Fall 2013

Establishing The Role Of The Pancreatic Transcription Factor Mist1 In Xbp1-Mediated Maintenance Of Pancreatic Acinar Cell Homeostasis

David Alan Hess
Purdue University

Graduate School ETD Form 9
(Revised 12/07)

PURDUE UNIVERSITY
GRADUATE SCHOOL
Thesis/Dissertation Acceptance

This is to certify that the thesis/dissertation prepared

By David A. Hess

Entitled
Establishing the role of the pancreatic transcription factor MIST1 in XBP1-mediated maintenance of pancreatic acinar cell homeostasis

For the degree of Doctor of Philosophy

Is approved by the final examining committee:

R. Claudio Aguilar
Chair

Stephen F. Konieczny

Julia Kirshner

Sophie Lelievre

To the best of my knowledge and as understood by the student in the *Research Integrity and Copyright Disclaimer (Graduate School Form 20)*, this thesis/dissertation adheres to the provisions of Purdue University's "Policy on Integrity in Research" and the use of copyrighted material.

Approved by Major Professor(s): Stephen F. Konieczny

Approved by: Peter J. Hollenbeck 5/31/2013
Head of the Graduate Program Date

ESTABLISHING THE ROLE OF THE PANCREATIC TRANSCRIPTION FACTOR MIST1 IN XBP1-MEDIATED MAINTENANCE OF PANCREATIC ACINAR CELL HOMEOSTASIS

A Dissertation
Submitted to the Faculty

of

Purdue University

by

David Alan Hess

In Partial Fulfillment of the

Requirements for the Degree

of

Doctor of Philosophy

December 2013

Purdue University

West Lafayette, Indiana

TABLE OF CONTENTS

Page

Page

Page

Page

LIST OF TABLES

LIST OF FIGURES

Figure Page

Figure Page

Figure Page

LIST OF ABBREVIATIONS

6-FAM	6-carboxyfluorescein
ADM	Acinar ductal metaplasia
ATF4	Activating transcription factor 4
ATF6	Activating transcription factor 6
ATP	Adenosine tri-phosphate
BiP	Binding immunoglobulin protein
CaCs	Centroacinar cells
CCK	Cholescystokinin
ChIP	Chromatin immunoprecipitation
CHOP	C/EBP homologous protein
DNA	Deoxyribonucleic acid
DTT	Dithiothreitol
ECM	Extracellular matrix
ER	Endoplasmic reticulum
ERAD	ER-associated degradation
ERSE	ER stress elements
GTP	Guanine tri-phosphate
HSPs	Heat shock proteins
IF	Immunofluorescence
IHC	Immunohistochemical
IRE1	Inositol-requiring enzyme 1
ISGs	Immature secretory granules
KC mice	$Mist1^{CreER/+}$; $LSL\text{-}Kras^{G12D}$
M6P	Mannose 6-phosphate
PACUC	Purdue Animal Care and Use Committee
PanINs	Pancreatic intraepithelial neoplasias
PaSCs	Pancreatic stellate cells
PCR	Polymerase chain reaction
PDA	Pancreatic ductal adenocarcinoma
PDI	Protein disulfide isomerase
PERK	PKR-like ER kinase
RT-qPCR	Real-time quantitative polymerase chain reaction
TGN	*Trans* golgi network
UAEs	Ubiquitin-activating enzymes
UPR	Unfolded protein response

UPRE	Unfolded protein response element
XBP1	Xbox binding protein 1
XBP1s	Xbox binding protein 1, spliced variant
XBP1u	Xbox binding protein 1, unspliced variant
XKC mice	$Mist1^{CreER/+}$; $Xbp1^{fl/fl}$; LSL-$Kras^{G12D}$
ZG	Zymogen granules

ABSTRACT

Hess, David A. Ph D., Purdue University, December 2013. Establishing the role of the transcription factor MIST1 in XBP1-mediated maintenance of pancreatic acinar cell homeostasis. Major Professor: Stephen F. Konieczny.

Pancreatic acinar cells (PACs) continuously produce more protein than any other cell type in the human body. As a result, PACs and other specialized secretory cells have a constant demand placed on their protein synthetic and packaging machinery. When demand for secreted products exceeds the capacity of the cell's basal protein production facilities, dangerous accumulations of misfolded proteins can build up, resulting in a condition known as ER stress. To ameliorate this stress, secretory cells activate a coordinated, three-part compensatory network collectively known as the unfolded protein response (UPR) to both expand the capacity of the ER and directly assist in refolding or degradation of aberrant peptides. Interestingly, others have hypothesized that the UPR branches largely overlap in their functions and targets, prompting us to investigate whether loss of the IRE1/XBP1 branch via conditional ablation of XBP1 in mature mouse PACs could be compensated for by the remaining UPR pathways. We show that survival and homeostasis of PACs is wholly dependent on the IRE1/XBP1 axis of the UPR. Specifically, ablation of *Xbp1* in mouse PACs results in a gradual but cumulative onset of irreversible ER stress. This results in abrogation of normal digestive enzyme synthesis, onset of extensive signs of pancreatic distress, and eventual apoptosis via ER stress-induced death pathways. Remarkably, we also show that the pancreas initiates a robust regenerative response via cell cycle reentry and proliferation of multiple adult cell types. This regenerative mechanism rapidly restores a functioning exocrine compartment and provides a novel means to study pancreatic damage and recovery from intrinsic stress events. Finally, we investigated the role of the acinar cell-specific transcription factor MIST1 as a downstream effector of XBP1. We verify that MIST1 is a direct target of XBP1, and a number of MIST1 target genes directly participate in facilitating cell recovery and survival during ER stress. Together, these data indicate that XBP1 and

MIST1 cooperate to sustain pancreatic acinar cells during times of high protein demand. Future disease research exploiting stress induction via modulation of the XBP1/MIST1 transcriptional network may be used to generate novel therapeutics for treatment of pancreatitis and pancreatic cancer.

CHAPTER 1. INTRODUCTION

1.1 Regulated secretion is a necessary component of metazoan survival

The generation and distribution of secreted cell products in higher eukaryotes occurs through regulated cellular pathways that ensure proper homeostatic maintenance. Internal- and externalization machinery is present in all multicellular organisms, and it facilitates cellular environmental responses and survival via its role in trafficking of signaling molecules to and from the cell surface, recycling and acquisition of necessary cell components, and transport of synthesized products to extracellular spaces. For many multicellular species including humans, specialized secretory cells are responsible for synthesis, packaging, and secretion of proteins necessary for regulation of life processes. In secretory cells, proteins destined for export are differentially processed and packaged to allow for expulsion from the cell and subsequent action upon a target tissue. At an organism level these secreted products often serve as vital components of maintenance and regulatory mechanisms including essential processes such as immunity and digestion. Due to the necessity of secreted products for survival, secretory cells have evolved unique mechanisms to regulate the synthesis and release of proteins.

Secretory cells possess extensive protein production and secretion capabilities, thus requiring a more developed regulatory system for ensuring proper protein production. Examples of secretory cells include plasma B cells that secrete antibodies as a component of the adaptive immune response, gastric chief cells that generate proteases and hydrolases in the stomach, and pancreatic acinar cells that synthesize and secrete inactive digestive enzyme precursors (zymogens) for eventual transport to the duodenum. Each of these cell types share common phenotypic and molecular characteristics including extensive ER and Golgi networks, a high degree of responsiveness to extracellular signals required to coordinate the actions of many cells, and expression of common transcription factors such as the basic helix-loop-helix transcription factor *Mist1* (discussed in section 1.5) (Acosta-Alvear et al., 2007; Pin et al., 2000). Additionally, secretory cells often cooperate and form structures that allow

multiple individual cells to secrete their contents into a shared lumen that relays the now concentrated products into a ductal network. These structures, termed acini, can be found in body tissues including lactating mammary glands and the pancreas. These cellular characteristics are essential to the regulation of the complex secretory process.

All eukaryotic cells utilize separate but overlapping pathways for internalization (endocytosis) of receptors and extracellular molecules and externalization (exocytosis) of required cell surface molecules, extracellular matrix components, and secreted factors (**Figure 1.01**). Vesicular endocytosis often initiates at clathrin- or caveolin-coated pits that form upon assembly of protein complexes at the membrane and initiate the internalizing process, although specialized pathways dependent on IL2Rβ, ARF6, flotillin and other proteins have also been described (Doherty and McMahon, 2009). Internalized vesicles are typically tagged and sorted into one of several categories including, but not limited to, the recycling endosome for return to the cell surface, the late endosome for sorting and transport along microtubules to various cell compartments, or the endolysosome for degradation (Mellman, 1996). This sorting process assures that the separate tasks of facilitating the relay of signals from the extracellular environment and acquisition and recycling of membrane and ECM components can utilize similar cellular machinery without interference.

Exocytosis, or more specifically protein secretion, is divided into two unique pathways; a constitutive and a regulated system **(Figure 1.02a)**. The constitutive pathway is utilized for packing of proteins into vesicles that are constantly released from the membrane, while regulated secretion is used to generate vesicles with highly concentrated protein contents that are stored and only secreted upon receipt of an external secretory signal, termed a secretagogue (Burgess and Kelly, 1987). Both pathways share early trafficking steps as peptides destined for secretion or requiring extensive protein modification enter the endoplasmic reticulum (ER) and proceed to the *cis* golgi network for processing **(Figure 1.1)** (Kelly, 1985). Specifically, membrane-bound ribosomes synthesize a pre-protein containing the complete amino acid sequence but lacking substantial secondary structure (Mains et al., 1987). These peptides typically contain signal sequences on their N-terminal tails that trigger translocation of the pre-proteins into the ER and subsequent cleaving or modification of the signal sequences (Mains et al., 1987). Once inserted into

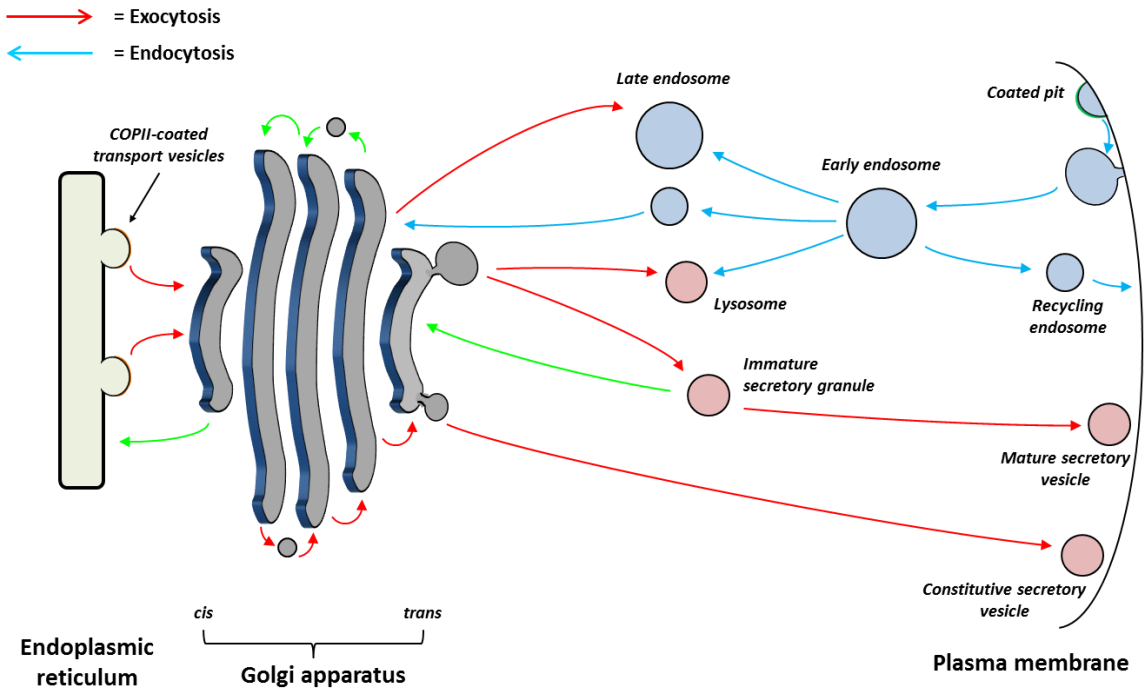

Figure 1.1 *Vesicular transport is utilized to convey signals and transport cell products to and from the plasma membrane.*

Exocytosis (red arrows) of secreted products involves vesicle-mediated transport from the ER to the *cis* Golgi, through the Golgi cisternae, and packaging into one of several types of secretory vesicle. Endocytosis (blue arrows) begins in coated pits that trigger vesicle formation around the internalized component and eventual sorting either back to the membrane or to other cell compartments. Retrograde movement of preexisting vesicles is also shown (green arrows).

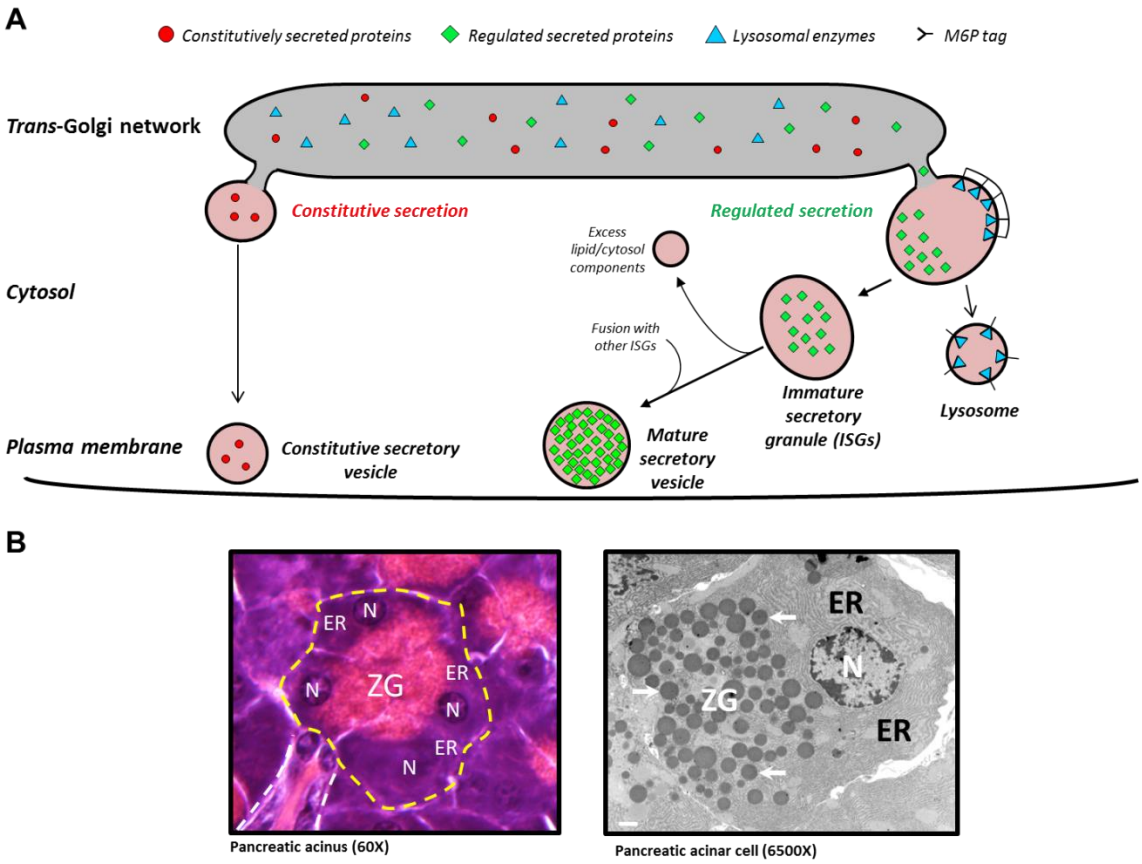

Figure 1.2 *Proteins requiring extensive folding or processing traffic through the trans Golgi*

(A) Constitutively secreted proteins (red circles) are packed loosely into vesicles and are delivered directly to the membrane (left). Both lysosomal enzymes and proteins undergoing regulated secretion are highly concentrated into budding vesicles (right). Lysosomal enzymes (blue triangles) form separate vesicles based on the presence of a mannose-6-phosphate tag. Proteins destined for regulated secretion (green diamonds) are packaged into immature secretory granules (ISGs) where excess lipid and cytosolic components are reclaimed. These vesicles then undergo fusion with other ISGs to become mature secretory vesicles. (B) Pancreatic acinar cells form polarized, multi-cellular structures called acini (left, yellow dotted line) with basally-localized nuclei (N) and ER and apically-localized zymogen granules (ZGs). These zymogen granules are coordinately secreted into an adjoining ductal network (left, white dotted line). Electron microscopy (right) reveals an extensive ER network and the apically localized zymogen granules (white arrows).

the ER lumen, glycoproteins destined for secretion or other cell fates are modified by the addition of carbohydrate groups, while the *cis* Golgi network serves to modify these attachments to allow for proper sorting and packaging into vesicles (Cooper, 2000). Upon entering the *trans* Golgi network (TGN), proteins fated for either the constitutive or regulated secretory pathways diverge and are packaged separately (Burgess and Kelly, 1987).

Sorting of processed proteins occurs in the TGN, where products can be diverted to lysosomes, passed directly to the membrane via constitutive secretion, or stored in secretory vesicles for regulated secretion. Lysosomal glycoproteins passing through the Golgi are heavily modified and tagged for transport to the lysosome via attachment of mannose 6-phosphate (M6P) to carbohydrate groups previously added in the ER **(Figure 1.02a, right)**. The M6P attachment is recognized by receptors in the TGN and triggers packaging of the tagged enzymes into clathrin-coated vesicles for transport to the lysosome (Glickman and Kornfeld, 1993). For secreted proteins, the constitutive secretion pathway serves as a default, as proteins lacking any other recognition sequences are directly trafficked to the plasma membrane (Burgess and Kelly, 1987). The constitutive pathway is utilized for targeting of necessary cellular components including plasma lipids and extracellular matrix components such as glycoproteins (Burgess and Kelly, 1987). Constitutive secretion does not generate vesicles that are stored within the cell for long periods of time; exocytosis takes place immediately after vesicle formation rather than in response to external stimuli **(Figure 1.02a, left)** (Kelly, 1985). Indeed, constitutive secretory vesicles often traffic from the TGN to the plasma membrane in as little as 10 minutes as compared to regulated secretory vesicles with a cytoplasmic lifetime from hours to days (Grampp et al., 1992). As a result, proteins secreted in this fashion do not achieve a high degree of protein concentration within vesicles, a feature unique to the regulated secretory pathway (Burgess and Kelly, 1987).

Regulated secretion defines a specific exocytosis pathway common to secretory cells in which synthesized products are diverted to specialized compartments within the TGN. The sequestering of secretory proteins within the TGN allows for a substantial increase in their concentration, often reaching densities ten to one hundred times higher than that

of the early Golgi (Burgess and Kelly, 1987). After deposition of proteins into the isolated compartment, the chamber is budded off from the TGN as an immature vesicle. This vesicle fuses with other immature vesicles and continues to be modified as excess membrane and cytosolic components are reclaimed and recycled, resulting in a mature secretory vesicle with a much higher concentration of protein than the initial compartment **(Figure 1.02a, right)** (Vitale and Denecke, 1999). These vesicles are carried via attachment to the cytoskeleton to specific locations within the cell for storage before eventual exocytosis in response to a hormonal or chemical signal (Burgess and Kelly, 1987; Wacker et al., 1997). Cytoskeletal trafficking to distinct membrane locations (required for apical/basal polarized cells) is accomplished via vesicle membrane-embedded tags as well as the action of multiple members of the Ras superfamily of small GTPases (Hsu et al., 2004). Standard light as well as electron microscopy of exocrine secretory cells reveal that secretory vesicles appear as electron-dense granules that are often localized to a specific location within the cell in order to allow for rapid, directional release into an adjoining ductal network **(Figure 1.02b)**. Due to the prodigious quantities of protein required for the generation of secretory vesicles, secretory cells utilize unique adaptive responses to control protein throughput.

All secreted proteins require ER processing, as correct peptide modifications and arrangement of hydrophobic amino acids into the interior of the protein structure are necessary for both membrane and extracellular fluid solubility. As such, secretory cells have a uniquely specialized cellular anatomy, often utilizing transcriptional networks to establish a physically expanded ER lumen in order to accommodate increased protein biosynthesis (Federovitch et al., 2005). This expansion was first noted during B lymphocyte differentiation into plasma B cells (Wiest et al., 1990), and has been demonstrated in both B cells and fibroblasts to be dependent upon expression of the ER stress-responsive transcription factor XBP1 (Shaffer et al., 2004; Sriburi et al., 2004). XBP1 serves to upregulate a number of genes as a component of the compensatory unfolded protein response (UPR), discussed at length in section 1.4. These gene targets both expand the ER and increase the production of protein transporters necessary for moving proteins in and out of the ER. Other transcriptional programs, discussed in section 1.3, also serve to ameliorate the stress placed on secretory cells by high protein synthesis demands. These responses serve as one component of an extensive quality

control system designed to guarantee both efficient synthesis and correct folding and packaging of proteins.

1.2 Quality control mechanisms ensure proper protein folding following synthesis

Eukaryotic cells utilize various quality control mechanisms throughout the cell to ensure that only properly synthesized and folded proteins are produced. This quality monitoring system begins during transcription, when the intrinsic 3'-5' exonuclease activity of some DNA polymerases allows them to excise incorrectly base paired nucleotides that are inadvertently added during replication and replace them with the correct base using the matching strand as a template (Khare and Eckert, 2002). Similarly, DNA integrity is monitored prior to synthesis by a checkpoint mechanism regulated by the p53 and Ataxia-Telangiectasia Mutated (ATM) proteins (Banin, 1998). Mutations in DNA damage regulators are intimately linked to human disease, particularly in the case of p53 which is known to be mutated in greater than 50% of human cancers (Olivier et al., 2010). The importance of correct transcription and translation of proteins beyond the DNA damage pathway is illustrated in RAS-driven cancers. The oncogenic form of the Kirsten rat sarcoma (KRAS) protein possesses a single point mutation and amino acid substitution ($G^{12}\rightarrow D$) that serves as the activating mutation in multiple cancers, including greater than 90% of tumors arising in pancreatic ductal adenocarcinoma (PDA) (discussed extensively in Chapter 6) (Hidalgo, 2010). As such, mechanisms to maintain the integrity of the DNA sequence serve as vital controls in prevention of disease. Maintenance of proper protein folding, however, is equally important for cell survival and homeostasis. The folding process is primarily regulated post-transcriptionally via production of chaperone and sensor molecules that control cellular responses to accumulations of misfolded proteins.

Protein denaturation can be triggered both physiologically and experimentally by exposing cells to short durations of heat. Heat exposure above normal physiological temperatures results in accumulation of misfolded or aggregated proteins in the cytosol as the denatured regions assume non-native conformations (Richter et al., 2010). In unstressed conditions, hydrophobic amino acids are internalized during protein folding or membrane embedding, and the presence of exposed hydrophobic residues in the cytoplasm can result in dangerous protein aggregates or anomalous activity, thus

necessitating a means for cells to sequester the misfolded proteins and to assist their refolding. Eukaryotic cells express a class of molecules known as molecular chaperones that aid in the refolding of these proteins as well as serving roles in the normal synthesis of certain peptides. These chaperones, typically referred to as heat shock proteins (HSPs) due to a characteristic increase in their expression following heat treatment, are present throughout the cell and bind to exposed hydrophobic surfaces in denatured or unfolded proteins (Richter et al., 2010). The specific means by which HSPs assist protein folding vary depending on the class of chaperone and subcellular location.

Some chaperones, including the predominantly mitochondrial-localized HSP60-like proteins, attach to exposed hydrophobic surfaces in denatured proteins and assume a conformation that forms a protective shell around the residues to isolate them from the surrounding cytosol **(Figure 1.03a)** (McClellan et al., 2005). This generates a favorable environment for refolding of the protein as well as preventing the interaction of the hydrophobic residues with other exposed proteins that could lead to protein aggregation. Additionally, this complex interacts with the pro-apoptotic proteins BAX and BAK, a binding that allows HSP60 to serve as an anti-apoptotic regulator while proteins are given time to assume their correct conformations (Itoh et al., 2002). Other classes of chaperones utilize different mechanisms to assist refolding.

The HSP70-like family of chaperones assists protein folding as new peptides assume their initial conformation following translation **(Figure 1.03b)** (Mayer and Bukau, 2005). Prior to interaction with an unfolded protein, HSP70-like chaperones are ATP-bound and have an open conformation with an exposed protein binding domain and exhibit only weak intrinsic ATPase activity (Mayer and Bukau, 2005). Upon binding to (and effectively sequestering) hydrophobic residues in a folding peptide, ATP hydrolysis takes place and the chaperone changes conformation, now exhibiting an increased affinity for the bound protein. During this time, mechanisms that have not been fully elucidated allow HSP70-like proteins to change conformation and directly assist in solubilization and folding of these substrates (Mayer and Bukau, 2005). Following dissociation of ADP

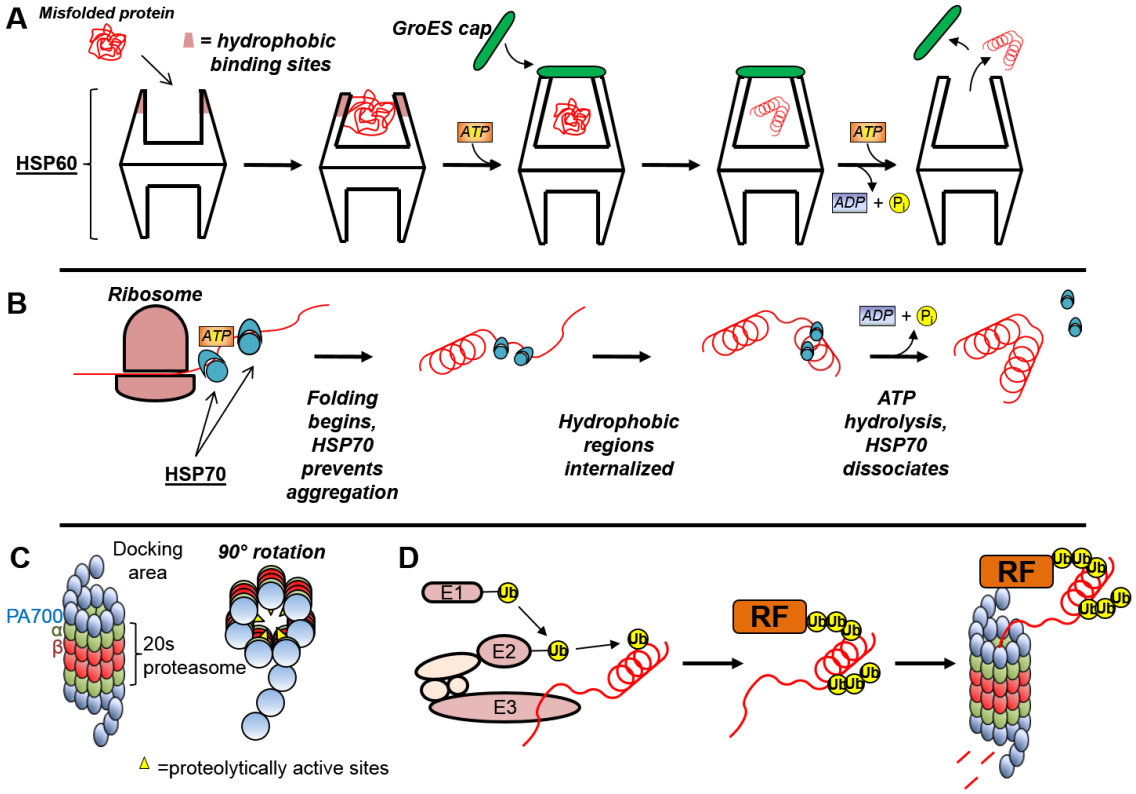

Figure 1.3 *Heat-shock proteins and the proteasome cooperate to repair or degrade misfolded proteins*

(A) HSP60 interacts with misfolded proteins via binding to exposed hydrophobic domains. An ATP-dependent interaction allows a GroES “cap” to bind, resulting in a protected, internal cavity that facilitates protein refolding. (B) HSP70 binds hydrophobic regions of proteins emerging from the ribosome in an ATP-dependent reaction. HSP70 remains bound until hydrophobic residues are sequestered inside the folding protein, then dissociates. (C) The proteasome is a multi-subunit complex that forms a hollow, tube-like structure with internal proteolytic activity. (D) The E1a-c proteins form a complex with E1 loading ubiquitin molecules onto E2, which subsequently adds the ubiquitin to a substrate held in place by E3. Ubiquitinated proteins are then bound by a recognition factor (RF) which promotes proteasome formation that subsequently degrades the tagged protein.

and P_i and reloading of the ATP, HSP70-like chaperones return to their open state and release their bound substrate. These two chaperone families, as well as most chaperone classes, all share common features that allow them to bind to unfolded protein regions in an attempt to generate a soluble or sufficiently protected structure (McClellan et al., 2005). When proteins are unable to assume their native conformations despite chaperone action, cells utilize alternative strategies to identify, tag, and destroy misfolded peptides.

The chaperone-mediated mechanism for assisted refolding operates alongside a destructive pathway that utilizes proteolytic enzymes to degrade proteins with exposed hydrophobic regions (Heinemeyer et al., 1991). This process is accomplished via an ATP-dependent, multi-subunit complex termed the proteasome that, in the case of misfolded proteins, uses embedded protease enzymes to unfold and cleave bound substrates **(Figure 1.03c)** (Elsasser and Finley, 2005). Misfolded proteins are marked for degradation via attachment of a polyubiquitin tag by a series of ubiquitin-activating enzymes (UAEs) termed E1, E2, and E3 ligases (Pines and Lindon, 2005). UAEs become targeted to misfolded proteins either via attachment of signal molecules by ER-resident sensors that can be recognized by E3 (discussed in section 1.3) or via recognition by E3 of certain hydrophobic motifs that are aberrantly exposed in denatured proteins (Pines and Lindon, 2005). The UAEs each function in a coordinated manner, with E1 enzymes loading ubiquitin molecules onto E2, while the E2 and E3 enzymes act in concert to target (a process mediated by the E3 subunit) to polyubiquitinate (via the E2 subunit) proteins that are to be destroyed (Pines and Lindon, 2005). The presence of the polyubiquitin tail added by the E2 subunit following recognition stimulates attachment of any of several targeting proteins that then trigger the formation and binding of the proteasome complex and subsequent proteolytic degradation of the tagged protein (Elsasser and Finley, 2005). While both the proteasome and the heat-shock proteins allow recovery and destruction of misfolded proteins, neither of these systems can regulate the process of translation that initially produces these peptides. This limits their responsiveness to intrinsic protein folding stresses that may be triggered by the sudden, rapid demand for protein synthesis often seen in secretory cells.

Correct protein folding is particularly important for peptides destined for membrane deposition or secretion from the cell. For proteins trafficked to the membrane, improper arrangement of hydrophobic and hydrophilic regions can lead to insolubility in the lipid bilayer, improper trafficking of receptors, or receptors that are unable to relay signals from extracellular stimuli, all conditions observed as causative agents in human disease (Kim and Rao, 2010). Improperly folded secreted proteins can also be detrimental due to the possibility of aggregation in extracellular spaces or loss of function at the target site. Indeed, secreted protein aggregates are believed to contribute to a number of human diseases including the aggregation of amyloid-β in neuronal spaces in Alzheimer's disease and the aggregation of islet amyloid polypeptide in the pancreas during type II diabetes (DeToma et al., 2012). In order to maintain efficient and effective protein synthesis, homeostatic mechanisms have evolved in order to sense and respond to accumulations of misfolded proteins while peptides are still progressing through the ER, a condition known as ER stress (Oslowski and Urano, 2011). These mechanisms, collectively termed the unfolded protein response (UPR), serve to regulate protein processing, folding, and degradation via upregulation of chaperones, increased expression of ER-associated degradation (ERAD) proteins, and direct modulation of translation initiation (Walter and Ron, 2011). Additionally, specific components of the UPR can trigger apoptosis if ER stress cannot be ameliorated. Recent work has demonstrated that the UPR plays a vital role in maintaining secretory cell viability.

1.3 The unfolded protein response (UPR) is a multi-component compensatory mechanism that maintains cellular homeostasis

In contrast to quality control mechanisms that respond to cytoplasmic protein denaturation, the UPR is initiated by an accumulation of misfolded proteins within the ER, a condition described as ER stress **(Figure 1.04)**. ER stress can be caused physiologically by a production demand that temporarily exceeds the physical capacity of the ER, including the high levels of synthesis required following clearance of secretory vesicles after signal-mediated release in secretory cells (Lee et al., 2005). ER stress can also be triggered experimentally by treatment of cells with any number of drugs including, but not limited to, thapsigargin (an inhibitor of sarco/endoplasmic reticulum Ca^{2+} ATPases), tunicamycin (an inhibitor of N-linked glycosylation), or dithiothreitol (a

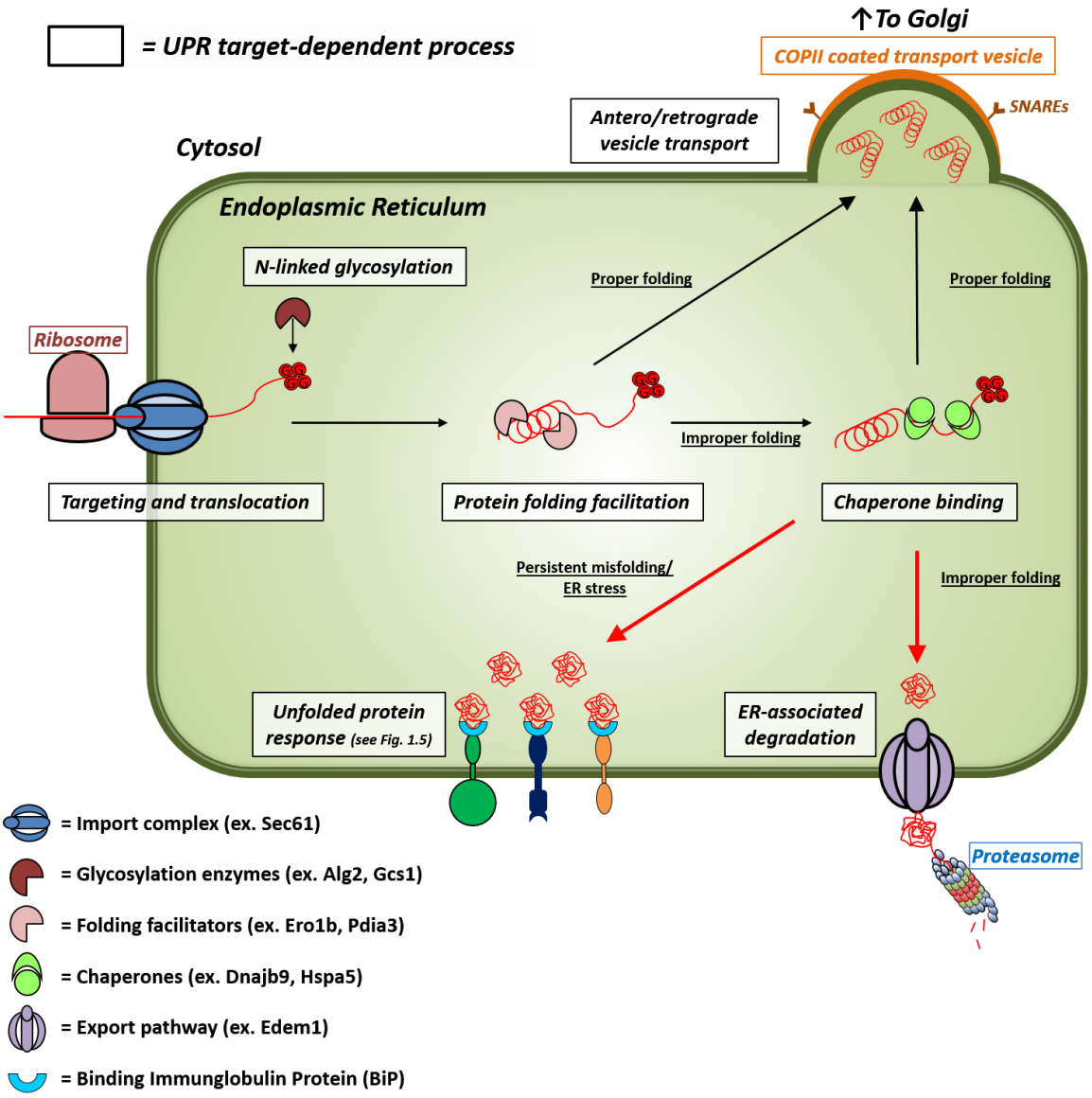

Figure 1.4 *The unfolded protein response regulates gene targets associated with all stages of protein synthesis*

Translated proteins are inserted via membrane import complexes (blue). Proteins are initially glycosylated via enzymatic modification (brown) before being acted upon by enzymes (pink) that facilitate folding. Improperly folded proteins are bound by chaperones (green) in an attempt to further facilitate folding. Successful folding results in transport to the Golgi via COPII-coated vesicles, while improperly folded proteins are exported from the cell (purple). Large accumulations of misfolded proteins generate increasing hydrophobic interactions with BiP that result in activation of the unfolded protein response.

reducing agent, also known as DTT) (Samali et al., 2010). These drugs all impair protein folding within the ER by disrupting either the transport of peptides/proteins into and out of the ER (thapsigargin) or the proper addition of necessary modifications (glycosylation for tunicamycin, disulfide bond formation for DTT) that are required for proteins to properly fold (Samali et al., 2010). During ER stress proteins with exposed hydrophobic resides begin to accumulate within the ER lumen. These residues interact with both ER-resident chaperones and embedded sensor molecules that traverse the ER membrane and initiate transcriptional cascades, altering protein synthesis and processing in an attempt to allow clearance of the misfolded peptides.

In eukaryotes, the UPR is primarily initiated through the action of the ER-resident chaperone Binding Immunoglobulin Protein (BIP), a member of the HSP70 class of chaperones (Haas, 1994). BIP serves as an ER lumen-specific chaperone by binding to exposed hydrophobic residues (similar to the previously discussed mechanism regarding HSP70) in order to prevent aggregation within the ER as well as allow for proper folding (Haas, 1994). BIP functions in concert with the ER-specific enzyme Protein Disulfide Isomerase (PDI) to maintain newly synthesized proteins in a non-aggregated and accessible conformation that allows PDI to modify disulfide bonds for structural arrangement of the protein (Mayer et al., 2000). BIP also functions to regulate calcium levels and prevent initiation of ER stress-induced apoptosis via an interaction with ER-resident caspase-7 (Reddy et al., 2003). While each of these functions aid in maintenance of normal protein production and cell homeostasis, BIP also serves as the primary sensor for each of the three transmembrane proteins that serve as master regulators of the UPR cascades.

In an unstressed state, steady-state levels of protein production require small amounts of BIP in order to facilitate proper folding of proteins as they initially enter the ER. BIP molecules normally remain docked to three separate transmembrane proteins; (PKR)-like ER kinase (PERK), activating transcription factor 6 (ATF6), or inositol requiring enzyme 1 (IRE1) (Walter and Ron, 2011). When unbound by misfolded peptides, BIP stably binds to all three proteins individually and serves as an inhibitor of their functions **(Figure 1.05)**. Upon binding exposed hydrophobic residues in folding peptides, BIP

dissociates from the UPR initiator protein it was bound to, allowing the UPR master regulators to initiate their downstream pathways (Ron and Walter, 2007). Once

sufficient dissociation has occurred, the UPR branches can initiate positive feedback loops that sustain the response until the ER stress is resolved. Recent studies have shown that IRE1 may also directly interact with misfolded proteins, although the bound BIP chaperone is still thought to serve as a modulator of this activity (Mori, 2009; Walter and Ron, 2011). The three branches coordinately trigger expression of both branch-specific and multi-branch gene targets in an attempt to ameliorate ER stress.

Each specific master regulator (PERK, ATF6, or IRE1) initiates a unique signaling cascade that ultimately aids in one of three general functional stress responses: adaptive response of the cell to ER stress, feedback control of the UPR process itself, or cell fate determination in cases of unresolved ER stress **(Figure 1.05)** (Oslowski and Urano, 2010). While ATF6 and IRE1 are uniquely activated in response to ER stress, PERK has substantial crosstalk with other pathways, as its primary effector (eIF2α) is also utilized by several other independent stress responses (Marchand et al., 2006).

During the adaptive response phase, protein throughput is attenuated while processing of misfolded proteins is increased. Attenuation is primarily accomplished via the PERK component of the UPR **(Figure 1.05, right)**. Upon dimerization within the ER membrane following BIP dissociation, PERK-dependent phosphorylation of eukaryotic translation initiation factor 2A (eIF2α) leads to a reduction in global mRNA translation via inhibition of the eIF2 complex (Chakrabarti et al., 2011). This slowdown preferentially allows for production of certain proteins, including activating transcription factor 4 (ATF4), a transcription factor that is involved in feedback regulation of the UPR (via expression of the transcription factor XBP1) and cell fate determination (via expression of C/EBP homologous protein, or CHOP) (Walter and Ron, 2011). Additionally, PERK phosphorylates NF-ED-related factor 2 (NRF2) in order to drive antioxidant and detoxification cascades along with proteasome components (Lee et al., 2012).

Independent of PERK activation, the ATF6 master regulator is released by BIP and undergoes a conformational change allowing its cytoplasmic domain to dissociate and

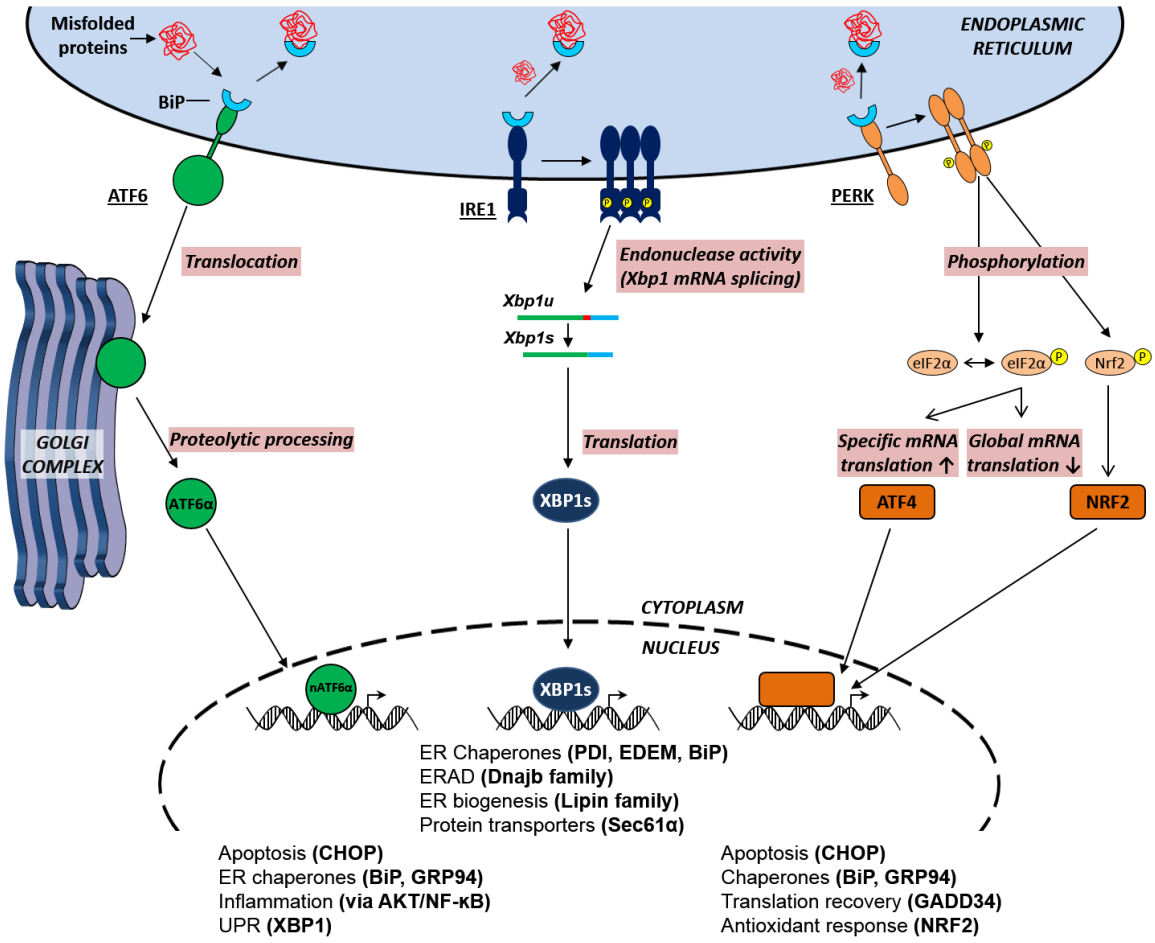

Figure 1.5 *Diagram of the mammalian unfolded protein response (UPR)*

The UPR consists of three separate pathways, each under the control of a different transmembrane master regulator. The ATF6 branch (left, green) is activated via proteolytic processing of the ATF6 receptor following activation and dissociation from the ER membrane. The IRE1 branch (center, blue) is activated via mRNA splicing of the *Xbp1* mRNA into a new form encoding a potent transcription factor, XBP1s. The PERK branch (right, orange) initiates a phosphorylation cascade resulting in global translation slowdown as well as activation of the ATF4 and NRF2 transcription factors. All branches are shown with examples of downstream cell responses/gene targets provided.

translocate to the Golgi **(Figure 1.05, left)**. The protein is then proteolytically processed prior to further translocation to the nucleus (now termed nuclear ATF6 or nATF6) where it upregulates expression of a number of chaperone proteins including BIP, XBP1, and glucose-regulated protein 94 (GRP94) (Okada et al., 2002). The ATF6-dependent expression of XBP1 is itself an example of the crosstalk and feedback control mechanisms that exist between UPR branches, as XBP1 is the primary effecter of the IRE1 branch via a unique activation mechanism (discussed extensively in section 1.4). IRE1 functions primarily to promote expression of XBP1s **(Figures 1.5, middle)**, an active form of XBP1 that translocates to the nucleus and activates a number of genes associated with adaptive response to ER stress including *ERdj4* (associated with the ER-resident degradation machinery) and *EDEM1* (associated with translocation of misfolded proteins from the ER back into the cytoplasm for degradation).

In higher eukaryotes, each of the UPR branches are utilized differently depending on cell type, with different responses observed following attenuation of the individual branches in various cells. Extensive characterization has been done on the IRE1 branch of the UPR in yeast, as it is both the only UPR branch present in the species and because it is the most conserved of the three branches among all metazoans. Increased UPR complexity is a hallmark of higher eukaryotes, as multiple ATF6 variants exist that function differently in the mammalian UPR. Similarly, IRE1 is expressed in two forms, α and β, that may specify unique mechanisms for different UPR functions depending on cell type (Walter and Ron, 2011). Interestingly, despite substantial overlap in function and targets among the three UPR branches, individual embryonic deletion of the three branches generates significant phenotypic differences varying from no substantial effect to embryonic lethality in the case of the IRE1/XBP1 branch (Reimold et al., 2000; Urano et al., 2000; Yamamoto et al., 2007; Zhang et al., 2002). This suggests a unique role for the IRE1/XBP1 axis during development and possibly as a principle component of the mammalian UPR.

1.4 XBP1 is the primary transcription factor utilized by the IRE1 branch of the UPR

IRE1 utilizes an unconventional mechanism to activate its portion of the mammalian UPR **(Figure 1.06b)**. Following oligomerization and autophosphorylation of multiple

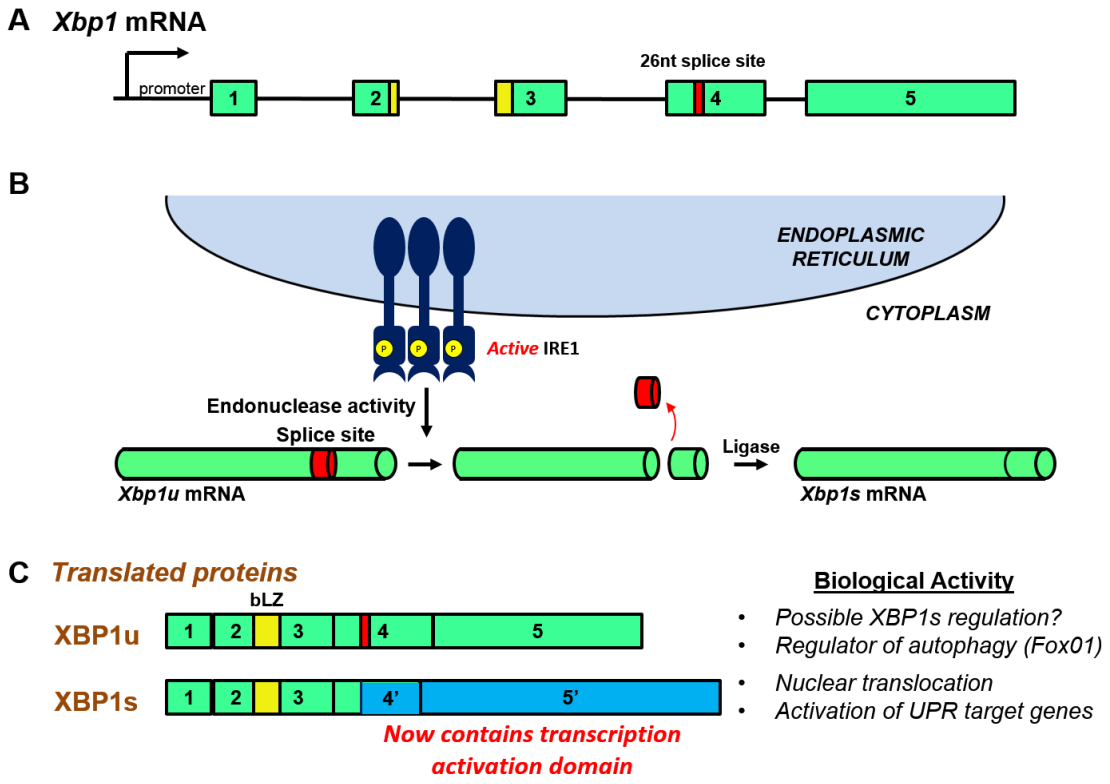

Figure 1.6 *IRE1-dependent splicing of the Xbp1 mRNA is responsible for generation of the XBP1s protein*

(A) The *Xbp1* mRNA contains a 26-nucleotide splice acceptor in Exon 4 (red). This mRNA is localized to vicinity of the ER by unknown mechanism. (B) Upon activation, IRE1 utilizes its endoribonuclease functions to excise the intron. A cytoplasmic ligase then anneals to two ends of the mRNA, generating a novel transcript. (C) The unspliced *Xbp1* transcript is translated into XBP1u, a short-lived protein that remains largely in the cytoplasm. The spliced transcript is translated into XBP1s. XBP1s has a unique C-terminus as the splice event causes a frameshift, resulting in a new transcriptionally active protein with a nuclear localization signal and transcription activation domain.

IRE1 proteins in the ER membrane, IRE1 activates an endoribonuclease domain located on the cytosolic side of the molecule (Chakrabarti et al., 2011). This endoribonuclease activity cleaves an ER-resident mRNA called *Xbp1u* (for *Xbp1*, unspliced variant). The exact role of the translated XBP1u protein generated by the unspliced *Xbp1u* transcript is unknown, although recent work has indicated a possible role as a regulator of autophagy via interaction with FOX01 (Zhao et al., 2013). The IRE1-dependent splicing event excises a 26-nucleotide long intron from the *Xbp1u* transcript (Lee et al., 2002). This excision generates a frameshift coding for a novel protein, termed XBP1s (for *Xbp1*, spliced variant) **(Figure 1.06c)**. Despite sharing extensive N-terminal homology with XBP1u including the basic leucine zipper motif, XBP1s has a distinct C-terminal domain. This unique C-terminus contains a potent nuclear localization signal as well as a transcription activation domain, while the XBP1u C-terminus has competing nuclear localization and nuclear exclusion domains as well as an uncharacterized “degradation domain” that prevents its accumulation in the cell (Yoshida et al., 2006).

A possible but not yet fully characterized mechanism for modulation of XBP1s utilizes dimerization of the unstable XBP1u with XBP1s and subsequent retention in the cytoplasm and proteasomal degradation (Yoshida et al., 2006). This mechanism is believed to serve only as a small component of the overall feedback control of the UPR, as XBP1s levels are drastically upregulated following splicing after ER stress onset, producing far more protein than the low levels of XBP1u could regulate via dimerization (Yoshida et al., 2006). Other research suggests a possible role for XBP1u as a transcriptional partner of XBP1s, but only for a very small subset of genes outside the canonical UPR targets (Guo et al., 2010), suggesting that XBP1s can regulate both UPR and non-UPR transcriptional networks, an idea discussed more thoroughly in chapter 5.

XBP1s is a potent basic leucine zipper (bLZ) transcription factor that, upon translation from the newly spliced mRNA, translocates to the nucleus and activates its target genes. The IRE1-dependent splicing of Xbp1 is conserved in metazoans and has been heavily studied in yeast where HAC1, an XBP1 homologue, is spliced by IRE1 and is responsible for initiation of the entire UPR (Cox and Walter, 1996). Mammalian XBP1s binds to a number of consensus sequences including ER Stress Elements (ERSE) I and II and the Unfolded Protein Response Element (UPRE) (Acosta-Alvear et al., 2007).

While binding to ERSE sequences and subsequent transcriptional activation is a common feature of both XBP1 and nATF6, XBP1 preferentially binds the UPRE while nATF6 shows very low affinity, indicating that XBP1 has a distinct role from ATF6 in the UPR (Yamamoto et al., 2004) **(Figure 1.07)**. Additionally, ATF4 (upregulated via the PERK UPR branch), has a unique binding site independent of nATF6 and XBP1, likely due to the fact that the phosphorylation of eIF2α carried out by PERK in the UPR is also utilized by other enzymes as part of unrelated stress pathways including amino acid deprivation and viral infection (Marchand et al., 2006). Recent work by the Yoshida group has also illustrated that XBP1, BiP, and CHOP can cross-regulate each other, and that CHOP can form a positive feedback loop via low-affinity binding to a number of promoter regulatory sequences including ERSE (Takayanagi et al., 2013). This is hypothesized to be a means of allowing a transition from a pro-survival, pro-recovery UPR state to one promoting apoptosis driven by steadily increasing expression of CHOP.

Embryonic knockout studies in mice have examined the roles of each of the three UPR master regulators, as well as XBP1. Deletion of PERK or its primary effector, ATF4, generates viable offspring, however $PERK^{-/-}$ mice have secretory cell defects in the pancreas, an unsurprising result given the extensive secretory load placed upon pancreatic cells (Tanaka et al., 1998; Zhang et al., 2002). Knockout of either ATF6α or ATF6β has no effect on embryonic development, however compound knockout of the two proteins results in embryonic lethality (Yamamoto et al., 2007). Interestingly, this study also revealed extensive dimerization between ATF6α and XBP1, indicating possible crosstalk between the two pathways independent of their co-activation of ERSE sequences. IRE1 or XBP1 deletion in mice results in embryonic lethality. However, targeting of a liver-specific XBP1 transgene (Liv^{Xbp1}) in $Xbp1^{-/-}$ mice rescues this phenotype, although mice die during post-natal development (Lee et al., 2005; Reimold et al., 2000). Interestingly, $Xbp1^{-/-}$;Liv^{Xbp1} post-natal pups have extensive abnormalities in secretory tissues, with the presumed cause of death attributed to lack of pancreatic enzyme production (Lee et al., 2005). The dependency of secretory tissues on an intact UPR has prompted numerous researchers to utilize mouse models in order to investigate the unique roles of XBP1 in various secretory cell types.

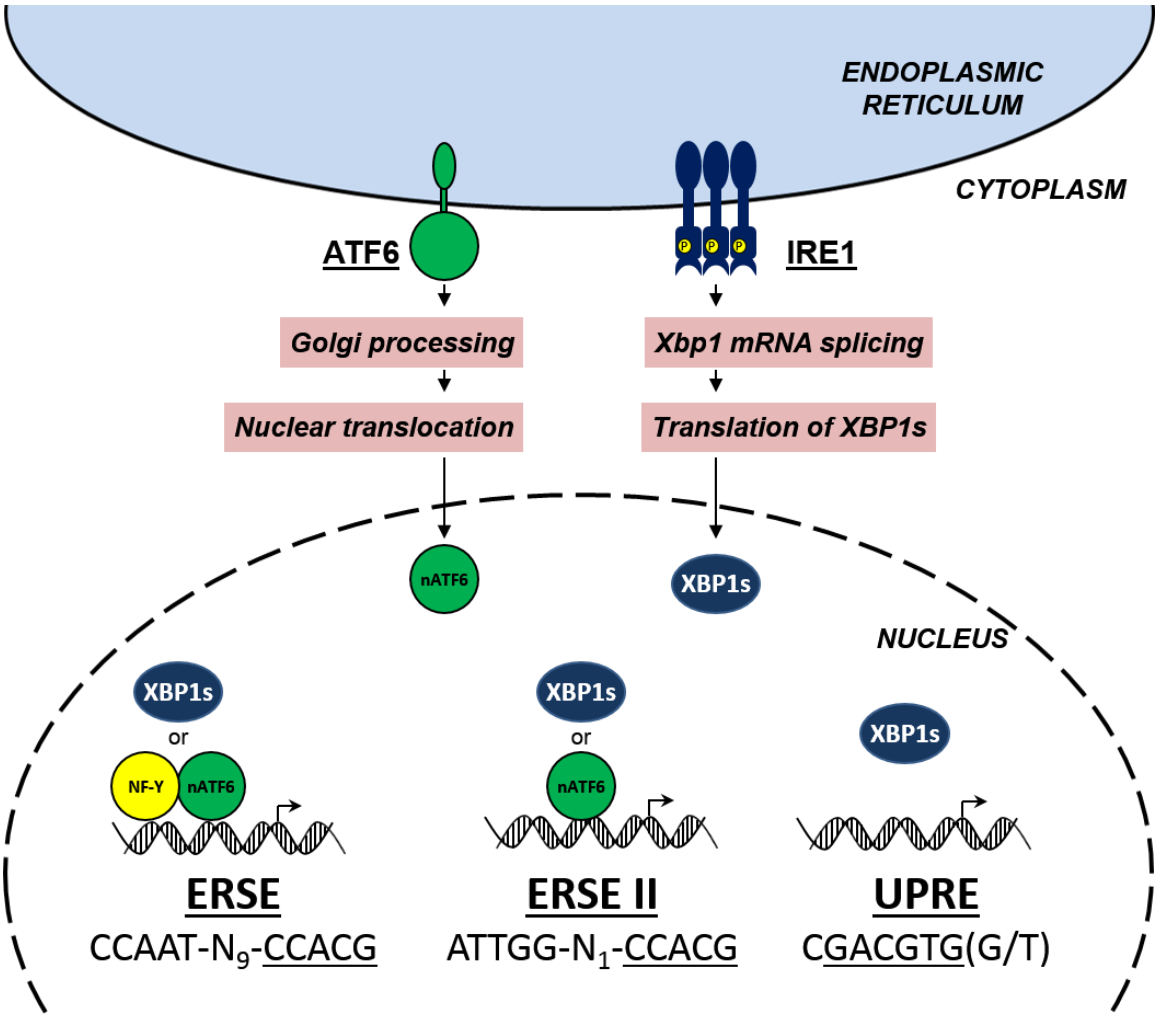

Figure 1.7 *XBP1 and nATF6 bind common and unique DNA consensus sequences*

Three ER stress-specific consensus sequences (ERSE, ERSEII, and UPRE) have been identified. ERSE can be bound by nATF6 only in concert with NF-γ, while XBP1s can bind by itself. ERII can be bound by either nATF6 or XBP1s. UPRE preferentially binds XBP1s and has only low affinity for ATF6. Underlined sequences represent core motifs bound by XBP1.

Multiple mouse models have been generated in order to interrogate the role of XBP1 in secretory cells and tissues. A mouse strain with a heterozygous deletion of *Xbp1* (*Xbp1*$^{+/-}$) has been used recently to show that impaired XBP1 function, due to reduced levels of its expression, results in exacerbated damage in an alcohol-induced model of exocrine pancreatic disease (Lugea et al., 2011). Chimeric mice generated from the previously described *Xbp1*$^{-/-}$ model are noticeably deficient in plasma cells and incapable of secreting substantial amounts of immunoglobulin (Reimold et al., 2001). A Cre-inducible *Xbp1* null mouse (*Xbp1*$^{fl/fl}$) was recently generated that was utilized to investigate the effects of adult ablation of *Xbp1* in the chief cells of the stomach (Huh et al., 2010). Interestingly, this work revealed little increase in ER stress but a marked failure of cells to establish a fully differentiated gene expression pattern. Taken together, these models have revealed variable roles for *Xbp1* that are highly dependent on cellular context. In addition to expression of *Xbp1*, the three cell types investigated (pancreatic exocrine cells, plasma B cells, and gastric chief cells) also share expression of a number of transcription factors linked to cell identity and secretion, among them the basic helix-loop-helix protein MIST1. This prompted a close examination of the possible role of MIST1 as a component of the XBP1 transcriptional network.

1.5 MIST1 is a transcription factor linked to proper functioning of secretory cells

The pancreas is responsible for endocrine-mediated regulation of blood glucose levels, for the production of digestive enzyme precursors, termed zymogens, and for the secretion of the zymogens via a ductal network that leads into the duodenum **(Figure 1.08a)**. The digestive exocrine component of pancreatic function is accomplished by coordinate action of multiple cell types including secretory acinar cells and duct cells **(Figure 1.08b)**. Spheres of acinar cells, termed acini (plural) or acinus (singular), are connected to a branched ductal network, often described as analogous to grapes on a vine. These duct networks merge, eventually becoming the main pancreatic duct that joins the common bile duct before emptying into the duodenum. Pancreatic acinar cells are responsible for production of the vast majority of digestive enzymes secreted into the duodenum (Williams, 2010), and in humans they synthesize more protein than any other cell type (Case, 1978). This function is facilitated via a characteristic cell organization in which an extensive ER is maintained at the basal surface of the cells while packaged

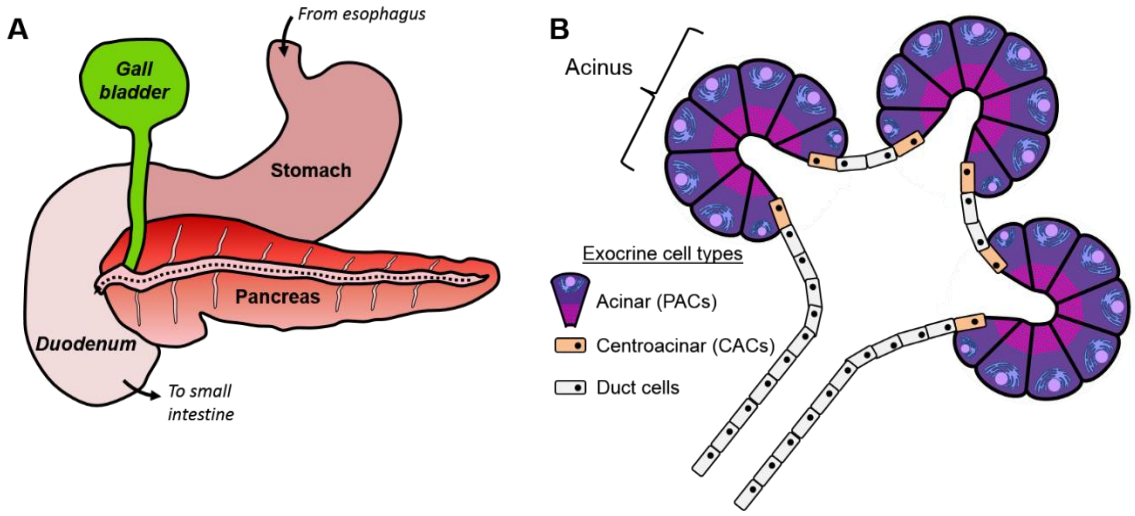

Figure 1.8 *Pancreatic acinar cells secrete digestive enzyme precursors into the duodenum*

(A) The exocrine pancreas consists of large numbers of acinar clusters, arranged in a “grapes on a vine” formation. These clusters are sites of zymogen synthesis and empty into centralized lumens that eventually join to the pancreatic duct before joining the common bile duct and emptying into the duodenum. (B) Acinar cells are arranged into a spherical cluster termed an acinus (plural = acini). These acini are polarized with zymogens clustered at the apical end. Additional cell types are present in the cluster including duct cells that form a tubular network for zymogen transport and centroacinar cells that connect the acini lumens to the ducts.

zymogens are stored at the apical side, awaiting secretion into an adjoining ductal lumen **(Figure 1.08b)**. This organization is dependent on specific cytoskeletal arrangements as well as surface attachment points for zymogen vesicles, all of which are controlled via specific transcriptional programs. In the pancreas, the transcription factor MIST1 has been extensively studied as a key factor in maintaining the organization and efficient functioning of pancreatic acinar cells.

MIST1 is a basic helix-loop-helix transcription factor that is exclusively expressed in secretory tissues including the serous secretory cells of the immunoglobulin secreting B cells, zymogenic gastric chief cells, and pancreatic acinar cells (Capoccia et al., 2011; Pin et al., 2000). Embryonic knockout or expression of a dominant negative *Mist1* construct leads to pancreatic acinar cells that exhibit a number of defects including disorganization of cell structures and loss of polarity, as well as impaired cellular communication due to loss of intracellular gap junctions (Jia et al., 2008; Pin et al., 2000; Rukstalis et al., 2003; Zhu et al., 2004). Additionally, deletion of *Mist1* causes an acceleration in Kras-induced development of pancreatic intraepithelial neoplasia, an early event observed in mouse models of pancreatic cancer (Shi et al., 2009b). These findings identify MIST1 as a critical regulator of pancreatic acinar cell organization and function. Recent work has also established that MIST1 may serve to maintain proper secretory function in acinar cells.

Intracellular communication via membrane channels is required for proper zymogen biosynthesis as well as packaging and secretion in the pancreas (Meda, 1996). Additionally, the polarized state of epithelial cells in multi-cell structures is highly dependent on effective cell-to-cell communication via intracellular channels (Mellman and Nelson, 2008). Recently, a system in which MIST1 expression is induced in a *Mist1*$^{-/-}$ animal (effectively a rescue of MIST1 expression, termed LSL-*Mist1*^{myc} model) was used to demonstrate that MIST1 is directly responsible for maintaining intracellular communication and coordinated secretion between pancreatic acinar cells (Direnzo et al., 2012). This facilitation is accomplished via transcriptional control of *Connexin 32* (*Cx32*), a protein that forms a functional channel between acinar cells that aids in coordination of secretory actions **(Figure 1.09a)** (Direnzo et al., 2012; Rukstalis et al., 2003). Gap junction-mediated communication is a key feature of the coordinated

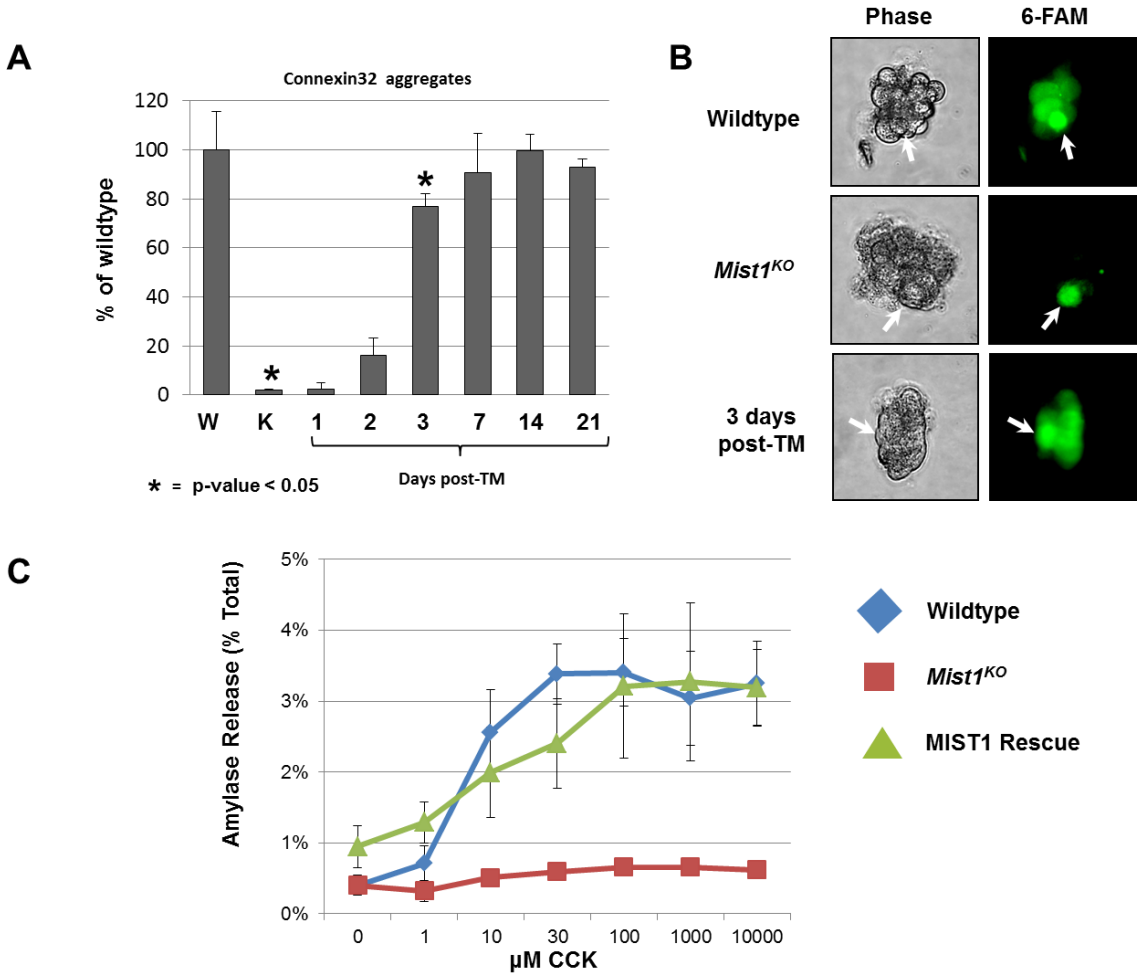

Figure 1.9 *MIST1 is essential for pancreatic acinar cell communication and secretion*

(A) Quantification of connexin 32 aggregates following in *Mist1*$^{-/-}$ pancreata reveals near complete loss of gap junction formation that is rescued upon ectopic expression of MIST1. (B) Single cell injection of 6-carboxyfluorescein (6-FAM) into acinar clusters indicates that *Mist1*$^{-/-}$ acinar cells do not communicate via gap junctions, as they are unable to pass the dye from cell to cell. (C) Measurement of amylase secretion from isolated acinar clusters following administration of cholescystokinin (CCK) demonstrates that *Mist1*$^{-/-}$ acinar cells have significantly less secretion than wildtype or MIST1 rescue cells. Figures A,B modified from Direnzo et al., 2012.

secretion process necessary for normal digestive processes. The loss of MIST1 impairs cell-to-cell communication as demonstrated by fluorescein dye injections of isolated acinar clusters from mice **(Figure 1.09b)**. This loss of communication was hypothesized to be an underlying cause for the drastic drop in secretory capability seen in MIST1$^{-/-}$ animals **(Figure 1.09c)**. In addition to its role in facilitating cell communication and coordination within the pancreatic acinus, MIST1 also directly enables successful secretory vesicle formation and secretion.

Rescue of MIST1 expression via the previously described LSL-*Mist1*^{myc} mouse model restores the secretory capability of pancreatic acinar cells after being significantly diminished when MIST1 expression is limited **(Figure 1.09c)**. Ultrastructural analysis reveals that acinar cells lacking MIST1 have decreased secretory vesicle size and number, as well as a general lack of apical ER localization and expansion, a similar defect as that seen in *Xbp1*-null pancreatic acini after birth (Direnzo et al., 2012; Lee et al., 2005). Bioinformatic screens in mouse models examining MIST1-positive chief cells and pancreatic acinar cells have also revealed that MIST1 regulates a subset of genes in the RAB protein family, specifically *Rab3D* and *Rab27a* (DiRenzo, 2012; Huh et al., 2010). The RAB3 family and RAB27a are typically associated with mature secretory vesicles and may function as sensors for mature vesicles, thus serving as a bridge between MIST1 and control of the final stages of exocytosis (Fukuda, 2008). These data collectively indicate that MIST1 is transcriptionally linked to the synthesis, packaging, trafficking, and coordinated secretion of zymogens in pancreatic acinar cells, making its possible actions and mode of regulation during ER stress a prime area for investigation.

1.6 The unfolded protein response and MIST1 both play roles in maintenance and recovery of acinar cell identity following damage in the exocrine pancreas

The mammalian pancreas is initially formed during development as two separate outgrowths of the primordial gut tube that merge to form the complete organ (Slack, 1995). All mature pancreatic cells, including both the endocrine and exocrine linages, derive from a common, multi-potent progenitor cell **(Figure 1.10, left)** (Jensen et al., 2005). These progenitor cells have a unique expression pattern for a number of

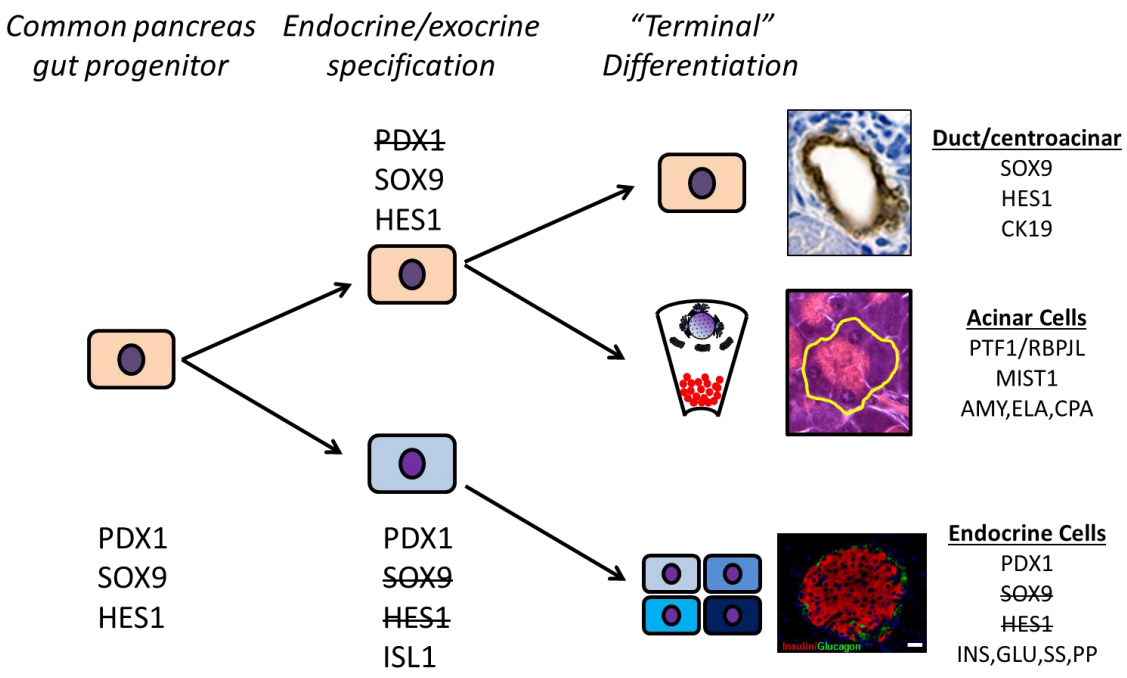

Figure 1.10 *Exocrine development in the pancreas involves expression of key transcription factors including MIST1*

All pancreatic cells begin as a common progenitor expressing PDX1, SOX9, and HES1. The endocrine lineage (lower path) loses expression of SOX9 and HES1 while gaining expression of ISL1. These cells eventually initiate unique transcription programs for each of the unique endocrine cell types. Exocrine cell differentiation (upper branches) is marked by a loss of PDX1, followed by a split into the duct/centroacinar program (marked by continued expression of SOX9 in both cases and HES1 in centroacinar cells) and the acinar cell program specified by expression of the PTF1a/RBPJL complex and MIST1.

transcription factors (TFs), including coexpression of pancreatic and duodenal homeobox 1 (PDX1), Sry/HMG box transcription factor 9 (SOX9), and active Notch signaling components including hairy and enhancer of split-1 (Hes1) (Jensen et al., 2005). Importantly, this unique progenitor signature is not fully recapitulated in any adult cell type in the pancreas.

Developing cells in the pancreas achieve their differentiated state via repression or expression of key transcription factors **(Figure 1.10)**. The endocrine lineage includes five distinct cell types (α, β, δ, ε, and PP) that upon maturation reside in the pancreatic islets of Langerhans (Elayat et al., 1995). Each of these cell types has a unique transcriptional program, although early endocrine specification involves continued expression of PDX1, loss of SOX9, and expression of insulin gene enhancer protein 1 (ISL1) (Edlund, 2002). Differentiated endocrine cells are identified via expression of their secreted products including glucagon (α), insulin (β), somatostatin (δ), ghrelin (ε), and pancreatic polypeptide (PP) (Elayat et al., 1995).

The mature exocrine lineage is marked by a lack of PDX1 expression and is divided into three cell types; duct cells, centroacinar cells, and acinar cells. Duct and centroacinar cells continue expression of the progenitor factor SOX9, while centroacinar cells also continue to express HES1, leading to the hypothesis that centroacinar cells may be the most “stem-like” cell within the pancreas (discussed in section 1.6). Acinar cells are specified via coexpression of PTF1a/ RBPJL complex as well as MIST1 (Jensen et al., 2005; Rooman and Real, 2011). The commitment of most pancreatic lineages to specific, terminally differentiated cell identities has prompted extensive discussion as to whether a persistent stem cell population exists within the adult pancreas. This question is of key importance to the study of human diseases, including pancreatitis, in which repair and replacement of damaged exocrine cells in required for proper organ function. Attempts to identify and characterize repair mechanisms and specific cell compartments that function to restore damaged acinar tissue have often yielded conflicting results.

Damage-responsive cell types exist both outside and within the exocrine compartment **(Figure 1.11a)**. Outside of the acinar/duct system, pancreatic stellate cells (PaSCs) are tissue-resident, myofibroblast-like cells that reside in the periacinar space between acini

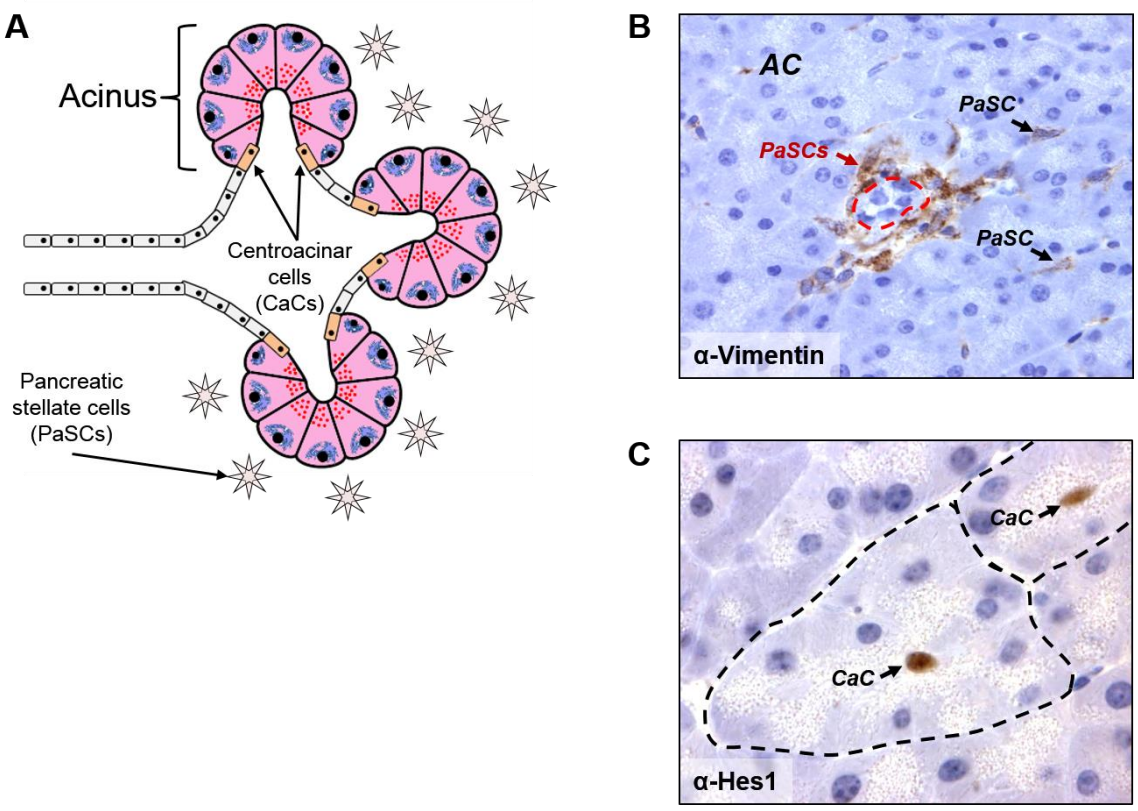

Figure 1.11 *Pancreatic cells outside the acinar compartment respond to damage*

(A) Pancreatic stellate cells (star-shaped) reside in the peri-acinar space between acini and are activated in response to damage. Centroacinar cells are found at the junction between acinar and duct cells and are also known to proliferate in response to damage. (B) Red dotted line marks a small, pre-cancerous metaplastic duct. Immunohistochemical staining for Vimentin reveals both tissue resident (black arrows) and damage-responsive (red arrows) pancreatic stellate cells. (C) Anti-HES1 stain shows localization of centroacinar cells at the center of a cross-sectioned acinus.

(Figure 1.11b) (Omary et al., 2007). PaSCs have been extensively studied, as they serve as damage-responsive remodelers of the extracellular matrix. When activated via tissue damage, PaSCs undergo a number of phenotypic and molecular changes including altered size and shape, increased size and prominence of the ER, and expression and secretion of ECM components including collagen I and II and fibronectin (Bachem et al., 1998; Omary et al., 2007). Stellate cells are responsible for generating new support structures when pancreatic damage results in substantial loss of acinar tissue. Extensive development of fibrosis resulting from continued pancreatic damage is a feature of many pancreatic tumors, often resulting in impaired treatment effectiveness and complications in surgical resection (Garber, 2010). Extracellular remodeling, however, is not capable of regenerating damaged tissue nor generating a primary tumor mass, thus prompting investigations into which cells repopulate the pancreas following injury.

A unique, non-secretory exocrine cell type, termed centroacinar cells (CACs), resides at the junction of the acinar lumen and the adjoining ductal network **(Figure 1.11c)** (Slack, 1995). These cells have high expression of aldehyde dehydrogenase 1, a known marker of stem cells in other organs, as well as a number of ductal genes, often making them indistinguishable from normal ducts (Rovira et al., 2010). Interestingly, isolation of CACs and subsequent growth in culture results in spontaneous reprogramming and differentiation of centroacinar cells into both endocrine and exocrine cell lineages (Rovira et al., 2010). Additional research has shown that following damage via pancreatic duct ligation, cells within the ductal compartment (including CACs) can give rise to β-cells, an endocrine cell type (Wang et al., 1995). This suggests that centroacinar cells may serve as multi-potent, tissue-resident stem cells, but their regenerative activity may vary based on the means in which damage is induced.

Most exocrine pancreas research focuses on two primary ailments: pancreatitis and pancreatic cancer. Pancreatitis is often subdivided into two specific forms; chronic and acute. Chronic pancreatitis is most commonly the result of alcoholism or familial mutations (Omary et al., 2007; Pandol et al., 2010). Chronic pancreatitis has also been linked to development of pancreatic cancer, although this correlation is largely limited to patients with an underlying mutation in the cationic trypsinogen gene (PRSS1) (Gao et

al., 2012; Hernández-Muñoz et al., 2008). Acute pancreatitis accounts for over 80% of diagnosed pancreatitis cases and is most frequently caused by gallstone-triggered blockage of the common bile duct or alcoholism (Dufour and Adamson, 2003; Pandol et al., 2010). Both chronic and acute pancreatitis have been extensively studied in mouse models, and they are both characterized by severe necrosis within the organ as well as by extensive localized and systemic inflammatory responses (Su et al., 2006).

Pancreatic cancer (discussed extensively in Chapter 6) has been demonstrated in mouse models to be the result of metaplastic conversion of acinar cells into precancerous ductal lesions, termed PanINs (Schmid, 2002). This plasticity in acinar cell identity (discussed in detail later) is also observed as part of the exocrine damage response during recovery from pancreatitis, possibly linking chronic pancreatic injury and cancer development. Additionally, chronic pancreatitis has been shown to exacerbate PanIN development in KRAS-transformed acinar cells (Guerra et al., 2007). This promotion may be linked to stromal and inflammatory interactions with acinar cells, as stromal factors allow senescent PanINs to reenter a proliferative cycle and contribute to cancer progression (Guerra et al., 2011). As demonstrated above, both pancreatitis and pancreatic cancer are associated with acute or long-term acinar distress, conditions replicated in the *Xbp1*$^{fl/fl}$ mouse model.

In order to study the effects of damage on the adult pancreas, multiple experimental systems utilizing wild-type mice have been devised. Alcohol-induced pancreatitis can be triggered by feeding mice alcohol-enriched diets, although this leads to only mild pancreatic damage triggered by oversecretion of the endogenous acinar secretagogue cholecystokinin (CCK) from duodenal cells (Su et al., 2006). Diet-induced models in which mice are fed choline-deficient chow supplemented with ethionine lead to severe necrotizing pancreatitis. This system, however, has a high mortality rate and does not resemble the cause or appearance of human disease (Lombardi et al., 1975; Su et al., 2006). One model that does mimic the changes in acinar structure seen in human pancreatitis patients utilizes the CCK analog caerulein (Su et al., 2006).

Caerulein can be administered via a number of techniques, most frequently using an intraperitoneal injection. Caerulein induces a supramaximal response in acinar cells,

leading to aberrant secretion across the basolateral membrane and into the pancreatic interstitial space rather than via the apical membrane into the ductal network (Jungermann et al., 1995). This accumulation of zymogens in the periacinar space triggers enzyme auto-activation and subsequent proteolytic digestion of the tissue (Jungermann et al., 1995). Digestion leads to extensive pancreatic edema, local inflammation and necrosis, and increases in serum levels of pancreatic enzymes as activated zymogens escape into the bloodstream (Mayerle et al., 2013). Advantageously, the damage induced in the caerulein model of pancreatitis is completely recoverable despite severe exocrine necrosis, making it ideal for study of pancreatic regeneration (Jensen et al., 2005).

Recovery following either disease-driven or experimentally-induced pancreatitis is marked by activation of pancreatic stellate cells and subsequent deposition of new extracellular matrix (Neubauer et al., 1995). This matrix fills voids left following acinar necrosis and must be generated and then extensively remodeled in order to allow regrowth of new cells, a task accomplished via coordinated secretion of ECM proteins, adhesion molecules, and matrix proteases (Lugea et al., 2006). Drawn out periods of injury can impair acinar cell repopulation and encourage continued deposition of extracellular stromal and matrix proteins, eventually leading to development of fibrosis that remains for the life of the organ (Hernández-Muñoz et al., 2008; Stetler-Stevenson, 1996). In addition to stimulation of organ repair and remodeling, pancreatic damage also induces a rapid change in the transcriptional state of the acinar cells themselves.

Acinar cell damage (either extrinsic as is the case in caerulein-induced pancreatitis or intrinsic in the case of activating oncogene expression) results in downregulation of acinar differentiation regulators including MIST1 and loss of zymogen expression **(Figure 1.12a,b)** (Rooman and Real, 2011). Acinar cells lacking high expression of these differentiation factors have altered duct-like morphology, drastically reduced levels of zymogen synthesis, and begin to express duct-restricted genes including the transcription factor *Sox9* **(Figure 1.12b)** (Kopp et al., 2012). This transdifferentiation from a mature acinar to a more duct-like state is called acinar-ductal metaplasia (ADM) and has been demonstrated in mouse models to be an key step in early development of pancreatic cancer (discussed extensively in Chapter 6)

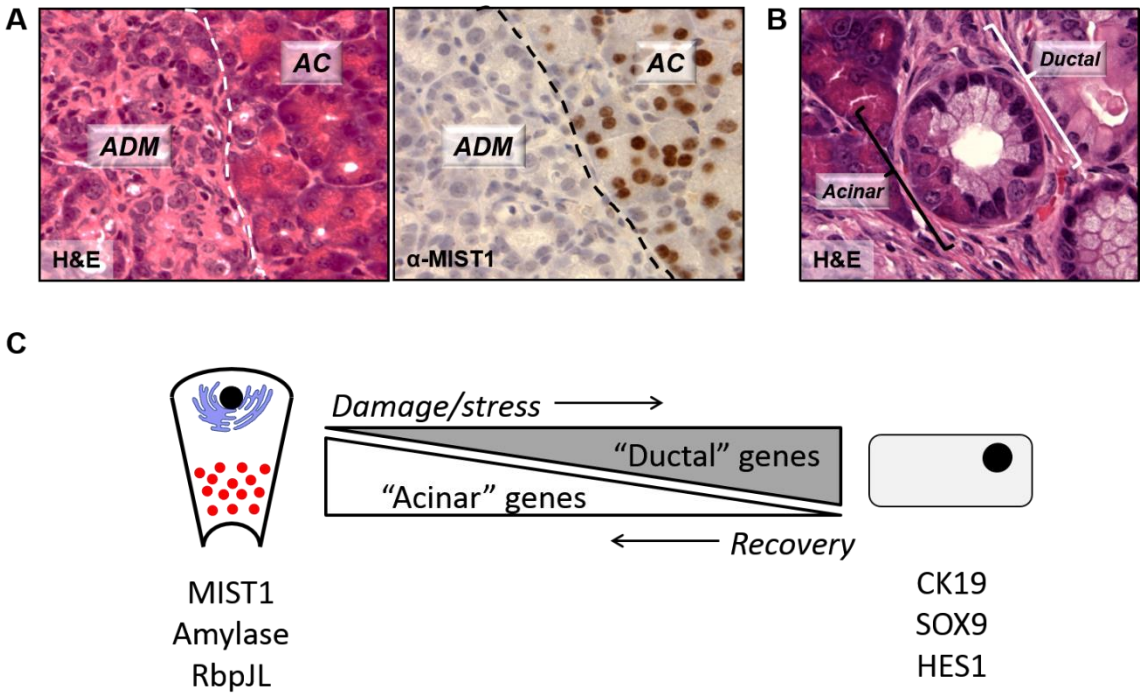

Figure 1.12 *Loss of acinar characteristics including expression of MIST1 occurs following pancreatic damage*

(A) H&E and IHC staining for MIST1 in mice with experimentally-induced pancreatitis. Cells undergoing ADM in response to damage (left sides of images) lose expression of MIST1, while healthy acinar cells (AC) retain expression. (B) H&E staining of a KRAS-induced precancerous lesion shows an acinus in which half of the acinar cells have lost acinar-like zymogen staining (labeled as "ductal") while half of the cells retain an acinar-like appearance. (C) Proposed model for acinar cell plasticity in which damage or stress causes a sharp decrease in acinar transcription factors including MIST1. This reduction is accompanied by increased expression of ductal genes CK19 and SOX9. Upon restoration of homeostasis, cells begin to express MIST1 and return to an acinar phenotype. Figures A, B courtesy Dr. Daniel DiRenzo.

(Shi et al., 2009b, 2012; Zhu et al., 2007). Cells undergoing ADM also activate previously silenced developmental signaling pathways including Notch signaling, frequently detected via expression of the HES1 protein **(Figure 1.12c)** (Rooman and Real, 2011). These transcriptional changes are believed to make acinar cells more capable of proliferation, a unique state as the adult pancreas is typically regarded as a quiescent organ, with unstressed rodents having less than 1% observed acinar cell turnover (Oates and Morgan, 1982).

Various techniques have been used to study pancreas regeneration, generating differing hypotheses regarding which cell type serves as the source of new acinar cells. In support of an acinar origin of regeneration, Jensen and colleagues utilized caerulein-induced pancreatitis and transcriptional profiling of recovering cells to establish that surviving acinar cells repress their terminal differentiation program and activate expression of PDX1 as well as activation of both the β-catenin and Notch signaling pathways (Jensen et al., 2005). Similar results were seen using Cre-mediated lineage tracing and multiple models of injury to investigate pancreatic plasticity, indicating that acinar cells in the damaged pancreas dedifferentiate, form a unique duct-like transitional state, and then give rise exclusively to new acinar cells (Houbracken et al., 2011; Means et al., 2005). Notably, the use of caerulein in these experiments mimicked the acinar structural changes seen in human disease but did not represent an endogenous stress, as human acinar cells do not respond to caerulein (Ji et al., 2002).

In contrast, work by Esni and others recently utilized a model in which diphtheria toxin receptors were expressed exclusively in acinar cells, allowing the selective ablation of the entire acinar compartment but sparing the duct and centroacinar cells (Criscimanna et al., 2011). In this system proliferative analysis revealed that the ductal/centroacinar compartment (which share expression of the SOX9 marker and were thus indistinguishable) was responsible for regenerating new acinar cells, also via activation of embryonic signaling pathways (Criscimanna et al., 2011). These data indicate that at least two distinct mechanisms for acinar repopulation may exist, although the lack of inflammatory response in the Esni model may reduce the clinical relevancy of the data. Mouse models utilizing endogenous stressors, including ER stress, and that also generate tissue inflammation would be ideal for painting a clinically relevant picture of

how acinar cells respond to damage. Notably, multiple experimental damage models have now demonstrated a correlation between pancreatic injury and activation of the unfolded protein response.

The UPR is activated in response to both alcohol- and L-arginine-induced experimental pancreatitis (Alahari et al., 2011; Kubisch et al., 2006; Lugea et al., 2011). Pandol and colleagues observed that impairment of XBP1 expression (and therefore only the IRE1 component of the UPR) results in reduced zymogen granule formation, increased autophagy, and acinar cell apoptosis (Lugea et al., 2011). This suggests that the IRE1 branch of the UPR may be a key component of the acinar cell damage response program. Interestingly, separate work by Pin and others utilizing *Mist1*$^{-/-}$ mice in an alcohol-induced pancreatitis model demonstrated that the absence of MIST1 leads to reduced UPR activity and an increase in pancreatic damage (Alahari et al., 2011). This suggests that MIST1 may be regulating acinar cell damage responses, a hypothesis recently confirmed in unpublished work by the Konieczny group showing that misregulation of MIST1 expression in a caerulein-induced pancreatitis model can trigger extensive acinar cell death. Indeed, given the extensive role that MIST1 plays in normal secretory function as well as its emerging role in mitigating exocrine damage, investigations as to whether MIST1 is a component of the pancreatic acinar cell UPR are warranted.

In this study, an acinar cell-specific, Cre-inducible *Xbp1* ablation model (*Mist1*$^{Cre/+}$;*Xbp1*$^{fl/fl}$) was used to investigate the role of XBP1 in maintaining homeostasis in pancreatic acinar cells. Specifically, targeted gene ablation was used to investigate the effects of XBP1 on acinar cell viability. Additionally, cells still expressing XBP1 in the pancreas were characterized following ER stress-induced organ damage as a means to study pancreatic proliferative and regenerative mechanisms. Finally, *in vitro* cell culture systems were used to investigate whether MIST1 is a direct target of XBP1 as well as its possible role as a component of the mammalian unfolded protein response.

CHAPTER 2. MATERIALS AND METHODS

2.1 Mouse strains

Xbp1^{fl}, Mist1^{CreER}, Rosa26^{LacZ}, LSL-Kras^{G12D}, and Mist1^{Kras} mouse lines have all been described previously (Habbe et al., 2008; Hetz et al., 2008; Jackson et al., 2001; Soriano, 1999; Tuveson et al., 2006). All mice were maintained on a C57Bl/6 background. Mouse experiments were conducted with approval and in accordance with PACUC regulations. Mouse euthanasia was conducted via CO_2 asphyxiation followed by cervical break.

2.2 Mouse genotyping

Mouse tail tips were harvested at post-natal day 21 in accordance with PACUC regulations. Tail tips were digested in tail lysis buffer supplemented with 0.2 mg/mL Proteinase K overnight at 56°C. Digested material was centrifuged for 10 minutes at 14,000 x g to remove tail debris. DNA isolation was accomplished via isopropanol precipitation of supernatants followed by washing of DNA pellets in 70% ethanol and subsequent resuspension in 100 µL of TE buffer at 65°C.

PCR genotyping using 1 µL of tail DNA was performed using standard protocols provided with the Mango Taq PCR system (BIO-21083, Bioline, Taunton, MA). PCR conditions included 35 cycles of 94°C for 30 seconds, 65°C for 90 seconds, and 72°C for 60 seconds. Tissue isolation and PCR conditions were identical for genotyping and for monitoring DNA recombination events. Primers for both types of reactions are listed in **Table 2.01**.

2.3 Tamoxifen administration for Cre-mediated induction

Tamoxifen (T5648, Sigma, St. Louis, MO) solution was prepared to a final concentration of 20 mg/mL in corn oil (C8627, Sigma, St. Louis, MO), then placed in a scintillation vial and heated with shaking at 37°C for five hours. Cre^{ERT2}-inducible mouse lines were given

Table 2.1 *Primer list for mouse genotyping and detection of recombination*

Genotyping Primers			
Transgene	**Forward**	**Reverse**	**Band Size (bp)**
Xbp1$^{fl/+}$	5'-acttgcaccaacacttgccatttc-3'	5'-caaggtggttcactgcct-3'	WT=141 FL=183
Mist1^{CreER} *	5'-ggttaaagcaaattgtcaagtacgg-3'	5'- atagtaagtatgtgcgtcagcg-3' 5'-gaagcattttccaggtatgctcag-3'	WT=750 Cre=520
Rosa26^{LacZ} *	5'-gcgaagagtttgtcctcaacc-3'	5'- ggagcgggagaaatggatatg-3' 5'-aaagtcgctctgagttgttat-3'	WT=650 LacZ=350
LSL-Kras^{G12D}	5'-tctgaattagctgtatcgtcaagg-3'	5'-gtcgagggacctaataacttcgta-3'	KR=500
Mist1^{Kras} *	5'-aggtgtccactaagcaccagt-3'	5'ctggaaggcattgttgagttt-3' 5'gctccaaccaccacaagttta-3'	WT=449 KR=200
Recombination Primers			
Allele	**Forward**	**Reverse**	**Band Size (bp)**
Xbp1^{WT}	5'-ttgggactctctcgtgtg-3'	5'-caaggtggttcactgcct-3'	1682
Xbp1$^{\Delta Ex2}$	5'-tggccacgtctacaaatgaa-3'	5'-caaggtggttcactgcct-3'	997

** Tripartite primers used to detect both WT and transgenic alleles*

tamoxifen via intraperitoneal injection into the left side to initiate nuclear Cre localization. Total volume of injected tamoxifen was 200 µL, for a total tamoxifen delivery of 4 mg. Mice were injected three times 24 hours apart, with the second injection set to time zero for experimental timings.

2.4 Tissue section preparation, immunohistochemistry, and immunofluorescent staining

For paraffin embedding, isolated tissues were placed in 10% neutral buffered formalin for overnight fixation following necropsy. Tissues were then dehydrated in a graded ethanol series proceeding from 70% to 100% ethanol before final dehydration in xylenes and embedding in paraffin using an automated tissue processor (Citadel 1000, Thermo Scientific, Waltham, MA). Tissues were subsequently embedded in paraffin blocks, and a microtome was used to generate 5 µM thick sections that were placed on charged microscope slides and heated to 40°C to ensure adherence to the glass.

For cryo-preserved tissues, isolated tissues were placed in a 4% paraformaldehyde/PBS solution for 1 hour at 4°C followed by transfer and gradual dehydration in a 30% sucrose solution for 4 hours at 4°C. Tissues were embedded in O.C.T. (4583, Sakura, Torrance, CA) in plastic tissue molds before snap freezing via placement of the molds into 2-methylbutane (78-78-4, Alfa Aesar, Ward Hill, MA) cooled in liquid nitrogen. Cryo blocks were stored at -20°C before sectioning via cryostat, with 5 µM sections placed on charged slides and stored at -80°C for subsequent staining.

Deparrafinization of tissue sections was accomplished by passing tissues from xylenes through a decreasing percentage of ethanol baths (2X 100%, 2X 95%, 1X 70%, 1X 50%) before final washing in distilled water. General histological analysis was accomplished via standard hematoxylin (47199-010, Lerner Labs, Pittsburgh, PA) and eosin (41799-028, Lerner Labs, Pittsburgh, PA) staining on deparaffinized tissue sections. Collagen staining was performed by incubating deparaffinized sections with Sirius red stain (365548, Sigma, St. Louis, MO) for 1 hour at room temperature followed by two washes in acidified water (0.5% glacial acetic acid in distilled water). X-gal staining for β-galactosidase activity was performed on cryo sections that were thawed for 5 minutes at room temperature before fixing with 10% neutral buffered formalin for 10 minutes and

incubation in X-gal staining solution (1 mg/mL X-Gal, 5 mM potassium ferricyanide, 5 mM potassium ferrocyanide, 2 mM MgCl in PBS) at 37°C for six hours. Paraffin sections were counterstained with hematoxylin while cryo sections were counterstained with nuclear fast red (H-3403, Vector Labs, Burlingame, CA).

Immunohistochemistry (IHC) and immunofluorescence (IFC) staining was performed on deparaffinized sections following antigen retrieval in antigen unmasking solution (H-3300, Vector Labs, Burlingame, CA) that was heated in a 2100-Retriever (PickCell Laboratories, Amsterdam, The Netherlands). Sections were then blocked using the MOM blocking reagent (BMK-2202, Vector Labs, Burlingame, CA) for one hour. Primary antibodies were diluted in MOM protein diluent and placed on sections for 1 hour at room temperature or overnight at 4°C. Secondary biotin-conjugated antibodies were then incubated with the sections for ten minutes. For IHC, Vectastain ABC reagent (PK-7100, Vector Labs, Burlingame, CA) was incubated on the sections for 1 hour at room temperature before development via Immpact DAB peroxidase substrate (SK-4105, Vector Labs, Burlingame, CA). For IFC, tertiary, avidin- and fluorescent-group conjugated antibodies were incubated with sections for 5 minutes along with DAPI. Following final staining/developing, IHC slides were passaged through baths of 95% ethanol, 100% ethanol, and xylenes and mounted using Vectamount (H-5000, Vector Labs, Burlingame, CA) while IFC slides were directly mounted using Vectashield Hard-mount Media (H-1400, Vector Labs, Burlingame, CA). Primary and secondary antibody information is provided in Table 2.02.

Analysis of images was performed using ImageJ with the cell counter plugin. All statistical analyses on cell and nuclear counts utilized a student's T-test with a significance threshold of 95%.

2.5 Electron microscopy

Harvested pancreata were fragmented and fixed in 3% paraformaldehyde/0.5% glutaraldehyde in PBS. Samples were dehydrated via graded ethanol series and embedded in Epon (Electron Microscopy Sciences, Hatfield, PA). Electron micrographs

Table 2.2 *Primary and secondary antibodies used*

Antigen	Dilution	Company	Cat #
Amylase	1:100	Calbiochem, San Diego, CA	171534
Amylase	1:1000	Santa Cruz Biotechnology, Santa Cruz, CA	sc-12821
β-gal	1:300	Novus Biologicals, Littleton, CO	NB100-65209
Chop	1:500	Cell Signaling, Boston, MA	2895S
CPA	1:1000	AbD Serotec, Raleigh, NC	1810-0006
E-Cadherin	1:1000	Abcam, Cambridge, MA	ab53033
Erk1/2	1:1000	Cell Signaling, Boston, MA	9102S
Glucagon	1:100	Dako, Carpinteria, CA	A0565
Hes1	1:1000	Gift of Tetsuo Sudo	-----
K19	1:100	Dev. Studies Hybridoma Bank, Iowa City, IA	Troma3
Ki67	1:500	Dako, Carpinteria, CA	M7249
LC3B	1:200	Cell Signaling, Boston, MA	3868S
Mist1	1:500	Pin et al, 2000	C175
nATF6a	1:1000	Santa Cruz Biotechnology, Santa Cruz, CA	sc-22799
p38	1:1000	Cell Signaling, Boston, MA	9212S
p-eIF2a	1:1000	Cell Signaling, Boston, MA	3597S
p-Erk1/2	1:1000	Cell Signaling, Boston, MA	9101S
pH3	1:100	Upstate (Millipore), Billerica, MA	06-570
S6	1:1000	Santa Cruz Biotechnology, Santa Cruz, CA	sc-74459
Sox9	1:500	Millipore, Billerica, MA	AB5535
Avidin (Alexa 594)	1:200	Invitrogen	S-11227
Avidin (Oregon Green)	1:200	Invitrogen	S-6368
Mouse (2°)	1:200	Vector	BA-9200
Rabbit (2°)	1:200	Vector	BA-1000
Rat (2°)	1:200	Santa Cruz	sc-2987

were taken of 100 nM ultra-thin sections on a Phillips CM-100 (Philips, Andover, MA) electron microscope with the assistance of Dr. Barbara Damsz.

2.6 RT-qPCR

Pancreatic RNA was isolated following initial harvesting of a small tissue piece for histology. PBS was then injected into the left ventricle of the heart to clear the tissues of blood and plasma fluids. A 1 mm^3 fragment of pancreatic tissue was then excised and harvested following homogenization with a Tissue Tearor (985-370, Biospec Products, Bartlesville, OK) using the Total RNA Kit 1 (R6664-02, Omega Biotek, Norcross, GA). Isolated RNA was converted to cDNA using the iScript cDNA synthesis kit (170-8891, Bio-Rad, Hercules, CA). Real-time PCR was performed using FastStart Universal SYBR Green (04913914001, Roche, Indianapolis, IN) in an ABI 7300 Real-Time PCR System (Applied Biosystems, Foster City, CA). PCR conditions involved 40 cycles of 95°C for 30 seconds, 59°C for 60 seconds, and 72°C for 30 seconds. Relevant Ct data were generated using the ABI 7300 software package followed by analysis using the $2^{-\Delta\Delta CT}$ (or ΔΔCT) method in which all values were normalized first to 18s expression levels as an internal control and then renormalized to a control biological sample for fold analysis.

2.7 Cell Culture

Cell culture experiments were conducted using mouse 266-6 pancreatic acinar cells (CRL-2151, ATCC, Manassas, VA) and primary mouse embryonic fibroblasts (MEFs). Wild-type MEFs were obtained from the Purdue University Transgenic Mouse Core Facility following isolation from harvested embryos and a single passage in 2D culture. *Xbp1*^{KO} MEFs were a generous gift from Dr. Ann-Hwee Lee at Harvard University.

266-6 cells were cultured in high-glucose Dulbecco's Modified Eagle Medium (hgDMEM) supplemented with 10% fetal bovine serum (FBS) and 1% Pen/Strep antibiotic solution (15140-122, Invitrogen, Grand Island, NY). MEFs were grown in hgDMEM supplemented with 10%FBS, 0.5% Pen/Strep, 1% L-Glutamine, 1% non-essential amino acids, and 1:10000 β-mercaptoethanol.

Table 2.3 *Primers used for RT-qPCR. All sequences are for mouse transcripts*

	Forward Primer	***Reverse Primer***
18S	5'-tgtctcaaagattaagccatgc-3'	5'-gcgaccaaaggaaccataac-3'
Amylase	5'-cagagacatggtgacaaggtg-3'	5'-atcgttaaagtcccaagcaga-3'
Arcn1	5'-agcagctttcccaaaactca-3'	5'-tcctctaaggctcggcaata-3'
Arfgap3	5'-tttgactgtggtgccaaaaa-3'	5'-ttgagttccctccaacttgc-3'
Atp2a2	5'-aaaccttgctggaacttgtga-3'	5'-ccacgattgcattggctac-3'
Bip	5'-gtgtcctctctggtgatcagg-3'	5'-tgtcttttgttaggggtcgtt-3'
Chop	5'-cctgaggagagagtgttccag-3'	5'-cagatcctcataccaggcttc-3'
Dnajb9/ERdj4	5'-ccccagtgtcaaactgtaccag-3'	5'-agcgtttccaattttccataaatt-3'
Dnajc1	5'-gacctggagttgttcgacttg-3'	5'-tgagtttgtgcattttcatcttt-3'
Dnajc3	5'-ccgacgccttatcacagttt-3'	5'-aagtccatcttcagcgcaat-3'
Edem3	5'-agcgtcatggagcctggt-3'	5'-gttgccataagcatgatcaaa-3'
Elastase	5'-actatgtccagctgggtgttc-3'	5'-cagtaagaggagctggagcag-3'
Gli1	5'-tttcttgaggttgggatgaag-3'	5'-ggtggagtcattggattgaac-3'
H47	5'-gcagagcagagaggagcag-3'	5'-agctgtctctgcctcaaagc-3'
Hes1	5'-agagaaggcagacattctgga-3'	5'-gtcacctcgttcatgcactc-3'
Htra2	5'-cattggagtgatgatgctgac-3'	5'-aatggccaagatcacatcac-3'
Mist1	5'-tggtggctaaagctacgtgt-3'	5'-catagctccaggctggtttt-3'
Nestin	5'-gagagtcgcttagaggtgcag-3'	5'-gatctgagcgatctgactctgt-3'
Os9	5'-ggtccaaatgtgatctcaacg-3'	5'-ggtcagtacgtaggagcagga-3'
Pdi1	5'-caagatcaagccccacctgat-3'	5'-agttcgccccaaccagtactt-3'
Piga	5'-gacccatttaggaggcatga-3'	5'-tggtccctctcctccaatta-3'
Ppib	5'-gcgcaatatgaaggtgctct-3'	5'-ttccaaagagtccaaagacga-3'
Ppp1r15b	5'-tcttgtaaggcccagctgtt-3'	5'-gccaatggcaacttctgttt-3'
Reg1	5'-atggctaggaacgcctacttc-3'	5'-cccaagttaaacggtcttcagt-3'
Rrbp1	5'-gctgccaatcagggtaaaaa-3'	5'-gcttccaaccgtagagacca-3'
Sec11c	5'-aaggcctgattgttctcacg-3'	5'-tcggaatgtctcttccttcaa-3'
Sec61a	5'-ctatttccagggctccgagt-3'	5'-aggtgtgtactggcctcggt-3'
Sec61b	5'-atccactgttcggcagag-3'	5'-cagcagcgatgaacagaaga-3'
Serp1	5'-agaaaaggcgtcggtaggac-3'	5'-cacatgcccatcctgatactt-3'
Sox9	5'-cttctgtgggagcgacaactt-3'	5'-agggagggaaaacagagaacg-3'
Spcs2	5'-ggatgactctgccaaaaagg-3'	5'-ctggcttggactcaggaaag-3'
Spcs3	5'-aactccctgttcgccttctc-3'	5'-tgtgatgaatcccaggtcac-3'
Ssr3	5'-cctgctccttcaggatttca-3'	5'-cattcttgtacgcgaaggcta-3'
Uso1	5'-cgcttagaagtgggaatcca-3'	5'-gagtgacattttctggctgct-3'
$Xbp1^{\Delta Ex2}$	5'-agaaagcgctgcggagaac-3'	5'-cctccacctctggaacctc-3'
Xbp1s	5'-tgagtccgcagcaggt-3'	5'-agagaaagggaggctggtaag-3'
Xbp1u	5'-tcagactatgtgcacctctgc-3'	5'-agagaaagggaggctggtaag-3'

ER stress induction was achieved via treatment with either 500 nM thapsigargin (T9033, Sigma, St. Louis, MO), 2.5μM tunicamycin (654380, EMDMillipore, Billerica, MA), or 5mM dithiothreitol dissolved in DMSO. DMSO alone was used as a control vehicle.

2.8 Generation of shCtrl, shXbp1, and shMist1 viruses and cell lines

Lentiviral plasmids (pLKO.1 backbone) were obtained from Sigma-Aldrich (St. Louis, MO) containing validated sequences for silencing of XBP1 or MIST1 as well as a control, non-targeting shRNA (sequences in **Table 2.04**). The plasmids were grown up in DH5α cells, mini-prepped, and transfected along with viral packaging plasmids in 293T cells.

Table 2.4 *Sequences of shRNA plasmid constructs against mouse transcripts*

Name	***Sequence***	***Target***
sh*Xbp1*	5'CCGGCCATTAATGAACTCATTCGTTCTCGAGAACGAATGAGTTCATTAATGGTTTTT-3'	3' UTR
sh*Mist1*	5'CCGGCGGATGCATAAACTCAACAATCTCGAGATTGTTGAGTTTATGCATCCGTTTTT-3'	CDS
sh*Ctrl*	5'CCGGCAACAAGATGAAGAGCACCAACTCGAGTTGGTGCTCTTGTTGTTTTT-3'	N/A

The transfected cells were allowed to synthesize virus for 24 hours before having supernatants collected at 12 hour intervals for 3 days (24 through 72 hours post-transfection). Supernatants were then spun at 25,000 x g for two hours and pellets were resuspended in 1 mL of TNE buffer (50 mM Tris-HCl – pH 7.4, 100 mM NaCl, 0.1 mM EDTA) and stored in 200 μL aliquots at -20°C.

To infect new cells, a 70% confluent 10cm plate of 266-6 cells was treated with a solution consisting of 2 mLs complete hgDMEM, 10 μg/mL polybrene, 10 mM HEPES, and 200 uL of thawed viral aliquot. Cells were given 24 hours to become infected before media was replaced with selection media consisting of complete hgDMEM with 1.0 μg/mL puromycin added. Complete control (uninfected) cell death was achieved in puromycin selection within three days, with virally infected cells being passaged twice to remove all traces of virus and then expanded and frozen down for future use.

2.9 Luciferase assays

Mist1-promoter luciferase vectors were generated by Dr. Jeff Ishibashi using the pBRIT-PURO viral backbone. 266-6 cells were transfected using standard protocols for PEI (polyethyleimine) (23966-2, Polysciences Inc., Warrington, PA) transfections. Briefly, this involved seeding 6 cm plates with 266-6 cells to 70% confluence. Transfection mixes contained 400μL serum-free, antibiotic-free hgDMEM at room temperature, 1.5 μg each of *Mist1*pr-luc vector and pBRIT-Xbp1s or pBRIT PURO control, 2 ng Renilla luciferase expressing vector (for internal control purposes), and 9 μL PEI (1 μg/μL stock). Mixes were created and allowed to incubate at room temperature for 15 minutes, then added dropwise to a culture dish in which the cells had been washed three times in media to remove any secreted growth factors. Cells were incubated for 48 hours before being harvested in passive lysis buffer (E194A, Promega, Madison, WI) and analyzed using the Luciferase Assay System (E1501, Promega, Madison, WI) and Renilla Luciferase Assay System (E2820, Promega, Madison, WI). 10 μL of each supernatant was added to both luciferin-containing and coelenterazine-containing glass vials (with each in its respective buffer from the Promega kits). Luminescence readings were obtained using a Lumat luminometer (LB9501, Berthold, Oak Ridge, TN). Luciferin luminescence values were normalized to coelenterazine luminescence values via simple division as an internal control, as all samples had the same amount of Renilla plasmid added at time of transfection.

2.10 Bioinformatic analysis of candidate MIST1 effectors

Generation of the initial list of candidate MIST1 effectors was accomplished via analysis of pooled data from multiple sources including: ChIP-Seq data generated from *Mist1*^{WT} mice in collaboration with Dr. Raymond MacDonald at UT Southwestern (unpublished), microarray data from a *Mist1* rescue mouse panel (Direnzo et al., 2012), a mouse UPR-specific PCR array (PAMM-089, SA Biosciences, Valencia, CA), published gene lists reporting secretory genes associated with XBP1- and nATF6-transfected NIH3T3 fibroblasts (Bommiasamy et al., 2009; Sriburi et al., 2007), and microarray data from tunicamycin-treated *Ire1*^{KO} liver samples (So et al., 2012).

Selection criteria for candidate genes initially involved selection of all general UPR and secretion-specific UPR genes available from the previously listed sources, generating a

184 candidates. These candidates were analyzed for ChIP enrichment (see Appendix A) using the MochiView software suite (Homann and Johnson, 2010). This eliminated 65 candidates that had no MIST1 enrichment within the target gene's promoter or first two exons/introns. We then used sequence analysis on the 500 base pair regions surrounding ChIP enrichment sites in the remaining genes and scanned for the presence of GC or TA E-boxes, known DNA binding sites for MIST1. We eliminated genes with no detectable E-boxes. We then analyzed the resulting genes via utilization of microarray data previously generated by Dr. Daniel DiRenzo that detected the relative gene expression differences between *Mist1*^{WT}, *Mist1*^{KO}, and *Mist1*^{KO};*LSL-Mist1*^{myc} transgenic mice. These animals expressed a *Mist1* transgene in a *Mist1*^{KO} background for 36 hours prior to RNA harvesting, thus allowing us to determine whether expression of any of the candidate effectors was significantly altered in *Mist1*^{KO} acinar cells and fully or partially rescued upon *Mist1*^{myc} expression (see Appendix B). By restricting our search to genes that displayed expression changes upon MIST1 expression, we reduced our list of possible targets to 54 candidates. As a final refining step, we checked our candidates against published microarray data (available in the NCBI Geo repository) analyzing WT and *Ire1*^{KO} liver samples treated with tunicamycin. We then grouped the remaining list of candidate effectors based on ChIP-Seq enrichment, expression levels after MIST1^{myc} expression, and demonstrated significance in ER stressed, *IRE1*^{KO} liver samples. This final list of candidate effectors contained 15 high-scoring genes, and we chose 6 additional effectors missing a single criteria but with highly significant ChIP enrichment or expression changes upon rescue. These genes are listed in **Table 5.02**, with a summary diagram of the selection criteria in **Figure 5.08**. All genes are shown in Appendices A-D with relative ChIP enrichment scores (Appendix A,B) and *Mist1* rescue array scores (Appendix C,D).

CHAPTER 3. XBP1 IS A NECESSARY COMPONENT OF THE PANCREATIC ACINAR CELL UNFOLDED PROTEIN RESPONSE

3.1 Introduction

Studying the unfolded protein response (UPR) requires consideration of a number of factors regarding cell type and function. As previously described, all cells utilize secretory pathways in some fashion, typically via constitutive secretion of membrane and extracellular matrix (ECM) components (Burgess and Kelly, 1987). Constitutively secreted proteins typically mature extensively in the Golgi, often requiring substantial modification including glycosylation of N-terminal protein signals, phosphorylation, sulfation or hydroxylation of specific residues, and early proteolytic processing steps (Mains et al., 1987). Constitutive secretion, however, generates vesicles with low protein titers, placing little stress on the ER/Golgi machinery and leading to low UPR activation (Grampp et al., 1992). As such, non-secretory cells typically have a reduced UPR activity and are not ideal models for studying UPR regulation.

One exception to reduced protein throughput being a characteristic of non-secretory cells is during development, when secreted protein families, including the bone morphogenetic proteins (BMPs), are essential to proper body planning (Hogan, 1996). Additionally, gene-trap experiments targeted specifically to secreted and transmembrane proteins have demonstrated the importance of secreted proteins and an intact secretory pathway during development (Mitchell et al., 2001). However, embryonic knockout studies utilizing a compound knockout of *Atf6α/β* or deletion of *Ire1*/*Xbp1* result in embryonic lethality, making developmental systems difficult to utilize in the investigation of the UPR (Lee et al., 2005; Reimold et al., 2000; Yamamoto et al., 2007). Therefore, an ideal experimental system for UPR research should utilize an inducible mechanism for ablation or activation of necessary UPR components. Such a system must also utilize a cell type that relies upon the UPR in order to observe any changes in cell phenotype following its disruption.

Non-secretory cell types, including the NIH3T3 fibroblast cell line, have been used to bioinformatically analyze the effects of *Xbp1s* via transfection studies. As summarized in Table 3.01, *XBP1s* transfection results in expression of target genes associated with nearly every step in the secretory pathway (see Figure 1.04 for matching classifications of XBP1 target genes) (Sriburi et al., 2007). This data illustrates the importance of XBP1 in driving cellular responses to ER stress. The exact means by which XBP1 controls homeostasis in secretory cells has been difficult to study, owing to a lack of normal secretory cell systems and the previously described lethality of *Xbp1*-knockout mice.

Dedicated secretory cells are typically polarized, thus requiring extensive interaction of the endo- and exocytic pathways, cytoskeletal regulatory mechanisms, and the secretory machinery (Deitcher, 2002). Exocrine cells therefore make extensive use of the UPR both during secretion and in the basal state. *In situ* hybridization analysis of developing mouse embryos revealed extensive Xbp1 mRNA expression in osteoblasts and exocrine glands (Clauss et al., 1993). This data also indicated that Xbp1 expression peaks at E14.5, suggesting a developmental role for XBP1 outside of its role in the UPR (Clauss et al., 1993). However, follow up studies utilizing XBP1s reporter mice established that XBP1 is constitutively expressed and spliced in the adult pancreas, indicating that a basal level of UPR activity is maintained there, making it ideal for studying the IRE1/XBP1 branch (Iwawaki et al., 2004).

XBP1 is of key interest in the study of pancreatic disease and cancer. Impaired expression via hemizygous gene deletion in mice demonstrated that XBP1 specifically protects the exocrine pancreas from alcohol-induced damage (Lugea et al., 2011). This is particularly interesting as alcoholism is a known risk factor. Pharmacological inhibitors of Xbp1 splicing with standard chemotherapeutics has shown synergistic effects in halting the growth of multiple myeloma cells (Mimura et al., 2012). for development of chronic pancreatitis, possibly linking XBP1 and pancreatic disease (Dufour and Adamson, 2003). XBP1 may also play a role in tumorigenesis, as transgenic models have revealed a positive correlation between rates of XBP1 splicing and tumor cell growth, indicating a possible avenue for new therapeutics (Spiotto et al., 2010). This development would be particularly important, as pancreatic ductal adenocarcinoma

1. Targeting and translocation	
Signal recognition particle	*Srp9, Srp19, Srp54a, Srp68, Srpr, Srprb*
Signal sequence receptor	*Ssr1, Ssr2, Ssr3, Ssr4*
Translocon	*Sec61a1, Sec61b, Sec61g, Sec63, Tram1*
Signal peptidase	*Spcs2, Spcs3, Sec11a, Sec11c*
2. N-linked glycosylation	
Core oligosaccharide synthesis	*Alg2, Alg12, Mgat2*
Oligosaccharyltransferase	*Ddost, Dad1, Rpn1, Rpn2*
Oligosaccharide processing	*Mogs*
3. Facilitation of protein folding	
Chaperones	*Dnajb2, Dnajb9, Dnajb11, Dnajc1, Dnajc10*
	Fkbp1b, Fkbp2, Fkbp7, Fkbp10, Fkbp11, Fkbp14
	Hspa5, Hspa13, Hsp90b1, Hyou1, Ppib
Disulfide bond formation	*Ero1lb, Erp29, Erp44, Pdia3, Pdia4, Pdia6, Selm, Txndc5, Txndc11*
ER-associated degradation	*Derl1, Edem1, Herpud1, Syvn1*
4. Vesicular trafficking and transport	
Anterograde transport (ER→Golgi)	
COPII vesicles	*Sec23a, Sec23b, Sec24d, Sec31a, Yipf5, Yif1a*
Cargo receptors	*Lman1, Mcfd2*
SNAREs	*Bet1, Betl1, Sec22b*
Retrograde transport (ER←Golgi)	
COPI vesicles	*Arcn1, Arfgap3, Copb1, Copb2, Cope, Copg, Copz1*
Cargo receptors	*Kdelr2, Kdelr3, Lman2*
Transport/recycling in the Golgi	*Blzf1, Cog3, Cog6, Gosr2, Rab33b, Uso1*
Exocytosis	
SNAREs	*Stx5a, Stx18, Vamp2, Vamp4, Vamp7*
Small GTPases	*Rab3a*
5. Others	
ER proteins	*Atf6, Atp2a2, Bfar, Creb3, Creb3l1, Crebl1, Dolpp1, Eif2ak3, Ggcx, H13, Hmox1, Lepre1, Ormdl3, Rrbp1, Rcn3, Piga, Sdf2l1, Surf4, Wfs1*
Golgi proteins	*Golga3, Golga4, Golgb1, Gcc1, Golph3, Golph3l, Gopc, Gorasp2, Rabac1*

Table 3.1. *XBP1 target genes are involved in multiple steps of normal protein synthesis and degradation in the ER*

Transfection of XBP1s in NIH3T3 fibroblasts results in expression of genes associated with facilitation of secretory protein synthesis (diagrammed in Figure 1.04).

(PDA) has a dismal 6% 5-year survival rate due in large part to ineffective chemotherapeutics (Siegel et al., 2013). In fact, recent pre-clinical work combining

Initial studies utilizing Xbp1$^{-/-}$ mice demonstrated that complete knockout of the gene is embryonic lethal, although liver-specific expression of an Xbp1 transgene (Xbp1$^{-/-}$;Liv^{Xbp1}) allows mice to survive into neonatal development (Lee et al., 2005). As shown in **Figure 3.01**, Xbp1$^{-/-}$;Liv^{Xbp1} mice die due to pancreatic insufficiency, an expected finding given previous data showing that XBP1 is required for initial development of the exocrine secretory machinery and that pancreatic acinar cells have the highest protein production level of any human secretory cell (Case, 1978; Lee et al., 2005). Interestingly, recent work utilizing an inducible XBP1-knockout model in gastric chief cells demonstrated that XBP1 was required for expression of the key differentiation marker MIST1, a basic helix-loop-helix transcription factor also expressed in differentiated pancreatic acinar cells (Huh et al., 2010). However, our analysis of *Xbp1*$^{-/-}$ post-natal pup pancreata revealed sparse acini with that surprisingly still expressed MIST1 despite lacking *Xbp1* **(Figure 3.01c, right panel)**. This indicates that the regulation of XBP1 target genes, and possibly the determinination as to whether a gene is actually a target, is likely cell-type dependent. These data prompted us to study whether XBP1 is essential for acinar cell UPR activation and homeostasis in the adult pancreas.

In this study, we addressed the issue of *Xbp1* knockout lethality via generation of an acinar cell-specific, Cre-inducible mouse line. Our work has demonstrated that acinar-specific *Xbp1* ablation results in a gradual onset of ER stress and activation of the PERK and ATF6 components of the UPR. Furthermore, the activities of the PERK and ATF6 branches are unable to restore normal protein throughput levels in acinar cells, resulting in visible distress including loss of ER staining and integrity, accumulation of autophagic vesicles, and decreased acinar cell zymogen synthesis. The loss of Xbp1 eventually leads to apoptotic cell death approximately four weeks after ablation. These findings demonstrate that XBP1 is an essential component of the pancreatic acinar cell UPR, and its expression is required for maintenance of acinar cell homeostasis.

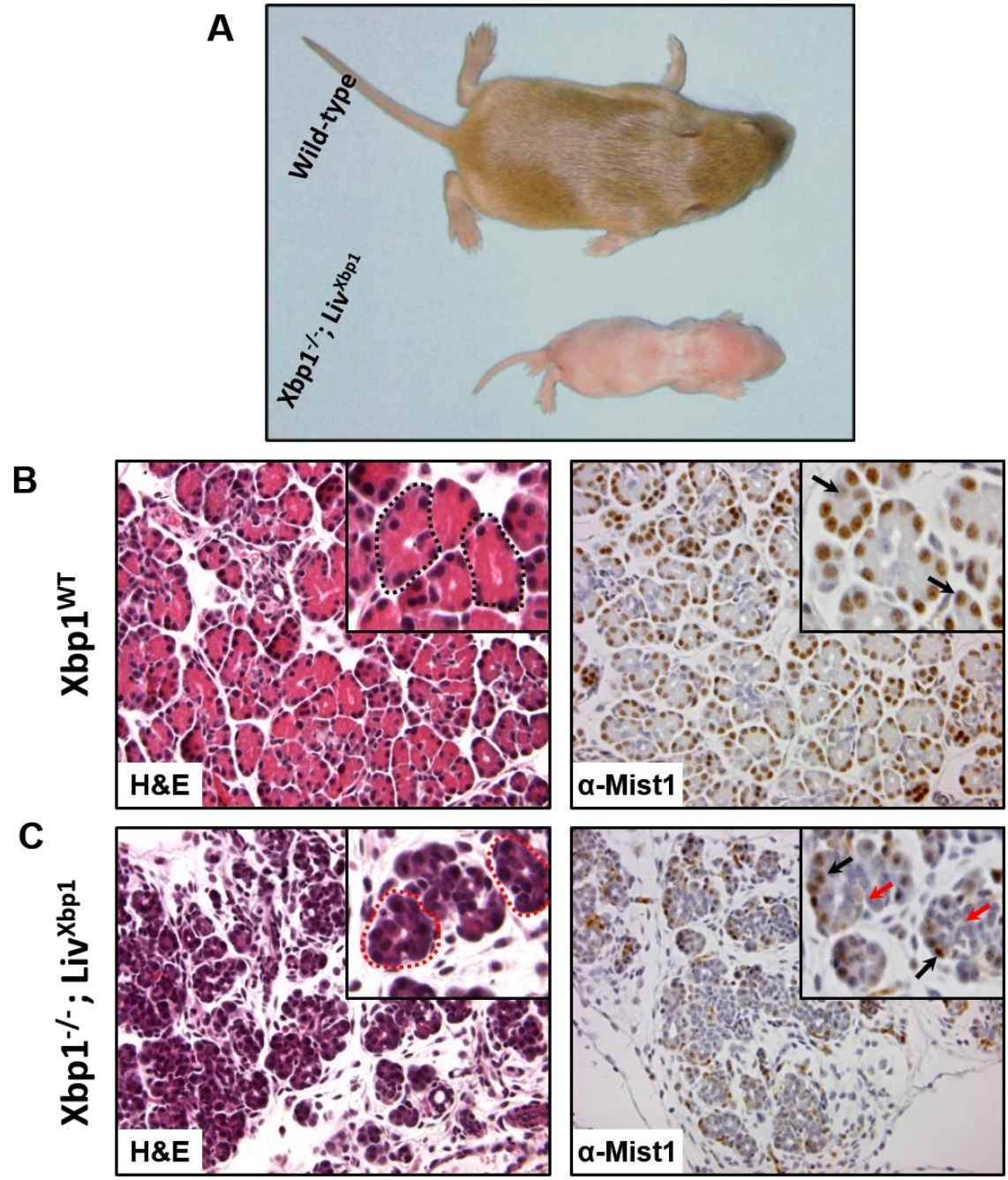

Figure 3.1 *Xbp1$^{-/-}$;Liv^{Xbp1} mice have malformed pancreata with sparse acini and patchy expression of MIST1*

(A) *Xbp1$^{-/-}$*;Liv^{Xbp1} mice (bottom) die during post-natal development and are substantially smaller than wild-type counterparts (top). (B) Wild-type pancreata at 10 days post-natal development have substantial zymogen accumulation (left image, pink staining) with strong expression of MIST1 (right image). (C) *Xbp1$^{-/-}$*;Liv^{Xbp1} pancreata have reduced zymogenic staining with reduced numbers and size of acinar cells (left image and inset) but maintain MIST1 expression. Panel A courtesy of Dr. Laurie Glimcher.

3.2 Generation and testing of Mist1$^{CreER/+}$; Xbp1$^{fl/fl}$ mice

The goal of this work was to generate a mouse line that would facilitate acinar-specific ablation of Xbp1 in the adult pancreas. This system allows the study of XBP1 as a component of the UPR in fully developed, wild-type acinar cells. Two established lines were crossed to generate a ^{CreERT2}-mediated system allowing ablation of Xbp1 via simple intraperitoneal (i.p.) injection of tamoxifen.

An established mouse line, termed Xbp1$^{fl/fl}$, was obtained from Dr. Laurie H. Glimcher at Harvard University in order to effectively study inducible Xbp1 ablation. The Xbp1$^{fl/fl}$ mouse line was originally generated in the Glimcher lab by Dr. Ann-Hwee Lee and is diagrammed in **Figure 3.02a/b** (Hetz et al., 2008). The wild-type Xbp1 gene (responsible for producing the Xbp1u transcript that can be spliced to Xbp1s) has five exons, with the DNA-binding and leucine zipper spanning exons 2 and 3 and the 26nt splice site located in exon 4 **(Figure 3.02a/b)**. Two loxP sites flanking exon 2 were engineered via standard techniques to generate the Xbp1$^{fl/fl}$ line. Upon Cre-mediated recombination, exon 2 is excised, resulting in transcription of a modified mRNA transcript that no longer encodes active XBP1s (Hetz et al., 2008). Importantly, despite being unable to be translated into a functional protein, the Xbp1^{fl} transcript still contains the intact 26nt splice site, allowing the monitoring of IRE1-dependent splicing, and thus UPR activity, via RT-qPCR with splice-specific primers (Hetz et al., 2008). This construct was then paired with an acinar cell-specific Cre recombinase line generated in the Konieczny lab.

The Mist1^{CreERER} line was designed by Dr. Guanglu Shi in collaboration with the Purdue Transgenic Mouse Core Facility **(Figure 3.02c)** (Shi et al., 2009b). Briefly, homologous recombination and embryo injection of ES cells were used to generate a knock-in mouse line in which the coding sequence of the Mist1 gene was replaced with a new sequence encoding the Cre-ER^{T2} fusion protein at the endogenous Mist1 locus. This fusion protein is a standard Cre-recombinase fused to a tamoxifen-sensitive mutant human estrogen receptor that forces cytoplasmic localization of the recombinase (Feil et al., 1997). The modified estrogen receptor is bound to the recombinase and prevents its nuclear localization until tamoxifen (typically administered to the animal via i.p. injection or oral gavage) crosses the cell membrane and binds the receptor, causing its dissociation from

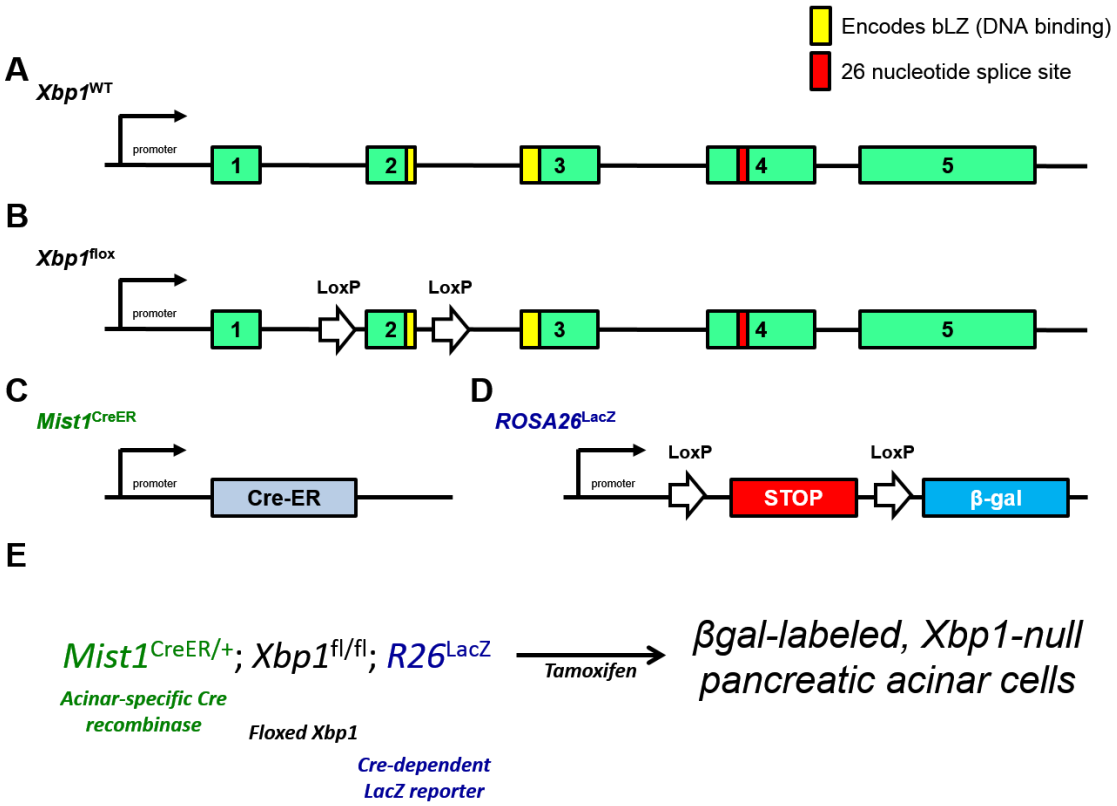

Figure 3.2 *Schematic of transgenes used in creation of the Mist1$^{CreER/+}$; Xbp1$^{fl/fl}$; R26^{LacZ} mouse line*

(A) Schematic of the normal Xbp1 locus, with boxes representing translated exons. The DNA-binding, basic leucine zipper (bLZ, yellow) domain spans exons 2 and 3, while the IRE1-dependent splice site (red) is in exon 4. (B) Schematic of the *Xbp1^{flox}* (*Xbp1^{fl}*) locus with loxP sites flanking exon 2 at the endogenous *Xbp1* locus. (C) Schematic of the Mist1^{CreERER} (Mist1^{CreER}) transgene that was knocked into the endogenous *Mist1* locus. (D) Schematic of the ROSA26^{LacZ} (R26^{LacZ}) locus, showing Cre-dependent, conditional expression of β-galactosidase. (E) Diagram of desired mouse lineage with its effects.

Cre and allowing nuclear translocation of the recombinase (Feil et al., 1997). Importantly, the cytoplasmic restriction of the protein prevents Cre-mediated ablation of Xbp1, thus creating a system in which intact XBP1 expression can be inducibly switched off. The knock-in model restricts expression of Cre-ER^{T2} to cells that natively express MIST1, including pancreatic acinar cells.

Mist1$^{CreERER/CreER}$; Xbp1$^{+/+}$ mice were mated to Mist1$^{+/+}$; Xbp1$^{fl/fl}$ over multiple generations, yielding mice with a Mist1$^{CreER/+}$;Xbp1$^{fl/fl}$ genotype as well as relevant variations used as experimental controls. Additionally, a transgene that conditionally encodes the β-galactosidase (LacZ) gene from the *ROSA26* locus was crossed into the line **(Figure 3.02d)**. The *ROSA26* locus, originally identified via gene-trap experiments in mouse ES cells, is constitutively active in all cells and is frequently utilized for transgenic expression of reporter genes (Casola, 2010; Friedrich and Soriano, 1991). In ROSA26^{LacZ} (R26^{LacZ}) mice, a lox-stop-lox (LSL) cassette containing multiple in-frame stop codons preceding the LacZ gene was knocked in to the ROSA26 locus. This results in a non-coding locus that becomes active upon Cre-mediated excision of the LSL cassette and begins low-level transcription of β-galactosidase. This results in permanent labeling of all cells in which Cre has been active or was active in a progenitor cell. Importantly, because this is a permanent recombination event, all progeny of β-gal-positive cells will remain β-gal-positive.

By combining all three transgenes through standard crosses, we generated a mouse line with inducible, cell-specific ablation of XBP1 along with coexpression of β-galactosidase for lineage tracing **(Figure 3.02e)**. As diagrammed in **Figure 3.03a**, ablation of Xbp1 exon 2 generates a frameshift that encodes an early stop codon six amino acids into XBP1 exon 3, resulting in a transcript that codes for a truncated protein lacking DNA-binding, transcriptional activation, and nuclear localization domains **(Figure 3.03b)**. This truncated protein (Xbp1$^{\Delta Ex2}$) has no transcriptional activity and is rapidly degraded, completely eliminating XBP1s in all progeny cells.

Initial testing for ^{CreER} efficacy using DNA extracts from tamoxifen-treated mice revealed expression of the recombined Xbp1^{fl} construct (termed Xbp1$^{\Delta Ex2}$) restricted to tamoxifen-

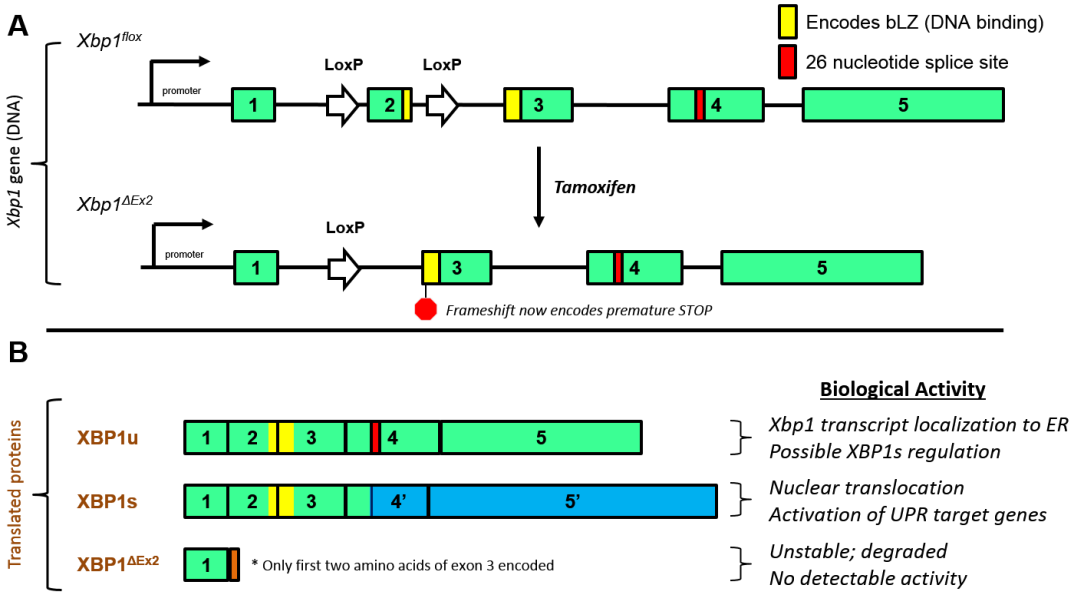

Figure 3.3 *Effects of Cre-mediated recombination at the Xbp1^{flox} locus*

(A) Cre-mediated recombination results in a modified gene that no longer encodes for a portion of the basic leucine zipper (bLZ). Additionally, a frameshift resulting from the loss of exon 2 encodes a STOP codon located six amino acids into exon 3 in the translated protein. (B) XBP1u is a direct translation of the unspliced *Xbp1* transcript and has few well-studied functions in cells. XBP1s has a unique C-terminus that contains a potent transcriptional activation domain and nuclear localization signal, resulting in its translocation to the nucleus and activation of its target genes. XBP1$^{\Delta Ex2}$ consists of exon 1 and six amino acids of exon 3 of the XBP1 proteins and is unstable.

administered pancreata and not in tail, kidney, or untreated tissues **(Figure 3.04a)**. These were selected as representatives of MIST1-expressing (pancreas) and non-expressing (kidney, tail) cell types. The restriction of Cre activity was mimicked using standard qPCR **(Figure 3.04b)**, confirming restriction of Cre-mediated recombination to MIST1-expressing tissues. Further analysis was conducted to determine the subset of pancreatic cells in which *Xbp1* had been ablated.

As a first step to monitor acinar-specific recombination, pancreatic sections were generated from Mist1$^{CreER/+}$; Xbp1$^{fl/fl}$; R26^{LacZ} mice treated with corn oil (vehicle) or tamoxifen (TM). As shown in **Figure 3.05a,b**, X-gal staining, a marker for β-galactosidase (β-gal) activity, revealed substantial staining of pancreatic acinar cells with no staining in the untargeted pancreatic islets or ducts. Histological analysis of harvested pancreata from these animals also showed normal appearance and protein expression in both the β-gal negative islets and duct cells **(Figure 3.05c,d)**. Quantification of β-gal activity via X-gal staining **(Figure 3.05e)** indicated virtually no recombination in untreated or MIST1-negative tissues. In contrast, approximately 90% of Mist1$^{CreER/+;}$ Xbp1$^{fl/fl}$; R26^{LacZ} acinar cells were positive for β-gal. These data demonstrated that Cre recombinase activity in *Mist1*$^{CreER/+}$; *Xbp1*$^{fl/fl}$; *R26*^{LacZ} mice was restricted to Mist1-expressing organs, and recombination is restricted within the pancreas specifically to acinar cells. Further testing was conducted to determine whether the tissue-specific expression of the Xbp1$^{\Delta Ex2}$ transcript resulted in loss of Xbp1 activity.

As previously shown in **Figure 1.05**, each UPR branch activates both branch-specific gene targets as well as shared effectors that are coactivated by one of the other master regulator cascades. IRE1/XBP1 is responsible for activation of a number of branch-specific UPR targets, among them protein disulfide isomerase (PDI, a regulator of disulfide bond formation in the ER), the related protein disulfide isomerase associated 2 (PDIA2/PDIp), and Sec61α (a component of the ER translocation apparatus used for moving proteins into and out of the ER) (Todd et al., 2008, 2009). Constitutive, low-level XBP1s activity has been previously observed in the pancreas **(Figure 3.07a)** (Iwawaki et al., 2004), prompting us to investigate the expression of known XBP1-specific target genes for confirmation of *Xbp1* loss of function.

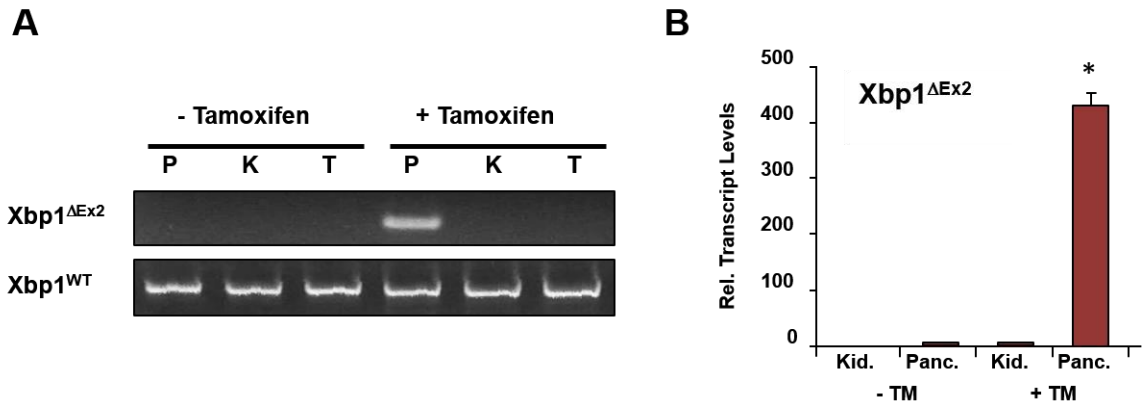

Figure 3.4 Mist1$^{CreER/+}$; Xbp1$^{fl/fl}$ *mice express the Xbp1^{dEx2} transcript in a pancreas-restricted fashion*

(A) Standard PCR utilizing primers specific for the *Xbp1$^{\Delta Ex2}$* transcript were used on homogenates from pancreas (P), kidney (K), and tail (T) tissues in tamoxifen-treated and untreated Mist1$^{CreER/+}$; Xbp1$^{fl/fl}$ mice. Expression of the recombined transcript is only detected in the pancreas of tamoxifen-treated mice. (B) qPCR for the *Xbp1$^{\Delta Ex2}$* transcript also reveals expression effectively restricted to tamoxifen (TM)-treated pancreata. (* = p-value < 0.001 relative to tamoxifen-treated kidney sample). RT-qPCR analysis completed in collaboration with Dr. Sean Humphrey.

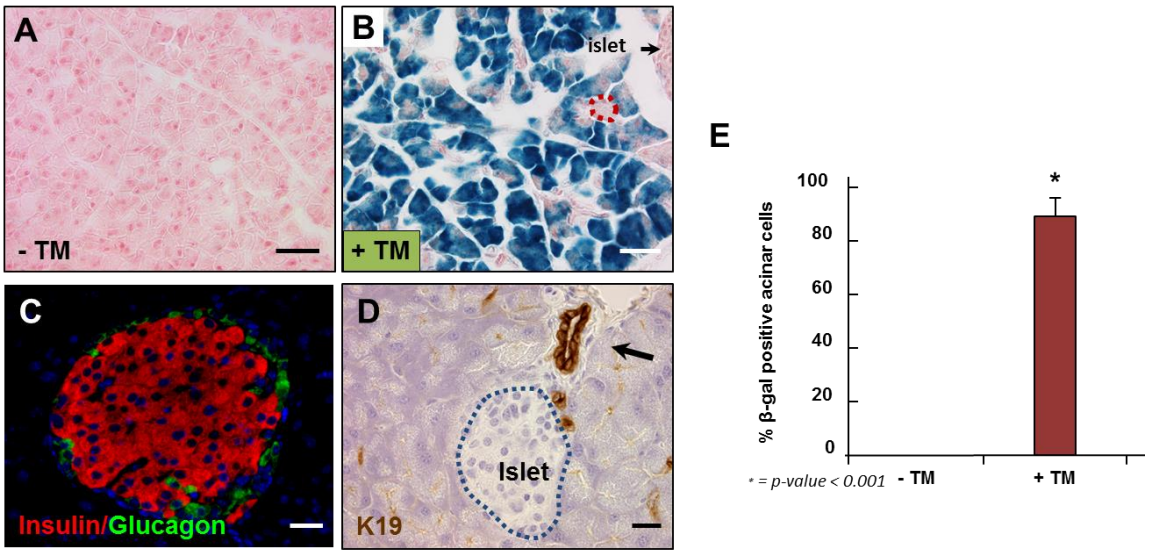

Figure 3.5 *Ablation of Xbp1 in tamoxifen-treated* Mist1$^{CreER/+}$; Xbp1$^{fl/fl}$; R26^{LacZ} *mice is restricted to the acinar cells in the pancreas*

(A) X-gal staining of pancreata from *Mist1*$^{CreER/+}$; *Xbp1*$^{fl/fl}$; *R26*^{LacZ} mice without tamoxifen shows no staining, indicating a lack of Cre activity. (B) X-gal staining of tamoxifen-treated *Mist1*$^{CreER/+}$; *Xbp1*$^{fl/fl}$; *R26*^{LacZ} mouse pancreata shows extensive β-galactosidase activity in acinar cells, but not islets (black arrow). Additionally, the red outline marks a β-gal negative centroacinar cell. (C) Staining for insulin and glucagon in *Mist1*$^{CreER/+}$; *Xbp1*$^{fl/fl}$; *R26*^{LacZ} mouse pancreata show normal arrangement of cells and protein expression. (D) Staining for cytokeratin 19 (K19) in *Mist1*$^{CreER/+}$; *Xbp1*$^{fl/fl}$; *R26*^{LacZ} pancreata reveals normal appearance and K19 expression in ducts (black arrows). (E) Quantification of acinar β-gal activity demonstrating Cre-activity in approximately 90% of pancreatic acinar cells in TM-treated samples.

As shown in **Figure 3.06a**, expression of PDI, PDIp, and Sec61α is immediately and significantly reduced in Mist1$^{CreER/+}$; Xbp1$^{fl/fl}$ samples within 48 hours of TM treatment. This is contrasted by expression of CHOP **(Figure 3.06a, right)**, an ER stress response gene regulated by multiple UPR branches that shows no significant change. These results suggest than *Xbp1* ablation effectively silenced the IRE1 component of the UPR without effect on the other branches.

We next sought to verify that ablation of *Xbp1* had not altered upstream UPR activators. To confirm that IRE1 was still actively splicing Xbp1 transcripts, IRE1 activity was assayed via RT-qPCR using splice-specific primers that detected IRE1-dependent excision of the 26 nucleotide intron still present in the Xbp1$^{\Delta Ex2}$ transcript (diagrammed in **Figure 3.03a**). As shown in **Figure 3.06b**, splicing of the Xbp1$^{\Delta Ex2}$ transcript confirmed robust IRE1 activity within the pancreas following tamoxifen-mediated Xbp1 ablation. This activity was sustained over several weeks, showing significant increases following ablation (discussed in section 3.3). Despite the high level of IRE1 activity, the XBP1 targets Sec61α and PDI were not significantly upregulated **(Figure 3.06c)**, indicating that tamoxifen-mediated Cre-dependent splicing abrogates XBP1 function in the pancreas. These mice will henceforth be referred to as Mist1$^{CreER/+}$; Xbp1$^{\Delta Ex2}$ mice.

3.3 Xbp1 ablation causes ER stress and activation of an incomplete UPR in Mist1$^{CreER/+}$; Xbp1$^{\Delta Ex2}$ acinar cells

Previous work performed by the Miura research group utilized transgenic mice to express an XBP1s-GFP fusion protein to be used as a reporter of ER stress (Iwawaki et al., 2004). These mice have substantial expression of the tagged fusion protein specifically in the pancreas, indicating that ER stress with corresponding UPR activation is constitutive in the normal adult pancreas (Iwawaki et al., 2004) **(Figure 3.07a)**. The constant secretory load and corresponding UPR makes the pancreas an ideal target for investigating the degree of crosstalk between the three master regulator molecules and their downstream signaling components. The extensive overlap in UPR targets and functions prompted us to ask whether XBP1 is an essential component for UPR-mediated resolution of ER stress in pancreatic acinar cells. Previous

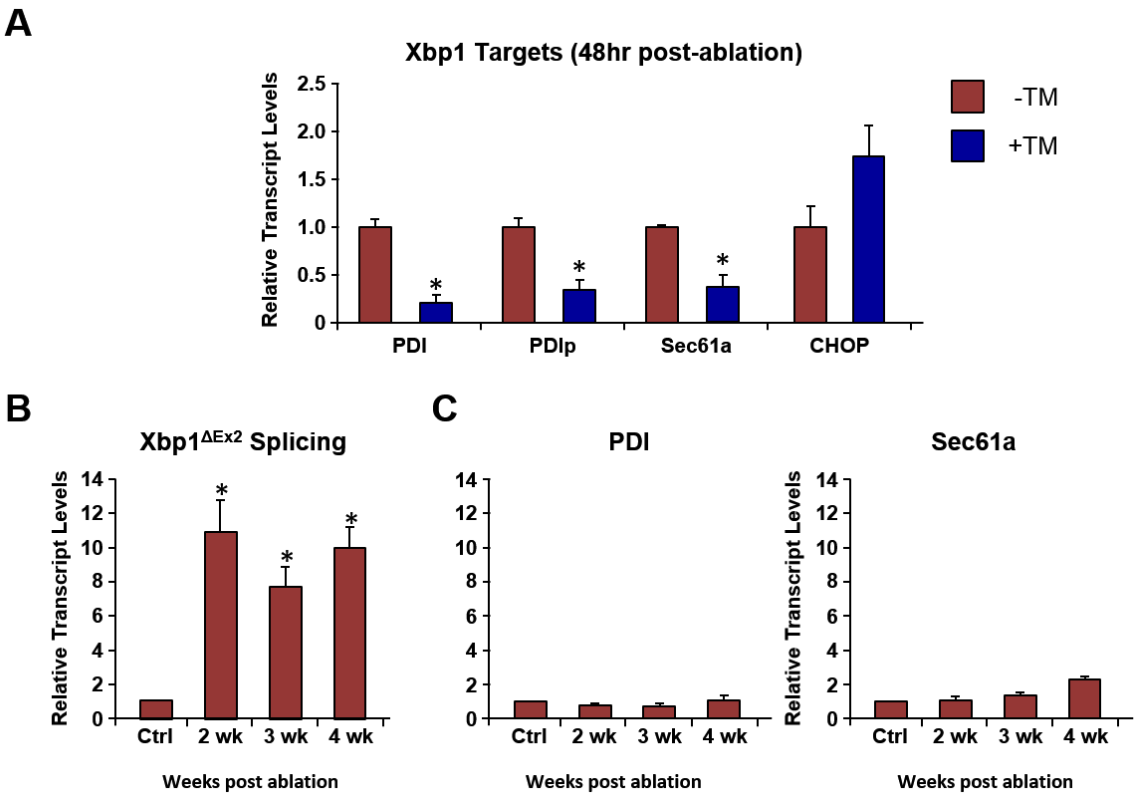

Figure 3.6 *Tamoxifen administration in* Mist1$^{CreER/+}$*;* Xbp1$^{fl/fl}$ *mice disables the XBP1-dependent expression of target genes*

(A) RT-qPCR analysis of pancreata from tamoxifen-treated *Mist1$^{CreER/+}$; Xbp1$^{fl/fl}$* mice indicates that expression of PDI, PDIp, and Sec61α is significantly reduced compared to CHOP. (B) RT-qPCR using primers specific for IRE1-mediated *Xbp1* RNA splicing indicates significant and sustained activity of IRE1. (C) RT-qPCR for XBP1-specific targets PDI and Sec61α show no significant increase in expression over control despite active splicing of the *Xbp1* transcript. (* = p-value < 0.05 relative to control samples, normalized to 18s expression) RT-qPCR analysis (Figure C) conducted in collaboration with Dr. Sean Humphrey.

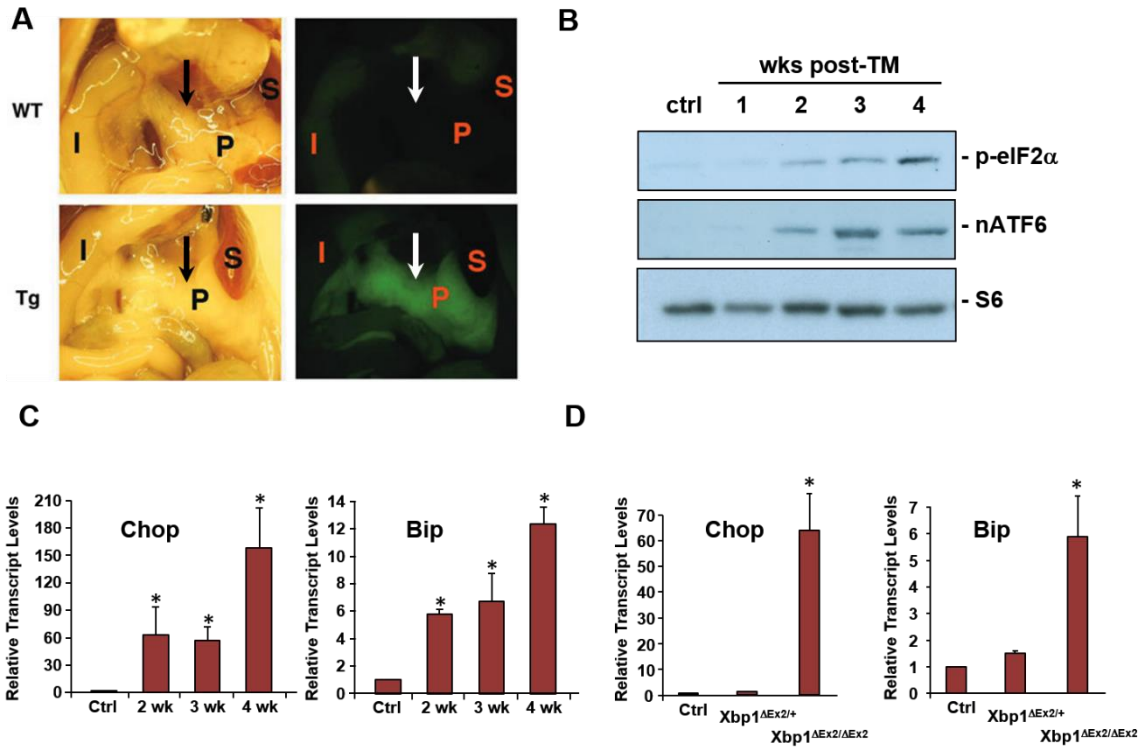

Figure 3.7 *Ablation of Xbp1 results in sustained and progressive activation of the unfolded protein response (UPR)*

(A) Gut isolates of ER stress-activated indicator (ERAI) mice expressing an *Xbp1*-Venus fusion protein that fluoresces upon splicing of the *Xbp1* transcript (Iwawaki et al., 2004). Transgenic mice reveal constitutive expression of XBP1s specifically in the mouse pancreas (P) but not the intestine (I) or stomach (S). (B) Protein isolates from Mist1$^{CreER/+}$; Xbp1$^{\Delta Ex2}$ pancreata reveal increasing activation of the PERK (assayed via phosphorylation of eIF2α) and nATF6 (primary effector of ATF6) pathways. (C) RT-qPCR analysis of ER stress indicators in pancreatic RNA isolates reveal progressively increasing expression of both *Chop* and *Bip*. (D) *Chop* and *Bip* are upregulated in RNA isolates from Mist1$^{CreER/+}$; Xbp1$^{\Delta Ex2}$ pancreata at three weeks post-ablation but not in Mist1$^{CreER/+}$; Xbp1$^{\Delta Ex2/+}$ or untreated Mist1$^{CreER/+}$; Xbp1$^{fl/fl}$ controls. (* = p-value < 0.05 relative to control samples, normalized to 18s expression). RT-qPCR analysis conducted in collaboration with Dr. Sean Humphrey.

investigations of other master regulators indicated that ablation of PERK or ATF6α failed to generate increases in ER stress indicators (Iida et al., 2007; Wu et al., 2007). Both of these studies concluded that the UPR could function in the absence of one of the three branches.

In order to monitor the effects of Xbp1 ablation, mice were administered tamoxifen and sacrificed at one week intervals. Pancreata were harvested for histology, protein, and RNA isolation to allow for complete analysis of each organ. As seen in **Figure 3.07b**, loss of Xbp1 was followed by steadily increasing detection of phosphorylated eIF2α (eIF2α) and nuclear ATF6 (nATF6), indicative of activation of the PERK and ATF6 master regulators, respectively. (see **Figure 1.05** for diagram). This increase in UPR pathway activation correlated with increasing transcript levels of both *Bip* and *Chop* **(Figure 3.07c)**, previously described as key UPR targets activated by multiple UPR master regulator branches. These data suggest that loss of XBP1 function leads to progressively increasing levels of ER stress.

Previous investigations by other groups have indicated that loss of one Xbp1 allele can substantially impair UPR function in mice with experimentally-induced acute pancreatitis (Lugea et al., 2011). We investigated whether the UPR activation we observed accompanying basal pancreatic functioning could be similarly triggered via heterozygous deletion of one copy of Xbp1. As shown in **Figure 3.07d,** *Xbp1*$^{\Delta Ex2/+}$ mice failed to show increased expression of *Bip* or *Chop* at three weeks post tamoxifen treatment, indicating a lack of significant ER stress due to loss of one *Xbp1* allele. This illustrates that the apparent increase in ER stress indicators *Bip* and *Chop* is specifically due to the complete loss of XBP1 function and that a single *Xbp1* allele is capable of sustaining the unfolded protein response during normal pancreatic functioning.

3.4 Loss of Xbp1 triggers progressive cell damage in acinar cells

Pancreatic acinar cells make extensive use of their protein production machinery in order to synthesize and secrete digestive zymogens. As such, zymogen production and activation are effective ways of measuring cell stress levels and protein throughput. Specifically, zymogen forms of amylase, elastase, and carboxypeptidase A (CPA) are all expressed at high levels in acinar cells. Additionally, accumulation of aberrantly auto-

activated CPA is a hallmark of improper acinar secretion that is triggered by pancreatic damage, leading to inflammation seen in pancreatitis patients (Jaffray et al., 2000). Certain acinar transcription factors, including MIST1, are also affected during stress, with a marked decrease in expression associated with pancreatic damage due to pancreatitis or oncogenic transformation (Shi et al., 2009b). We thus sought to investigate the overall health of Mist1$^{CreER/+}$*;* Xbp1$^{\Delta Ex2}$ acinar cells via analysis of MIST1 levels and the presence of intact and damage-associated zymogen forms.

In contrast to the increased ER stress markers seen previously, expression of amylase and elastase transcripts progressively declined following ablation of *Xbp1*, suggesting that there may be a reduction in overall protein throughput **(Figure 3.08a)**. This finding is also seen at the protein level, along with an inversely correlated accumulation of activated CPA, indicative of acinar cell distress **(Figure 3.08b)**. These data prompted an investigation of whether visible signs of distress could be observed via histological analysis.

Due to the limited efficacy of Cre-mediated recombination, a small subset of acinar cells (<10%) were expected to continue expressing normal XBP1s derived from the unrecombined Xbp1^{flox} allele. This fortuitously allowed a comparison of Xbp1$^{\Delta Ex2}$ acinar cells to unablated cells within the same tissue. LacZ staining of four week post-tamoxifen tissue samples revealed isolated acini which had not responded to tamoxifen induction and thus failed to activate β-gal expression or ablate Xbp1 **(Figure 3.08c, red outlines)**. The previously described loss of zymogen and Mist1 expression known to be a consequence of acinar cell damage was restricted to the β-gal positive cells, confirming that “normal” acini were unaffected by neighboring cell loss of Xbp1 **(Figure 3.08d)**. These two distinct populations were thus dubbed the zymogenic (XBP1-expressing) and non-zymogenic (Xbp1$^{\Delta Ex2}$) populations. The presence of two distinct populations provided an opportunity to comparatively analyze the cell architecture within the Xbp1$^{\Delta Ex2}$ acinar cells.

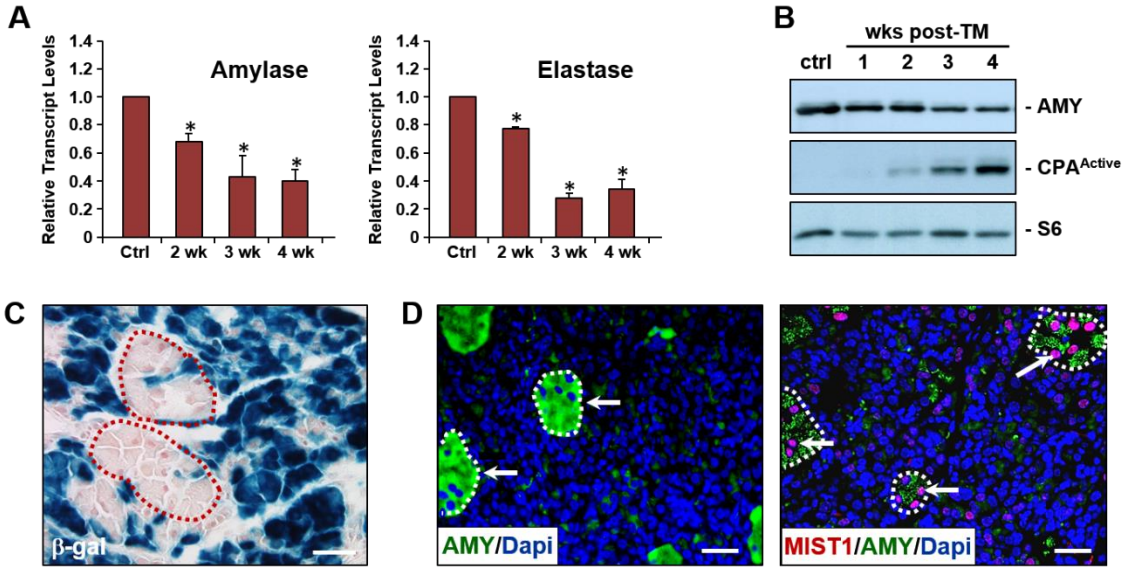

Figure 3.8 *Ablation of Xbp1 results in reduction of protein expression that is accompanied by increased damage indicators*

(A) RT-qPCR for amylase and elastase transcripts show a progressive drop in steady-state levels following loss of XBP1. (B) Protein blot for amylase (AMY) and activated CPA (CPA^{Active}) levels show a decrease in amylase protein while activated CPA, a marker for pancreatic damage, accumulates over the same period. (C) LacZ staining reveals isolated acini that failed to ablate *Xbp1* (β-gal negative) and retain expression of acinar hallmark proteins. (D) Immunofluorescence staining for amylase and MIST1 reveals a loss of both proteins in the $Mist1^{CreER/+}; Xbp1^{\Delta Ex2}$ population with continued expression in the cells that failed to ablate *Xbp1*. (* = p-value < 0.05 relative to control samples, normalized to 18s expression) RT-qPCR analysis done in collaboration with Dr. Sean Humphrey.

As previously described, expression of XBP1s is linked to expansion of the ER in cells undergoing ER stress, implying that ablation of Xbp1 could result in altered cellular ER morphology (Federovitch et al., 2005; Shaffer et al., 2004; Sriburi et al., 2004). Consistent with this idea, hematoxylin and eosin (H&E) staining of isolated pancreata **(Figure 3.09a-c)** showed a progressive loss of basophilic (dark purple) ER staining, along with a decrease in eosinic (pink) zymogen staining. Notably, this loss in zymogen staining is absent in the zymogenic population **(Figure 3.09c, white outlines)**.

Comparative electron microscopy between zymogenic and non-zymogenic cells at 4 weeks post-ablation **(Figure 3.09d,e)** showed a marked change in endoplasmic reticulum appearance, with overall disorganization of the ER, disruption of the nuclear envelope, and a near absence of secretory/zymogen vesicles. The ER itself was swollen and lacked the orderly stacking seen in normal cells. Additionally, loss of *Xbp1* triggered an increase in protein degrading autophagy as determined by increased expression of the autophagy-related protein LC3B and direct observation of autophagosomes by TEM in Xbp1$^{\Delta Ex2}$ acinar cells **(Figure 3.09f)**.

3.5 Acinar cells lacking Xbp1 die approximately four weeks after ablation

Unchecked ER stress and continued activation of the UPR results in initiation of an apoptotic cascade via coordinated action of all three master regulators of the UPR (Szegezdi et al., 2006). A key regulator of this process is the C/EBP homologous protein (CHOP) transcription factor that is activated by all three pathways but only dependent on activation of the PERK branch (Harding et al., 2000). CHOP leads to numerous pro-apoptotic expression changes including a decrease in expression of pro-apoptotic BCL2 and an increase in expression of pro apoptotic proteins such as GADD34, ERO1α, and TRB3 (Szegezdi et al., 2006). Notably, the IRE1 component of the apoptotic arm is not XBP1-dependent but rather relies on a direct interaction of IRE1 and TRAF2, a known upstream regulator of the BCL2 family of proteins that prevent apoptotic initiation (Szegezdi et al., 2006). Though the exact mechanism of ER stress-induced cell death is still being elucidated, it is apparent that persistent activation of the UPR results in activation of an apoptotic cascade that initiates and develops through non-XBP1

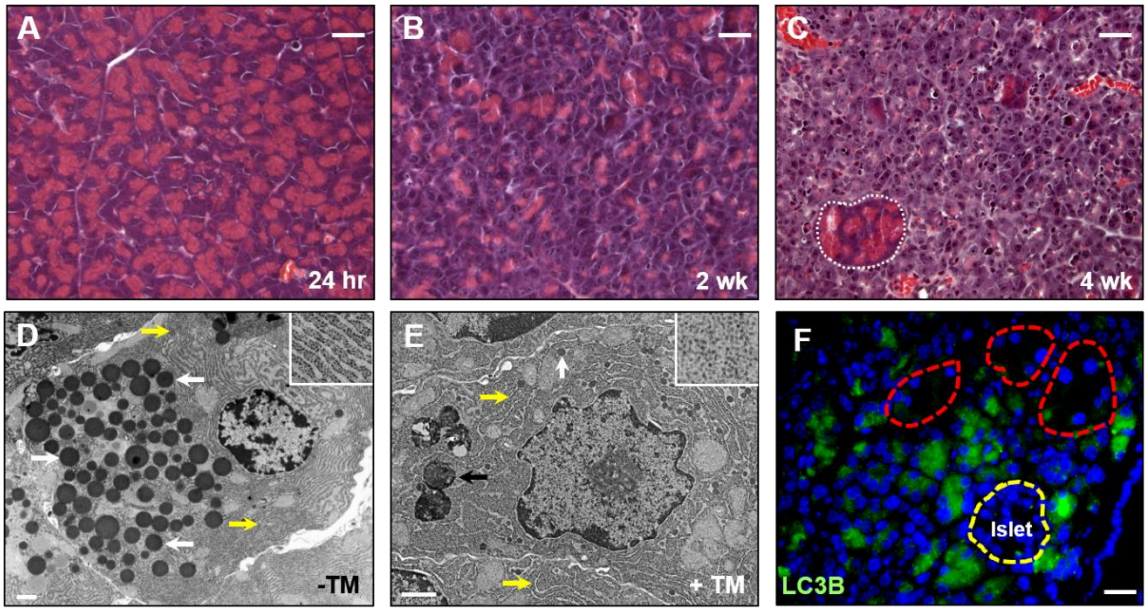

Figure 3.9 *Loss of Xbp1 triggers altered acinar morphology, ER disorganization, and increased autophagy*

(A) Hematoxylin and eosin (H&E) staining of *Mist1*$^{CreER/+}$*; Xbp1*$^{\Delta Ex2}$ pancreata 24 hours post-TM with normal morphology. (B) *Mist1*$^{CreER/+}$*; Xbp1*$^{\Delta Ex2}$ pancreata two weeks after *Xbp1* ablation. (C) *Mist1*$^{CreER/+}$*; Xbp1*$^{\Delta Ex2}$ pancreata four weeks after *Xbp1* ablation. White outline denotes a zymogenic region. (D) Transmission electron micrograph (TEM) of a zymogenic acinar cell four weeks post-ablation. Yellow arrows denote normal stacked ER (also shown in high magnification inset). White arrows denote zymogens with a normal, electron-dense appearance. (E) TEM of a *Mist1*$^{CreER/+}$*; Xbp1*$^{\Delta Ex2}$ non-zymogenic acinar cell. White arrows and inset show disorganized ER with free ribosomes (inset). Yellow arrows denote aberrant zymogen granules and a black arrow denoting an autophagosome, indicative of autophagy. (F) Immunofluorescence staining for LC3B reveals increased autophagy in the non-zymogenic population at four weeks post-*Xbp1* ablation (red outlines denote zymogenic clusters).

dependent pathways. This prompted us to investigate the fate of the Xbp1$^{\Delta Ex2}$ acinar cells.

As noted in section 3.2, Xbp1$^{\Delta Ex2}$ acinar cells exhibit a progressive activation of the UPR following Xbp1 ablation **(Figure 3.08)**. The noted increase in CHOP transcripts discussed earlier is correlated with increased expression of CHOP protein that is restricted to the Xbp1$^{\Delta Ex2}$ acinar cells **(Figure 3.10a)**. This marked increase in CHOP expression is not observed until four weeks post-ablation. Additionally, at the four week time point electron microscopy allowed for direct observation of large numbers of autophagosomes, again indicating an increase in autophagy likely related to extensive protein misfolding **(Figure 3.10b)**. This time point coincides with the onset of cell death as determined by labeling of tissue sections via terminal deoxynucleotidyl transferase dUTP nick end labeling (TUNEL), again restricted to the non-zymogenic population **(Figure 3.10c)**. Isolated protein homogenates from this time point also reveal increases in stress pathway markers pERK1/2 (MAPK pathway) and p38 **(Figure 3.10d)**. All of these data indicate that the non-zymogenic, Xbp1$^{\Delta Ex2}$ acinar cells die via apoptosis following a period of progressive increasing ER stress.

3.6 Discussion

The unfolded protein response (UPR) plays an essential role in maintenance of homeostasis within secretory cells. While the mechanics of activation and execution of each master regulatory branch have been well studied, the complex interplay between branches and their reliance on each other for full effectiveness is still being investigated. Indeed, various studies have indicated that the substantial overlap between the three UPR networks can largely compensate for each other, as elimination of individual branches typically results in no increase in ER stress (Huh et al., 2010; Iida et al., 2007; Wu et al., 2007). Understanding this interplay between branches is essential as knowledge of the UPR is increasingly being utilized to design novel therapeutics against various malignancies (Wang et al., 2010). This emphasis is due to increasing numbers of studies

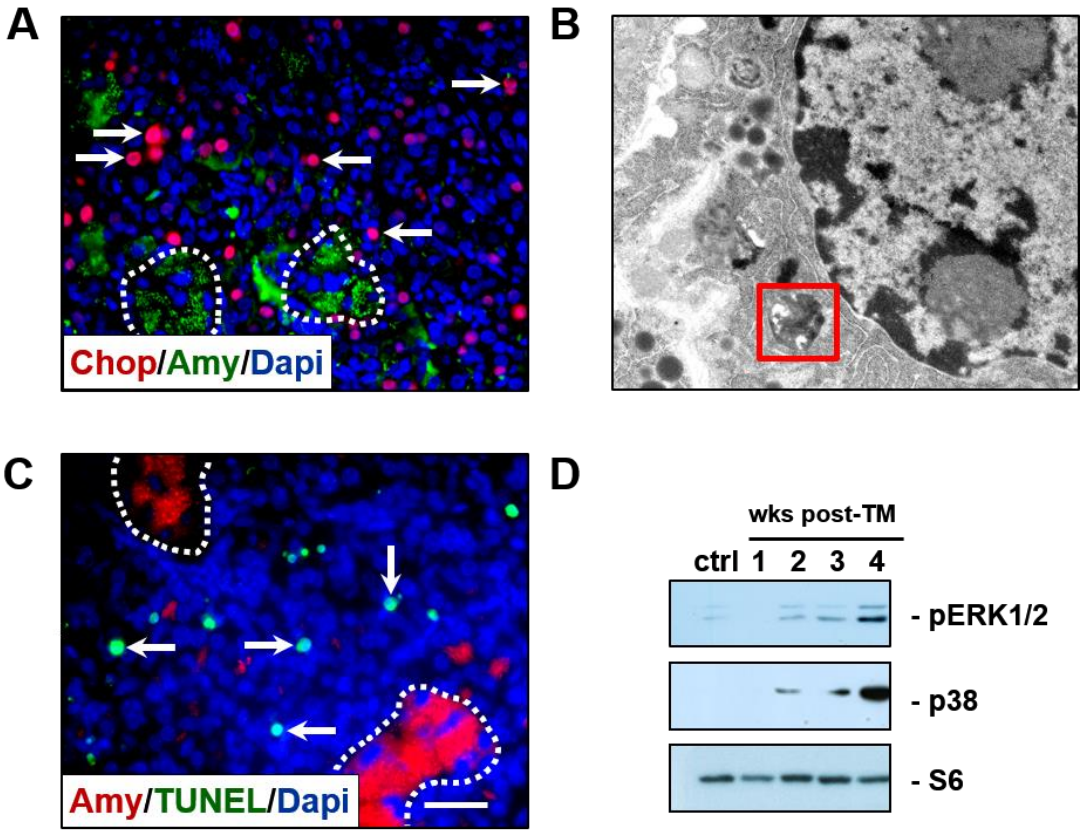

Figure 3.10 *Xbp1 ablation leads to activation of apoptotic UPR pathways and eventual cell death*

(A) Immunofluorescent analysis of 4-week post-ablation pancreata shows strong expression of CHOP localized to the non-zymogenic population. Zymogenic cells remain CHOP-negative. (B) Transmission electron micrograph of a non-zymogenic acinar cell reveals an autolysosome, indicative of end stage autophagy. (C) TUNEL staining of 4-week post-ablation pancreata reveals positive staining in the non-zymogenic acinar population. (D) Protein blots on isolated pancreatic extracts reveal extensive, progressive activation of the MAPK and p38 stress pathways. Panel D courtesy Dr. Sean Humphrey.

indicating that ER stress is a common hallmark in cancerous cells (Cyr and Hebert, 2009; Kaufman, 2002; Koong et al., 2006; Walter and Ron, 2011; Wang et al., 2010) as well as a viable means of inducing cell death in combination with standard chemotherapeutics (Martins et al., 2011; Nawrocki et al., 2005a, 2005b). The need for such novel approaches is particularly important in pancreatic ductal adenocarcinoma (PDA), a nearly untreatable malignancy with a five-year survival rate of only 6% (Siegel et al., 2013). In this study a cell-specific, inducible *Xbp1*-knockout mouse model was utilized to determine if nullification of the IRE1 branch of the UPR could be compensated for by the PERK and ATF6 networks in pancreatic acinar cells.

The pancreas has been shown previously to have a basal activation of the unfolded protein response **(Figure 3.07a)**. This is presumed to be due to the high secretory demands placed on pancreatic acinar cells. Based on this information, we hypothesized that impairment of proper UPR function via ablation of *Xbp1* would result in a sustained ER stress response. Indeed, we observed a progressively increasing activation of the PERK and ATF6 branches of the UPR **(Figure 3.07)**, consistent with an inability to properly resolve basal ER stress in acinar cells. UPR activation reached a maximum at four weeks post-ablation, which also correlated with the highest degree of cell death. These results suggest that XBP1, while essential to provide a full unfolded protein response, is not required for the action of the other two branches. Indeed, the PERK and ATF6 branches appear fully functional and active via analysis of their immediate effectors. Thus, the incomplete UPR initiated in the absence of XBP1 might be sufficient to counter short, minor periods of stress in cells with lower protein loads, but the PERK and ATF6 branches are not sufficient to mitigate chronic ER stress.

As shown in **Figure 3.09**, two distinct acinar cell populations are present in *Mist1*$^{CreER/+}$*; Xbp1*$^{\Delta Ex2}$ pancreata, likely due to limitations in Cre efficacy. Fortuitously, the 90% recombination frequency permits observations of the 10% XBP1-expressing, "zymogenic" acinar cells in contrast to their *Xbp1*$^{\Delta Ex2}$ counterparts. This served as an excellent system for analyzing the effects of XBP1-null cells vs. normal cells under identical conditions. Electron micrographs revealed substantially altered morphology in *Xbp1*$^{\Delta Ex2}$ acinar cells including degradation of the ER **(Figure 3.09d,e)**. These findings are consistent with previous data showing that XBP1 is responsible for the physical

remodeling of the ER during periods of ER stress (Shaffer et al., 2004; Sriburi et al., 2004). Indeed, loss of XBP1 and the associated disruption of ER architecture results in a swelling of the ER, possibly due to insufficient protein transport out of the ER, a process known to be regulated by the XBP1-target EDEM1 **(Table 3.01)**. It is thus likely that XBP1 functions primarily as a mediator of the adaptive phase of the UPR, remodeling the ER to expand capacity and increasing export of misfolded proteins.

Ablation of *Xbp1* also has apparent cell-wide consequences. As shown via immunofluorescent staining for the autophagy marker microtubule-associated protein light chain 3b (LC3B) **(Figure 3.09f)**, cells lacking XBP1 have increased autophagy, a likely consequence of accumulating large amounts of improperly folded proteins that are no longer being modulated by the remaining UPR branches. This finding is of particular importance, because induction of autophagy in transformed cells is emerging as a possible druggable mechanism for tumor suppression (Suh et al., 2012), supporting the idea that modulators of XBP1 could serve as a novel therapeutic intervention in human disease.

Long-term loss of XBP1 function is deleterious to acinar cells, as non-zymogenic cells express high levels of CHOP four weeks after ablation **(Figure 3.10)**. This again demonstrates that the PERK and ATF6 of the UPR are unaffected by loss of XBP1. CHOP expression is primarily under the control of the PERK UPR master regulator, although recent work has implicated XBP1 as a coregulator (Takayanagi et al., 2013). Indeed, the gradual accumulation of CHOP over the four weeks following *Xbp1* ablation supports recent work by the Yoshida group showing that CHOP expression may be auto-regulatory in nature (Takayanagi et al., 2013).Thus, our studies lead to a model in which ablation of XBP1 causes mounting ER stress, resulting in continuous expression of CHOP that eventually triggers a switch to an apoptotic cell fate **(Figure 3.11)**. Indeed, the extended window of ER stress seen in the $Mist1^{CreER/+}; Xbp1^{\Delta Ex2}$ model may serve as a novel tool for investigating regulation of the unfolded response.

Complete loss of XBP1 activity is ultimately fatal in pancreatic acinar cells **(figure 3.10)**. The observed co-localization of CHOP and TUNEL staining to the non-zymogenic, $Xbp1^{\Delta Ex2}$ acinar cell population indicates that the cells likely died via activation of the

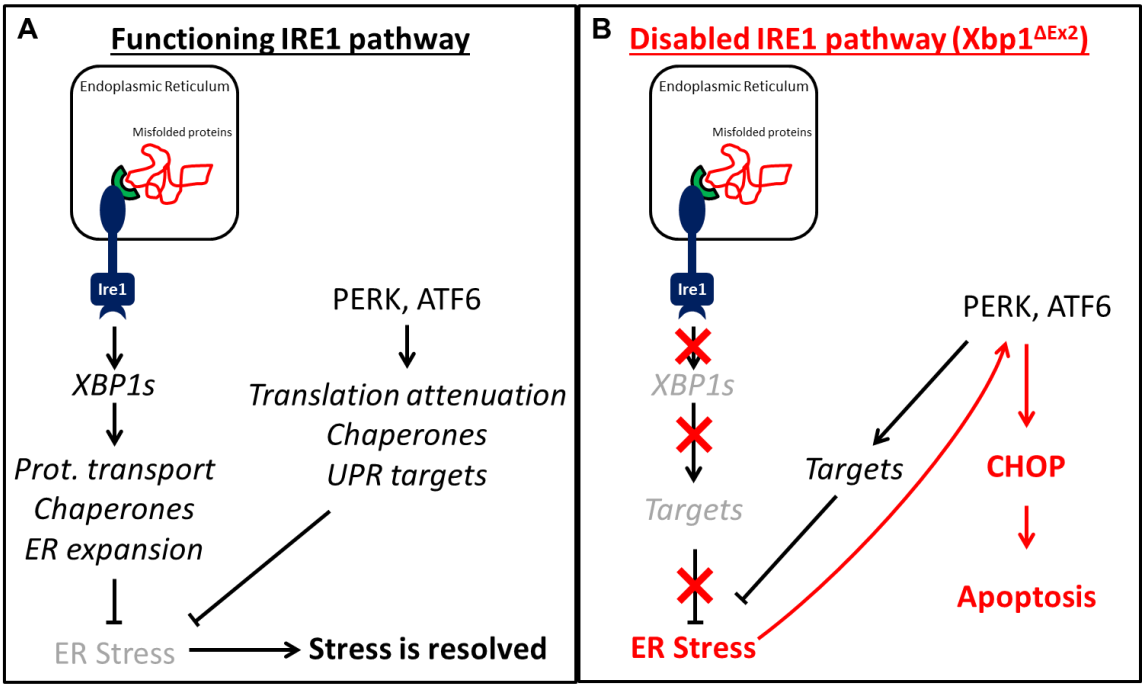

Figure 3.11 *Proposed model regarding the effects of* Xbp1 *ablation on ER stress in pancreatic acinar cells*

(A) Standard model of XBP1s action in which IRE1-dependent splicing of *Xbp1* leads to production of XBP1s. This in turn leads to expression of target genes which work in concert with the other pathways to resolve ER stress. (B) In *Xbp1*$^{\Delta Ex2}$ acinar cells, XBP1s cannot be synthesized, resulting in disabling of the entire IRE1 branch of the UPR. This leads to increasing ER stress, which eventually feeds back to the PERK and ATF6 master regulators and triggers expression of CHOP and the apoptotic portion of the UPR.

apoptotic arm of UPR. The progressive activation of both the MAPK and p38 stress pathways also indicates that acinar cells are under substantial stress due to basal metabolic demands but that the effect is sub-lethal for an extended period of time. This observation could indicate that modulation of the UPR may be an effective means of controlling the viability of stressed cells, including those undergoing oncogenic transformation. This hypothesis is supported via studies of bortezomib, a chemotherapeutic drug used to treat multiple myeloma that induces ER stress while suppressing the UPR (Mimura et al., 2012; Nawrocki et al., 2005a). Future studies are required to see if induction of ER stress in acinar cells is sufficient to prevent cancerous transformation. Preliminary data regarding the interaction of ER stress and oncogenesis in Mist1$^{CreER/+}$; Xbp1$^{fl/fl}$ mice will be presented in Chapter 4.

This study revealed that XBP1 is essential for the homeostasis and viability of pancreatic acinar cells via its role in the unfolded protein response. Future studies will investigate whether specific, downstream effectors of XBP1 are similarly capable of controlling viability in stressed cells (see Chapter 6). Additional work, detailed in Chapter 5, has focused on a specific XBP1-target, MIST1, which itself has been shown to be a key regulator of acinar cell identity during pancreatic disease (Kowalik et al., 2007; Shi et al., 2009b, 2012; Zhu et al., 2004). Together, this work demonstrates that XBP1 and its targets may be an effective means of regulating homeostatic mechanisms in secretory cells.

CHAPTER 4. PANCREATIC DAMAGE IN *Mist1*$^{CreER/+}$; *Xbp1*$^{\Delta Ex2}$ MICE TRIGGERS A COORDINATED, MULTI-CELL COMPARTMENT REGENERATIVE RESPONSE

4.1 Introduction

Damage in the exocrine pancreas is generally caused by one of two insults; oncogenic transformation or pancreatitis. Oncogenic transformation refers to the transdifferentiation of acinar cells into duct-like structures via acinar-ductal metaplasia (ADM). Acinar cells undergoing ADM can then develop into pre-cancerous lesions called pancreatic intraepithelial neoplasia (PanINs), eventually progressing into pancreatic ductal adenocarcinoma (PDA). This transition occurs after initial expression of mutated, constitutively active *Kras*^{G12D} oncogene, thus representing an intrinsic stress on the cells (Hruban et al., 2006). Pancreatitis is an inflammatory disease in which autoactivation of digestive enzymes (experimentally induced by secretagogue treatment) results in acinar cell death, pancreatic edema, and the appearance of ductal structures also from acinar-ductal metaplasia (Klöppel and Maillet, 1993; Strobel et al., 2007). Multiple mouse models have been generated to investigate both of these exocrine pancreas diseases.

As shown in **Figure 4.01a**, PanIN development is governed by expression of constitutively active forms of the KRAS protein, a downstream effector of extracellular growth factor (Maitra and Hruban, 2008). At least ten mouse model systems have been made utilizing activated KRAS, primarily differing in whether KRAS is expressed via constitutive or inducible promoters (Hruban et al., 2006). The most prevalent model system uses Cre-mediated induction of activated *KRAS*^{G12D} via deletion of a STOP cassette, generating a Cre-inducible mutant KRAS allele with tissue specificity based on the choice of Cre used **(Figure 4.01b)** (Jackson et al., 2001). These systems have been used extensively to characterize early oncogenic transformation events in mice, demonstrating alongside human patient samples that pancreatic cancer development is associated with an intense desmoplastic response resulting from extensive inflammation (Pandol et al., 2009). The pronounced inflammatory environment seen during PDA development is a shared trait also observed in mouse models of pancreatitis.

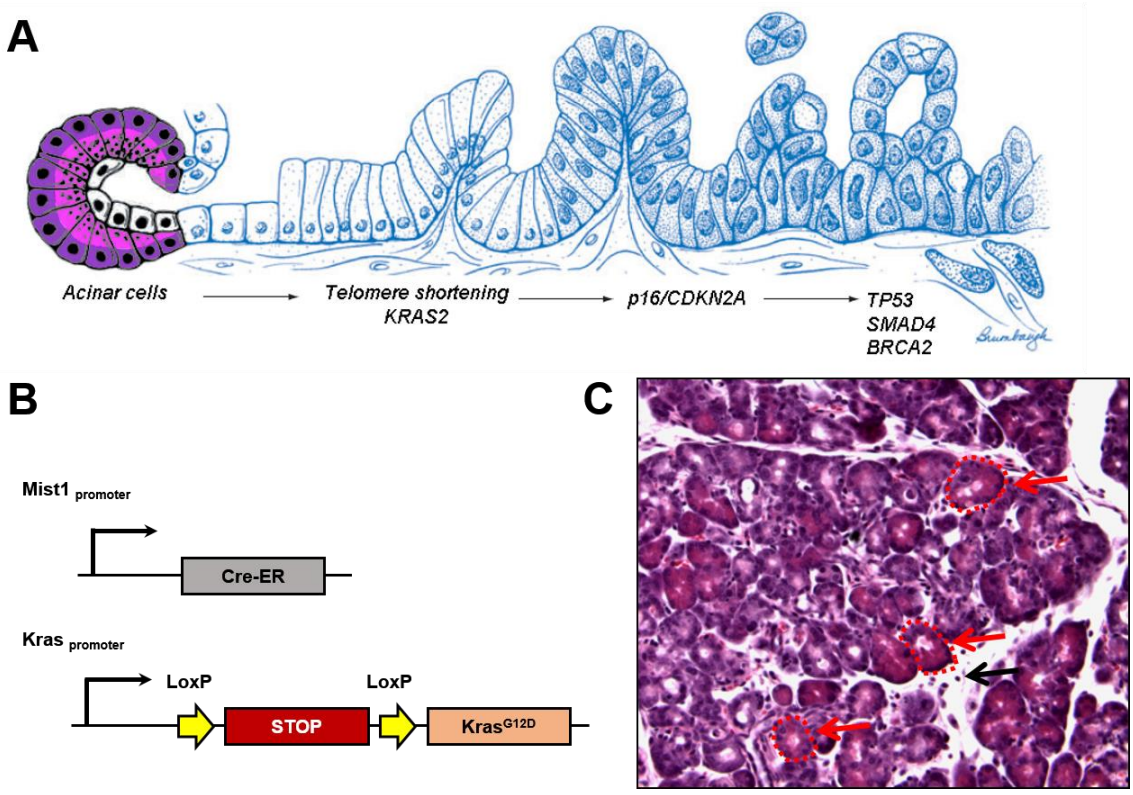

Figure 4.1 *Exocrine pancreas damage leads to acinar-ductal metaplasia and inflammation*

(A) Illustration of PanIN development showing initial conversion of acinar cells to duct-like cells via expression of mutant KRAS, a mutation found in approximately 90% of human pancreatic cancers. Later steps involve mutations in the *p16* gene followed by mutations in the *TP53, Smad4,* and *Brca2* genes. Figure modified from Maitra and Hruban, 2008. (B) Schematic showing the Mist1$^{CreER/+}$; LSL-Kras mouse line with acinar cell-specific expression of *Kras*^{G12D}. Activation of Cre removes the STOP cassette and allows for expression of the mutant *KRAS*^{G12D} protein. (C) Representative image of caerulein-induced pancreatitis showing intralobular stromal deposition (black arrow) as well as open lumened, acinar cells undergoing ADM (red arrows). Figure A adapted from Maitra and Hruban, 2008. Figure C courtesy of Dr. Daniel DiRenzo.

Multiple mouse models of pancreatitis also exist, differing primarily in how exocrine damage is inflicted. Model systems based on surgical obstruction of the pancreatic duct (Watanabe et al., 1995), feeding of alcohol (Su et al., 2006) or L-arginine (Lerch and Adler, 1994), or administration of the cholesystokinin (CCK) homologue caerulein (Jungermann et al., 1995) have all been used extensively in the literature with varying degrees of success. Caerulein injection has become the predominant model system due to its ease of delivery via intraperitoneal injection. Caerulein administration triggers supramaximal levels of acinar cell zymogen secretion, resulting in aberrant release of digestive enzymes across the basal acinar membrane as well as autoactivation of intracellular granules (Jungermann et al., 1995). This results in proteolytic tissue digestion, edema, and inflammation that mimics the appearance of human disease **(Figure 4.01c)** (Dawra et al., 2007). Interestingly, acinar-ductal metaplasia is also observed during pancreatitis, linking both oncogenic and inflammatory damage to maintenance of acinar cell identity, discussed extensively in Chapter 5.

Acinar-ductal metaplasia serves as a prime example of the plasticity of adult pancreatic cells. The ability of acinar cells to convert into a duct-like progenitor state when damaged has been demonstrated in response to oncogenic transformation (Zhu et al., 2007), caerulein-induced pancreatitis (Strobel et al., 2007), and following dissociation of human tissue explants in culture (Houbracken et al., 2011). Additionally, the use of growth factors on cultured acinar cells can trigger conversion of the exocrine-lineage, digestive enzyme-producing acinar cells to endocrine-lineage, insulin-producing β-cells, a transition that occurs through a duct-like intermediate (Baeyens et al., 2009; Minami et al., 2005). These transitional events indicate that damaged or stressed acinar cells become more duct-like via dedifferentiation, presumably entering a damage-refractory progenitor state and subsequently redifferentiating following resolution of stress. The specific transcriptional networks and stress signaling pathways active within acinar cells are therefore particularly important in maintaining the differentiated identity of the cell.

ADM has been studied using numerous model systems. Isolated acinar cells have been observed to transdifferentiate into duct-like cysts in culture (Means et al., 2005), while lineage tracing studies in mice with activated KRAS expression have confirmed that acinar cells contribute to duct-like PanIN structures *in vivo* (Habbe et al., 2008; Shi et al.,

2009b). The use of these model systems has identified specific signaling pathways that are required for ADM, including the mitogen-activated protein kinase (MAPK) pathway, a key regulatory pathway known to be affected by the activating *Kras*^{G12D} mutations that initiate pancreatic cancer (Habbe et al., 2008; Houbracken et al., 2011). ADM can also be accelerated via loss of key acinar differentiation factors including MIST1, discussed in Chapter 5 (Shi et al., 2009b, 2012). Signaling studies using caerulein-induced pancreatitis models have similarly revealed a need for activation of embryonic signaling pathways during pancreatic regeneration, specifically the Hedgehog and Notch pathways (Fendrich et al., 2008). A combination of oncogenic and inflammatory damage can also synergize in regards to ADM and disease progression, with some studies indicating that a chronic inflammatory environment is essential for oncogenic progression in mouse models expressing activated KRAS proteins (Guerra et al., 2007, 2011). Interestingly, both cancer progression and pancreatitis have been linked to activation of the unfolded protein response.

Expression of the key UPR mediator BiP has been associated with poor prognosis and lack of chemo-sensitivity in multiple secretory organ cancers including prostate (Daneshmand et al., 2007), hepatocellular (Su et al., 2010), and breast (Lee et al., 2006) malignancies. Additionally, multiple chemotherapeutics have been utilized to induce ER stress as a means of inducing cancer cell cycle arrest or apoptosis (Martins et al., 2011; Nawrocki et al., 2005b; Wang et al., 2010). UPR activation is also observed in several experimental models of pancreatitis including L-arginine, alcohol, and caerulein-induced systems (Alahari et al., 2011; Kubisch et al., 2006; Lugea et al., 2011), with full activation of the unfolded protein response and all of its branches observed within 8 hours of pancreatitis induction (Kubisch et al., 2006). Specific studies of *Xbp1*$^{+/-}$ mice have indicated that loss of a single copy of *Xbp1* also impairs acinar cell recovery in alcohol-induced pancreatitis, supporting the idea that the UPR is a necessary component in maintaining pancreatic homeostasis during damage. Existing models of pancreatic damage, however, have produced conflicting data regarding cellular maintenance and regeneration during damage, necessitating the development of new ways of examining both pancreas recovery and the role that the UPR may be playing.

Current pancreatic damage models, while useful, have limitations regarding their applicability to human disease. Secretagogue-induced mouse models mimic the histological appearance of human disease but this model relies on the use of caerulein, a chemical that does not produce a response in human acinar cells and thus may not accurately replicate the molecular signature of recovering human patients (Ji et al., 2002). Non-inflammatory, endogenous stress models, including acinar-specific expression of diphtheria toxin receptors, generate striking levels of acinar cell destruction and regeneration (Criscimanna et al., 2011). The lack of inflammation in these models, however, does not mimic the environment of a diseased or damaged pancreas and thus fails to account for complex epithelial-stromal interactions that may take place during damage. An ideal system for studying pancreatic damage would generate sufficient inflammation to mimic human disease while also generating damage via an intrinsic acinar mechanism known to affect humans. We sought to investigate whether pancreatic damage resulting from ER stress-induced acinar cell loss in the *Mist1*$^{CreER/+}$*; Xbp1*$^{fl/fl}$ model system could recapitulate known histological and gene expression patterns associated with pancreatic damage and regeneration.

In this study we analyzed the effects of extensive, progressive damage on the murine pancreas following the loss of the *Xbp1*$^{\Delta Ex2}$ acinar cell population. We determined that ER stress-induced acinar cell loss is compensated for by cell cycle reentry by both the acinar and centroacinar compartments, with subsequent regeneration of exocrine tissue. Furthermore, we demonstrate that recovering acinar cells are histologically unusual, with swollen zymogen compartments and increased cell and nuclear dimensions that may indicate a compensatory response to exocrine destruction. Finally, we show that loss of *Xbp1* results in long-term pancreatic remodeling and damage, but this damage does not appear to predispose the pancreas to oncogenic transformation.

4.2 *Xbp1*$^{\Delta Ex2}$ pancreata develop a pronounced inflammatory response and activate embryonic signaling components

As described in Chapter 3, acinar cells in *Mist1*$^{CreER/+}$*; Xbp1*$^{\Delta Ex2}$ mice fail to execute a sufficient unfolded protein response, leading to progressive UPR activation and eventual ER stress-induced crisis. One of the hallmarks of exocrine pancreatic damage in both human patients and rodent models is a pronounced mixed inflammatory/desmoplastic

response involving tissue-resident macrophage activation and systemic B and T cell infiltration (Kim, 2008; Whitcomb, 2004). Post-damage tissue regeneration is also linked to expression of normally silenced pancreas-specific progenitor markers including *Pdx1*, *Hes1* (a Notch signaling component) and *Nestin* (Jensen et al., 2005; Means et al., 2005). We sought to determine whether ER stress-induced damage within the acinar compartment of *Xbp1*$^{\Delta Ex2}$ mice was sufficient to generate an inflammatory response and activation of embryonic signaling pathways.

Histological examination of pancreatic sections isolated from two-week post-crisis (6 week post-ablation) *Mist1*$^{CreER/+}$*; Xbp1*$^{\Delta Ex2}$ mice revealed extensive cell remodeling within the intra-acinar spaces. This remodeling included formation of tubular complexes **(Figure 4.02a, white arrows)**, a common feature seen in caerulein pancreatitis models and caused by either acinar-ductal metaplasia or reorganization of preexisting ductal cells (Strobel et al., 2007). These tubular complexes were themselves surrounded by extensive collagen deposits as determined by Sirius Red staining **(Figure 4.02b)**. Immunohistochemical staining for the T-cell marker CD3 revealed an extensive influx of T-cells surrounding the tubular complexes **(Figure 4.02c, red arrows)**. Additional staining for the B-cell marker F4/80 also revealed the presence of B-cells among the non-epithelial, tubular complex-adjacent cells **(Figure 4.02d, red arrows)**. These data indicated that a mixed stromal/inflammatory response occurred within the intra-acinar spaces in post-crisis pancreata.

We next sought to determine whether *Mist1*$^{CreER/+}$*; Xbp1*$^{\Delta Ex2}$ pancreata had altered progenitor marker expression. RNA isolates from *Mist1*$^{CreER/+}$*; Xbp1*$^{\Delta Ex2}$ mice taken weekly from two to six weeks post-*Xbp1* ablation were analyzed for expression of the progenitor marker/genes *Nestin*, *Hes1*, and *Pdx1*. As shown in **Figure 4.03a-c**, all three genes exhibited a similar expression pattern, with significantly upregulated expression following ablation that progressively increased until four weeks post-*Xbp1* ablation. This was then followed by decreasing expression of all three genes to wild-type levels by six weeks, with the exception of *Pdx1* which still had significantly higher expression levels, albeit at lower levels than the peak at four weeks. This pattern strongly suggested a

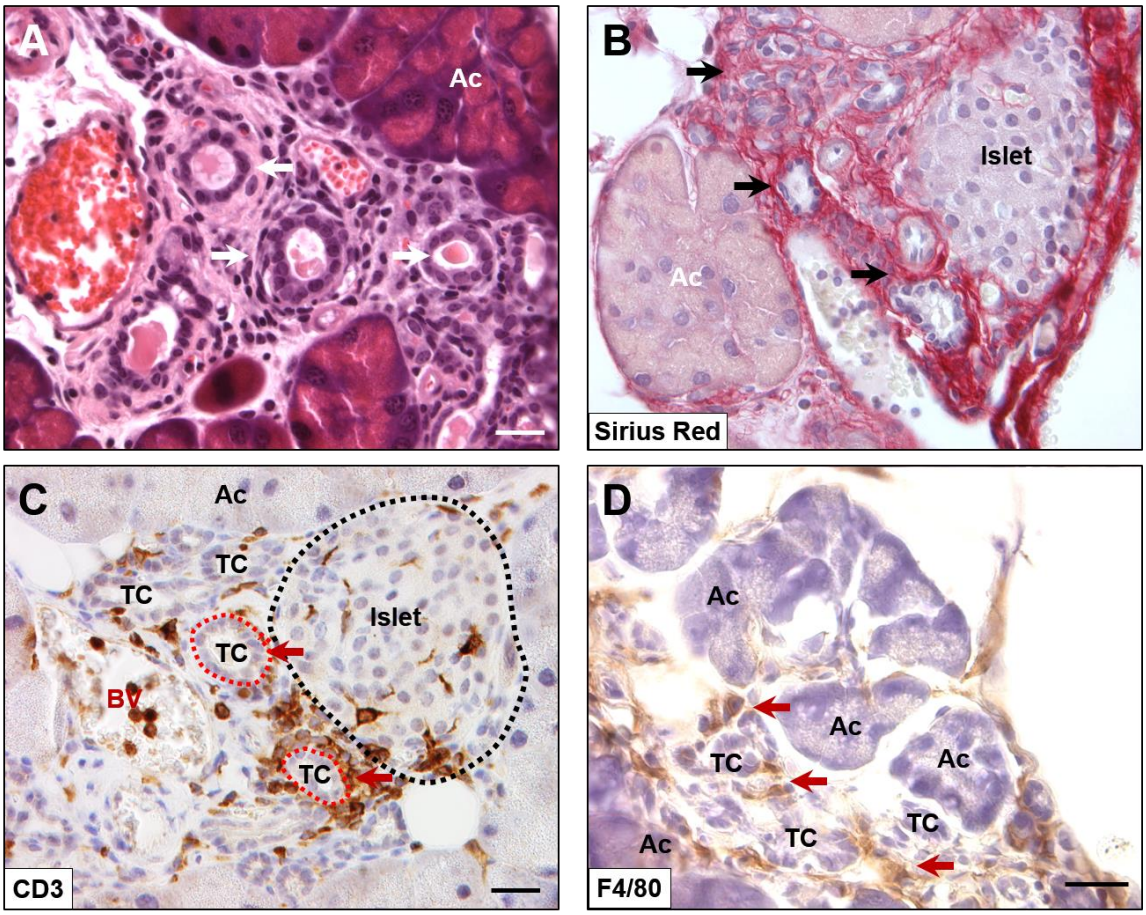

Figure 4.2 *Mixed inflammatory response occurs in recovering pancreata of* *Mist1*$^{CreER/+}$*;* *Xbp1*$^{\Delta Ex2}$ *mice*

(A) H&E image of pancreatic section taken from recovering pancreas showing development of mucinous, duct-like tubular complexes (TCs) (white arrows). (B) Sirius Red staining of 6 week post-ablation pancreatic section showing extensive collagen deposition surrounding tubular complexes (black arrows). (C) Histological stain of stromal infiltrate and tubular complexes (red outlines) for CD3, showing CD3-positive T-cells (red arrows) surrounding the TCs. (D) Histological stain of stromal infiltrate showing for F4/80 showing F4/80-positive B-cells surrounding the TCs.

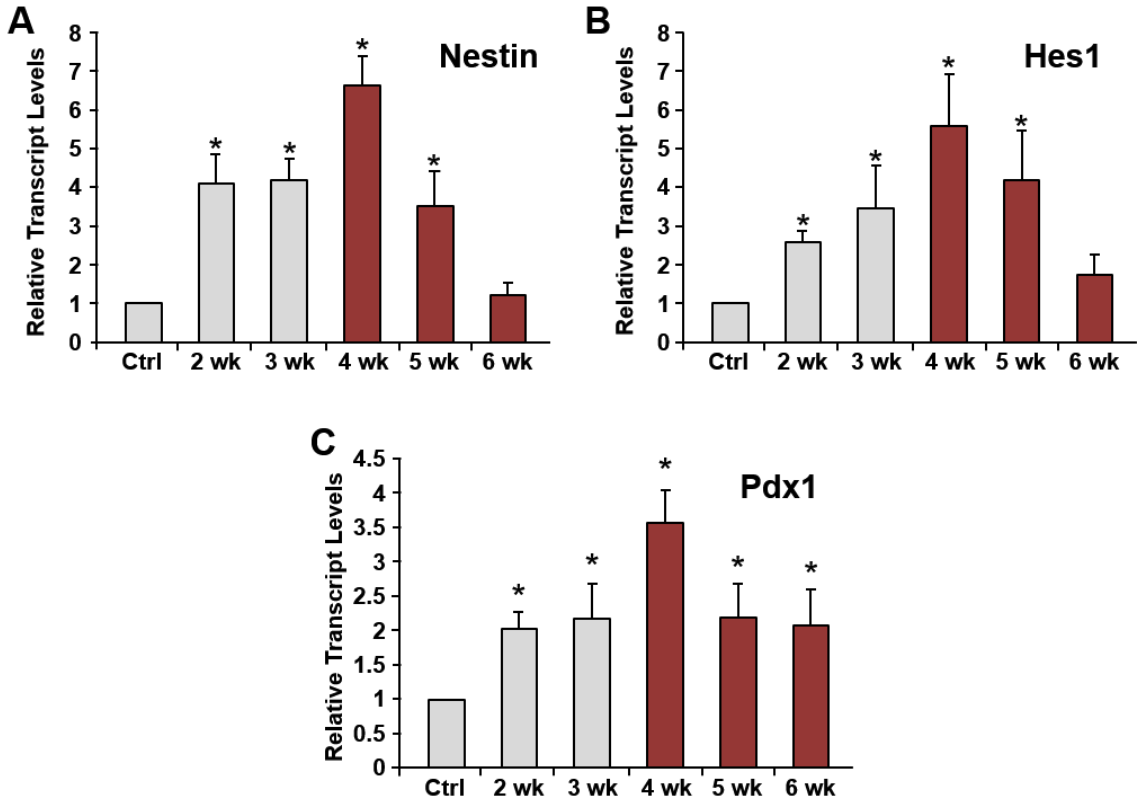

Figure 4.3 *Recovering pancreata in Mist1$^{CreER/+}$; Xbp1$^{\Delta Ex2}$ mice have increased expression of progenitor genes*

RNA isolates from *Mist1$^{CreER/+}$; Xbp1$^{fl/fl}$* pancreata taken at weekly intervals following *Xbp1* ablation. Relative transcript levels for progenitor genes (A) *Nestin*, (B) *Hes1*, and (C) *Pdx1* are shown. All genes were progressively expressed, peaking at 4 weeks post-ablation before to near basal levels. (* = p-value < 0.05 relative to control samples, normalized to 18s expression)

correlation between the increasing levels of ER stress described in Chapter 3 and the expression of known, damage-responsive progenitor genes associated with pancreatic regeneration.

4.3 Pancreata in post-crisis *Xbp1$^{\Delta Ex2}$* mice have diminished UPR activation and recover normal exocrine parameters

Despite the pronounced inflammatory and transcriptional responses to ER stress in the *Mist1$^{CreER/+}$; Xbp1$^{\Delta Ex2}$* mice, we were interested in determining if the pancreata retained long-term damage or whether there might be a post-crisis restoration of the exocrine compartment. Histological examination of four-week post-*Xbp1* ablation pancreatic isolates undergoing ER stress-induced crisis revealed a nearly complete lack of acinar zymogen staining in *Xbp1$^{\Delta Ex2}$* cells relative to wild-type tissue **(Figure 4.04b,e)**. This pronounced exocrine deficiency, however, did not result in early lethality in these mice, prompting us to investigate how the pancreas was capable of continued function despite a diminished exocrine compartment. Specifically, we sought to identify whether the remaining acinar cells compensated for the loss of the *Xbp1$^{\Delta Ex2}$* population or whether a regenerative response was mounted to replace the damaged cells. We first attempted to establish if post-crisis *Mist1$^{CreER/+}$; Xbp1$^{\Delta Ex2}$* mice were histologically normal.

As shown in **Figure 4.04c/f**, increased eosinic (zymogen) staining is observed in samples isolated two weeks after ER stress-induced crisis (6 weeks post-ablation). The observed acinar cells have substantially increased zymogen staining relative to the four week post-ablation pancreata, although isolated regions of tissue **(Figure 4.04c/f, black arrows)** continue to show signs of residual damaged acinar cells as well as open tubular structures **(yellow arrow)**. We also noted a pronounced increase in the size of the acinar compartment (discussed in section 4.5). Given the reestablishment of acinar cells with substantial zymogen staining, we sought to quantify whether the previously observed increase in UPR activation seen in *Xbp1$^{\Delta Ex2}$* acinar cells had been resolved.

Monitoring of the IRE1 branch of the UPR was accomplished via RT-qPCR using *Xbp1* splice-specific primers. As seen in **Figure 4.05a**, IRE1 activity (measured by *Xbp1* splicing) was significantly reduced following loss of the *Xbp1$^{\Delta Ex2}$* acinar population,

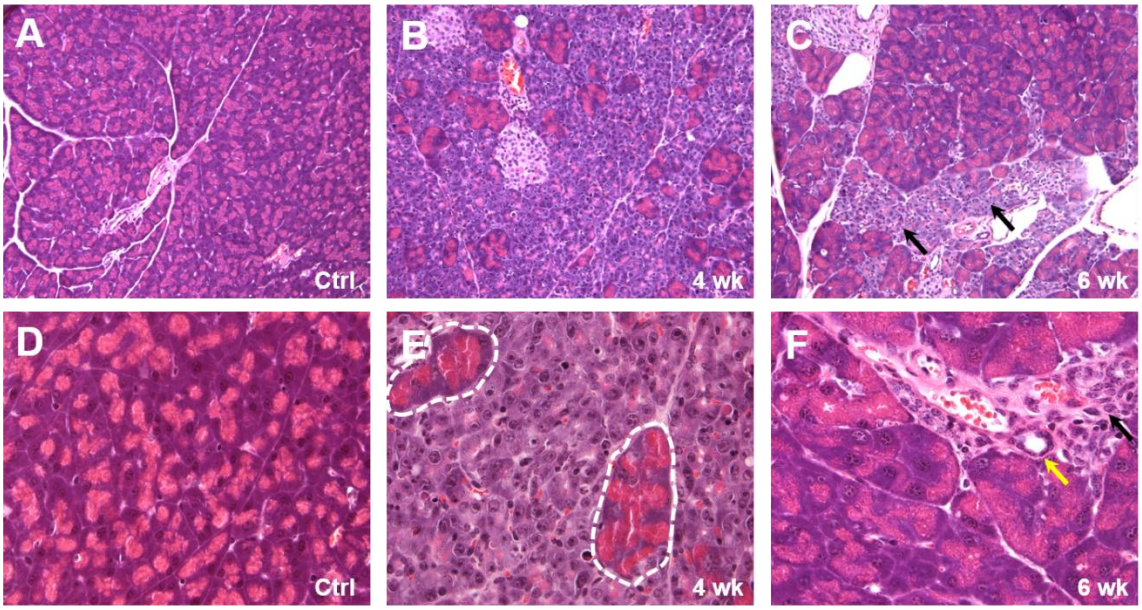

Figure 4.4 *Damaged pancreata in Xbp1$^{\Delta Ex2}$ mice regenerate the acinar cell compartment*

All images are paired at 20X (A-C) and 60X (D-F) magnification. (A,D) Control (no tamoxifen) pancreatic sections with normal strong eosinic staining (pink) surrounded by dense ER and polarized nuclei (purple). (B,E) Four week post-ablation pancreata with near complete loss of zymogenic staining outside the small, zymogenic clusters of cells (white outlines). (C,F) Recovering, six week post-ablation pancreatic sections with dense stromal infiltrate (black arrows) and tubular complexes (yellow arrow). The majority of the acinar compartment has been restored.

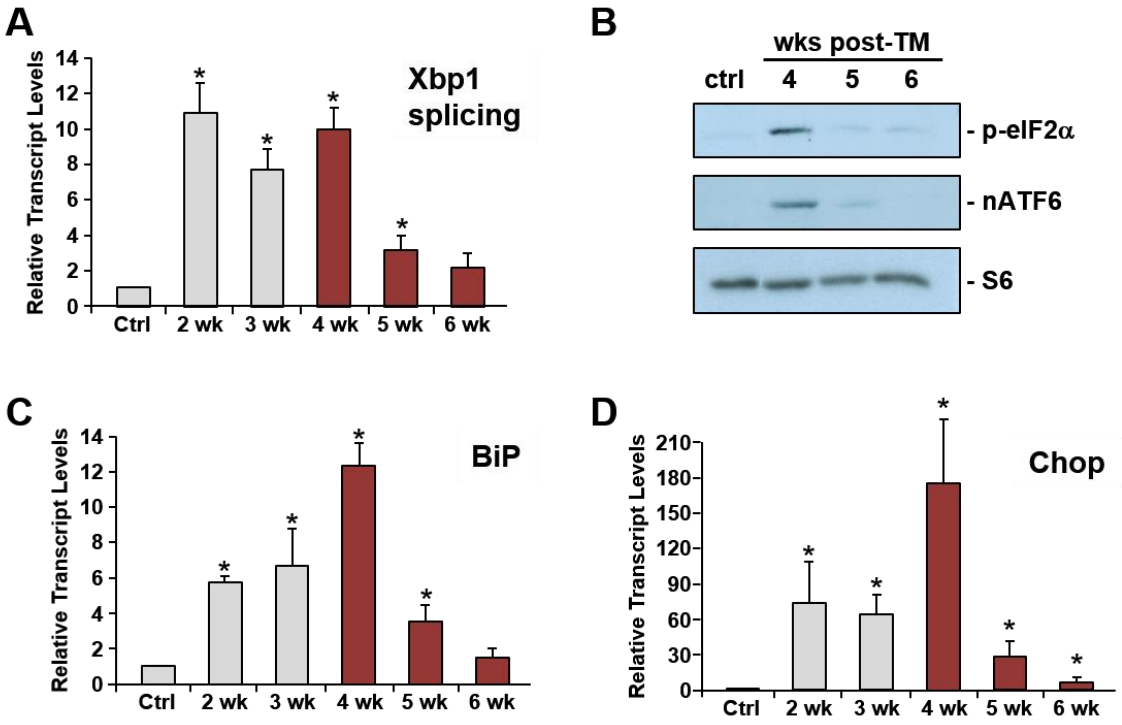

Figure 4.5 *Pancreas-wide UPR activity returns to near-basal levels following loss of the Xbp1$^{\Delta Ex2}$ acinar population*

(A) IRE1 activity (as determined by RT-qPCR analysis of splicing of the *Xbp1* transcript) escalates up to four weeks post-ablation and then returns to control levels by six weeks. (B) Protein blot of pancreatic homogenates shows that activation of the PERK (p-eIF2α) and ATF6 (nATF6) branches also returns to control levels by 6 weeks. (C) Downstream effector *BiP* was elevated and then returned to control levels as determined by RT-qPCR. (D) Expression of *Chop* was drastically reduced in recovering pancreata, although not quite reaching control levels. (* = p-value < 0.05 relative to control samples, normalized to 18s expression)

reaching wild-type levels by six weeks post-ablation. This was accompanied by a similar reduction in UPR activity in the PERK and ATF6 UPR branches as determined by protein analysis of pEIF2α and nATF6 levels **(Figure 4.05b)**. RT-qPCR analysis was conducted on the UPR downstream effectors *BiP* and *Chop*, both of which were reduced to control (*BiP*) or near-control (*Chop*) levels by six weeks post-ablation **(Figure 4.05c-d)**. These results indicated that UPR activation had returned to basal levels following ER stress crisis in the *Xbp1*$^{\Delta Ex2}$ acinar cells. As a next step, we investigated whether zymogen production and localization were similarly returned to wild-type levels in the post-crisis acinar cells.

RT-qPCR analysis of *Amylase* transcripts revealed a pronounced increase in expression following the ER stress crisis observed at four weeks post-ablation in *Mist1*$^{CreER/+}$; *Xbp1*$^{\Delta Ex2}$ mice **(Figure 4.06a)**. This was accompanied by increased protein levels for amylase as well as a reduction in aberrantly activated carboxypeptidase A **(Figure 4.06b)**, indicating reduced zymogen autoactivation and thus damage within the exocrine compartment. Immunofluorescence for amylase staining on 4-week post-ablation pancreatic sections revealed tightly concentrated pockets of amylase expression restricted to the previously described zymogenic, *Xbp1*$^{fl/fl}$ acinar cell population **(Figure 4.06c, white outlines)**. This was in stark contrast to 6-week post-ablation sections **(Figure 4.06d)** in which amylase was more diffused throughout the pancreas. This confirmed that the reestablished acinar population observed in **Figure 4.04** was correctly expressing and localizing intracellular zymogens. The 6-week exocrine compartment also showed an increased presence of ductal cells and duct-like structures, previously described in section 4.2 **(Figure 4.06d, red outlines)**.

Closer analysis of six week post-ablation pancreatic sections indicated that the recovery process within the pancreas was accompanied by increased fat deposition **(Figure 4.07a,b)**. Fat deposition is a known hallmark of acute pancreatic damage, and in this model it is a likely consequence of acinar cell destruction following loss of the *Xbp1*$^{\Delta Ex2}$ population (Klöppel et al., 2004). Additionally, the intra-acinar spaces were analyzed for expression of the ductal marker SOX9. As shown in **Figure 4.07b**, large numbers of

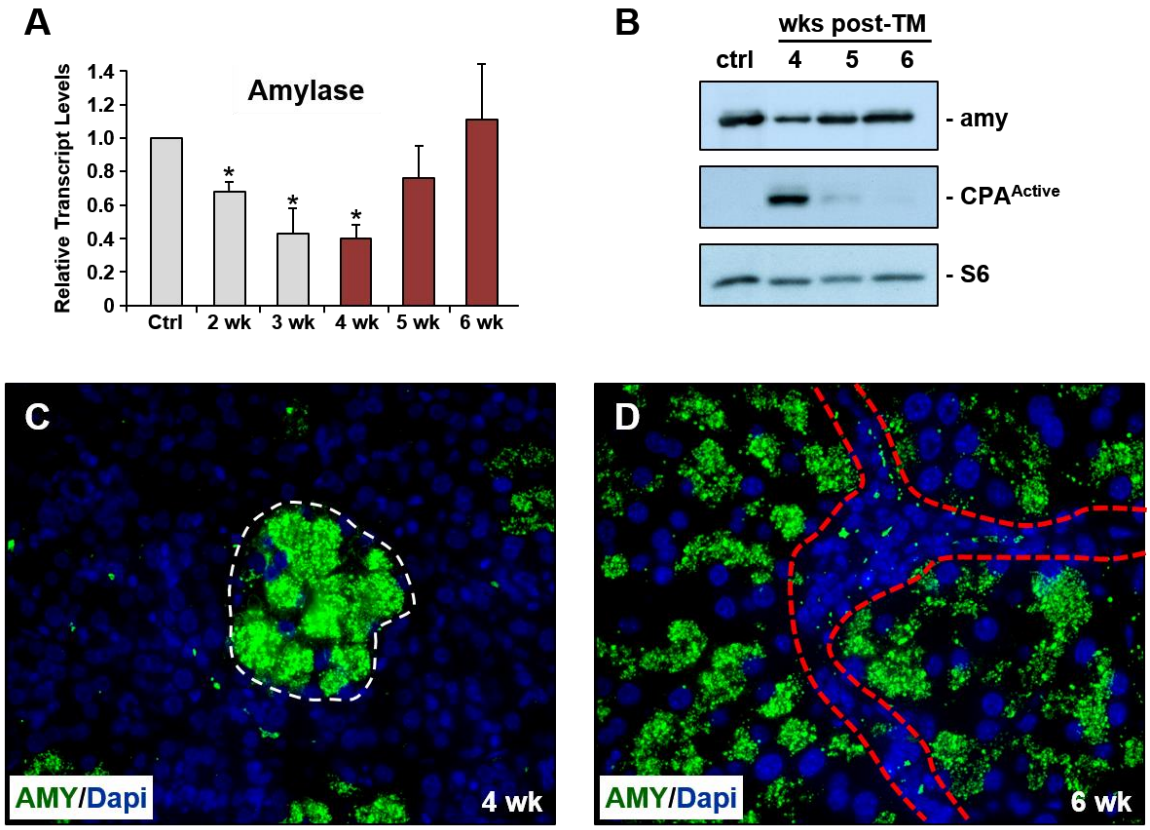

Figure 4.6 Acinar parameters including *zymogen synthesis, localization, and activation all return to normal in recovering Xbp1$^{\Delta Ex2}$ pancreata*

(A) RT-qPCR of amylase transcripts reveals a return to control expression levels during recovery. (B) Protein blot of amylase (amy) and damage-induced activated carboxypeptidase-A (CPA^{Active}) indicating that amylase protein increases to control levels during recovery while CPA^{Active} disappears. (C) Immunofluorescence staining showing the restriction of strong amylase staining to the zymogenic, *Xbp1$^{fl/fl}$* acinar cells (white outlines) in 4 week post-ablation pancreata. (D) Immunofluorescence staining showing a return to clustered, distributed amylase in recovering pancreata. Red outlines depict amylase-negative ductal and stromal cells in the periacinar space. (* = p-value < 0.05 relative to control samples, normalized to 18s expression)

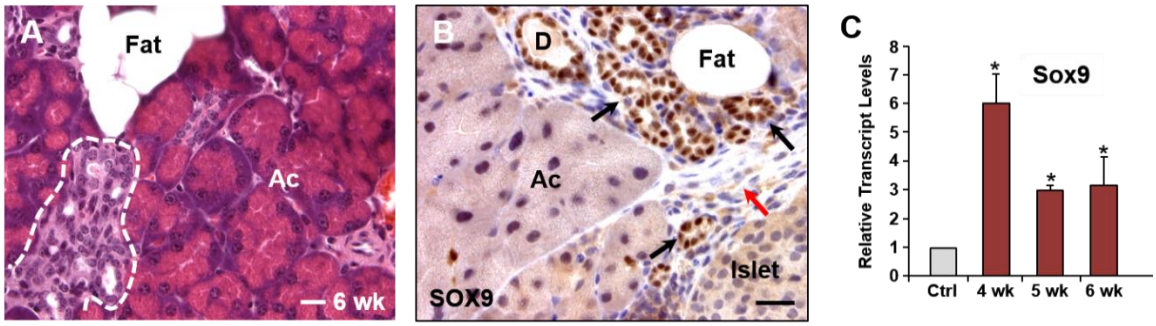

Figure 4.7 Recovering pancreata express high levels of the ductal/progenitor marker SOX9

(A) Six week post-ablation pancreatic sections have signs of damage including fat deposition and formation of duct-like tubular complexes (white outlines). (B) Staining for the ductal marker SOX9 shows extensive expression in normal ducts (D) and ductal/tubular complexes (black arrows) but not in the stromal cells (red arrow) or acinar tissue (Ac). (C) *Sox9* transcripts are elevated during peak damage but remain high in recovering pancreata. (* = p-value < 0.05 relative to control samples, normalized to 18s expression)

ductal cells **(black arrows)** accumulate in recovering pancreata, a separate response from the previously described mixed inflammatory cells **(red arrow)**. These duct-like cells are primarily in the form of tubular complexes, also a known facet of pancreatic damage (Strobel et al., 2007). RT-qPCR similarly revealed increased expression of *Sox9* during and continuing after acinar cell crisis **(Figure 4.07c)**. This is likely due to the persistent ductal cell population observed in these pancreata.

4.4 Exocrine regeneration following loss of *Xbp1$^{\Delta Ex2}$* acini is accompanied by proliferation of both the acinar and centroacinar compartments

The restoration of normal acinar parameters in the recovering *Mist1$^{CreER/+}$*; *Xbp1$^{\Delta Ex2}$* exocrine compartment, coupled with the TUNEL-labeled non-zymogenic acinar cells reported in Chapter 3, strongly suggested that cells lacking XBP1 died and were replaced with new acinar cells. There was, however, a possibility that the restored acinar compartment could have been composed of acinar cells that managed to overcome the lack of XBP1 and resume their normal program. Indeed histological analysis of pancreatic sections in 6 week post-ablation mice revealed areas with small acini expressing low levels of zymogen **(Figure 4.08a, white outlines)**. Additionally, expression analysis of RNA samples utilizing primers specific for the *Xbp1$^{\Delta Ex2}$* transcript revealed persistent, low levels of expression **(Figure 4.08b)**, possibly indicating a subpopulation of *Xbp1$^{\Delta Ex2}$* cells that survived within the pancreas.

In order to test whether *Xbp1$^{\Delta Ex2}$* acinar cells were contributing to the restored acinar compartment, we performed lineage tracing experiments using the *Mist1$^{CreER/+}$; Xbp1$^{\Delta Ex2}$; R26^{LacZ}* reporter line. As described in Chapter 3 **(Figure 3.02)**, cells in *Mist1$^{CreER/+}$*; *Xbp1$^{\Delta Ex2}$* ; *R26^{LacZ}* mice express the β-galactosidase gene in response to Cre activity. This expression occurs following a permanent, Cre-mediated DNA splicing event that marks both Cre-expressing cells and their progeny. As shown in **Figure 4.08c**, staining of stressed 4 week post-ablation pancreatic sections for β-galactosidase expression revealed that the minor zymogenic acinar population was β-gal negative, while the majority of the non-zymogenic acinar cells were β-gal positive and thus lacked XBP1. Matched staining performed on 8 week post-ablation pancreata **(Figure 4.08d)** showed

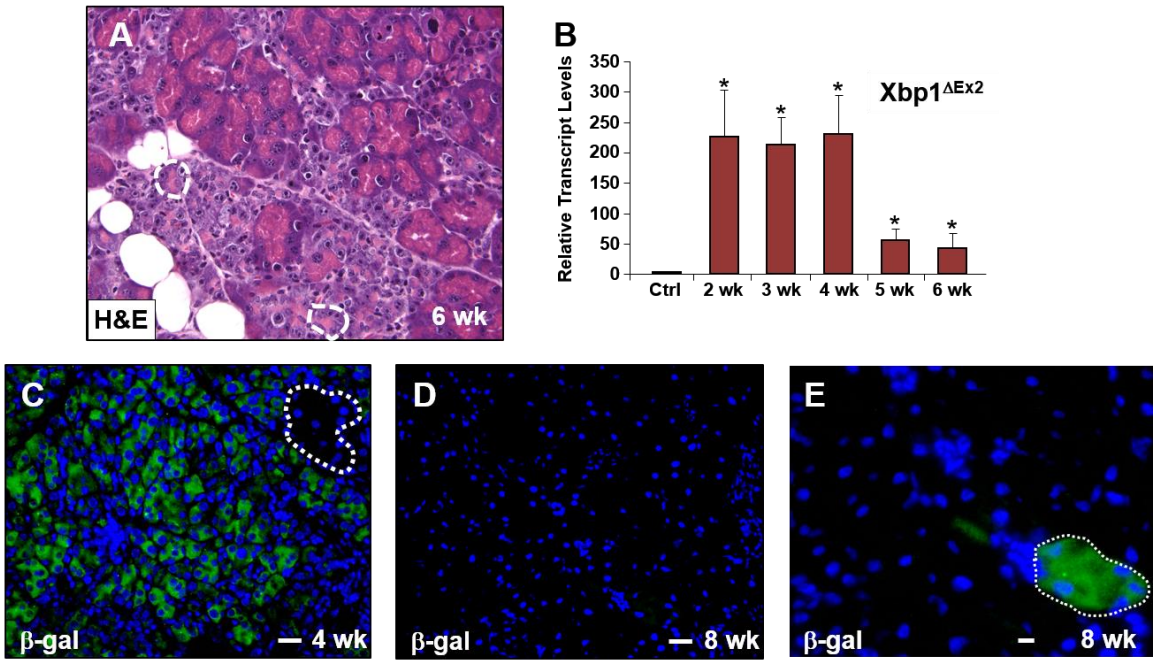

Figure 4.8 Regenerated acinar cells are derived from a non-Xbp1$^{\Delta Ex2}$ lineage

(A) Histological stain showing persistent, small acini (white outlines) within recovering (6 week post-ablation) pancreata. (B) RT-qPCR analysis of the Cre-remodeled *Xbp1$^{\Delta Ex2}$* transcript shows a significant reduction in levels during recovery, although still above control (no tamoxifen) values. (C) β-galactosidase (β-gal) immunofluorescence analysis of four week post-ablation pancreatic sections indicates that non-zymogenic cells expressed active Cre for recombination while the zymogenic acini (white outline) did not. (D) β-gal analysis of 8 week post-ablation pancreata indicates that restored acinar cells are not derived from cells that underwent Cre-mediated DNA recombination. (E) β-gal analysis shows rare isolated acini that were positive for β-gal but with normal zymogen content and no signs of ER stress. (* = p-value < 0.05 relative to control samples, normalized to 18s expression)

that the recovered acinar compartment was almost entirely β-gal negative, indicating that these acinar cells were not derived from the *Xbp1*$^{\Delta Ex2}$ population. Interestingly, a small minority of isolated acini remained β-gal positive despite no obvious cell defects **(Figure 4.08e).** These cells likely represent acinar cells in which the open ROSA26 (reporter) locus was recombined while both copies of the endogenous *Xbp1*$^{fl/fl}$ locus was not. Given the overwhelmingly β-gal negative state of the restored acinar compartment, we sought to investigate which pancreatic lineage was responsible for the acinar regeneration response observed in this model.

Initial investigation of recovering pancreata revealed visual evidence of proliferating acinar cells via the presence of mitotic figures **(Figure 4.09a)**. This was supported by immunohistochemical staining for the proliferation marker Ki67 which showed a distinct and significant increase in proliferative cells following ablation of *Xbp1* **(Figure 4.09b)**. Regeneration was further confirmed by coexpression of Reg1, a protein known to be associated with regenerating pancreatic cells (Okamoto, 1999). These data suggested that the restoration of normal acinar properties in recovering acinar cells was due to both proliferative and regenerative mechanisms.

We next sought to investigate the nature of the exocrine restoration via population analysis of proliferative staining patterns. As shown in **Figure 4.10a,b**, cells positive for both Ki67 and the mitosis-associated phospho-histone 3 (pH3) were found within the zymogenic, *Xbp1*$^{fl/fl}$ acinar population in 4 week post-ablation pancreata. This is consistent with previous findings utilizing caerulein-induced pancreatitis that indicated that preexisting acinar cells give rise to new acinar cells during pancreatic damage (Strobel et al., 2007). Interestingly, however, proliferative analysis also revealed Ki67 staining within the centroacinar compartment **(Figure 4.10c-e)**, a HES1/SOX9-positive cell type that has also been implicated in separate studies as a possible source for regenerating acinar cells (Criscimanna et al., 2011). Unfortunately, it is not possible to use lineage tracing in these cells because neither the zymogenic acinar nor centroacinar compartments would express β-gal, since zymogenic cells did not undergo Cre-mediated recombination and centroacinar cells do not have an active *Mist1* promoter to express the Cre protein. Therefore, the restored acinar compartment could be regenerated by either the preexisting acinar or centroacinar compartments.

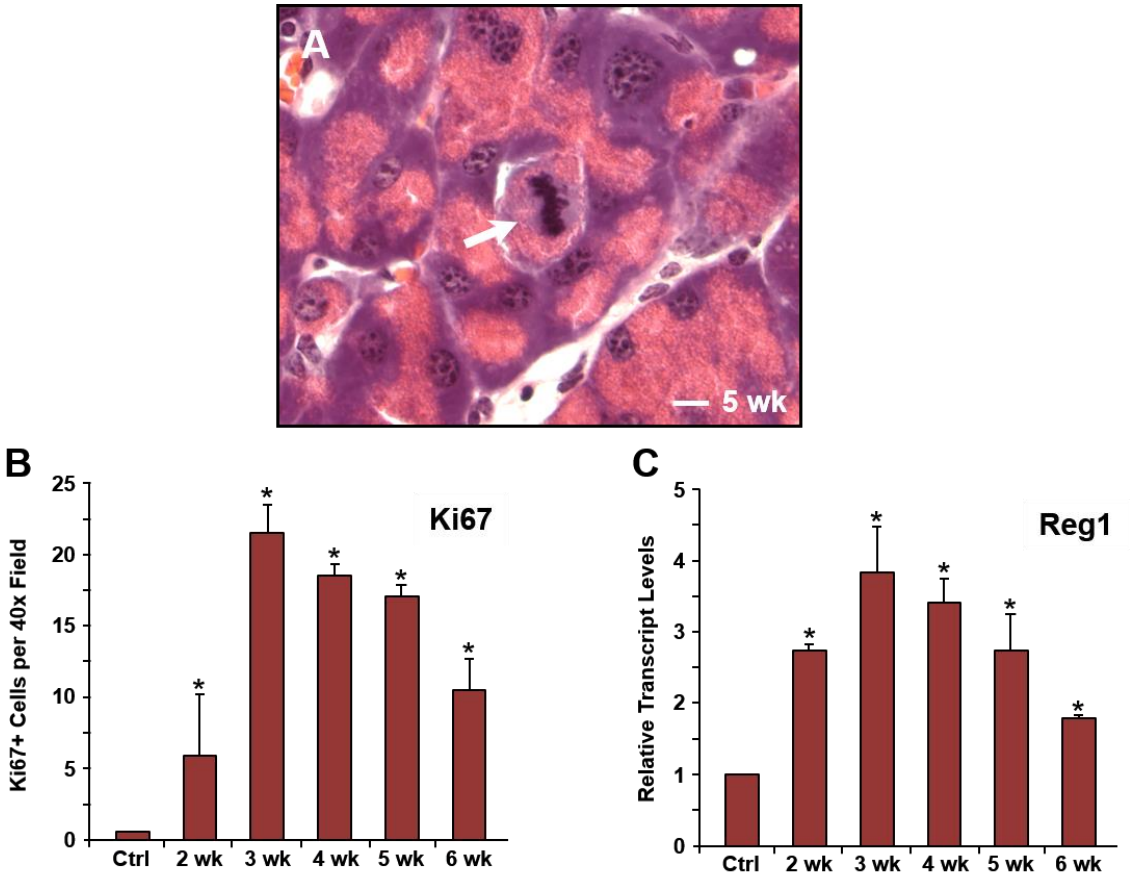

Figure 4.9 *Recovering pancreata display visible signs of proliferation and express proliferative and regenerative markers*

(A) Histological examination of early recovering pancreata (5 weeks post-ablation) reveals the presence of mitotic figures in the regenerating acinar compartment. (B) Analysis of immunohistochemical stains for the proliferative marker Ki67 shows a significant increase in proliferation as cell damage peaks followed by a reduction in staining during late recovery. (C) RT-qPCR analysis of RNA isolates shows an increase in the pancreatic recovery-associated factor *Reg1* as ER stress accumulates followed by a reduction during recovery. (* = p-value < 0.05 relative to control samples, Fig. C normalized to 18s expression)

4.5 Recovered pancreata retain abnormal long-term histological features but show no evidence of increased pancreatic malignancies

Fully regenerated acinar cells (12 weeks post-ablation) in *Mist1*$^{CreER/+}$; *Xbp1*$^{\Delta Ex2}$ mice display no evidence of higher than normal ER stress and express wild-type levels of amylase. From a morphological perspective, however, the process of regeneration was seen to alter the structure of the restored cells. As shown in **Figure 4.11a**, the overall area of localized zymogens per acinus **(white outlines)** increased in *Mist1*$^{CreER/+}$; *Xbp1*$^{\Delta Ex2}$ mice relative to control animals. This effect is quite striking at high magnification **(Figure 4.11b, right)**, where immunofluorescence analysis of amylase revealed a nearly membrane-to-membrane distribution of zymogen granules within a recovered acinus. This pattern was very different from the focal, apically-localized zymogen granules observed in control cells. Quantification of cell and nuclear area in post-ablation cells via analysis of E-cadherin stained pancreatic sections showed a progressive increase in both attributes **(Figure 4.11c)**. This increase began to lessen by 12 weeks post-ablation, though still remained significantly higher than wild-type animals.

Given the previously reported link between inflammation and increased likelihood of pancreatic cancer development (Farrow and Evers, 2002), we also sought to investigate whether ablation of *Xbp1* would increase the likelihood of developing pancreatic malignancies. *Mist1*$^{CreER/+}$; *Xbp1*$^{\Delta Ex2}$ mice were allowed to age for 12 months following ablation. As shown in **Figure 4.12a**, pancreata in these animals have a largely unremarkable acinar compartment populated by histologically normal acinar cells. Extensive fat deposits, first observed at six weeks post-ablation, remained throughout the pancreas **(Figure 4.12b-d)**, although tubular complexes are largely absent, indicating a return to steady-state conditions. Examination of the tissue for precancerous lesions revealed a general lack of PanINs, although several small proliferative ductal lesions were apparent **(Figure 4.12c,d – black boxes)**. The observed lesions were presumably derived from the *Xbp1*$^{fl/fl}$ tissues in response to the inflammatory environment generated, since we had previously demonstrated that these mice had nearly complete loss of the *Xbp1*$^{\Delta Ex2}$ acinar population. These lesions expressed high levels of mucin (light pink staining) but did not show any degree of nuclear stacking, a

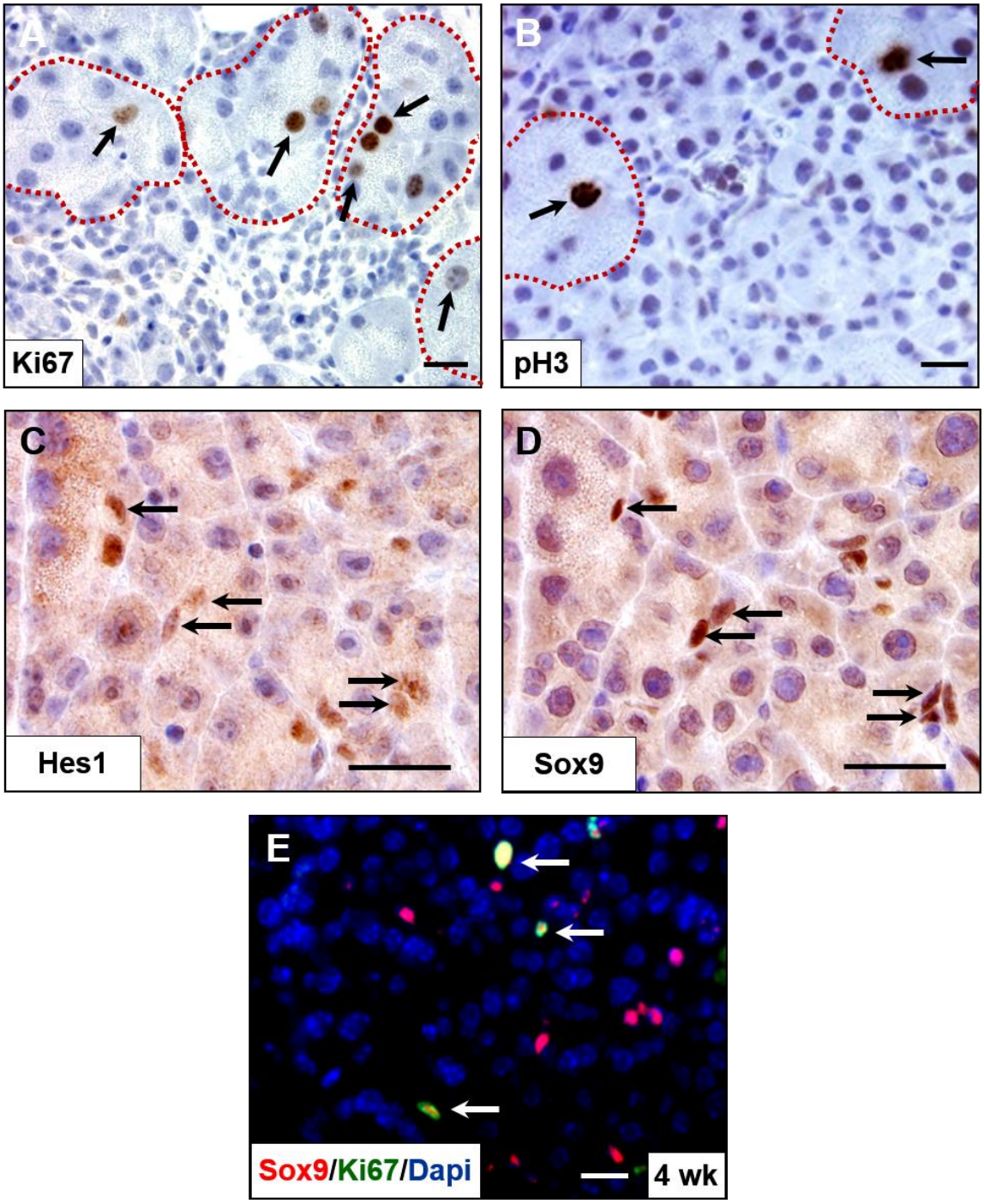

Figure 4.10 *Proliferation takes place in multiple cell compartments following ER stress-induced death of the Xbp1$^{\Delta Ex2}$ acinar cells*

(A,B) Ki67 and phospho-Histone 3 (pH3) stainings of 4 week pancreatic sections show expression (black arrows) and proliferation in the *Xbp1$^{fl/fl}$* acinar population. (C,D) Staining shows coexpresion of HES1 and SOX9 in centroacinar cells (black arrows). (E) SOX9 and Ki67 colocalize (white arrows) in centroacinar cells following damage.

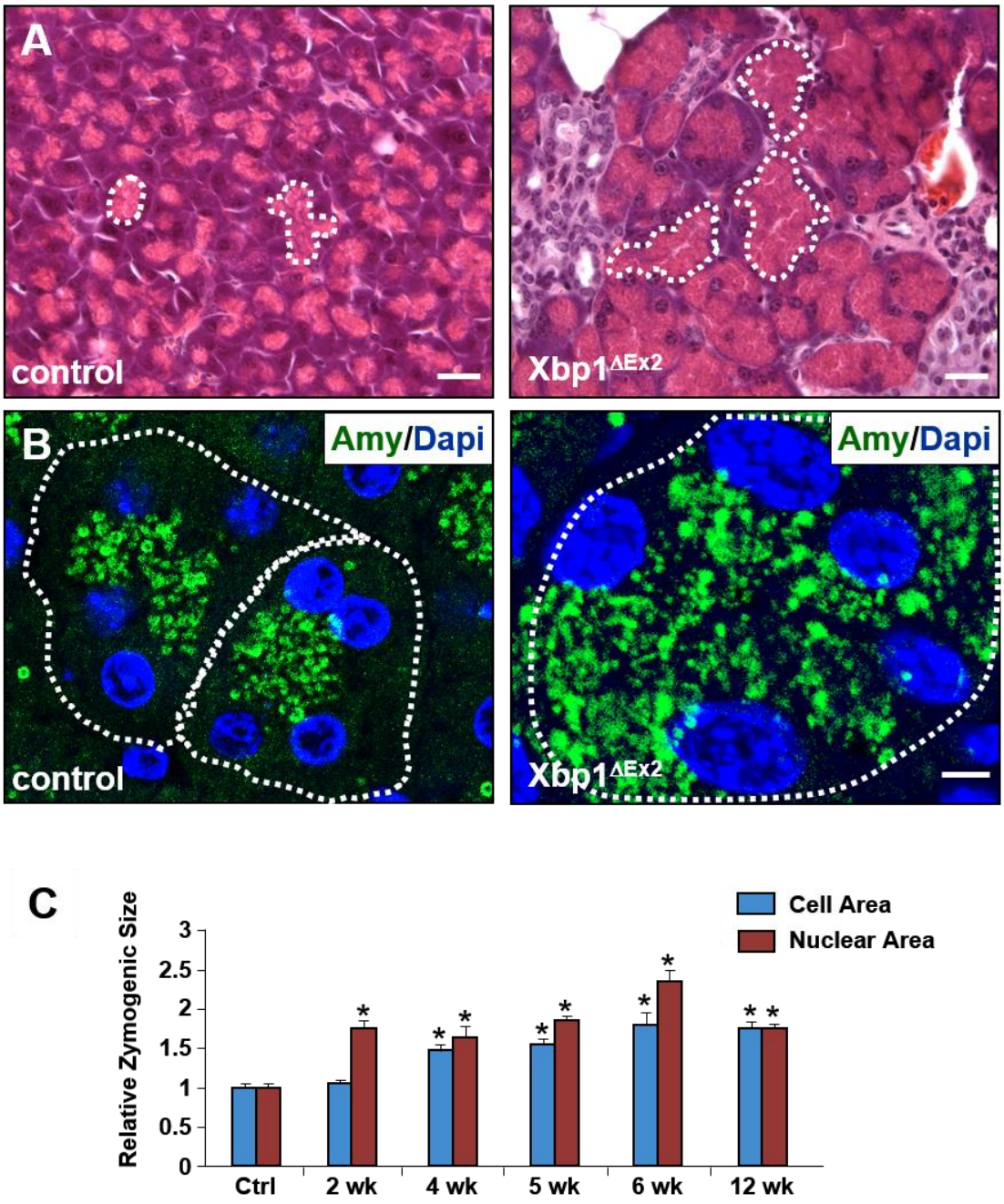

Figure 4.11 *Regenerated acinar cells are larger than control cells and contain more widely distributed zymogen granules*

(A) Comparison of control and 12 week post-ablation pancreata showing a larger zymogen compartment (white outlines). (B) Amylase stain revealing cell-wide zymogen localization of amylase vs. tight, apical localization in control pancreata. Outlines denote cell boundaries among individual acini. (C) Quantification of cell and nuclear size shows increases relative to control that persist through 12 weeks post-ablation. (* = p-value < 0.05 relative to control samples)

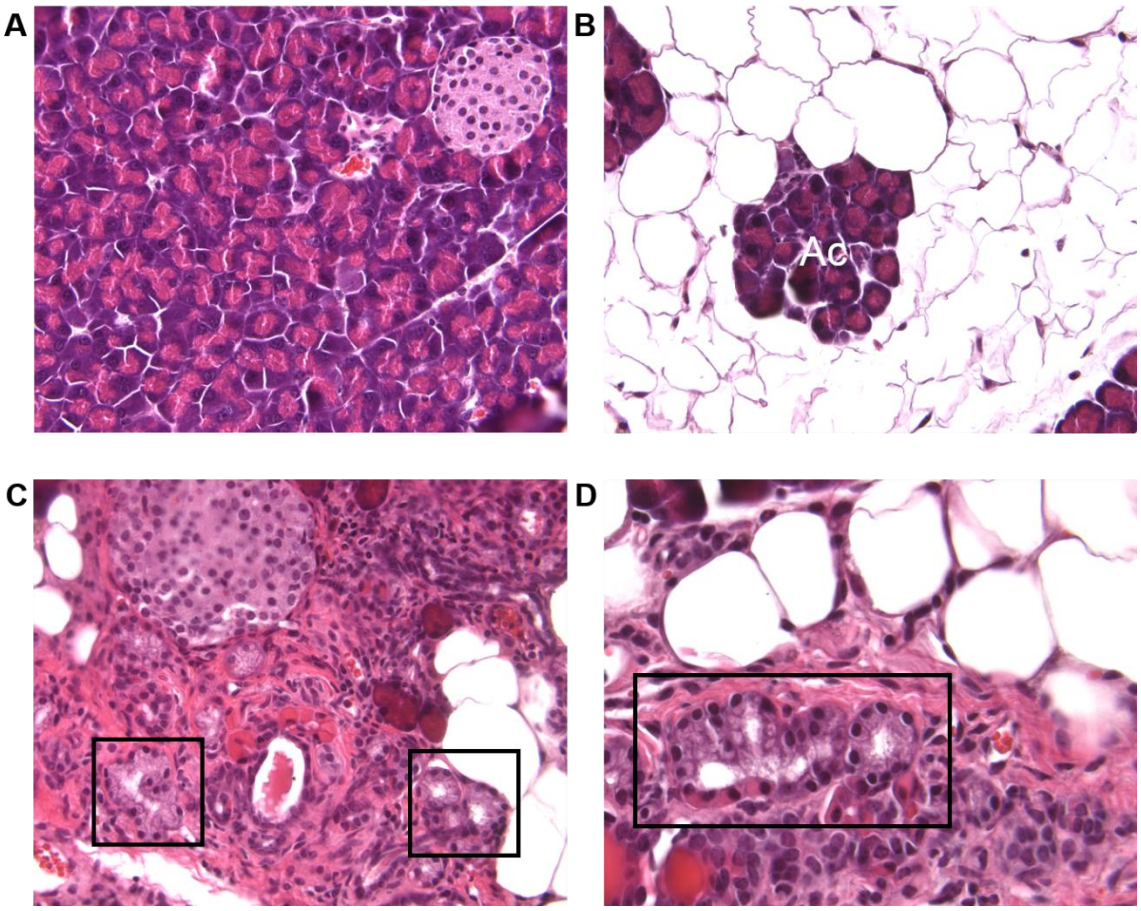

Figure 4.12 *12 month post-ablation pancreata have normal acinar compartments but persistent signs of damage*

(A) 12 month post-ablation acinar cells have normal histological appearance and zymogen localization. (B) Fat deposition remains throughout the pancreas, although healthy acinar cells (Ac) exist within the deposits. (C) Histologically unusual areas exist in 12 month post-ablation pancreata including ductal structures (black boxes). (D) High-magnification image of a ductal structure (black box) showing mucinous deposition (purple stain) but no nuclear atypia.

known histological feature of developing PanINs **(Figure 4.01a)**. The lack of typical precancerous lesions is not unexpected, as previous reports have shown that even the presence of the potent the *Kras*^{G12D} oncogene is unable to rapidly generate pancreatic tumors without the addition of either other oncogenes or inflammation via induced pancreatitis (Guerra et al., 2007; Hruban et al., 2006). We thus sought to investigate whether addition of a Cre-inducible *Kras*^{G12D} transgene (LSL-Kras) into the *Mist1*$^{CreER/+}$*; Xbp1*$^{fl/fl}$ line would lead to increased development of PanIN lesions immediately following ER stress-induced acinar cell loss.

Mist1$^{CreER/+}$*; Xbp1*$^{fl/fl}$*; LSL-Kras*^{G12D} (XKC) mice were generated through standard breeding techniques. These mice underwent acinar-specific *Xbp1* ablation with simultaneous expression of the *Kras*^{G12D} oncogene **(Figure 4.01b)**. Activation of the *LSL-Kras*^{G12D} transgene in otherwise normal mice (*Mist1*$^{CreER/+}$*; LSL-Kras*^{G12D}, or KC mice) leads to formation of small, focal PanIN lesions with occasional advanced, mucinous neoplasms and desmoplasia by six weeks post-Cre administration **(Figure 4.13 a,b, yellow outlines)**. We therefore administered tamoxifen to KC and XKC mice and sacrificed the animals at six weeks post-ablation/activation to determine whether these animals exhibited increased susceptibility to PanIN formation.

As shown in **Figure 4.13c**, XKC mice have extensive stromal infiltration of their periacinar spaces by six weeks post-tamoxifen. This is consistent with standard *Mist1*$^{CreER/+}$*; Xbp1*$^{\Delta Ex2}$ mice that are recovering from loss of the *Xbp1*$^{\Delta Ex2}$ acinar population, indicating that a similar apoptotic fate was encountered by the *Xbp1*$^{\Delta Ex2}$*; LSL-Kras* acinar cells as their counterparts lacking Kras expression. We then used standard histological stains on isolated pancreatic extracts in order to identify and quantify the types and numbers of lesions found in both Mist1$^{CreER/+}$*; Xbp1*$^{\Delta Ex2}$*; LSL-Kras* mice and control animals lacking the *Xbp1*$^{fl/fl}$ allele. As shown in **Figure 4.13d**, mice in which *Xbp1* had been ablated had significantly fewer small lesions as well as half as many advanced lesions. These data show that ablation of *Xbp1* results in significantly fewer small lesions per section as well as half as many advanced lesions indicating either a refraction to KRAS^{G12D}-induced lesion formation of or a loss of KRAS-transformed cells.

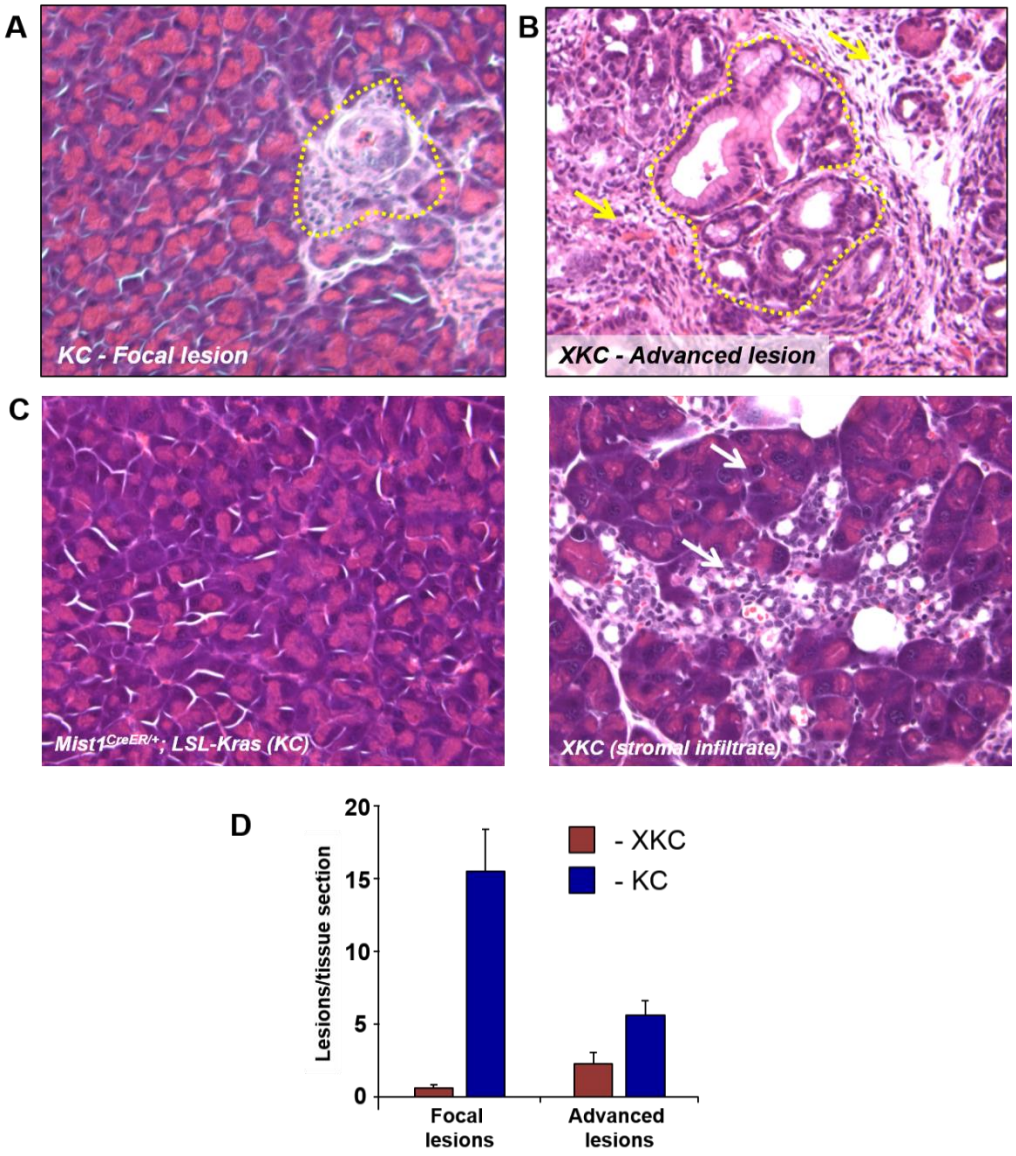

Figure 4.13 *Ablation of Xbp1 reduces occurrence of ADM and early PanINs in XKC mice*

(A) H&E stain of a focal, KRAS-derived lesion (yellow outline). (B) H&E stain of an advanced lesion (yellow outline) with extensive stromal infiltrate (red arrows). (C) Comparison of the acinar compartments of 6 week post-tamoxifen *Mist1*$^{CreER/+}$*; LSL-Kras*^{G12D} (KC) mice and *Mist1*$^{CreER/+}$*; Xbp1*$^{fl/fl}$*; LSL-Kras*^{G12D} (XKC) mice reveals extensive stromal infiltrate and tubular complex formation (white arrows) in XKC mice. (D) Histogram showing numbers of focal and advanced lesions in XKC vs. KC mice per tissue section. There is a nearly 16-fold reduction in focal lesions along with a 2-fold reduction in advanced lesions in XKC mice.

4.7 Discussion

Studies of pancreatitis damage often focus on rapid, organ-level responses or long term development of malignancies. Specifically, the use of rodent models to study damage as it relates to oncogenesis often utilizes expression of activated mutant forms of KRAS, an intrinsic stressor that drives transformation (Hruban et al., 2006). These studies allow an exquisite level of genetic and chemical cell manipulation for studying acinar responses, but fail to account for the effects of chronic damage or inflammation on cancer progression. In contrast, research involving pancreatitis typically uses administration of the secretagogue caerulein to trigger supramaximal levels of aberrant zymogen secretion (Jungermann et al., 1995). This damage event mimics the appearance of severe acute pancreatitis in human patients including the appearance of inflammatory infiltration of the periacinar spaces, loss of exocrine tissue, and edema (Niederau et al., 1985). Supramaximal zymogen secretion, however, is not a recognized cause of pancreatitis in human patients, most of whom exhibit acinar cell loss and inflammation following pancreatic duct obstruction by gallstones (Jha et al., 2009). Additionally, induction via large doses of caerulein produces inconsistent disease states with mild to severe inflammation and a large degree of variability in time until recovery (Su et al., 2006). Other pancreatitis model systems have similar issues with variable inflammatory induction and variable timing until recovery, making none of the existing systems ideal for investigating acinar and organ regeneration in response to severe instrinsic stresses including ER stress. In this study we characterized recovering pancreata in *Mist1*$^{CreER/+}$*; Xbp1*$^{\Delta Ex2}$ mice **(Figure 4.14)** following extensive ER stress-induced acinar cell death in order to establish that a near complete exocrine recovery is accompanied by expansion of the acinar and centroacinar compartments.

The extensive acinar cell death observed in *Mist1*$^{CreER/+}$*; Xbp1*$^{\Delta Ex2}$ mice **(Figure 3.10)** triggered formation of ductal tubular complexes, collagen and stromal matrix deposition, and infiltrating immune cells **(Figure 4.02)**. The stromal and immune components of this response are a key finding as recent studies have indicated that stromal-epithelial interactions may play a substantial role in progression of cancer (Hwang et al., 2008). Furthermore, the activation of embryonic signaling pathways **(Figure 4.03)** mimics both *in vitro* (Means et al., 2005) and *in vivo* (Fendrich et al., 2008) work demonstrating

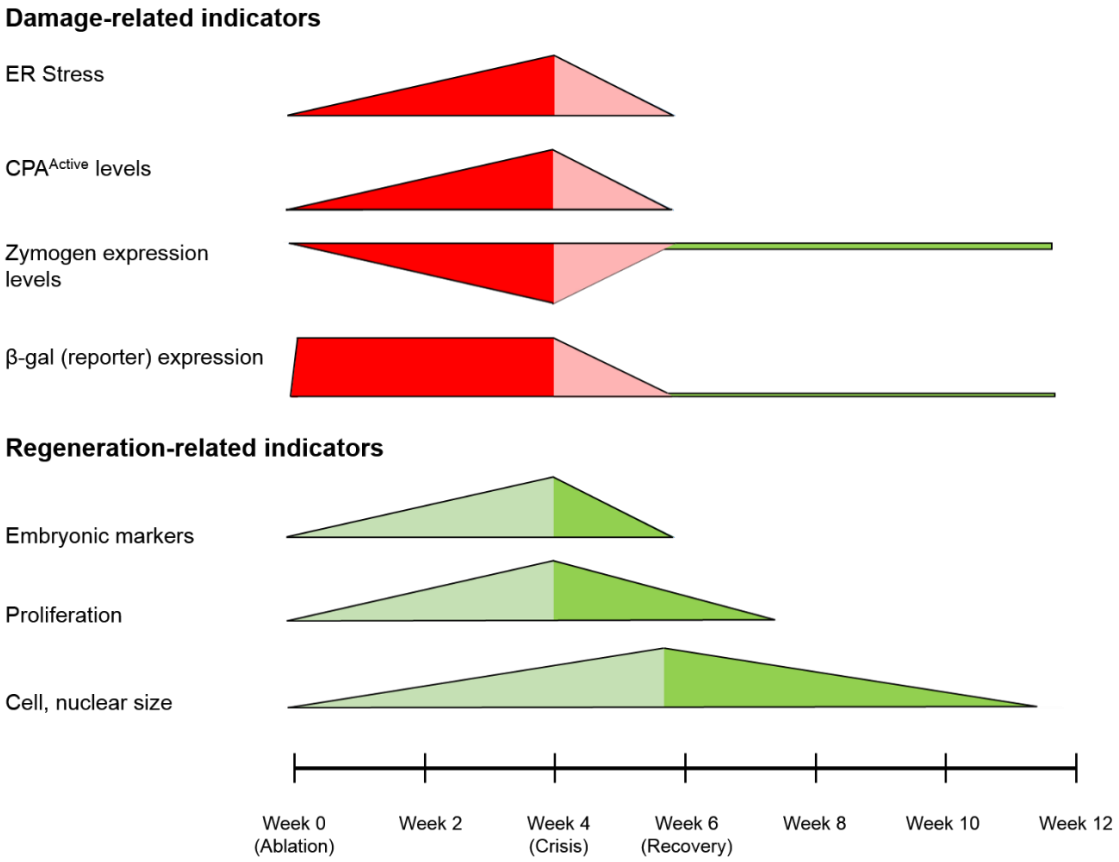

Figure 4.14 *Timeline of damage and regeneration in Mist1$^{CreER/+}$; Xbp1$^{\Delta Ex2}$ pancreata*

(A) Schematic summarizing the effects of ablation of *Xbp1* on ER stress, damage, and reporter gene expression before and after crisis. (B) Schematic summarizing the regeneration and recovery phenotypes observed following *Xbp1* ablation.

that the recovery mechanisms following ER stress-induced exocrine damage are consistent with other forms of injury. Additionally, the timing of recovery from the ER stress-induced apoptotic crisis may increase the utility of the *Mist1*$^{CreER/+}$*; Xbp1*$^{\Delta Ex2}$ model for studying pancreatic regeneration, as an extended, two-week window would allow for increased observation of molecular events that occur fleetingly during recovery.

As previously described, caerulein-induced pancreatitis is highly variable in terms of its severity and timing of recovery (Su et al., 2006). In contrast, mice undergoing ER stress-induced acinar cell death in the *Mist1*$^{CreER/+}$*; Xbp1*$^{\Delta Ex2}$ model exhibit an extended and consistent period of damage and recovery. Acinar tissue succumbs to apoptosis on or about the fourth week following ablation **(Figure 4.04)**, with the majority of recovery occurring during a two week period four to six weeks after *Xbp1* ablation. This recovery completely ameliorates the ER stress condition **(Figure 4.05)** while restoring normal exocrine parameters **(Figure 4.06)** and exhibiting stromal and ductal cell remodeling in the periacinar spaces **(Figure 4.07)**. Additionally, acinar cell zymogen compartments remain dilated for at least 12 weeks following ablation **(Figure 4.11)**, but resolve to normal size by 12 months **(Figure 4.12)**. Compensatory mechanisms may be necessitating this altered acinar morphology during the recovery period, but the regenerative process eventually allows cells to resume their normal structure and function. These events all take place over a span of weeks or months and allow for a thorough analysis of cellular and organ responses. This is a distinct advantage over the highly variable and rapid regeneration observed in response to caerulein which fully restores the organ 9-12 days following cessation of treatment (Adler et al., 1979).

While the exact source of regenerated acinar cells in *Mist1*$^{CreER/+}$*; Xbp1*$^{\Delta Ex2}$ pancreata cannot be determined due to limitations in lineage tracing in the system, proliferation analysis indicates that both the acinar and centroacinar compartments reenter the cell cycle **(Figure 4.10)**. This finding could lead to a reexamination of how these two cell types may play a role in regeneration. Indeed, analysis of pancreata 12 months after *Xbp1* ablation indicated persistent damage in the form of fat deposition and ductal lesion formation **(Figure 4.12)**, a unique long-term affect not typically seen in caerulein-induced models of acute pancreatitis. As a result, the *Mist1*$^{CreER/+}$*; Xbp1*$^{\Delta Ex2}$ system could be ideal

for developing intervention strategies, including treatments for pancreatitis, as the long-term effects are persistent and unique compared to those seen in other model systems.

Finally, we examined whether damage inflicted via ER stress-induced acinar cell destruction could exacerbate *Kras*^{G12D}-driven transformation. Our initial hypothesis was that the pro-inflammatory environment generated by loss of the *Xbp1*$^{\Delta Ex2}$ population would increase the occurrence of ductal lesion formation. However, as shown in **Figure 4.13d**, we actually observed a drastic reduction in focal and advanced lesions. Upon further consideration, this is likely due to the high levels of stress that were placed on the *Xbp1*$^{\Delta Ex2}$; *Kras*^{G12D}-expressing acinar cells, who likely succumbed to apoptosis prior to any substantial oncogenic development. Interestingly, while this hypothesis explains the overall lack of small PanIN lesions in the pancreas, the presence of several advanced growths could imply that the inflammatory environment generated by *Xbp1*$^{\Delta Ex2}$-driven apoptosis created a permissive environment for development of lesions from acinar cells that only recombined the LSL-Kras gene without ablation of *Xbp1*. Alternatively, the advanced lesions could represent acinar cells whose transformation had occurred before the onset of *Xbp1* ablation-mediated ER stress, implying that current work investigating ER stress as a means of therapy may need to focus on specific stages of cancer progression. Both hypotheses can be tested in future work utilizing independent induction systems for the *Xbp1*^{flox} allele and expression of KRAS^{G12D}.

This study demonstrates that the *Mist1*$^{CreER/+}$*; Xbp1*$^{fl/fl}$ system is a viable system for generating intrinsic, ER stress-derived damage in the exocrine pancreas. Furthermore, recovery from this damage is prolonged, recapitulating several known characteristics of pancreatic regeneration including stromal deposition, immune cell infiltration, and proliferation of pre-existing cells. This regeneration is consistent in terms of timing, with animals reaching peak pancreatic damage four weeks after *Xbp1* ablation and subsequent full recovery taking place over a period of at least eight weeks. These characteristics make the *Mist1*$^{CreER/+}$*; Xbp1*$^{fl/fl}$ system ideal for studies of acinar cell renewal and pancreatic remodeling during damage and recovery.

CHAPTER 5. MIST1 FUNCTIONS AS A TRANSCRIPTIONAL SCALING FACTOR IN THE XBP1-MEDIATED BRANCH OF THE UNFOLDED PROTEIN RESPONSE

5.1 Introduction

As discussed previously and later in Chapter 6, multiple forms of stress can lead to acinar-ductal metaplasia in the mature pancreas. This ability of acinar cells, once considered a terminally differentiated cell population, to alter their identity to deal with stress reveals the remarkable plasticity governed by transcriptional networks in adult pancreatic tissues. One of the key transcription factors linked to maintenance of the acinar differentiation program is the acinar cell-specific transcription factor MIST1.

MIST1 is a basic helix-loop-helix (bHLH) transcription factor found exclusively in secretory tissues including secretory B cells, zymogenic chief cells, and pancreatic acinar cells (PACs) (Capoccia et al., 2011; Pin et al., 2000). In the pancreas, MIST1 is restricted to healthy acinar cells **(Figure 5.01a)** and is known to be downregulated as an early feature seen in human ADM lesions **(Figure 5.01b)**. While MIST1 is not essential for pancreatic development, its presence is refractory to ADM lesion formation, as *Mist1*^{KO} mice develop spontaneous ductal lesions as they age (Pin et al., 2001). This suggests that MIST1 plays a role in maintaining acinar cell identity via regulation of its transcriptional targets.

MIST1 has also been shown to be essential for a number of normal acinar cell properties including cell communication, coordinated secretion, and refraction to oncogenic and pancreatitis-induced acinar cell damage (Direnzo et al., 2012; Kowalik et al., 2007; Shi et al., 2012). Importantly, these phenotypes are all reversed upon exogenous expression of a Cre-inducible MIST1 transgene in adult pancreata, indicating that MIST1 actively maintains adult PACs rather than merely facilitating their proper development (Direnzo et al., 2012). The nature of how MIST1 activates its targets is still under active investigation.

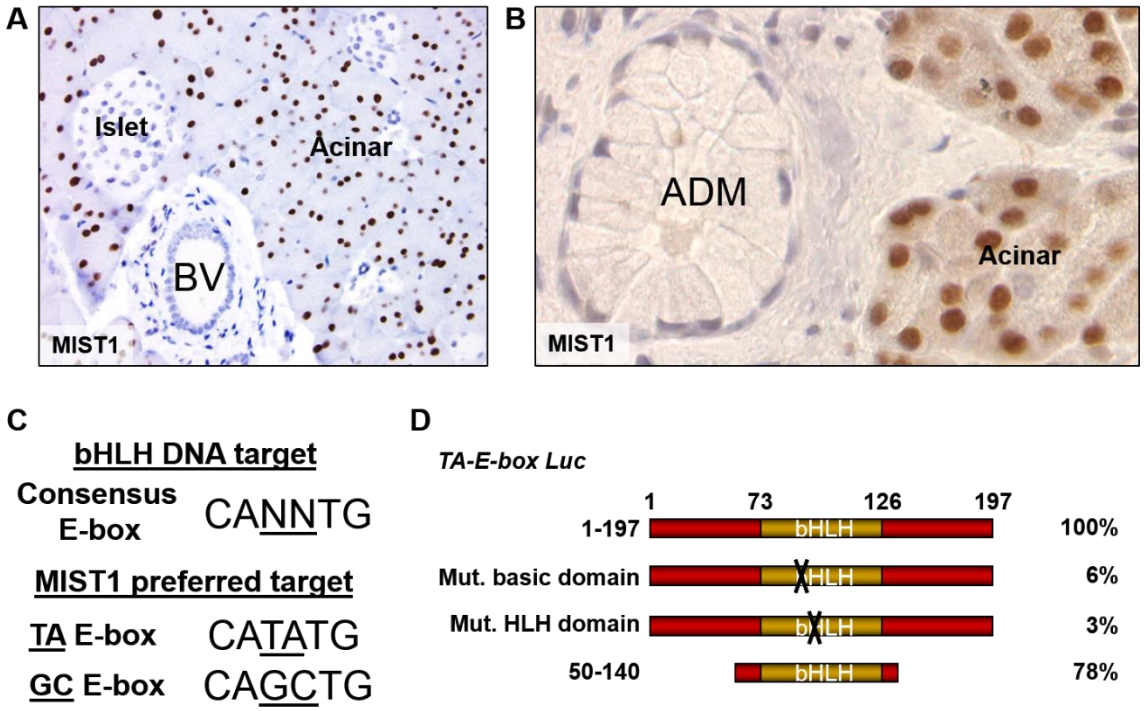

Figure 5.1 *MIST1 is a basic helix-loop-helix transcription factor expressed in pancreatic acinar cells*

(A) Immunohistochemical (IHC) stain for MIST1 shows expression in acinar tissue but not in islets or blood vessels. (B) IHC stain on a human tissue specimen reveals a lack of MIST1 expression in ADM lesions. (C) Consensus sequences for a general E-box as well as the preferred MIST1 binding sequences. (D) Diagram of MIST1 truncations and relative transcriptional activity, revealing that the bHLH region is sufficient to activate MIST1 target gene expression.

MIST1 is a classic bHLH transcription factor, binding to DNA target sequences termed E-boxes (enhancer boxes) and, more specifically the TA and GC variants **(Figure 5.01c)** (Direnzo et al., 2012). However, MIST1 has been shown to lack a recognized transcriptional activation domain (Tran et al., 2007). In fact, MIST1 can still activate or repress its transcriptional targets even when truncated down to only its DNA binding bHLH domain **(Figure 5.01d)** (Tran et al., 2007). This activity is under current investigation in the Konieczny lab in an attempt to identify whether MIST1 serves as the DNA targeting component of a bHLH protein:protein complex with a transcriptional activator or repressor. Recent work by others, however, has postulated that MIST1 is part of a relatively new class of transcriptional regulators termed “scaling factors” (Mills and Taghert, 2012).

The concept of a scaling factor purports that cells utilize unique transcription factors to more effectively specialize in specific tasks following initial differentiation during development (Mills and Taghert, 2012). These factors would function to scale up certain features including expansion of an extensive secretory compartment or a regulated, polarize cellular architecture in secretory cells. Importantly, these genes would not be required for the initial establishment of many cell features, but adult cells would require their constitutive expression in order to maintain a fully functional repertoire of unique, cell-specific capabilities. MIST1 is a prime candidate for classification as a scaling factor, as it is not essential for development of the acinar cell secretory machinery or for initial specification, but mature acinar cells lacking MIST1 have impaired secretion and a predisposition to transdifferentiate (Direnzo et al., 2012; Pin et al., 2001). Interestingly, MIST1 is also found exclusively in serous secretory cells, indicating that its scaling capabilities may be responsible for increasing the secretory capacity of specialized cells (Pin et al., 2000). This characterization of MIST1’s role in acinar cells is remarkably similar to the description of many features of the unfolded protein response, which is itself a specialized transcriptional network designed to facilitate high protein throughput in secretory cells.

The UPR is a reactive transcriptional response in which misfolded proteins trigger activation of three distinct ER-embedded sensors; (PKR)-like ER kinase (PERK), activating transcription factor 6 (ATF6), or inositol requiring enzyme 1 (IRE1) (See

Figure 1.05 for summary) (Walter and Ron, 2011). IRE1 activates its targets via a unique endoribonuclease domain that cleaves a 26 nucleotide fragment from the mRNA of the *Xbp1* gene, which causes a frameshift in the translated XBP1 protein (Ron and Walter, 2007). This protein, termed XBP1s, then proceeds to the nucleus where it activates its transcriptional targets. We previously have shown that XBP1s is essential for proper functioning of the UPR in PACs (Hess et al., 2011).

From a transcriptional standpoint, XBP1 shares extensive overlap in targets with nATF6, the downstream effector of the ATF6 branch of the UPR (Yamamoto et al., 2004). In fact, both are capable of binding a specific DNA sequence termed the ER stress element (ERSE), a variable consensus sequence with a five base pair CCACG core but generally described as CCAAT-N_9-**CCACG** (Acosta-Alvear et al., 2007). Interestingly, XBP1 is capable of binding the CCACG core directly while nATF6 requires the co-binding of NF-γ at the upstream CCAAT site before binding. XBP1 also has a unique binding site with a four-nucleotide ACGT core and a general sequence of C**GACGTG**(G/A). The relative abundance of the short CCACG and ACGT sequences in the genome, coupled with the highly variable nature of the consensus binding sequences, has made bioinformatics identification of XBP1 direct targets difficult.

MIST1 has been previously linked to expression of XBP1 in a developmental context, as zymogenic chief cells (ZC) in the stomach of $Xbp1^{\Delta Ex2}$ mice fail to express MIST1 when differentiating (Huh et al., 2010). Surprisingly, these cells did not show signs of ER stress despite the lack of XBP1 and MIST1, implying that the effects and targets of XBP1 may be specific to certain cellular contexts. ZCs and other stomach cells are constantly regenerating, as opposed to the adult pancreas which, in an unstressed condition, has a turnover rate of less that 1% (Oates and Morgan, 1982). As previously shown in **Figure 3.01** and in contrast to ZCs, acinar cells in $Xbp1^{KO}$ mice express MIST1 , again indicating that the developmental role of XBP1 as a regulator of MIST1 may not be the same for all cell types.

Generally speaking, XBP1 targets tend to facilitate protein folding including components expressed throughout the ER and secretory pathway (Sriburi et al., 2007). ER stress, however, is relatively unique in that it occurs infrequently outside of development or in

unusual environmental conditions such as hypoxia (Tsang et al., 2010). The exception to this general rule is in secretory cells, whose primary function is to generate large volumes of proteins that must properly traffic through the ER and Golgi. Highly secretory cells, such as pancreatic acinar cells (PACs), have constitutive activation of the UPR due to the demand placed on their synthetic machinery (Iwawaki et al., 2004). As a result, one can envision a scenario in which the UPR in secretory cells could regulate expression of scaling factors that proceed to independently facilitate secretory cell homeostasis. Such factors could either regulate the expression of unique target genes outside the canonical UPR pathways, or could aid in increased expression of existing target genes. We sought to investigate whether ER stress in PACs triggers expression of the scaling factor MIST1 and its downstream targets

In this study, we utilized *in vitro* studies with cell lines to characterize the expression of *Mist1* following chemically-induced ER stress. We show a similar expression phenotype in acinar cells from mice lacking XBP1 or MIST1 in a 3D culture system. We also demonstrate that expression of XBP1 following ER stress leads to upregulation of *Mist1* via direct interaction with its promoter. Furthermore we show via bioinformatic analysis that a subset of likely MIST1 target genes are induced during periods of ER stress and share a similar expression pattern to *Mist1*. We thus conclude that *Mist1* is a direct target of XBP1 and that it functions to control target genes as a component of the unfolded protein response.

5.2 Induction of ER stress leads to activation of MIST1

ER stress frequently results when increased demand for protein synthesis surpasses the limit of what the basal cellular machinery is capable of producing. Such a condition was likely in the $Xbp1^{\Delta Ex2}$ pancreata during crisis (4 weeks post-*Xbp1* ablation), as the minority $Xbp1^{fl/fl}$ acinar cells were forced to synthesize sufficient quantities of zymogens to maintain the health of the animal. In order to test this, we stained pancreatic sections from $Xbp1^{\Delta Ex2}$ mice during crisis (4 weeks post-*Xbp1* ablation) for phosphorylated eukaryotic initiation factor 2 (pEIF2α), the primary target in the PERK UPR branch. As shown in **Figure 5.02b**, both zymogenic (red outlines) and non-zymogenic (yellow outlines) were positive for pEIF2α while associated blood vessels (BV) and stromal cells (blue outlines) were negative. This confirmed that the zymogenic, XBP1-expressing

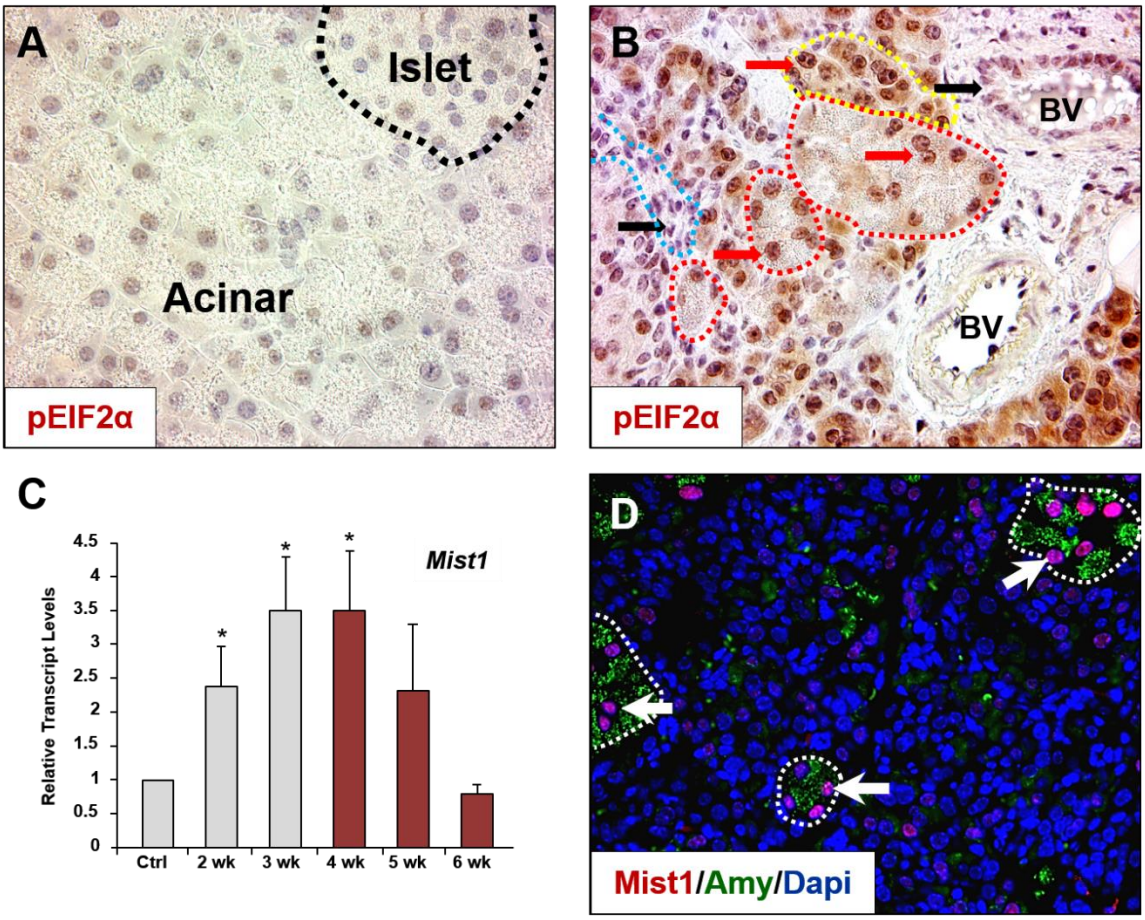

Figure 5.2 *Xbp1$^{fl/fl}$ acinar cells undergo ER stress and express higher than normal levels of MIST1 during pancreatic crisis*

(A) IHC stain for phospho-EIF2α (pEIF2α) shows little to no staining in wild-type pancreata. (B) IHC stain for pEIF2α in 4 week post-*Xbp1* ablation pancreata reveals extensive staining (red arrows) in zymogenic (red outlines) and non-zymogenic (yellow outline) cells. No staining (black arrows) is present in blood vessels (BV) or associated stromal tissue (blue outline). (C) RT-qPCR for *Mist1* shows increased expression following *Xbp1* ablation up until apoptotic crisis, then decreasing to wild-type levels by 6 weeks. (D) Immunofluorescence image showing high levels of MIST1 staining largely restricted to the zymogenic acinar population (white outlines). (* = p-value ≤ 0.05 relative to control samples, normalized to 18s expression)

acinar population also underwent ER stress, but did not express CHOP or initiate an apoptotic cascade, likely due to an intact UPR.

We next sought to determine whether *Mist1* expression was affected by ER stress induction. *Mist1* transcript levels were quantified using pancreatic RNA isolated from *Xbp1*$^{\Delta Ex2}$ mice following *Xbp1* ablation. As shown in **Figure 5.02c**, MIST1 expression increased over control pancreata by 3.5 fold, peaking during apoptotic crisis before returning to normal. This was surprising as *Mist1* is constitutively expressed in normal acinar cells and is not generally associated with dying cells. We proceeded to stain pancreatic sections taken at 4 weeks post-*Xbp1* ablation **(Figure 5.02d)** and saw high expression of MIST1 (white arrows) that was restricted to the zymogenic acinar population, with only minimal MIST1 staining in the non-zymogenic, *Xbp1*$^{\Delta Ex2}$ cells. This indicated that the 3.5-fold increase in *Mist1* expression levels was due to the <10% of acinar cells that had retained XBP1 expression. This prompted us to investigate whether MIST1 expression was a common feature of cells undergoing ER stress.

In order to investigate whether MIST1 expression was a common hallmark of cells undergoing ER stress we turned to *in vitro* cell lines. Cell lines have a distinct advantage versus mice as they can be induced to enter ER stress via treatment with a number of chemicals, including thapsigargin (a sarco/endoplasmic reticulum calcium ATPase inhibitor that slows protein transport in and out of the ER), tunicamycin (an inhibitor of n-linked glycosylation that prevents ER sorting of peptides), and DTT (a reduction agent that cross-links protein disulfide bonds). Each of these induces transient ER stress and a subsequent UPR within treated cells, allowing analysis of downstream signaling pathways and molecular events.

We first screened a number of non-transformed and transformed cell lines for normal UPR initiation, since the tumors that were used to derive transformed lines are usually subjected to and survive hypoxia and UPR-mediated apoptosis, possibly indicating an aberrant cellular response to stress (Ma and Hendershot, 2004). As shown in **Figure 5.03a-b**, analysis of non-transformed mouse embryonic fibroblasts (MEFs) and mouse 266-6 cells (SV40 large T antigen immortalized, non-transformed pancreatic acinar cells) showed significant *Xbp1* splicing following ER stress induction via thapsigargin that

remained high at 36 hours post treatment. In contrast, HEK293 (human embryonic kidney), MDA231 (human mammary gland adenocarcinoma), and PANC1 (human pancreatic cancer) cell lines all lacked significant *Xbp1* splicing following treatment despite strong induction of BiP expression, confirming that these cells also exhibited increased ER stress **(Figure 5.03c-e)**. Thus, we concluded that non-transformed cell lines would be the most effective cells for studying UPR targets.

We next sought to determine whether we could replicate the induction of *Mist1* expression following ER stress that we observed in $Xbp1^{fl/fl}$ acinar cells in cultured cells with a normal UPR response. This involved treating cell lines with thapsigargin and harvesting RNA, protein, and fixed cells for closer analysis. Despite increased *Mist1* transcript levels following thapsigargin treatment in MEFs **(Figure 5.04a)**, no MIST1 protein could be detected by protein blot or immunohistochemical staining **(Figure 5.04b)**. Interestingly, a MEF line derived from reporter mice in which β-galactosidase was knocked into the *Mist1* locus revealed that the *Mist1* locus was transcriptionally active during ER stress, but only in a minority of cells. This led us to conclude that *Mist1* expression in MEFs may be alternatively regulated, either in a cell cycle-dependent fashion or possibly via post-translational silencing of MIST1.

266-6 cells are known to express acinar cell digestive enzyme transcripts and respond to some secretagogues, making them among the most “acinar-like” cell lines available. Protein analysis performed in the Konieczny lab by Patrick Schweickert confirmed MIST1 expression in wild-type cells, making them relatively unique among pancreatic cell lines that are usually derived from ductal cancers in which MIST1 is silenced. Characterization of the 266-6 cell line following ER stress induction revealed increased *Mist1* transcripts and MIST1 protein, with strong expression maintained up to 36 hours post-thapsigargin treatment **(Figure 5.04c-d)**. Immunohistochemical staining of fixed 266-6 cells also showed a strong induction of MIST1 protein after ER stress onset **(Figure 5.04e-f)**. These data confirmed our hypothesis that *Mist1* is indeed expressed following ER stress.

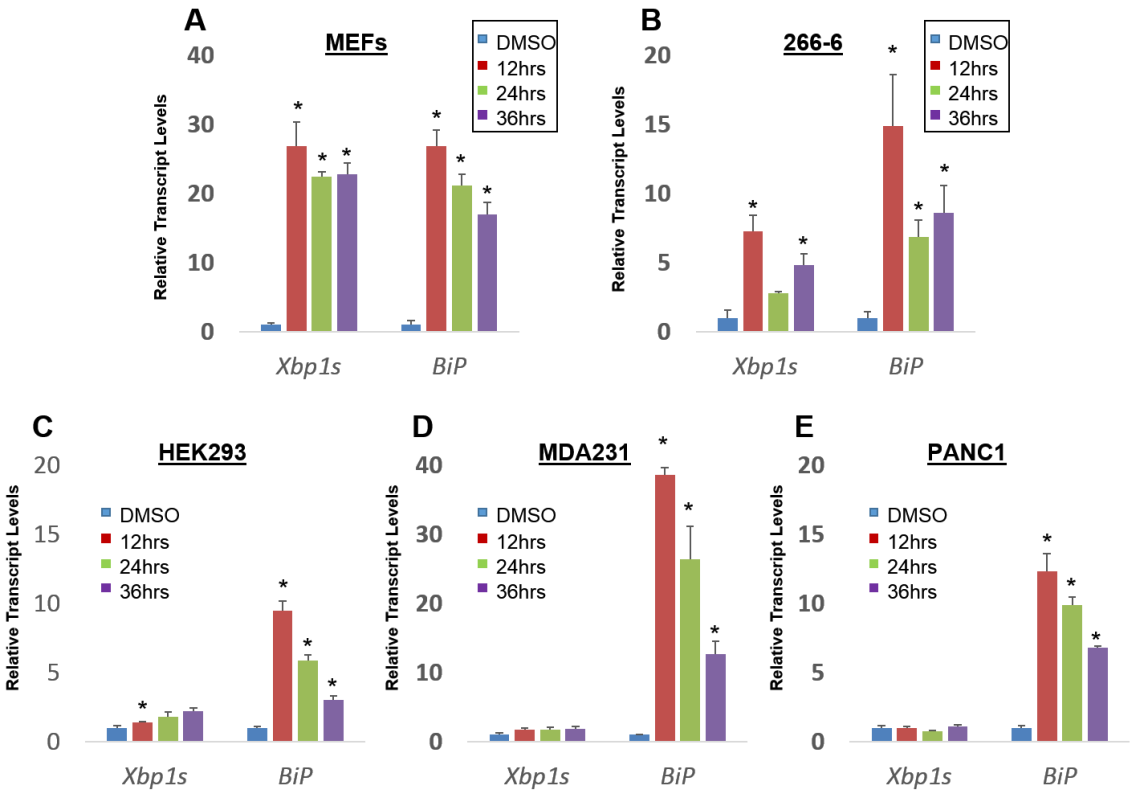

Figure 5.3 *266-6 cells and mouse embryonic fibroblasts splice Xbp1 in response to thapsigargin*

RT-qPCR using primers for spliced *Xbp1* and *BiP* transcripts following thapsigargin treatment in: (A) Mouse embryonic fibroblasts, high expression of both transcripts. (B) 266-6 cells, high expression of both transcripts. (C) HEK293, little expression of *Xbp1s* despite *BiP* induction. (D) MDA231, high levels of *BiP* induction without associated *Xbp1s* expression. (E) Panc1, high levels of *BiP* with no *Xbp1s*. (* = p-value ≤ 0.05 relative to control samples, normalized to 18s expression)

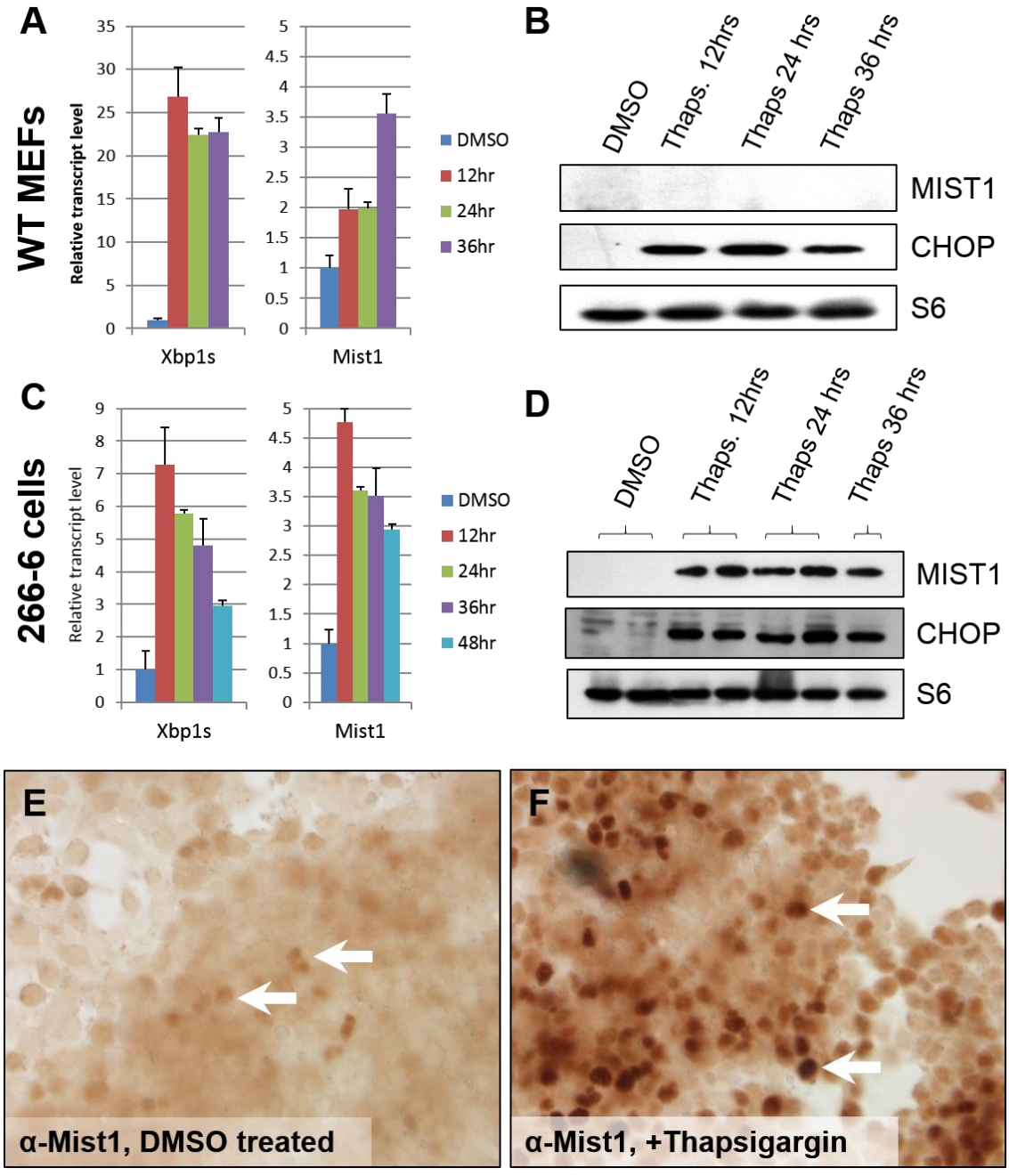

Figure 5.4 *266-6 cells express MIST1 in response to ER stress*

(A,B) RT-qPCR and protein blot on thapsigargin-treated WT MEFs reveals increased *Mist1* transcripts but no detectable MIST1 protein. (C,D) RT-qPCR/western blot in thapsigargin-treated 266-6 cells shows increased *Mist1* transcripts and protein. (E,F) IHC stain for MIST1 reveals few positively-stained cells (white arrows) in basal-state 266-6 cells and extensive staining following ER stress induction via thapsigargin. (* = p-value ≤ 0.05 relative to control samples, normalized to 18s expression)

5.3 *Mist1* is specifically targeted by XBP1 under conditions of ER stress

Following confirmation of increased *Mist1* expression during ER stress, we next sought to investigate whether XBP1 activity could be correlated with *Mist1* expression or its activities. Since MIST1 is known to control acinar identity and differentiation, we utilized a collagen-based 3D acinar cell culture system to study whether ablation of *Xbp1* would cause any changes in *Mist1* levels or acinar differentiation status. We harvested $Xbp1^{\Delta Ex2}$ acinar cells 48 hours post-ablation and embedded them in a 3D collagen matrix. As shown in **Figure 5.05a**, $Xbp1^{\Delta Ex2}$ acinar cells are initially deficient in *Mist1* and become moreso by 48 hrs post-embedding (96 hours post-*Xbp1* ablation). We also gauged acinar differentiation status by quantifying the degree to which the embedded acinar clusters converted to duct-like cysts upon treatment with TGFα, an extracellular growth factor receptor agonist that mimics activated KRAS signaling **(Figure 5.05b)**. $Xbp1^{\Delta Ex2}$ acinar cells showed an increased tendency to undergo ductal cyst transdifferentiation when treated with TGFα, a similar phenotype seen in embedded $Mist1^{KO}$ acinar cells (Shi et al., 2012). Interestingly, $Xbp1^{\Delta Ex2}$ acinar cells also showed a marked tendency to spontaneously convert in the absence of TGFα **(Figure 5.05c)**, implying an intrinsic differentiation defect that may be related to a lack of *Mist1* induction.

We next sought to experimentally determine whether *Mist1* was expressed in response to UPR and *Xbp1* activation. To accomplish this we acquired $Xbp1^{KO}$ MEFs, a generous gift from Dr. Ann-Hwee Lee at Harvard University. These cells were derived from $Xbp1^{KO}$ embryos, avoiding the problem of post-natal lethality known to occur in $Xbp1^{KO}$ neonates and allowing analysis in a mouse cell completely devoid of XBP1 protein. Similar to the $Xbp1^{\Delta Ex2}$ allele, these mice have a missing second exon, resulting in a truncated, nonfunctional protein but still undergoing IRE1-mediated RNA splicing, allowing splice-specific primers to be used to measure ER stress induction (Lee et al., 2003). We repeated our initial characterization studies of MEFs, this time utilizing WT and $Xbp1^{KO}$ lines to assay whether *Mist1* transcript levels were induced following ER stress in the absence of XBP1. Intriguingly, $Xbp1^{KO}$ MEFs failed to upregulate *Mist1* gene expression upon ER stress induction, indicating that XBP1 was responsible for *Mist1* expression **(Figure 5.06a)**. We further confirmed that MIST1 expression was not a result of

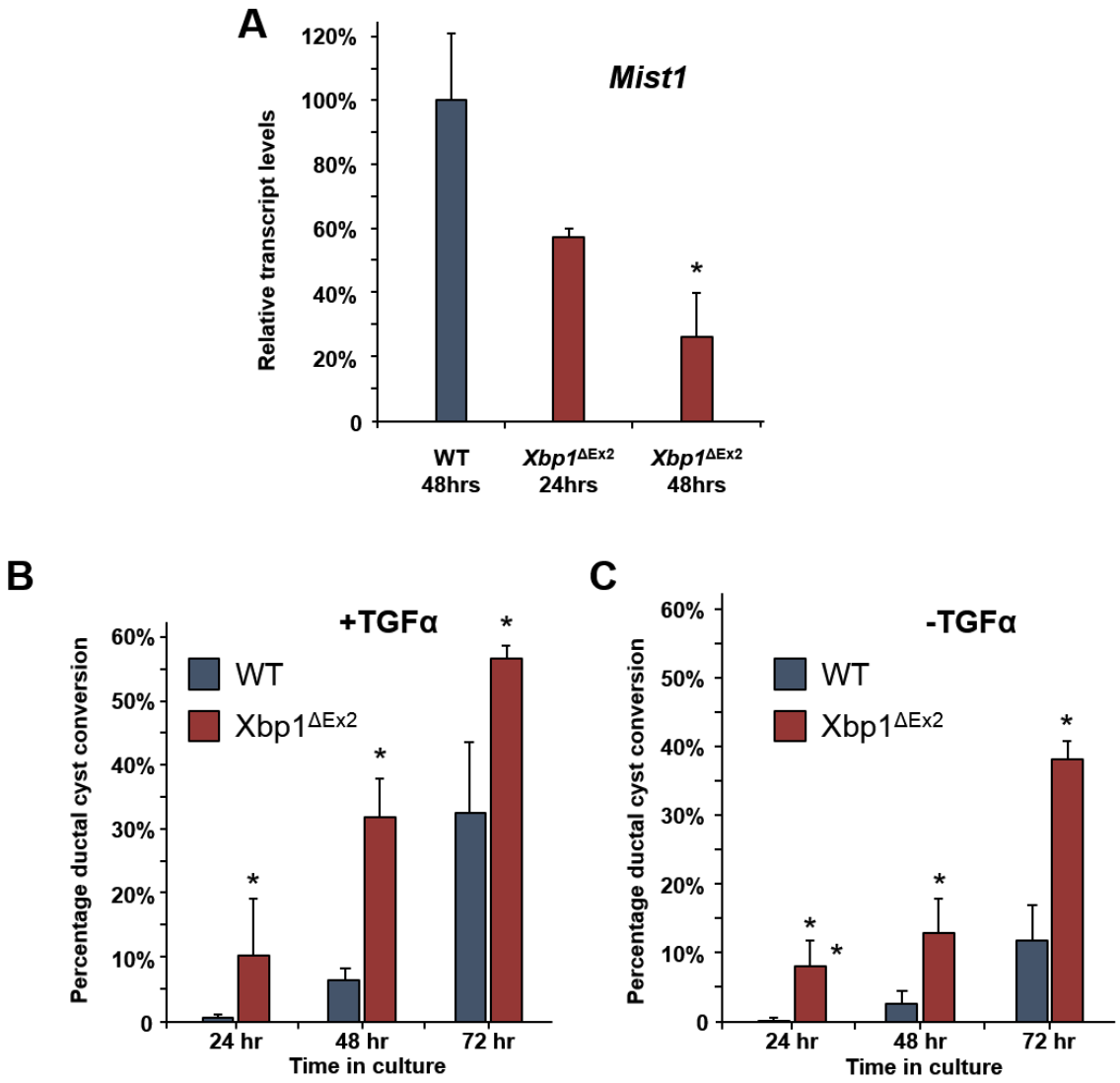

Figure 5.5 *Loss of* Xbp1 *in vitro results in increases in induced and spontaneous ductal cyst formation*

(A) RT-qPCR data on isolated acinar clusters in our collagen-based 3D culture system showing a precipitous drop in *Mist1* expression in *Xbp1*$^{\Delta Ex2}$ acinar cells relative to isolated wild-type acini. (B) Counts of ductal cyst formation in wild-type vs. *Xbp1*$^{\Delta Ex2}$ acinar cells shows significantly increased cyst generation in *Xbp1*$^{\Delta Ex2}$ acinar cells following TGFα treatment. (C) Ductal cysts spontaneously form at a significantly higher rate in *Xbp1*$^{\Delta Ex2}$ acinar cells. (* = p-value ≤ 0.05 relative to control samples, Fig. A normalized to 18s expression)

activation by other UPR branches by transfecting MEFs with an Xbp1s-encoding plasmid that caused increased *Mist1* transcript levels similar to those seen in response to thapsigargin **(Figure 5.06b)**. These data indicated that XBP1 activity was directly responsible for increased *Mist1* expression during ER stress.

We next sought to determine whether the *Mist1* gene was a direct transcriptional target of XBP1. This initially involved a sequence analysis of both the human (*huMist1*) and mouse (*muMist1*) promoters, which encode similar proteins but are structurally distinct due to the presence of an untranslated first exon in the mouse sequence **(Figure 5.07a)**. We scanned the 1000 base pairs preceding the transcriptional start site of *msMist1* and the corresponding region of *huMist1* through to the end of the gene and identified no ER stress element (ERSE) consensus sequences, eliminating the possibility of a joint ATF6/XBP1 induction of MIST1. Analysis of the same sequence in the *msMist1* gene for the XBP1-specific unfolded protein response element (UPRE) **(Figure 5.07b)** revealed two candidate sites within the mouse gene, termed site A and site B, both matching 7/8 nucleotides of the consensus UPRE sequence. Intriguingly, these sites are either partially (site A) or fully (site B) conserved in the *huMist1* promoter, with the partially conserved *huMist1* site A (termed A') actually matching 8/8 nucleotides of the consensus UPRE.

In order to determine whether XBP1 could bind to and activate these regions of the *Mist1* promoter, we utilized luciferase containing fragments of the *msMist1* promoter through intron 1 sequences. These plasmids were cotransfected into 266-6 cells along with an expression plasmid encoding XBP1. As shown in **Figure 5.07c**, the promoter fragment containing both candidate sites was capable of producing a 7-fold increase in luciferase expression relative to control, indicating XBP1s could directly bind that region of the *Mist1* promoter. Intriguingly, when we tested mutated reporter plasmids in which either Site A (mutA) or Site B (mutB) had been mutated to remove the UPRE (GACGTG -> ACTAGT), it was the partially conserved site A that had reduced luciferase activity while mutation of site B had no significant impact on luciferase expression. We thus concluded that site A was directly bound by XBP1 while site B was not.

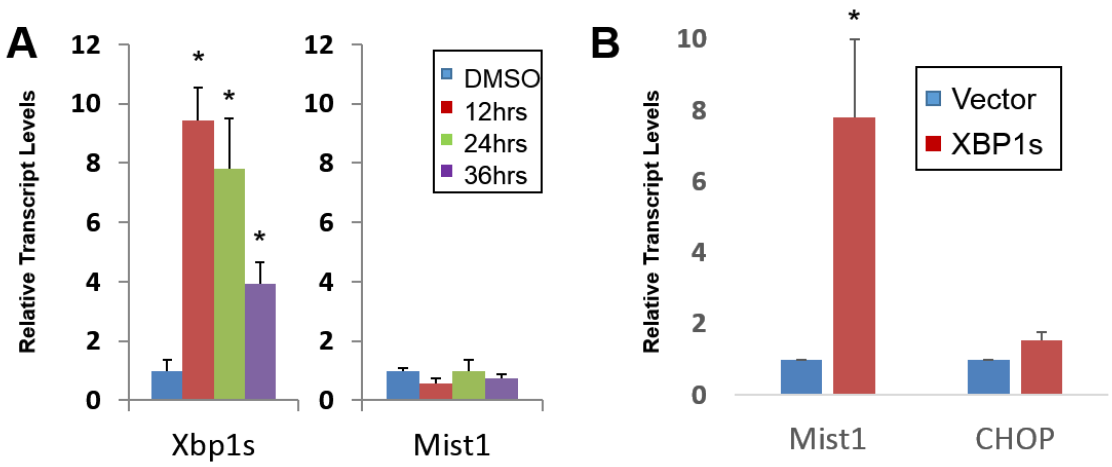

Figure 5.6 *XBP1 is directly responsible for inducing Mist1 expression*

(A) RT-qPCR on spliced *Xbp1* transcripts in *Xbp1*^{KO} MEFs indicates ER stress induction following thapsigargin treatment but with no increase in *Mist1* expression levels. (B) RT-qPCR analysis of vector (control) or *Xbp1s* transfected MEFs shows a significant increase in *Mist1* transcripts in cells expressing XBP1s. (* = p-value ≤ 0.05 relative to control samples, normalized to 18s expression)

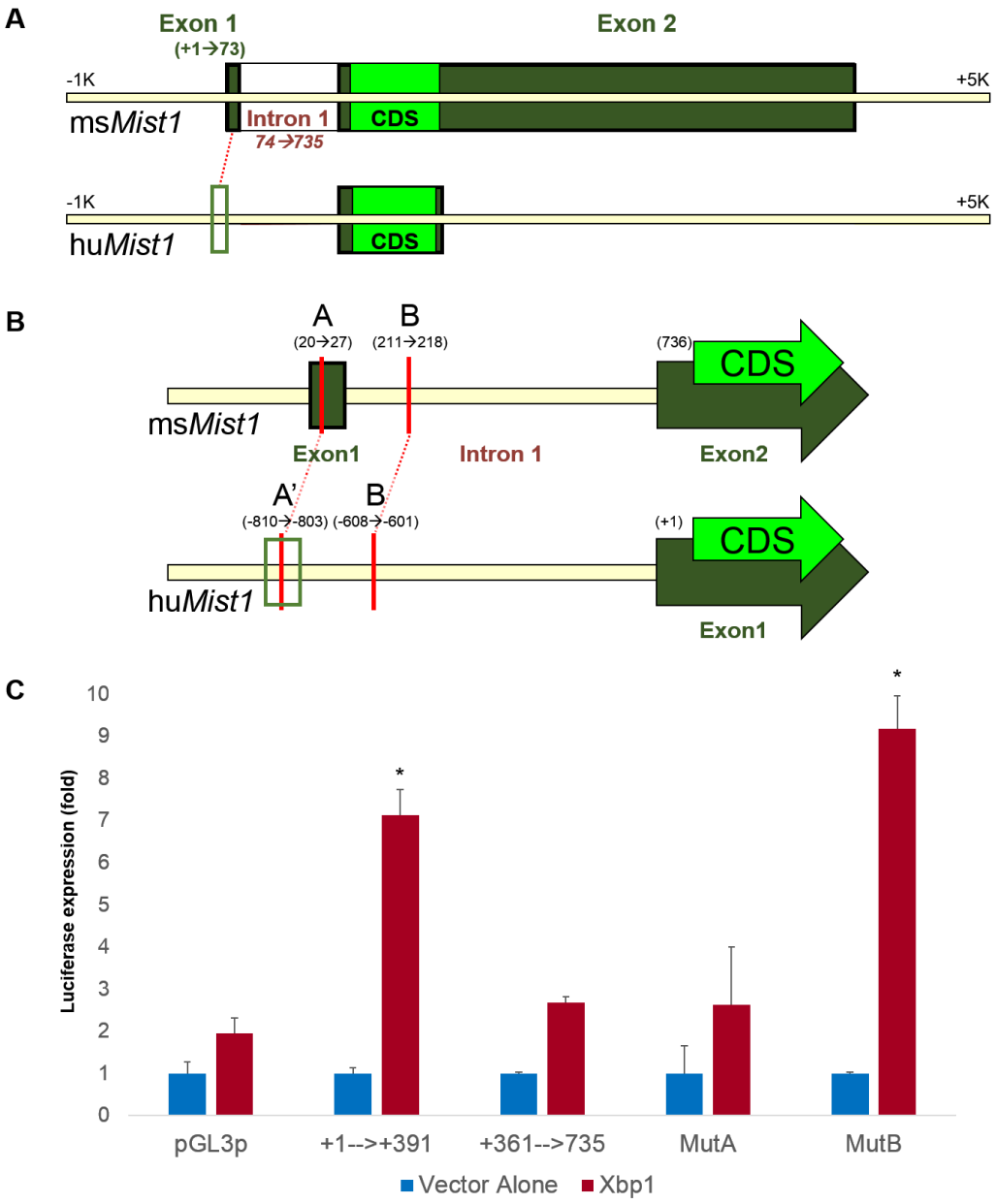

Figure 5.7 *XBP1 activates reporter gene expression in Mist1-promoter region constructs*

(A) Schematic of the mouse and human *Mist1* genes (*msMist1* and *huMist1*, respectively). *HuMist1* contains only one exon that consists of mostly the entire coding sequence (CDS), although a 87% sequence match exists between *msMist1* exon 1 and an upstream *huMist1* region (green box). (B) Sequence analysis of *huMist1* and corresponding region of *msMist1* showing the location of two conserved putative XBP1s binding sites (A/A', B). (C) Luciferase expression data following XBP1/Mist1$_{pr}$-Luc constructs in 266-6 cells, showing increased expression in the construct containing both UPREs. Increased expression is lost by mutating site A but unaffected by mutating site B. (* = p-value ≤ 0.05 relative to pGL3p luciferase value after *Xbp1* transfection)

As a final verification that XBP1-mediated activation of MIST1 was an important component of MIST1's activity, we expanded our sequence analysis to an additional eight species to determine whether either of the two candidate UPRE sites were conserved. As shown in **Table 5.01**, site A (found in exon 1) is conserved in human, mouse, and rat while site B (found in intron 1) is 100% conserved across five species. Interestingly, four of the remaining five species also have putative XBP1 binding sites matching the UPRE consensus sequence, indicating that XBP1 binding to the *Mist1* promoter plays an important role across higher eukaryotes.

5.4 Proposed MIST1 targets are induced during ER stress

We found no published data analyzing pancreatic acinar cells in the context of ER stress. Rather than conducting costly microarray or RNA-seq genome-wide expression studies, we chose to bioinformatically search for possible MIST1-regulated genes by correlating available published microarray data on XBP1 and the Konieczny lab's own data regarding unstressed pancreata. A detailed description of this analysis can be found in Chapter 2, and selection criteria are summarized in **Figure 5.08**. Briefly, we generated a list of 184 possible MIST1 effectors based on published microarray data utilizing fibroblasts transfected with XBP1 as well as general UPR-associated genes gleaned from literature searches and commercially available UPR PCR arrays. We then refined this list using data generated previously by the Konieczny lab by selecting only genes with significant ChIP-Seq enrichment scores, expression changes following induction of a *Mist1* transgene in a $Mist1^{KO}$ acinar cells, and the presence of either TA or GC E-boxes in the promoter and first two exons and introns of each candidate gene. Finally, we cross-checked our remaining candidate effectors against available microarray data from $Ire1^{KO}$ liver samples treated with tunicamycin as a final selection criteria, selecting for genes with significantly altered expression levels in WT vs. $Ire1^{KO}$ samples. This analysis resulted in a short list of 15 high-scoring candidates satisfying all criteria, with a further 6 genes with strong scores in most areas but that failed to satisfy one criteria. These genes are listed in **Table 5.02.**

Table 5.1 *Evolutionary conservation of UPRE sites in the Mist1 gene*

Sequence analysis indicates a 100% conservation of the putative UPRE binding site in intron 1 across five species. Four additional species have variants on UPRE sites in similar locations, with only one species lacking any identified XBP1 binding site.

	Intron 1 (Site 2)		***Exon 1 (Site 1)***	
Species	*Sequence*	*UPRE Match*	*Sequence*	*UPRE Match*
Human	CCACGTGG	7/8	CGACGTGT	8/8
Mouse	CCACGTGG	7/8	CTACGTGT	7/8
Rat	CCACGTGG	7/8	CGACGTGT	8/8
Chimp	CCACGTGG	7/8	N/A	N/A
Wolf	CCACGTGG	7/8	N/A	N/A
Killer Whale	CGACGTGT	8/8	N/A	N/A
Tasmanian Devil	AGACGTGA	6/8	N/A	N/A
Drosophila	GGACGTGG	7/8	N/A	N/A
Zebrafish	CAACGTGC	6/8	N/A	N/A
Chicken	N/A	N/A	N/A	N/A

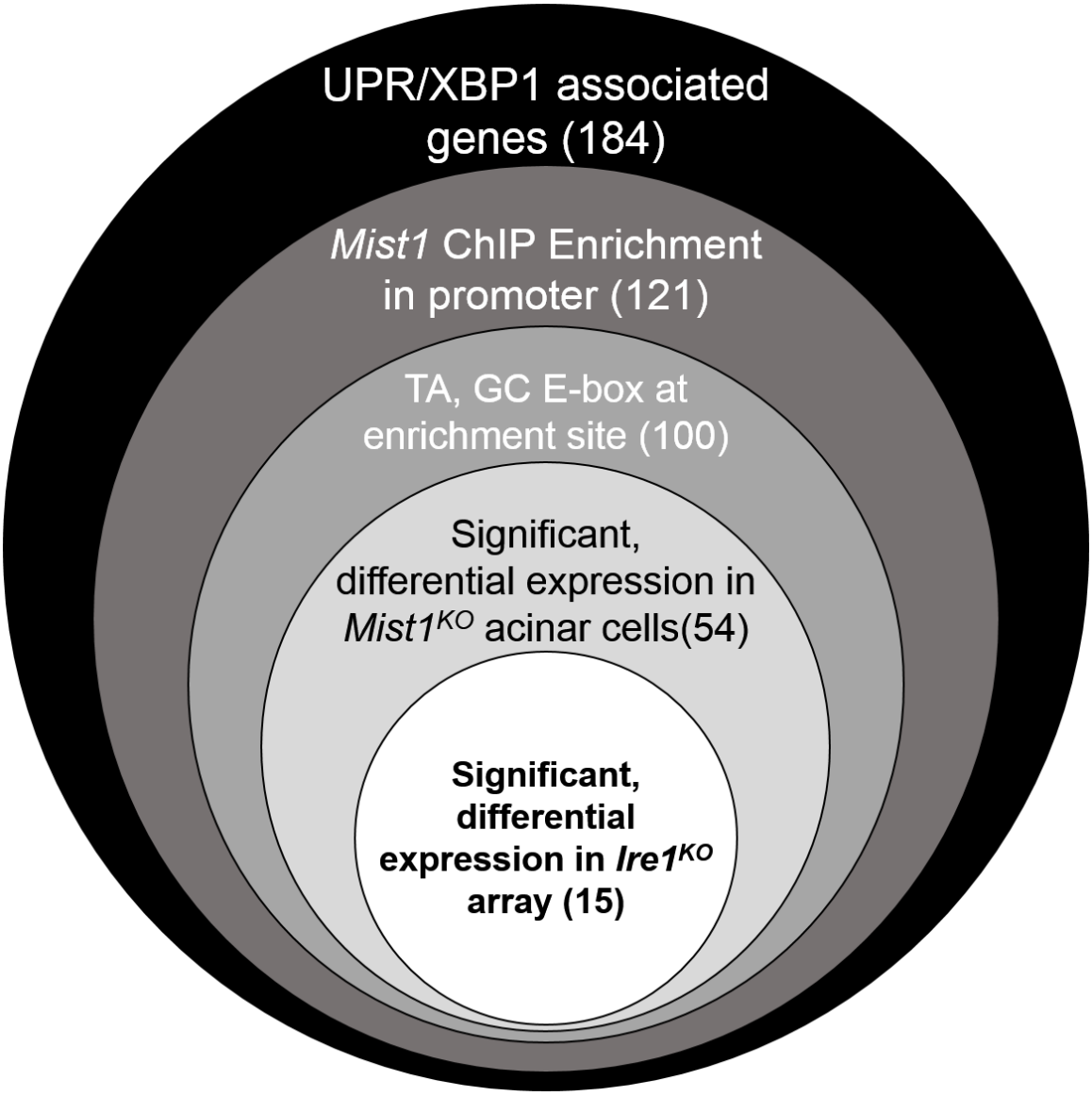

Figure 5.8 *Summary diagram of candidate gene selection criteria*

Selection criteria for putative MIST1-dependent UPR target genes. Each circle represents an additional criteria, with the number of genes possessing that criteria and all previous ones shown in parentheses. Only 15 of the original 184 genes met all five selection criteria.

Following the selection of likely MIST1 targets, we next sought to determine if any of the purported effectors were upregulated following ER stress induction. Given the previously discussed cell context specificity of XBP1's targets, we determined that an investigation of MIST1's role in the UPR necessitated a viable system for triggering ER stress specifically in pancreatic acinar cells at higher levels than normally present under basal conditions. However, the available *Xbp1*$^{fl/fl}$ mouse model generated extensive and cumulative ER stress in acinar cells, but removed XBP1, our hypothesized MIST1 activator. Published reports on targeted deletions of other UPR master regulators in mice did not show extensive ER stress as a consequence of their deletion (Reimold et al., 2000; Urano et al., 2000; Yamamoto et al., 2007; Zhang et al., 2002). Our own efforts at inducing ER stress induction *in vivo* via intraperitoneal injection of both thapsigargin and tunicamycin showed that such agents either resulted in animals that became rapidly nonresponsive and ill or a cellular response that was insufficient to initiate a UPR. We thus determined that 266-6 cells would be our best system for monitoring how MIST1 functions in the UPR.

We conducted a time course on 266-6 cells treated with thapsigargin to induce ER stress. These cells were harvested every 12 hours for RNA in order to study expression changes of candidate genes. Interestingly, analysis of transcript levels over repeated thapsigargin challenges indicated that *Xbp1s* expression following thapsigargin challenge in 266-6 cells rapidly climbs and diminishes, while *Mist1* expression increases and remains elevated for 36 hours after induction **(Figure 5.09a)**. Because of the sustained *Mist1* expression levels, we hypothesized that MIST1 targets would follow a similar expression pattern, with an initial increase following thapsigargin treatment and subsequent prolonged elevation. We proceeded to design primers for each candidate target gene to test the expression pattern of each following ER stress in 266-6 cells.

As shown in **Figure 5.09c**, 14 of the 21 candidate MIST1 target genes behave similarly to *Mist1*, with an initial spike in expression at 12 hours post-ER stress induction followed by sustained expression over the following 24 hours. This expression pattern is consistent with our hypothesis regarding MIST1 targets being expressed in a similar fashion as the *Mist1* gene. Five remaining candidates **(Figure 5.09b)** all have a spike

Table 5.2 *Summary of candidate effectors of MIST1 within the UPR pathway*

Catalog of 15 highest scoring and 6 highly-scored putative MIST1 targets. Each gene is shown with its relative ChIP enrichment score, E-box content at enrichment sites, fold change in *Mist1*^{WT} vs. *Mist1*^{KO} pancreata, fold change with significance in published *Ire1*^{KO} + tunicamycin liver sample microarray (So et al., 2012), and associated function. Commas are used to separate ChIP enrichment and E-box locations when multiple enrichment sites were identified.

	Gene name	ChIP Fold Enrichment	# of Eboxes		*Mist1*^{KO} Rescue Array		*Ire1*^{KO} array signif.		Putative Function (from GeneCards)
			GC	TA	*Mist1*^{KO} Fold Diff.	Rescued	*Ire1*^{KO} Fold Diff.	P-value	
HIGHEST SCORE	Arcn1	5.0	0	1	-1.21	Partial	-1.00	0.0013	ER to Golgi transport
	Arfgap3	5.8, 3.8	1, 2	0	-2.23	Partial	-4.12	<0.0001	Transport to Golgi (GAP)
	Atp2a2	8.0	1	0	-1.34	Full	-0.37	0.0209	Calcium pump (sarcoplasmic reticulum)
	Dnajc3	3.5	0	2	-1.216	Partial	-1.02	<0.0001	Chaperone, pEIF2a inhibitor
	Dnajb9/ERdj4	3.0	0	1	1.19	None	-2.54	<0.0001	Chaperone
	Edem3	7, 4.5	1, 1	0, 1	-1.75	Partial	-1.83	<0.0001	ER-associated degradation
	H47	2, 10	2, 1	0, 0	-1.16	Partial	-1.17	<0.0001	Peptide transport out of ER
	Os9	10, 4	1, 0	0, 2	-1.77	Partial	-1.21	0.0008	Misfolded protein binding
	Piga	8.0	1	0	2.56	Partial	-0.84	0.0044	Glycosyltransferase (tagging)
	Ppib	3.5	2	0	1.13	Full	-0.67	0.0027	Protein folding (secretory specific)
	Sec11c	4.5	1	1	-2.62	Partial	-1.95	0.0005	Peptide transport/modification into ER
	Sec61b	3.8	2	1	-1.33	Partial	-2.99	<0.0001	Peptide transport/modification into ER
	Serp1	2.7	1	0	-1.567	Partial	-1.63	<0.0001	Peptide transport/modification into ER
	Spcs3	9, 12, 16	1, 0, 2	0, 1, 1	-1.61	Partial	-1.55	<0.0001	Peptide transport/modification into ER
	Ssr3	3.5	0	2	-1.16	Full	-2.05	0.0001	Peptide transport/modification into ER
HIGH SCORE	Dnajc1	7.8, 8.0	0, 2	1, 0	-1.82	Partial	0.07	0.8000	Chaperone
	Htra2	2.1	4	0	-2.78	Partial	-0.22	0.3790	ER-associated cell death
	Ppp1r15b	7.7	2	0	-1.22	Full	0.34	0.0364	pEIF2 regulation
	Rrbp1	7.0	1	0	1.21	None	-1.31	0.0001	Peptide tranport into ER (ribosome binding)
	Spcs2	6.0	1	0	-1.16	None	-1.65	<0.0001	Peptide transport/modification into ER
	Uso1	3.7	2	0	-1.18	Partial	-1.65	<0.0001	Transport in Golgi

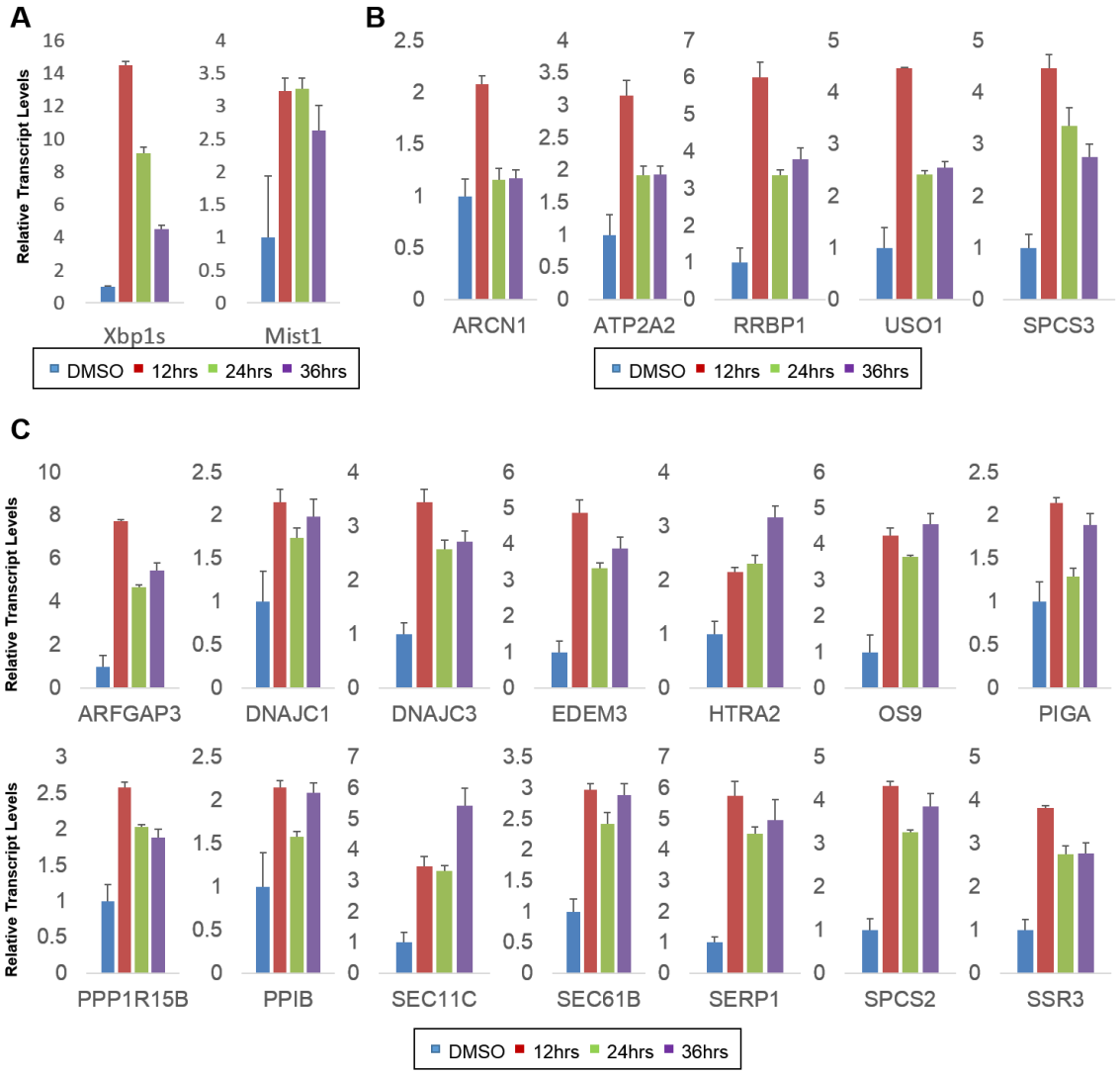

Figure 5.9 *Candidate MIST1 targets display predicted expression patterns upon ER stress induction*

RT-qPCR data from 266-6 cells treated with thapsigargin. (A) Combined *Xbp1s* and *Mist1* expression data from multiple experiments showing rapid increase and decrease in *Xbp1s* levels and comparatively long, persistent elevation of *Mist1* expression. (B) Five of the 19 putative MIST1 targets share a common expression pattern, with high expression at 12 hours post-ER stress induction followed by approximately 50% expression at 24 hours that remains by 36 hours. (C) Remaining putative MIST1 targets all share a similar expression profile to *Mist1*, with initial elevation and continued, nearly constant levels at later time points. (* = p-value ≤ 0.05 relative to control samples, normalized to 18s expression)

in expression at 12 hours followed by a decline to approximately half that level at 24 and 36 hours, suggesting that they may be targets for direct XBP1 and MIST1 binding, but not necessarily MIST1 alone.

5.5 A subset of putative MIST1 targets are expressed in a MIST1-dependent fashion following ER stress

Following our expression analysis, we sought to directly determine whether knock-down of *Mist1* via expression of a *Mist1*-targeting shRNA would significantly alter expression levels of the putative target genes. We generated both sh*Ctrl* (non-targeting control shRNA) and sh*Mist1* (targeting the *Mist1* CDS) viral constructs and infected 266-6 cells to generate stable lines. We then proceeded to challenge these cells with thapsigargin and harvested RNA at 12 hours post-ER stress induction to measure expression levels. As shown in **Figure 5.10**, there was no significant difference in *Xbp1* activation between the two groups, although both were significantly induced vs. DMSO-treated controls (data not shown). Interestingly, nine of the previously identified candidate Mist1-effector genes had significantly reduced expression following ER stress induction (**Figure 5.10b**). This is consistent with a model in which MIST1 is serving as the primary regulator of these ER stress-responsive genes in pancreatic acinar cells.

5.6 Discussion

Molecular mechanisms behind complex cell phenomena are increasingly being utilized to design modern therapeutics. As more and more knowledge regarding how cells utilize signaling pathways and feedback mechanisms to regulate their survival accumulates, so too do the opportunities to target these control circuits more precisely in order to manipulate aberrant cell behaviors. The unfolded protein response is an emerging target of interest in cancer treatment, as it utilizes unique pathways to regulate gene expression and cell survival independent of the more frequently targeted growth signaling and developmental gene networks (Koong et al., 2006). Ideally, novel therapeutics would modulate expression of downstream components of a pathway, making scaling factors such as MIST1 ideal targets as they are not essential for cell survival or pathway initiation but do facilitate homeostasis and overall cellular health. In

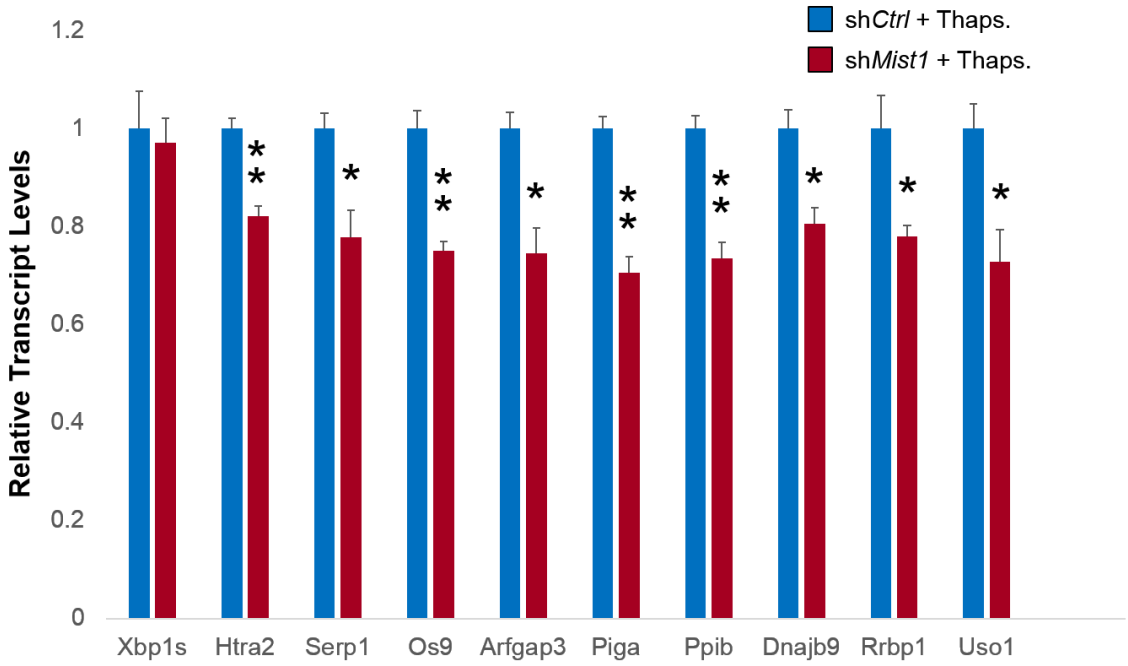

Figure 5.10 *Expression of a subset of Mist1 candidate target genes is significantly decreased in shMist1 266-6 cells following thapsigargin treatment*

Expression analysis of transcripts from sh*Ctrl* and sh*Mist1* 266-6 stable cell lines treated with thapsigargin (12 hours post-induction) reveals nine putative MIST1 gene targets with significantly reduced expression. Splicing of *Xbp1*, a measure of ER stress levels, was not affected by *Mist1* knockdown. Expression values are scaled to sh*Ctrl* values for illustrative purposes. (* = p-value ≤ 0.05, ** = p-value ≤ 0.01 relative to control samples, normalized to 18s expression)

this work we set out to establish if and how MIST1 plays a role in the XBP1-mediated branch of the unfolded protein response.

Our analysis established that *Mist1* is directly upregulated by pancreatic acinar cells undergoing ER stress **(Figure 5.02)**. Indeed, stressed acinar cells increased total *Mist1* expression to over 3.5 fold higher than basal levels, a particularly surprising finding as this expression took place with less than 10% of the total acinar cell population contributing to the result. This data indicates that the actual enrichment of MIST1 protein in the zymogenic population may be far higher than shown in transcript analysis, further supporting the idea that *Mist1* expression is important in regulating acinar cell health during periods of heightened stress.

We next proceeded to establish that the 266-6 immortalized acinar cell line has increased MIST1 expression in response to ER stress that mimics our *in vivo* mouse findings **(Figure 5.03c-d)**. We also showed that ablation of *Xbp1* in cells embedded in a collagen-based 3D culture system resulted in a general reduction in *Mist1* levels and a drastically increased rate of acinar cell transdifferentiation that mimics the phenotype of *MIST1*^{KO} acinar cells **(Figure 5.05)** (Shi et al., 2012). Furthermore, we established that *Mist1* expression is directly correlated with expression and binding of XBP1 to the *Mist1* promoter **(Figure 5.07)**, indicating that MIST1 is involved in the UPR via direct interaction with one of its primary initiating transcription factors. This provides a link between previous research showing that *Mist1* is developmentally regulated by XBP1 (Huh et al., 2010) and our own work showing a connection between *Mist1* expression and ER stress. Interestingly, we also showed a strong evolutionary conservation between possible XBP1-binding sites in the human and mouse *Mist1* genes, indicating that the regulation of *Mist1* by XBP1 may be an important feature of *Mist1*-expressing secretory cells across species.

We lastly sought to identify candidate MIST1 targets that were modulated in response to ER stress. Using a number of bioinformatic data sets we were able to identify a suite of 21 likely MIST1 targets, with eleven of candidates associated with various protein transport mechanisms into and out of the ER. This is consistent with recent reports of MIST1 regulating the *Atp2c2* gene, a sarcoplasmic reticulum calcium ATPase known to

be associated with the secretory pathway and involved in shuttling proteins across the ER membrane (Garside et al., 2010). In fact, our analysis also independently identified HTRA2, a protein involved in ER-associated degradation that has also been demonstrated to be a direct target gene of MIST1 (Direnzo et al., 2012). *Htra2* also shares a similar expression pattern to 13 of the 21 candidate genes upon thapsigargin treatment **(Figure 5.08c)**. These data support the validity of our approach, and they also add further support to the idea that one of the primary functions of MIST1 is to facilitate secretory networks via activation and expression of downstream genes in response to stress conditions. Indeed, the previously described constant UPR and XBP1 activity present in the pancreas may be the reason why MIST1 is found constitutively expressed in exocrine tissue (Iwawaki et al., 2004).

Finally, we validated that nine of our candidate genes have altered expression following thapsigargin treatment of 266-6 cells and shRNA-mediated knockdown of *Mist1*. This prompted us to conclude that *Mist1*, and not *Xbp1*, was directly responsible for expression of this subset of candidate genes, as differences between *Xbp1* levels in the two cell lines were insignificant. Further testing is planned on this suite of genes including anti-MIST1 ChIP experiments to verify direct binding of MIST1 to each candidate gene's respective promoter. Additionally, whole-genome approaches including ChiP-Seq and RNA-Seq may be utilized to further investigate MIST1 targets in the UPR.

Based on our data, we propose that MIST1 functions as a scaling factor for the unfolded protein response via activation by XBP1. This role as a facilitating influence rather than as a critical UPR regulator is also in agreement with published literature showing altered ER stress responses in *MIST1*^{KO} mice, which likely survive despite aberrant UPR functioning due to the supportive nature of MIST1's target genes. This work serves as a jumping-off point for possible therapeutic design targeting the UPR and its downstream networks. While direct disabling of key molecules, such as XBP1, has been shown by us and others be deleterious to cell survival, targeted modulation of MIST1 or its gene targets could impair UPR function sufficiently to allow increased cell sensitivity to chemotherapeutics. We believe that the MIST1 transcriptional network may present an accessible and effective means of controlling secretory cell survival as a means to treat human disease.

CHAPTER 6. HIGH-LEVEL KRAS^{G12D} EXPRESSION IN DEVELOPING PANCREATIC ACINAR CELLS LEADS TO ACINAR-DUCTAL METAPLASIA THAT IS MITIGATED BY MIST1

6.1 Introduction

Pancreatic ductal adenocarcinoma (PDA) is one of the most lethal malignancies, with a five-year survival rate of less than 6% (Siegel et al., 2013). The high fatality rate of PDA is primarily attributed to a lack of early diagnostic markers and a clear understanding of early transformation events. The median survival time following diagnosis plummets from a high of 24 months in patients with small, isolated pancreatic tumors to less than 10 months in patients with local lymph node invasion and less than 5 months in patients with detectable metastases (Hidalgo, 2010). As a result, extensive research in humans and mouse models has focused on classifying and investigating how PDA develops and progresses.

Molecular analysis of pancreatic tumors shows mutations in the RAS proto-oncogene in greater than 90% of PDA tumor specimens (Hidalgo, 2010). The RAS protein is a molecular switch that couples activation of membrane-embedded receptor tyrosine kinases (RTKs) to cytoplasmic and nuclear effectors **(Figure 6.01a)** (Spaargaren et al., 1995). RAS binds to activated RTKs via adapter proteins, including growth factor receptor-bound protein 2 (GRB2) and Son of Sevenless (SOS), that couple the signal generated by activation and phosphorylation of ligand bound receptors to RAS activation (McCormick, 1993; Spaargaren et al., 1995). The activation of RAS is governed by GTP binding facilitated by guanine nucleotide exchange factors (GEFs) while RAS deactivation is accomplished via hydrolysis of the bound GTP, a process that is dependent on GTPase activating proteins (GAPs) **(Figure 6.01b)** (Cox and Der, 2003). RAS mutations that prevent GTP hydrolysis (including the previously described KRAS^{G12D} mutation) are among the most prevalent in pancreatic and other cancers, since RAS activity drives downstream pathways that positively affect cell growth and

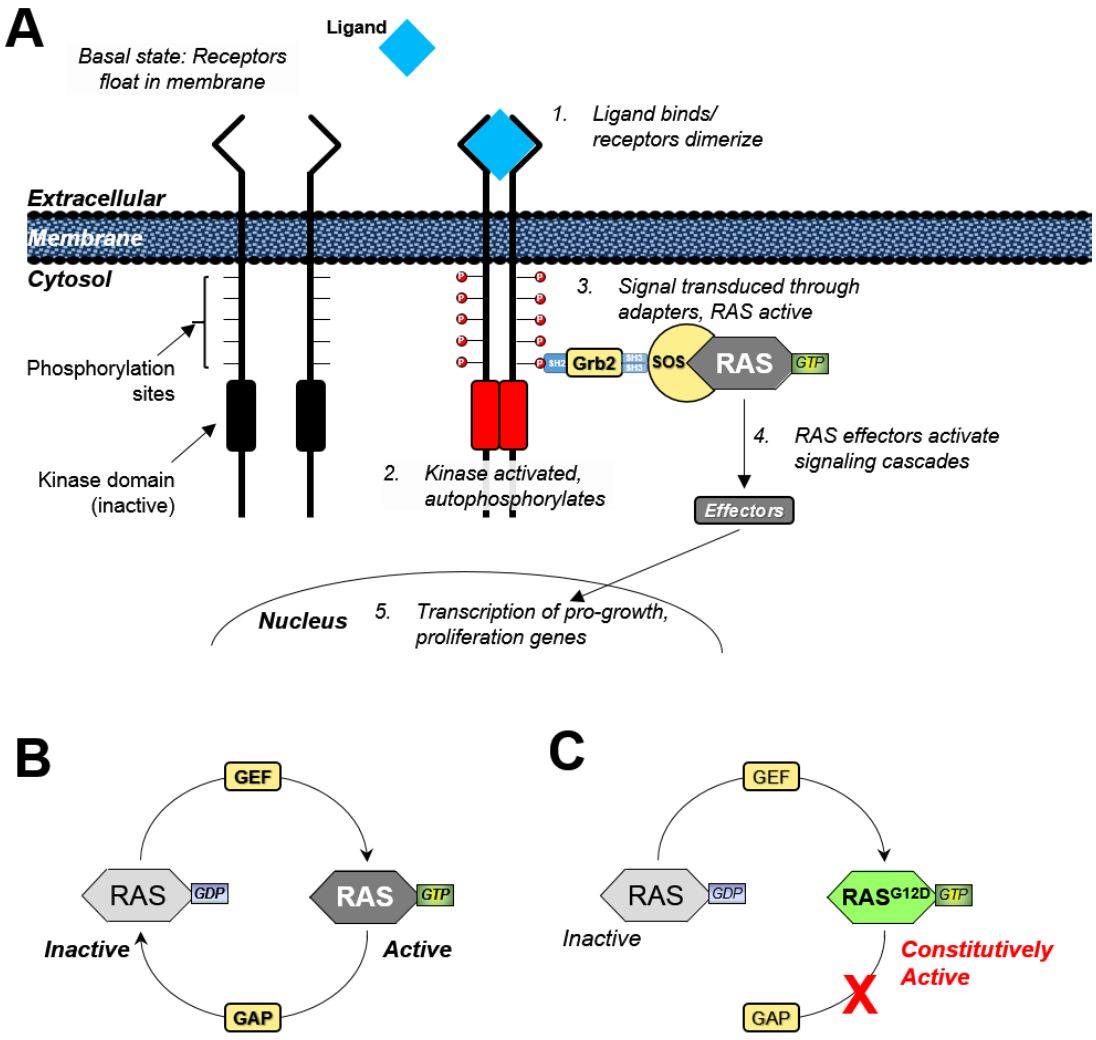

Figure 6.1 *Diagram of normal and mutant RAS-based signal transduction*

(A) Receptor tyrosine kinase signaling in which ligand binding promotes dimerization of receptors which then auto/transphosphorylate themselves. Adapter proteins bind to phosphorylated receptor sites, tethering the RAS molecule and causing it to become active and initiate signal cascades promoting growth and proliferation. (B) Diagram of normal RAS activity in which activated GTP-bound RAS hydrolyzes the bound GTP with the assistance of GTPase activating proteins (GAPs). Reactivation of the molecule involves exchange of GDP for a new GTP molecule and is facilitated by guanine nucleotide exchange factors (GEFs). (C) RAS^{G12D} has a mutant 12^{th} amino acid (G→D) that prevents RAS inactivation by GAPs and thus is constitutively active.

proliferation events **(Figure 6.01c)** (Hingorani and Tuveson, 2003). Interestingly, PDA progression is believed to require additional genetic insults including deregulation of cell death pathways via mutations in the p16Ink4A and p53 proteins (Maitra and Hruban, 2008). The disease, however, may still be RAS dependent, as recent work has shown that inactivation of RAS in a mouse model of RAS-driven pancreatic cancer can cause tumor regression (Collins et al., 2012).

Advanced PDA is characterized by extensive stromal infiltration of the pancreas that is often seen alongside epithelial structures resembling enlarged and abnormal ductal structures termed pancreatic intraepithelial neoplasias (PanINs) (Hruban et al., 2006). A proposed model for progression from small PanINs into advanced disease utilized findings that the stromal deposition observed in patients is often focused on specific pancreatic lobes, termed lobulocentric atrophy (Brune et al., 2006).

The observed fibrous stroma deposition seen in early PDA samples is restricted to lobes also containing PanINs (Brune et al., 2006). Further analysis of post-mortem pancreatic samples taken from elderly patients with no evidence of pancreatic disease also found foci of fibrosis associated with PanIN structures (Detlefsen et al., 2005). These data led to a proposed model in which PanIN development obstructs normal ducts, preventing normal zymogen secretion and triggering autoactivation of digestive enzymes leading to localized tissue damage (Hruban et al., 2008). Localized damage then triggers inflammation and regeneration via prolonged mitogenic signaling, suppressing normal cellular mechanisms for preserving DNA integrity and suppressing proliferation. This allows the expansion of the existing PanIN lesion and development of more extensive fibrosis, initiating a feedback loop in which the initial lesion promotes an inflammatory environment that gives rise to other lesions. These findings, coupled with the ductal expression phenotype and ductal histological appearance prompted many researchers to conclude that PDA was derived from ductal cells that acquire an activating KRAS mutation **(Figure 6.02a)** (Hruban et al., 2008).

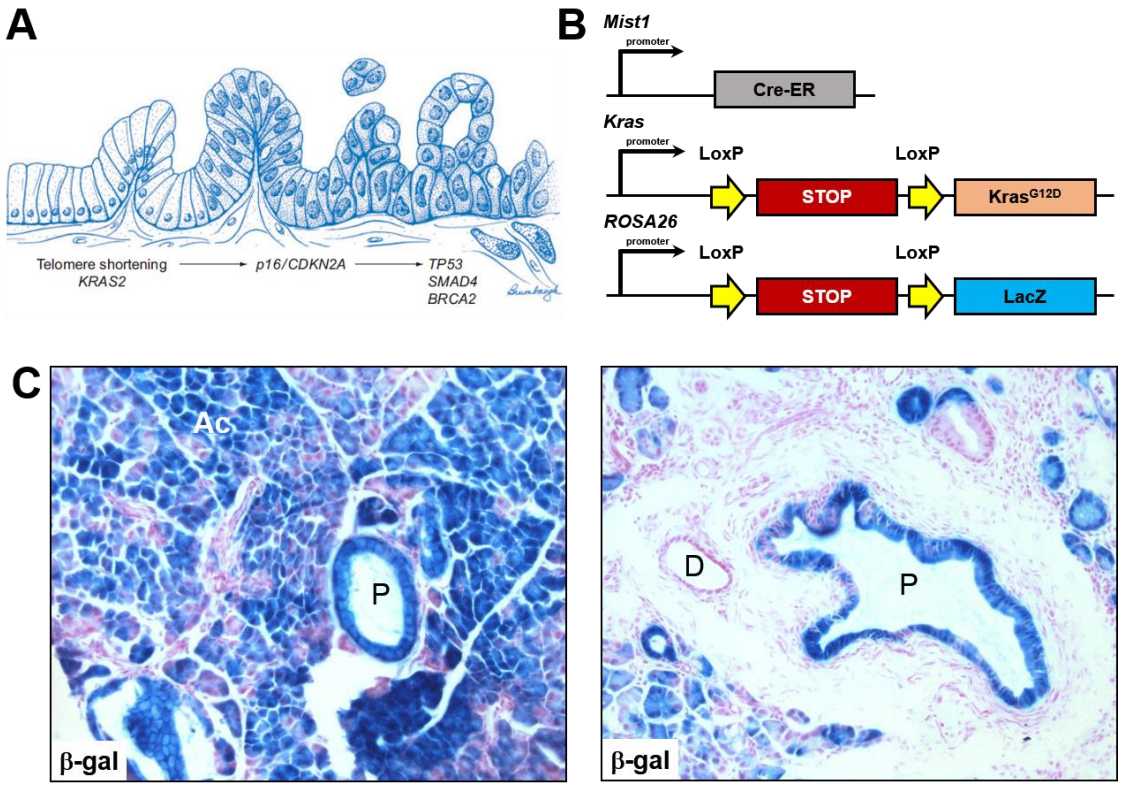

Figure 6.2 *Acinar cells directly contribute to PanIN lesions*

(A) Proposed model for PanIN development in which duct cells give rise to PanIN lesions(Hruban et al., 2008). (B) Schematic of genetic loci in *Mist1*$^{CreER/+}$*; LSL-Kras; R26*^{LacZ} reporter mice coupling acinar-specific KRAS^{G12D} expression to β-galactosidase. (C) PanIN lesions in *Mist1*$^{CreER/+}$*; LSL-Kras; R26*^{LacZ} reporter mice are positive for β-gal expression, indicating an that these PanINs are initially derived from acinar cells. Image adapted from Shi et al., 2009b.

Questions regarding the ductal origin of PDA arose when mouse models in which oncogenic KRAS was expressed from the duct-specific *cytokeratin 19* (K19) promoter failed to produce PanINs or PDA (Brembeck et al., 2003). Other researchers utilized lineage tracing models with Cre-mediated acinar-specific activated KRAS expression coupled to expression of the β-galactosidase gene **(Figure 6.02b)** (Habbe et al., 2008; Shi et al., 2009b). This construct labels all cells expressing KRAS as well as their progeny, allowing tracing of acinar cells that undergo Cre-mediated recombination regardless of any transdifferentiation events tied to oncogenic transformation. The appearance of β-gal positive PanIN structures following $KRAS^{G12D}$ expression allowed investigators to conclude that PanIN lesions were being derived from acinar cells via a process known as acinar-ductal metaplasia (ADM) **(Figure 6.02c)** (Habbe et al., 2008; De La O et al., 2008). Updated models of PanIN progression that include data from mouse studies now include acinar cells as possible sources of PanIN lesions, although the exact transcriptional networks that are required for ADM have not been fully elucidated.

Acinar-ductal metaplasia is frequently seen associated with PanIN lesions in human and mouse models (Brune et al., 2006; Zhu et al., 2007). ADM is accompanied by reduced digestive enzyme synthesis, altered acinar morphology resulting in cells resembling duct cells, and expression of duct-restricted proteins including mucin and transcription factor Sox9 **(Figure 6.03)** (Kopp et al., 2012). ADM conversion also involves downregulation of the acinar cell-specific transcription factor MIST1 (Rooman and Real, 2011), although the exact role MIST1 plays in maintaining acinar cell identity is still under investigation.

Loss of MIST1 in transgenic mice is associated with cell disorganization, polarity loss, loss of intracellular gap junctions/communication, and increased acinar lumen size **(Figure 6.04)** (Direnzo et al., 2012; Jia et al., 2008; Pin et al., 2000; Rukstalis et al., 2003; Zhu et al., 2004). These mice, however, show no significant decrease in lifespan. Interestingly, *Mist1* knockouts have increased ADM and PanIN formation in $KRAS^{G12D}$ expressing mice (Shi et al., 2009b). However, even in KRAS-expressing, $MIST1^{KO}$ mice, PanIN formation is sparse and temporally dispersed with only a small subset of acinar cells undergoing ADM at any given time. This has made studies of KRAS-derived ADM and its role in PDA development difficult.

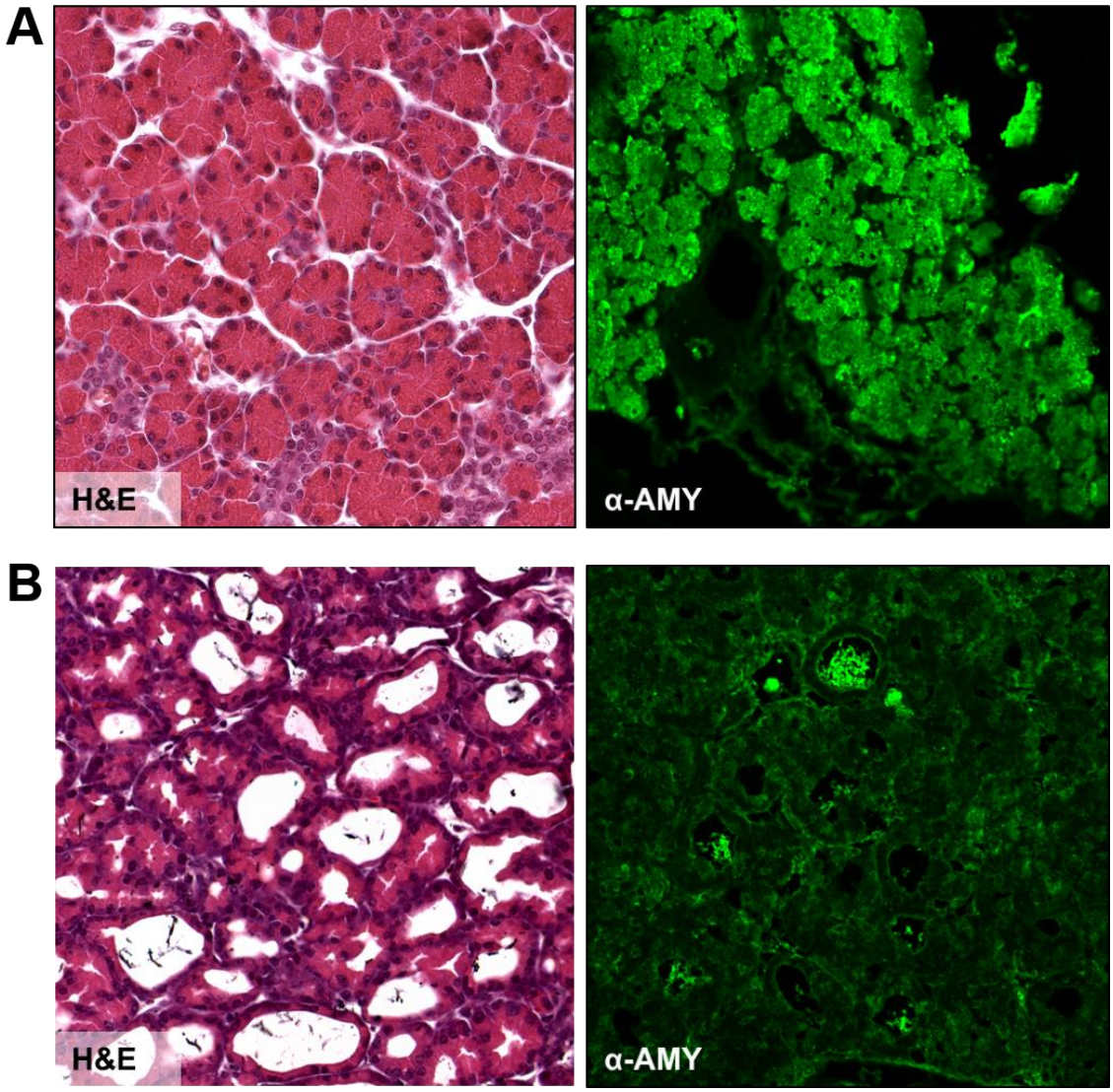

Figure 6.3 *Acinar-ductal metaplasia involves alterations to acinar cell morphology and protein expression*

Early PN1 neonatal pancreata have little endoplasmic reticulum staining but still abundantly express amylase, the highest-produced zymogen in the pancreas. Mist1$^{Kras/+}$ (discussed later) PN1 mouse pancreata with extensive ADM have multiple open-lumened acini (B, left) and drastically reduced amylase production (B, right).

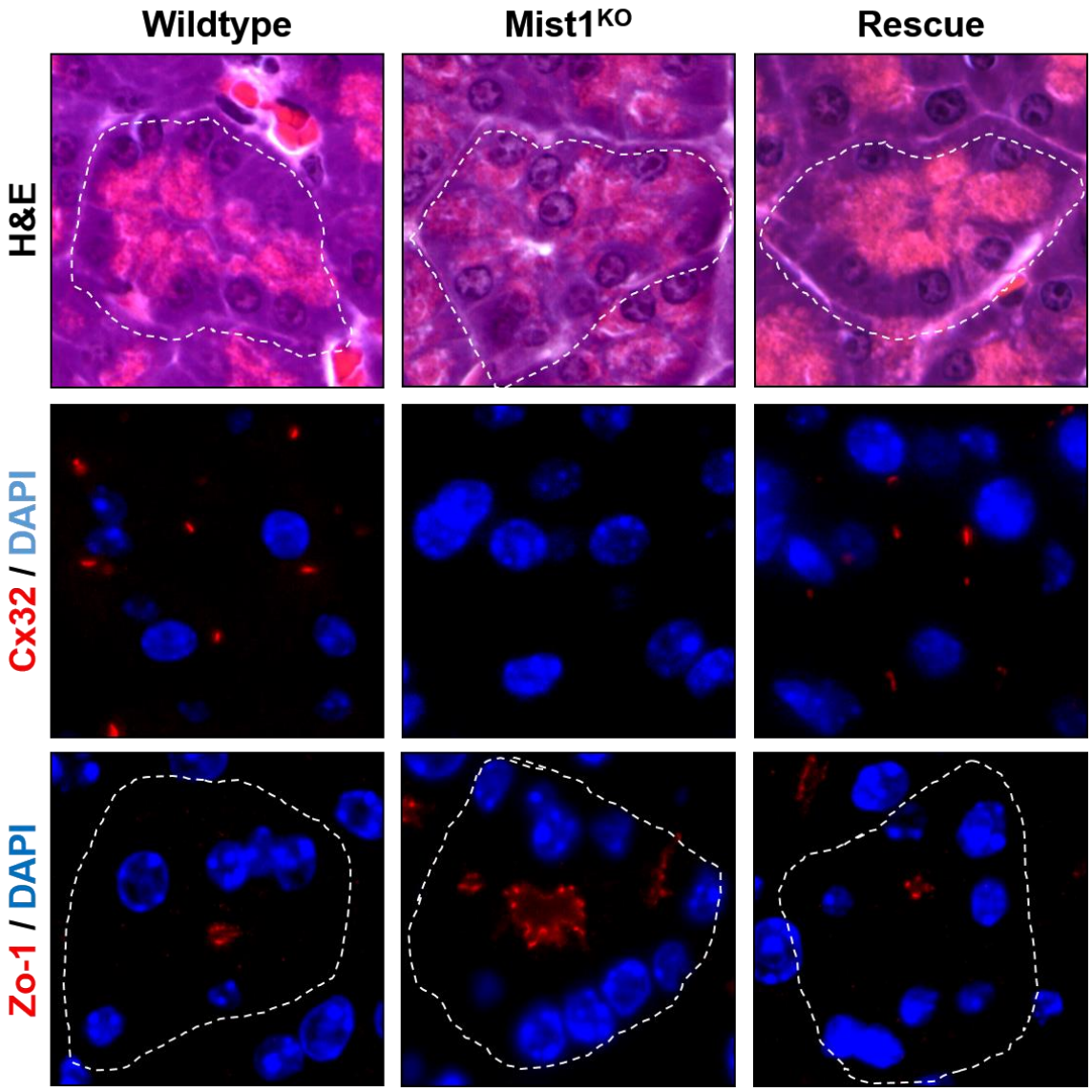

Figure 6.4 *MIST1 regulates cell polarity, gap junction formation, and lumen size in pancreatic acinar cells*

(Left panels) Wildtype adult pancreata with characteristic acinar morphology including apical-basal polarity (H&E image), expression of CONNEXIN32 (Cx32), and tight acinar lumens marked by ZONA OCCLUDENS 1 (Zo-1). (Middle panels) Mist1^{KO} pancreata lack apical-basal polarity and Cx32 expression and have enlarged lumens. (Right panels) *Mist1^{KO}* pancreata expressing a *Mist1^{myc}* transgene have restored polarity, Cx32 expression, and lumen size.

Correlative studies utilizing human patient samples found that ADM can be observed in both stand-alone and PanIN-associated states (Shi et al., 2009a). When isolated for genetic analysis via laser capture microdissection, stand-alone ADMs were found to be $KRAS^{WT}$ while ADM-containing RAS-mutations were exclusively found associated with PanINs. This data suggests that ADM is not exclusively derived from KRAS mutants in pancreatic cancer patients, necessitating a further investigation of ADM to determine how and if RAS governs the ADM process. This has proven to be very difficult in human patients and existing mouse models, since mutant RAS expression triggers only limited transformation events despite high penetrance in many mouse systems (Guerra et al., 2003). More recent work has shown that this refractory response to $KRAS^{G12D}$ expression is due to the need for KRAS activation via initiation of extrinsic mitogenic signaling (Huang et al., 2013). Indeed, multiple studies have confirmed that oncogenic RAS mutations within the pancreas do not necessarily lead to development of PDA or metastatic disease (Lu et al., 2002; Parsons and Meng, 2009; Yan et al., 2005). These findings indicate that cellular context must be accounted for in developing systems for studying ADM.

Mouse model work studying pancreatic cancer development has shown that even single occasions of acute pancreatitis following expression of mutant KRAS can drastically accelerate PDA progression (Carrière et al., 2009). Pancreatitis leads to development of extensive ADM, however, it also induces extreme damage throughout the pancreas and may complicate studies of the KRAS-specific component of ADM development. Therefore, it seems that the ideal model for studying ADM should utilize a suitable cellular context to allow KRAS-induced ADM formation without chemical or damage-induced exacerbation. We thus sought to investigate whether high-level expression of oncogenic RAS in developing mouse pancreata could be used to study acinar-ductal metaplasia.

In this study, we utilized a mouse model in which activated $KRAS^{G12D}$ is expressed from the acinar cell-specific *Mist1* promoter during embryonic development and in the adult exocrine pancreas. Herein we demonstrate that high-level, acinar cell-specific expression of activated RAS during embryogenesis generates extensive ADM ductal structures both during and following development. Furthermore, we show that these

ductal structures bear the hallmarks of ADM structures including decreased zymogen synthesis and increased proliferative capacity. Finally, we show that the severity of ADM formation is mitigated by the MIST1 protein, indicating that MIST1 likely plays a role in maintaining the acinar cell phenotype during KRAS-induced ADM formation.

6.2 Generation of *Mist1*$^{Kras/+}$ mice

The *Mist1*$^{Kras/+}$ line was generated via collaboration between the Konieczny and the Tuveson research group at the University of Pennsylvania. This line expresses oncogenic KRAS^{G12D} from the *Mist1* promoter, previously described in this report as restricted to acinar cells in the pancreas. The mouse line was generated via standard "knock in" techniques utilizing generation of chimeric mice following homologous recombination of the *Kras4B*^{G12D} cDNA into embryonic stem cells **(Figure 6.05a)** (Tuveson et al., 2006). Median survival time for *Mist1*$^{Kras/+}$ mice was decreased by approximately 55% **(Figure 6.05b)**. Notably, *Mist1*$^{Kras/LacZ}$ mice (not included on the plot) appear externally normal at birth but are severely undersized and die by three days post-birth, revealing the importance of MIST1 to normal acinar cell function.

In order to investigate the effects of KRAS^{G12D} expression driven by the Mist1 promoter, we bred *Mist1*$^{Kras/+}$ mice to *Mist1*$^{LacZ/+}$ animals **(Figure 6.05c)**. This crossing scheme generated control *Mist1*$^{+/+}$ and *Mist1*$^{LacZ/+}$ animals as well as *Mist1*$^{Kras/+}$ and *Mist1*$^{Kras/LacZ}$ experimental mice. This design allowed us to investigate the effects of KRAS^{G12D} expression both in the presence and absence of MIST1. Of note, *Mist1*$^{Kras/+}$ females are incapable of nursing their young due to expression of KRAS^{G12D} in the lactating mammary gland. As a result, only male *Mist1*$^{Kras/+}$ mice were used as breeders, however female mice were used in embryo studies.

6.3 *Mist1*$^{Kras/LacZ}$ mice develop extensive ADM that can be rescued by expression of a MIST1myc transgene

Previous work in mouse models had demonstrated that embryonic expression of high levels of RAS can lead to development of hyperplasia (Perez-Mancera and Tuveson, 2006). In order to investigate whether *Mist1*$^{Kras/+}$ mice develop ADM during development,

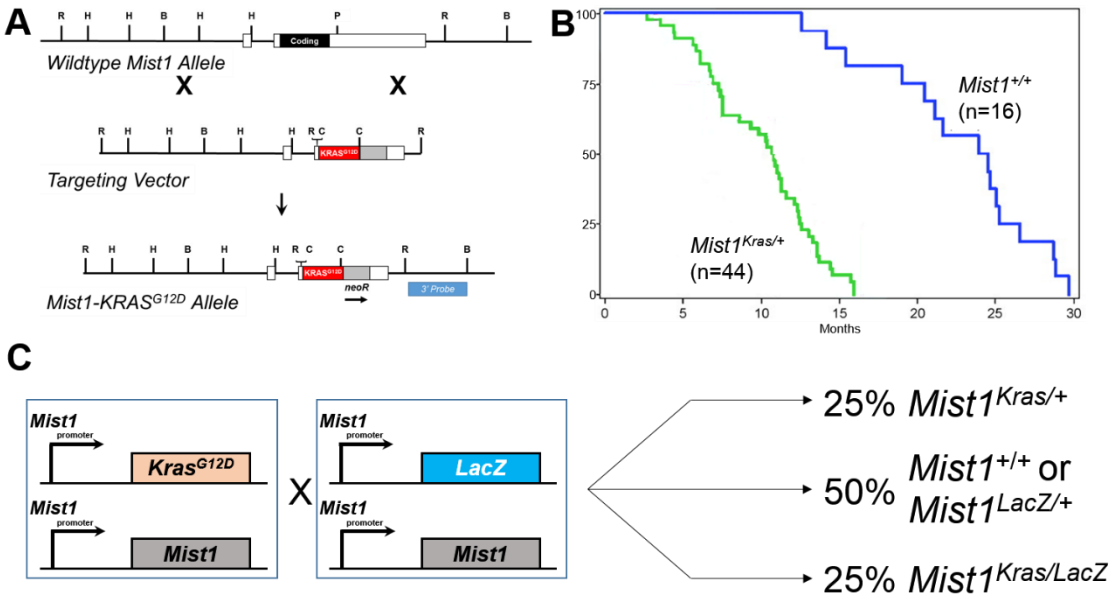

Figure 6.5 *Crosses for generating the Mist1$^{Kras/+}$ line and relevant controls for embryonic studies*

(A) Targeting strategy for generation of the *Mist1$^{Kras/+}$* mouse line. (B) Kaplan-Meier plot showing median survival time of 10.8 months for *Mist1$^{Kras/+}$* mice vs. 24.2 months for *Mist1$^{+/+}$* mice. (C) *Mist1$^{Kras/+}$* mice were mated to *Mist1$^{LacZ/+}$* mice to generate both control (Mist1$^{+/+}$) animals as well as mice bearing the *Kras^{G12D}* allele either with or without *Mist1* (*Mist1$^{Kras/+}$* and *Mist1$^{Kras/LacZ}$* respectively). Figures A and B adapted from Tuveson et al., 2006.

we first harvested pancreata from post-natal day 1 (PN1) embryos from the previously described mouse cross. Histological examination of sections from fixed pancreata showed that *Mist1*$^{+/+}$ acini have normal apical-basal polarity with basally-localized nuclei **(Figure 6.06a)**, but they lack strong staining of the ER, presumably due to decreased need for digestive hydrolases during development and while still nursing. Additionally, acini in these animals had closed lumens, indicating no basal levels of damage or developmentally- associated acinar-ductal metaplasia **(Figure 6.06a, blue arrows)**. In contrast, *Mist1*$^{Kras/+}$ PN1 pancreata had a pronounced increase in the occurrence of ADM-like, open-lumened acini **(Figure 6.06b, red outlines and arrows)**, although normal acini with closed lumens were also present **(Figure 6.06b, blue outline and arrow)**. *Mist1*$^{Kras/LacZ}$ mice had no normal acini. Instead, pancreata in *Mist1*$^{Kras/LacZ}$ mice contained a mix of ADM-like open-lumened acini **(Figure 6.06c, red outlines and arrows)** and larger duct-like complexes **(Figure 6.06c, D.C.)**.

The striking difference between *Mist1*$^{Kras/+}$ and *Mist1*$^{Kras/LacZ}$ was confirmed to be due to a deficiency in MIST1 following an experiment performed by Dr. Yan Sun in the Konieczny lab (Shi et al., 2009b) in which *Mist1*$^{Kras/LacZ}$ mice were mated to mice expressing a Mist1^{myc} transgene from the acinar cell-specific elastase promoter (*El$_{pr}$-Mist1*^{myc}). As shown in **Figure 6.07b,c**, expression of MIST1^{myc} rescues the *Mist1*$^{Kras/LacZ}$ phenotype, eliminating the appearance of large ductal complexes and returning the pancreas to a *Mist1*$^{Kras/+}$ appearance. We next sought to determine whether we could observe the earliest stages of ADM development via analysis of embryonic pancreata from *Mist1*$^{Kras/+}$ and *Mist1*$^{Kras/LacZ}$ animals.

6.4 *Mist1*$^{Kras/+}$ pancreata develop increasing numbers of proliferative ductal structures during embryogenesis

Embryos were obtained via timed pregnancies at three specific ages; E13.5, E 16.5, and E18.5. MIST1 expression (and thus KRAS^{G12D} expression) was first detected at day E13.5 and was only present in cells coexpressing amylase **(Figure 6.08b, c)**. However, no phenotypic difference could be observed between *Mist1*$^{+/+}$, *Mist1*$^{Kras/+}$, and *Mist1*$^{Kras/LacZ}$ animals at E13.5 as distinct, properly organized acini were not yet distinguishable.

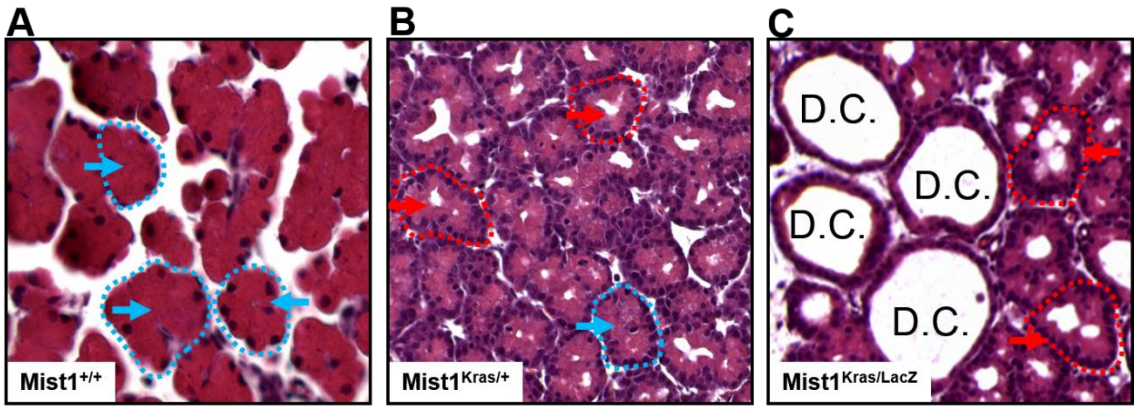

Figure 6.6 *Mist1$^{Kras/+}$ and Mist1$^{Kras/LacZ}$ animals have disrupted pancreata at birth*

(A) *Mist1$^{+/+}$* neonatal pancreata at post-natal day 1 (PN1) have acini (blue dotted lines) with normal, basal-localized nuclei and closed apical lumens (blue arrows). (B) *Mist1$^{Kras/+}$* PN1 pancreata have both normal acini (blue outline, arrow) and abnormal acini (red outlines) with open lumens (red arrow) resembling acinar-ductal metaplasia. (C) *Mist1$^{Kras/LacZ}$* PN1 pancreata have predominantly abnormal acini with open lumens (red outlines, arrows) as well as large duct-like complexes (D.C.).

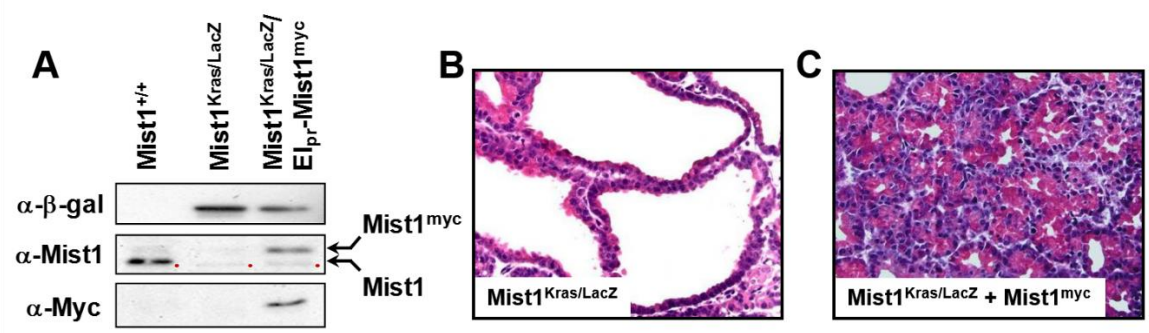

Figure 6.7 *ADM formation in Mist1$^{Kras/LacZ}$ mice can be rescued via expression of a Mist1^{myc} transgene*

(A) Protein blots on neonatal (PN1) pancreatic isolates for β-galactosidase (β-gal), MIST1, and MYC. *Mist1$^{Kras/LacZ}$* mice lack expression of MIST1 while *Mist1$^{Kras/LacZ}$*/El$_{pr}$-Mist1^{myc} mice regain expression of MIST1. (B) *Mist1$^{Kras/LacZ}$* PN1 pancreata have large ductal complexes. (C) *Mist1$^{Kras/LacZ}$/El$_{pr}$-Mist1^{myc}* PN1 pancreata do not have predominant ductal complexes and resemble *Mist1$^{Kras/+}$* pancreata. Images courtesy from Shi et al., 2009b.

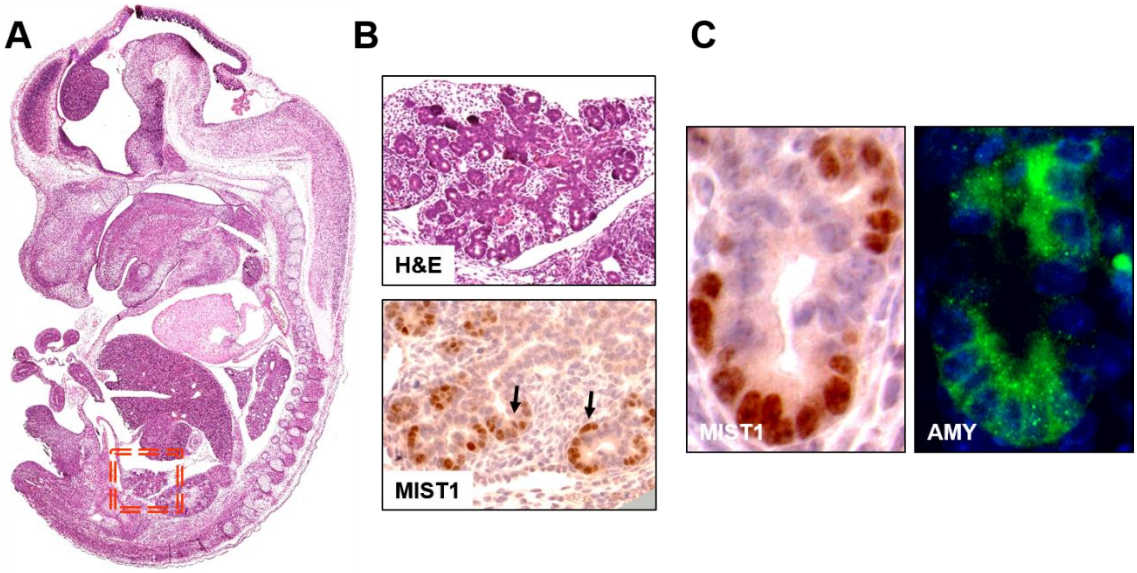

Figure 6.8 E13.5 pancreata express MIST1 in cells coexpressing AMYLASE

(A) Low-magnification of E13.5 embryo. Red box indicates location of the developing pancreas. (B) H&E and anti-MIST1 IHC images of pancreatic sections from E13.5 embryo. MIST1 is expressed in the terminal buds of the developing pancreas (black arrows). (C) High magnification image of a pancreatic terminal bud showing coexpression of MIST1 and AMYLASE, both markers exclusive to acinar cells.

ADM/open-lumened acini were first observed at E16.5 in all three genotypes **(Figure 6.09b)**. However, the majority of *Mist1*$^{+/+}$ acini exhibited normal polarity and closed lumens with a scant minority of open-lumened structures **(Figure 6.09b, left panel insets)**. In contrast, acini from *Mist1*$^{Kras/+}$ and *Mist1*$^{Kras/LacZ}$ pancreata were largely of the open lumen variety **(figure 6.09b, center and right panels)**. This difference in the KRAS^{G12D}-expressing mice was drastically increased by E18.5 **(Figure 6.09a)**. *Mist1*$^{Kras/+}$ pancreata, however, had a marked increase in both open-lumened acini and ductal complexes **(Figure 6.09a, middle)**. Interestingly, *Mist1*$^{Kras/LacZ}$ pancreata were even more severe, with the pancreas consisting almost entirely of ductal complexes with few surviving normal acini **(Figure 6.09a, right)**.

In order to confirm that the ADM/open-lumened acini had decreased acinar properties we quantified amylase expression via serial section fluorescence imaging on isolated pancreata. As shown in **Figure 6.10a,b**, the diffuse amylase content throughout the exocrine compartment in *Mist1*$^{+/+}$ pancreata was vastly diminished in *Mist1*$^{Kras/+}$ and *Mist1*$^{Kras/LacZ}$ animals, with the majority of zymogen content present in the lumens of the large ductal complexes (to be discussed later). Quantification of relative amylase intensity of non-lumenal areas via pixel analysis showed a significant reduction in amylase content in both KRAS^{G12D}-expressing groups relative to control, with no significant difference between either of the KRAS groups.

Finally, we sought to determine whether the ADM/open-lumened acini were more highly proliferative, a common observation in ADM and PanIN lesions in human patients. We stained embryonic sections for the proliferation marker Ki67 and quantified the numbers of positive nuclei per field as a percentage of total nuclei. As shown in **Figure 6.11b**, *Mist1*$^{Kras/+}$ and *Mist1*$^{Kras/LacZ}$ pancreata have a significantly higher proliferative index during embryonic development relative to Mist1$^{+/+}$. Both also remain elevated at birth, although only the *Mist1*$^{Kras/LacZ}$ pancreata reached the significance threshold of ≥95%.

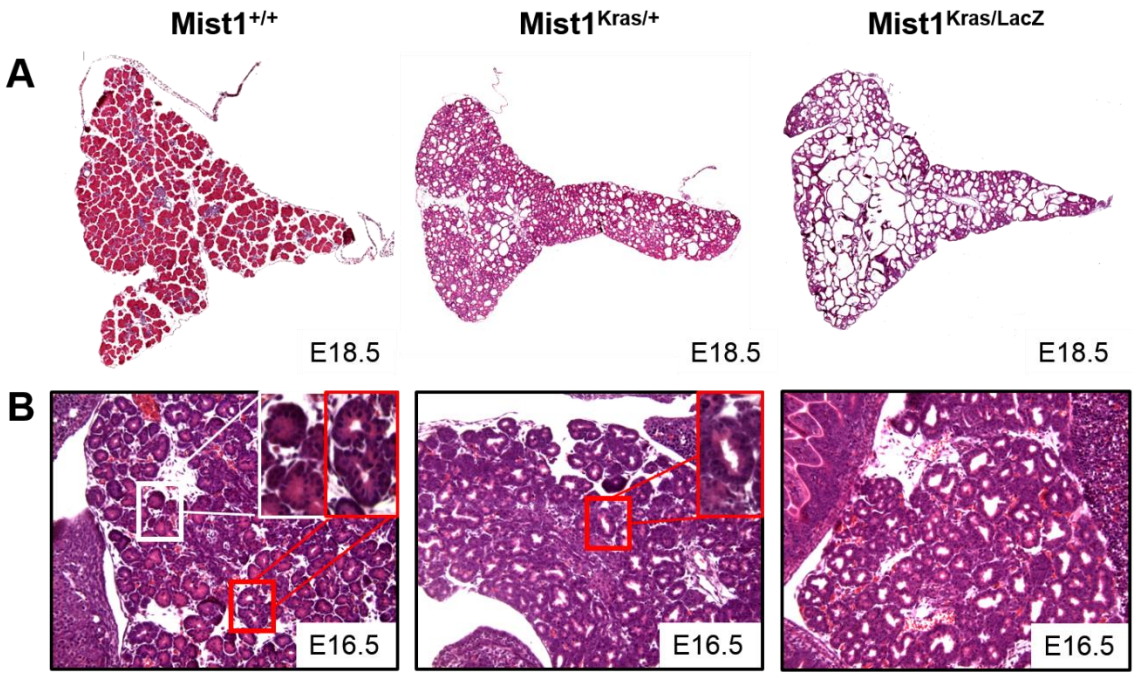

Figure 6.9 *ADM and ductal lesion formation precede birth in Mist1$^{Kras/+}$ and Mist1$^{Kras/LacZ}$ animals*

(A) Low magnification images of whole pancreata isolated from E18.5 mice. Mist1$^{+/+}$ pancreata appear normal, while *Mist1$^{Kras/+}$* pancreata have extensive open lumen acinar structures and *Mist1$^{Kras/LacZ}$* mice have almost entirely large ductal complexes. (B) Pancreatic sections from E16.5 animals reveal that *Mist1$^{+/+}$* acinar cells have predominantly closed lumens (inset, white box) with occasional open lumened acini (inset, red box). *Mist1$^{Kras/+}$* acinar cells are predominantly open lumened (inset, red box), while *Mist1$^{Kras/LacZ}$* acinar cells are entirely open lumened.

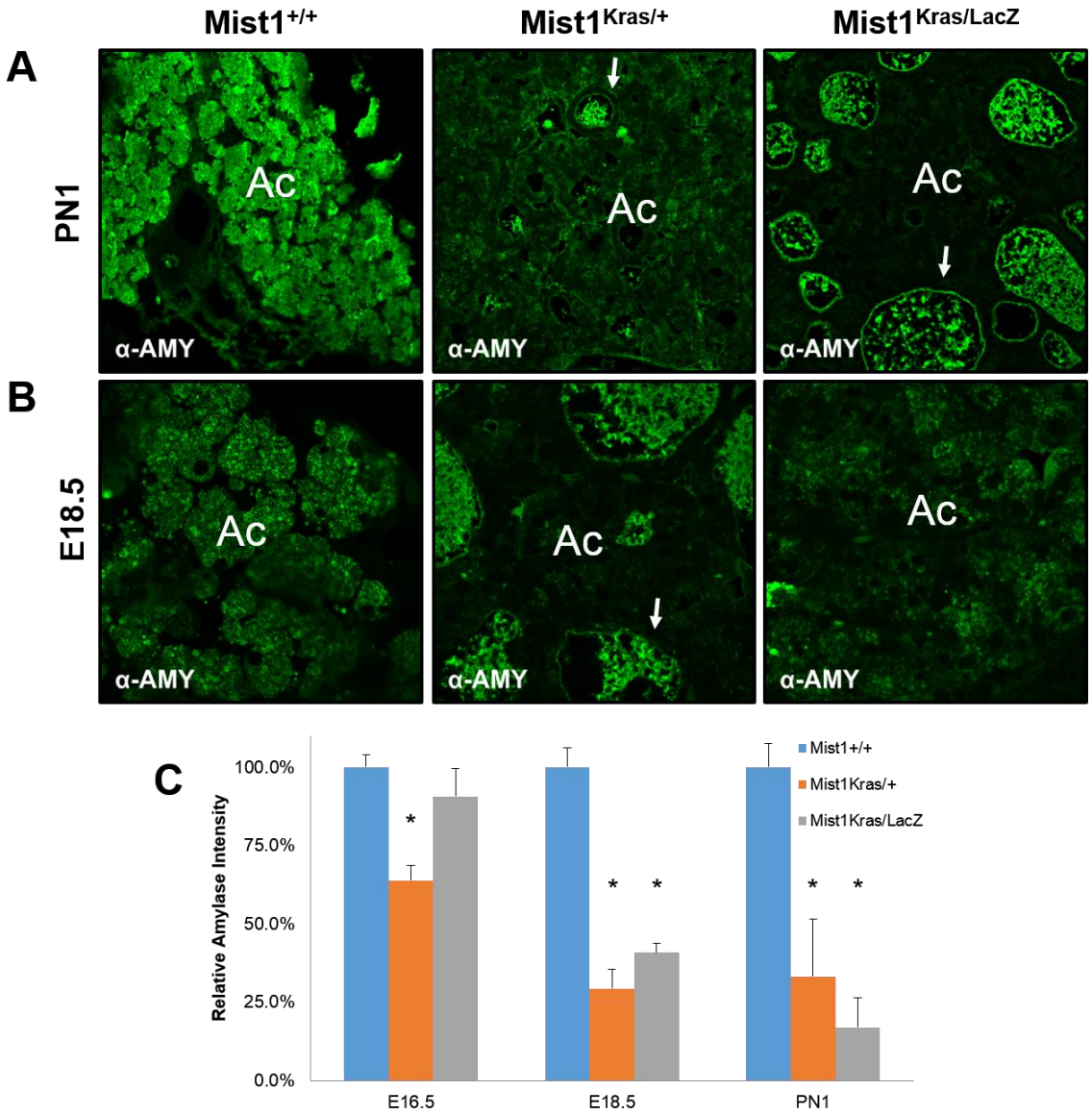

Figure 6.10 *Zymogen production is reduced in Mist1$^{Kras/+}$ and Mist1$^{Kras/LacZ}$ pancreata throughout development*

(A, B) Confocal microscopy of PN1 and E18.5 pancreata reveal diffuse amylase staining in *Mist1*$^{+/+}$ acinar cells (Ac) with little amylase content outside of duct-like complex lumens (white arrows) in *Mist1*$^{Kras/+}$ and *Mist1*$^{Kras/LacZ}$ animals. (C) Quantification of relative intensity of amylase staining in acinar areas shows significantly reduced expression in both *Mist1*$^{Kras/+}$ and *Mist1*$^{Kras/LacZ}$ animals by E18.5. (* = significantly different with p-value <0.01 relative to Mist1$^{+/+}$)

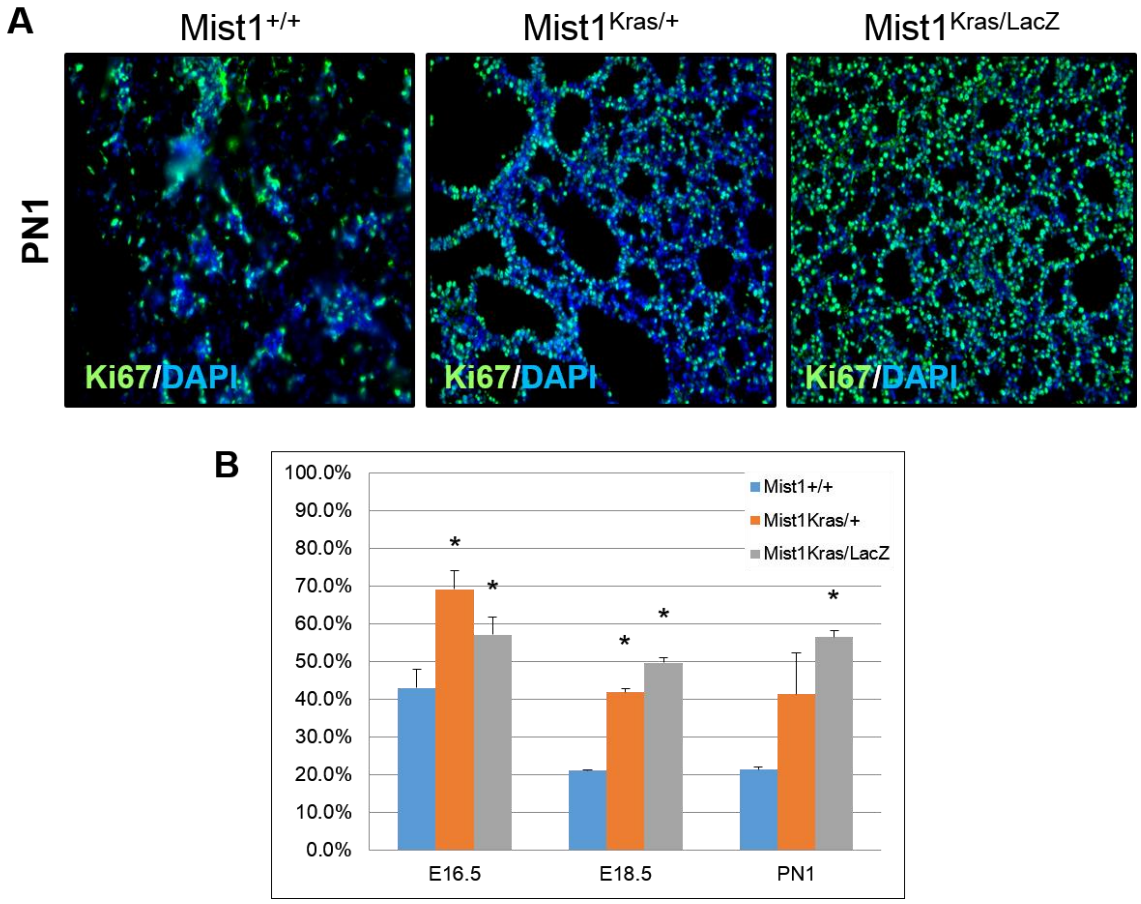

Figure 6.11 *Mist1$^{Kras/LacZ}$ pancreata have significantly increased proliferative capacity throughout development*

(A) Immunofluorescence staining for the proliferation marker Ki67 in PN1 pancreatic sections. (B) Counts of Ki67-positive nuclei per 10X field in E16.5, E18.5, and PN1 pancreatic sections as a percentage of total nuclei. *Mist1$^{Kras/LacZ}$* pancreata have significantly increased proliferative capacity relative to *Mist1$^{+/+}$* throughout development while *Mist1$^{Kras/+}$* pancreata are significantly increased until birth when they remain elevated. (* = significantly different with p-value < 0.05 relative to *Mist1$^{+/+}$*)

6.5 Ductal complex size is correlated with expression of MIST1

Since MIST1 appeared to have a substantial effect on phenotype severity between *Mist1*$^{Kras/+}$ and *Mist1*$^{Kras/LacZ}$ mice, we sought to determine if the previously stated link between ADM formation and downregulation of MIST1 could be observed in our embryonic mice. We first stained E16.5 *Mist1*$^{Kras/+}$ pancreatic sections for MIST1, as they previously had been seen to have large numbers of ADM/open-lumened acini. Surprisingly, the open-lumened acinar structures in E16.5 pancreata were all MIST1 positive **(Figure 6.12a, black outlines and arrows)**. We proceeded to stain E18.5 *Mist1*$^{Kras/+}$ pancreatic sections and found extensive MIST1 expression in the ADM structures **(Figure 6.12b, black stars)**. Interestingly, upon closer examination we determined that while small ADMs were MIST1 positive, larger ductal complexes were almost uniformly MIST1 negative **(Figure 6.12c)**. This expression pattern was consistent in ductal complexes that were larger than their acinar cell counterparts, however smaller open-lumened acini consistently expressed MIST1.

In order to determine if the downregulation of MIST1 in ductal complexes was associated with any secretory phenotypes, we stained E18.5 pancreatic sections for the zymogens amylase and carboxypeptidase A. As shown in **Figure 6.13a-c**, the lumens of the ductal cysts in *Mist1*$^{Kras/+}$ and *Mist1*$^{Kras/LacZ}$ pancreata were positive for both amylase and CPA but negative for a non-zymogen control (α-MIST1, unretrieved). This is unique as normal ducts in *Mist1*$^{+/+}$ pancreata have no zymogen staining. This may be a byproduct of the ductal complexes being forced to expel the remaining zymogen granules before completing the conversion from acinar to duct-like cells, although further analysis is required.

6.6 Adult *Mist1*$^{Kras/+}$ acinar cells are predisposed to ductal complex and cyst formation

In order to determine whether the observed ADM and ductal cysts seen in embryonic sections from *Mist1*$^{Kras/+}$ mice would give rise to ductal lesions in adult mice, we performed *ex vivo* and *in vivo* analyses of mature *Mist1*$^{Kras/+}$ pancreata. We first utilized the collagen-based 3D culture system described in detail in Chapter 4. Briefly, we

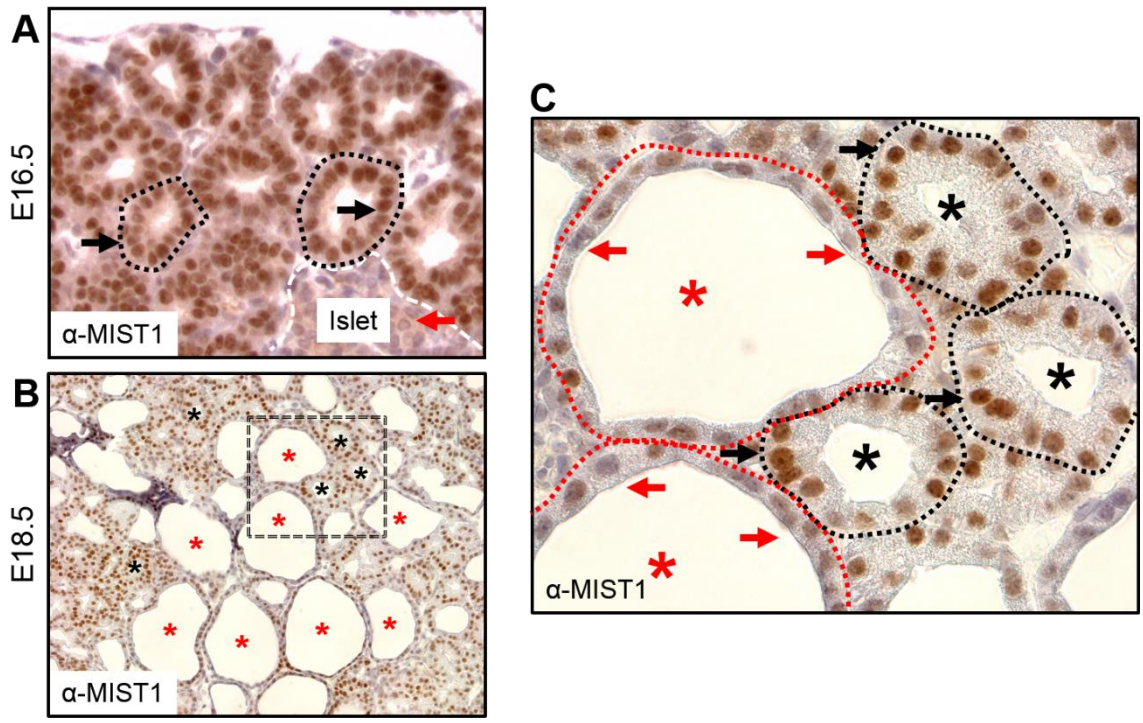

Figure 6.12 *Ductal complexes in Mist1$^{Kras/+}$ mice have a correlation between expression of Mist1 and reduced size*

(A) Immunohistochemical (IHC) stain for MIST1 in *Mist1$^{Kras/+}$* mice at E16.5 shows open-lumened acini (black outlines) with MIST1-positive nuclei (black arrows). MIST1-negative islet nuclei (red arrows) shown for reference. (B) IHC for MIST1 in *Mist1$^{Kras/+}$* E18.5 pancreata shows the presence of both ADM (black stars) and large ductal complexes (red stars). (C) High magnification image of black boxed area from image B showing ADM lesions with MIST1-positive nuclei (black outlines, arrows) while ductal complexes have predominantly MIST1-low or MIST1-negative nuclei (red outlines, arrows).

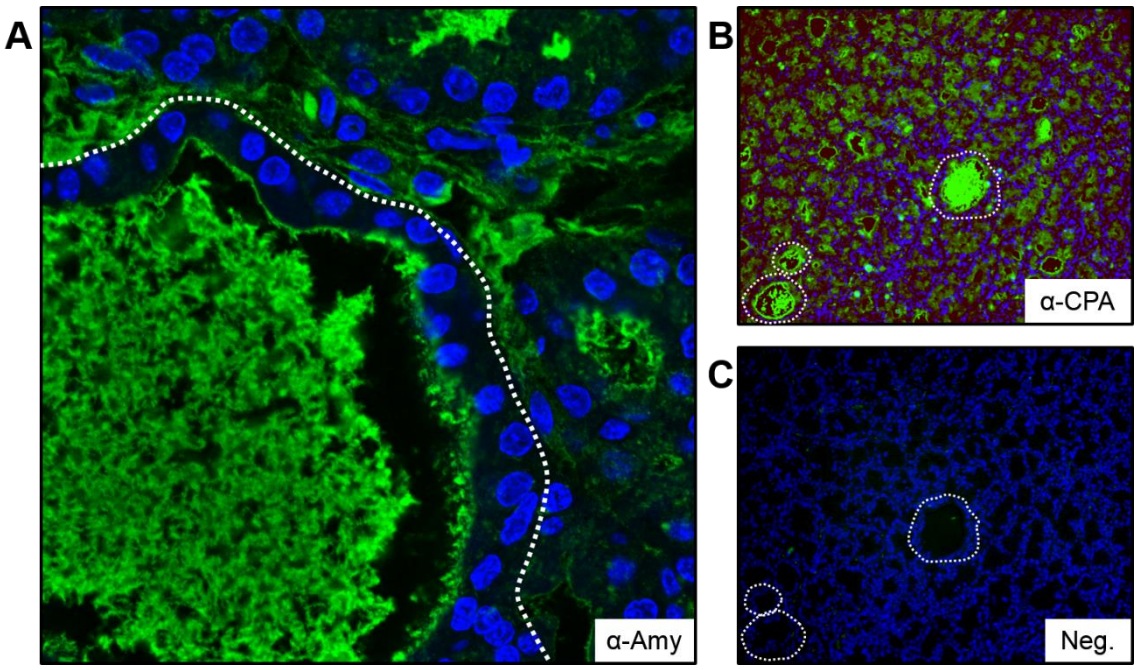

Figure 6.13 *Ductal structures aberrantly secrete zymogens into their lumens in Mist1$^{Kras/+}$ and Mist1$^{Kras/LacZ}$ pancreata*

(A) High-magnification confocal immunofluorescence image of representative ductal lumen in E18.5 *Mist1$^{Kras/+}$* pancreata. Amylase is largely absent from the cells but is present in the ductal lumen. White outlines represent boundaries of the ductal structures. (B) Low-magnification stain for carboxypeptidase A (CPA), another zymogen, also shows strong staining in the ductal lumens. White outlines represent boundaries of the ductal structures. (C) Non-zymogenic antibody control (α-MIST1, unretrieved) does not stain ductal lumens. White outlines represent boundaries of the ductal structures.

isolated acinar cells from 3 month-old *Mist1*$^{Kras/+}$ mice via collagenase digestion and subsequent size exclusion filtering before embedding the resulting clusters in a collagen matrix. As shown in **Figure 6.14**, *Mist1*$^{Kras/+}$ acinar clusters begin forming ductal cysts **(Figure 6.14, red boxes)** within 24 hours of embedding. These clusters subsequently grew and merged, becoming a large cluster of duct-like cysts with no remaining acinar clusters by day 5 in culture. Interestingly, this conversion to ductal cysts was accompanied by a pronounced degradation of the collagen matrix, seen in **Figure 6.14** as a pronounced transparency in the collagen by day 5. *Mist1*$^{+/+}$ acinar clusters remained quiescent over the duration of the experiment with a minimum of ductal cyst conversion.

In order to see whether the pronounced tendency of *Mist1*$^{Kras/+}$ acinar clusters to convert to ductal cysts would lead to *in vivo* disease, we isolated pancreata from 3-9 month old *Mist1*$^{Kras/+}$ animals. These animals all had palpable masses in the pancreas area of the gut, although the size of the masses was highly variable. Pancreata were isolated and sectioned, and representative images are shown in **Figure 6.15**. Pancreata from *Mist1*$^{Kras/+}$ mice were deficient in acinar tissue **(Figure 6.15, right panel - labeled Ac)**, with most of the pancreatic bulk being composed of small ductal complexes **(Figure 6.15 - black stars)** and larger, encapsulated mucinous structures. Following analysis of the sections conducted with the assistance of Dr. Michael Logan, a certified pathologist, we concluded that the large encapsulated complexes most closely resembled mucinous cystic neoplasms (MCNs), a less common oncogenic lesion that progresses slowly and does not generally give rise to pancreatic ductal adenocarcinoma.

6.7 Discussion

PDA remains a highly lethal human cancer due primarily to insufficient methods of early diagnosis and understanding of early disease. Mouse models utilizing inducible expression of oncogenic KRAS variants can give rise to ADM and PanIN precursor lesions, but typically do so in a wide spatial and temporal window, making analysis of early events in ADM formation difficult to observe. We sought to determine whether the *Mist1*$^{Kras/+}$ mouse model expressing high levels of acinar-cell specific oncogenic KRAS^{G12D} throughout embryogenesis could serve as a means to investigate early acinar-ductal metaplasia.

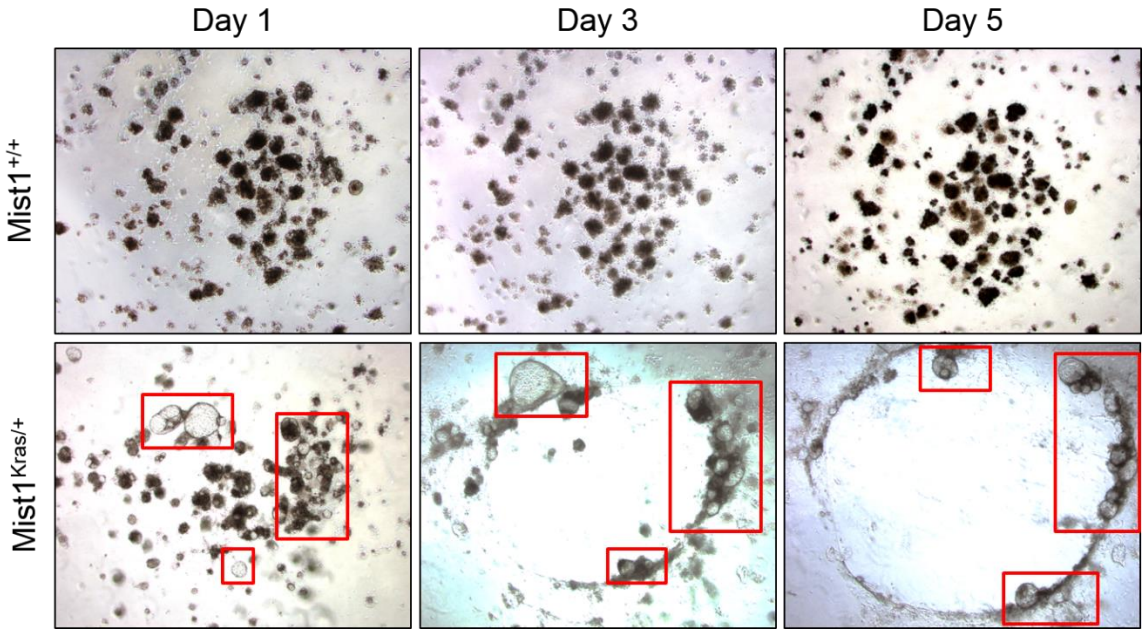

Figure 6.14 *Mist1$^{Kras/+}$ acinar cells rapidly develop into duct-like cysts in 3D culture*

(Top panel) *Mist1$^{+/+}$* acinar clusters grown in a collagen 3D-culture model remain largely quiescent over five days. (Lower panel) *Mist1$^{Kras/+}$* acinar clusters begin forming duct-like cysts (red boxes) in culture within 24 hours of collagen embedding. These clusters grow and combine over subsequent days and also appear to migrate as the collagen disk degrades.

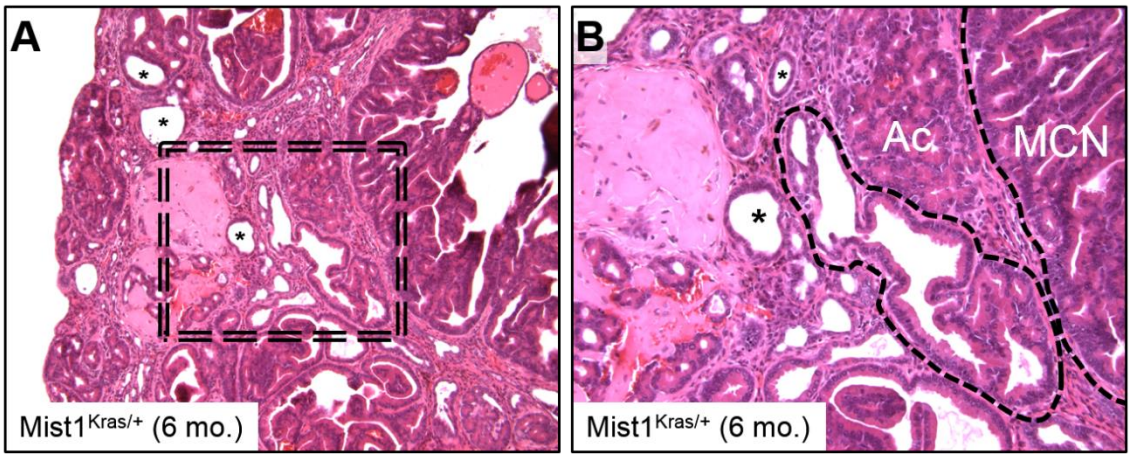

Figure 6.15 *Mist1$^{Kras/+}$ mice develop extensive mucinous neoplasms but not PanINs*

(A) Low-magnification image of pancreatic section from a 6 month old *Mist1$^{Kras/+}$* mouse. The vast majority of acinar tissue has been replaced by ductal complexes (black stars) and other ductal tissues of mixed pathology. (B) High-magnification image of boxed area from 6.13a shows small pockets of acinar tissue (Ac) as well as well-encapsulated ductal structures (black outlines). Analysis by a certified pathologist identified these structures as MCNs, not PanINs.

As demonstrated in **Figure 6.05b**, *Mist1*$^{Kras/+}$ mice have a drastically shortened lifespan compared to *Mist1*$^{+/+}$ littermates. This decreased lifespan was hypothesized to be due to advanced pancreatic cancer, although hepatocellular carcinomas resulting from either metastasis or transient MIST1 (and thus KRAS^{G12D}) expression in hepatic stem cells were also observed (Tuveson et al., 2006). Importantly, *Mist1*$^{Kras/+}$ mice develop large ADM and ductal cyst populations at least as early as E18.5 **(Figure 6.09)**, indicating that use of the model to observe ADM development would necessitate embryonic tissue isolation.

ADM and ductal cyst development in both *Mist1*$^{Kras/+}$ and *Mist1*$^{Kras/LacZ}$ animals was accompanied by a significant decrease in amylase expression **(Figure 6.10)** and a significant increase in proliferative capacity **(Figure 6.11)**. Interestingly, the decrease in amylase expression was observed alongside an aberrant depositing of zymogens into the ductal lumens of the large complexes **(Figure 6.13)**. This was surprising as ductal lesions *in vivo* are frequently disconnected from established ductal networks. This could indicate that early conversion to ductal cysts is accompanied by aberrant secretion of digestive enzymes into the periacinar space, providing an alternative reason as to why ductal cyst formation is closely associated with fibrous stromal deposition (Brune et al., 2006; Detlefsen et al., 2005).

Reduced MIST1 expression is a hallmark of early ADM and PanIN development, as well as a general response to damage in acinar cells (Rooman and Real, 2011). Here, we showed that the absence of MIST1 drastically enhances the effects of embryonic expression of KRAS^{G12D} **(Figures 6.07, 6.09)**. Indeed, recent work by the Konieczny group utilizing acinar cells isolated from LSL-Kras^{G12D} transgenic mouse showed that forced overexpression of MIST1 in 3D cultured acinar cells attenuated ductal cyst formation (Shi et al., 2012). This further establishes that MIST1 serves as a critical regulator of acinar cell transdifferentiation, either via direct interaction with KRAS downstream signaling pathways or through enforcement of acinar cell differentiation programs.

Isolation of acinar clusters from adult *Mist1*$^{Kras/+}$ mice indicated a predisposition for these cells to spontaneously convert to duct-like cysts in culture **(Figure 6.14)**. This finding is likely due to the high level of RAS expression driven by the MIST1 promoter prompting a

more rapid damage response following dissociation of the acinar clusters. This is in agreement with recent work indicating that normal levels of oncogenic RAS are insufficient to generate substantial lesion development but that high levels of RAS expression can lead to a pancreatitis-like phenotype and development of cystic carcinomas and metastatic PDA (Ji et al., 2009). This work is also consistent with our finding of cystic neoplasm development in adult *Mist1*$^{Kras/+}$ mice.

Future directions involving the *Mist1*$^{Kras/+}$ line are complicated due to the numerous pitfalls of high-level RAS expression in MIST1-expressing tissues. The previously described inability of *Mist1*$^{Kras/+}$ females to nurse pups either necessitates the use of foster mothers for rearing or reduces the available breeding pool to only males. Additionally, the occurrence of pancreatic malformations as early as PN1 **(Figure 6.06)** leads to often severe pancreatic disease by breeding age onset. Anecdotal observations indicate a reduced drive in *Mist1*$^{Kras/+}$ males, making breeding of sufficient numbers of mice difficult. Nevertheless, the *Mist1*$^{Kras/+}$ line does develop extensive ADM throughout the pancreas, making it ideal for future studies of molecular mechanisms of ADM conversion using whole pancreatic isolates. Additionally, the correlation of ductal cyst size with lack of MIST1 expression in E18.5 *Mist1*$^{Kras/+}$ pancreata would allow for molecular analysis of the role of MIST1 in the two structures via laser capture microdissection of embryonic pancreas sections. Finally, the development of non-PDA advanced cancer in *Mist1*$^{Kras/+}$ mice could be used to investigate the causes and molecular characteristics of mucinous cystic neoplasms, a form of pancreatic cancer that receives infrequent attention due to its less common occurrence.

CHAPTER 7. SUMMARY AND FUTURE DIRECTIONS

Pancreatic ductal adenocarcinoma (PDA) is the most prevalent form of pancreatic cancer, a malignancy that has become the 4th leading cause of national cancer-related deaths despite being primarily considered a disease of the elderly (Siegel et al., 2013). The astonishingly high mortality rate is due to poor understanding of the mechanisms of development, progression, and spread of the disease. While behavioral and genetic insults are suspected to be a link between pancreatic cancer and inflammatory pancreatitis, few studies have attempted to explore the novel cellular response and transcriptional networks that may link the two diseases and provide novel treatment options (Farrow and Evers, 2002). This has resulted in a lack of knowledge regarding possible overlap between the damage responsive pathways of the pancreas and alternative approaches to preventing malignant progression.

Pancreatic cancer and inflammatory pancreatitis both present substantial hurdles for researchers and physicians attempting to improve disease understanding and management. Scientists researching possible causes and treatments of PDA are hampered by a plethora of mouse models that often fail to recapitulate the full spectrum of disease conditions (Hruban et al., 2006). Additionally, controversy regarding the applicability of data based on mouse model systems to human patients has also delayed possible treatment developments (Rooman and Real, 2011). Physicians face a difficult problem as well, as patients suffering from either PDA or chronic pancreatitis are increasingly turning to surgical resection as the only available treatment for either condition (Ho et al., 2005). Despite technical improvements that have reduced the exceptionally high mortality rate that once saw over half of patients die from post-operative complications, surgical intervention still carries a morbidity rate as high as 60% (Ho et al., 2005). These data point to a glaring need for increased knowledge of cancer development, damage responses, and regenerative mechanisms in the pancreas in order to provide efficacious, non-surgical treatment options in human disease.

Recent work in designing targeted cancer therapeutics that are based on a molecular understanding of the disease have yielded astonishingly effective pharmaceutical treatments, including drugs such as trastuzumab (an antibody to the Her2 receptor overexpressed in breast cancer) and imantiinib (an inhibitor to the aberrant Bcr-Abl tyrosine kinase expressed in certain forms of chronic myelogenous leukemia). Other approaches, however, have proven less successful, including the long history of attempted inhibition of the Ras signaling pathway. Ras mutations are among the most frequent occurrences in human cancers, but represent a difficult-to-drug pathway due to the incredibly high occurrence of off-target effects and the importance of Ras signaling to normal cell processes (Chappell et al., 2011). The struggles with Ras have led to new approaches to chemotherapeutics, particularly a refocusing on small, downstream signaling pathway and pathway components that may allow sensitization of cancer cells to broad spectrum chemotherapy options. The unfolded protein response (UPR) is an emerging pathway of interest for design of new drugs to weaken transformed cancer cells (Wang et al., 2010).

Transforming cells must initially acquire mutations or genetic insults that promote their aberrant growth and proliferation. Once acquired, however, cells must then meet the challenge of increased need for nutrients and oxygen, requiring extensive use of protein folding in the ER (Ma and Hendershot, 2004). The UPR can initiate adaptive or apoptotic signaling cascades in transformed cells, making it an ideal target for pharmacological intervention (Li et al., 2011). Indeed, recent drugs taking advantage of ER stress induction, coupled with UPR inhibition (Mimura et al., 2012) or novel small molecules that specifically activate the apoptotic arm of the UPR (Flaherty et al., 2010), have shown promise in treating various malignancies. These approaches necessitate advances in understanding how the UPR maintains cell homeostasis as well as the downstream targets that may be viable options as drugable targets.

Several recent investigations have turned to mouse models in order to investigate the inner workings of the UPR. While yeast studies have long established that the IRE1/XBP1 branch of the UPR is the most prevalent and conserved of the three master regulatory arms (Kimmig et al., 2012), higher eukaryotes have evolved a more complex interacting response utilizing downstream signaling from the ATF6 and PERK embedded

ER sensors (Chakrabarti et al., 2011). This finding prompted numerous groups to generate developmental knock-out mouse lines of each of the respective UPR master regulators, producing a wide range of effects from no observable phenotypic differences at birth (ATF6) to embryonic or neonatal lethality (IRE1) (Reimold et al., 2000; Urano et al., 2000; Yamamoto et al., 2007; Zhang et al., 2002). The lethality associated with either IRE1 or XBP1 germline knockouts made investigations of this particular UPR branch difficult, a problem that was addressed via generation of a Cre-inducible knockout line by Drs. Ann-Hwee Lee and Laurie Glimcher at Harvard University (Hetz et al., 2008). This line, termed the *Xbp1*$^{fl/fl}$ mouse line, has been used by multiple groups to investigate XBP1's role in both the UPR and development.

Early investigations of XBP1 revealed that its expression was required for normal liver development and survival of developing mouse embryos (Reimold et al., 2000). When XBP1 expression was rescued in the liver, a key observation was made that secretory machinery in a number of exocrine tissues was disrupted, demonstrating that XBP1 was required for generating normal protein synthetic organelles (Lee et al., 2005). This prompted the Mills group at Washington University to use the *Xbp1*$^{fl/fl}$ mouse line to generate an inducible adult knock-out line lacking XBP1 expression in the constantly renewing zymogenic chief (ZC) cells of the stomach (Huh et al., 2010). This research revealed a deficiency in newly generated ZCs following *Xbp1* ablation that was attributed to failure of these cells to express MIST1, a bHLH transcription factor associated with maintenance of secretory function in serous secretory cells throughout the body (Huh et al., 2010). Interestingly, no observable changes in levels of ER stress were observed despite a lack of XBP1, the primary effector of IRE1 in the UPR. This prompted us to ask whether XBP1 was essential for UPR functioning and, if so, whether *Mist1* was itself a downstream target of XBP1 playing a previously uncharacterized role in the unfolded protein response.

In order to better study XBP1 in the context of a highly secretory cell type, our research utilized pancreatic acinar cells (PACs) that produce more protein than any other cell type in the human body (Case, 1978). PACs have low-level, constitutive expression of XBP1s, indicating a basal level of ER stress (Iwawaki et al., 2004). PACs also constitutively express MIST1, previously shown to be essential for acinar cell

organization and identity (Direnzo et al., 2012; Pin et al., 2001; Shi et al., 2012). We thus sought to generate a PAC-specific, Cre-inducible line in which we could ablate *Xbp1* in adult pancreata. These mice (*Mist1*$^{CreER/+}$;*Xbp1*$^{fl/fl}$) were then utilized to conduct timed observations of the effects of *Xbp1* ablation on PACs.

Our data revealed that PACs are entirely dependent on the IRE1/XBP1 branch of the UPR, with strong activation of the other two UPR master regulators failing to ameliorate basal levels of ER stress. This resulted in an apparent cumulative effect, with PACs developing increasing signs of zymogen deficit, damage, and ER structural changes consistent with ER stress, ultimately culminating in expression of CHOP, a key mediator of the apoptotic component of the UPR, and cell death. This gradual stress accumulation shows promise for XBP1-mediated therapeutic development, as acinar cells can tolerate *Xbp1* ablation for an extended period of time. While our own studies attempting to combine *Xbp1* ablation with activated KRAS expression were hampered by the simultaneous ablation/activation necessitated by our Cre-mediated model system, future investigations utilizing shRNA or small molecule inhibitors of XBP1 in the context of transformed cells may reveal a novel solution to sensitizing these growing, highly proliferative masses to chemotherapeutics in a way that spares normal acinar cells. This could represent an ideal system for preventing expansion of tumors in a way that spares the organ-devastating effects of pancreatic resection.

Existing models of damage often produce sub-optimal results, requiring either extensive chemical treatment or genetic “second hits” in order to generate physiologically relevant levels of exocrine damage and regeneration (Lerch and Adler, 1994). Additionally, these model systems often produce conflicting results regarding the cell of origin for regenerated exocrine cells, with some studies implicating pre-existing acinar cells (Strobel et al., 2007) and others suggesting that the centroacinar/ductal compartment (Criscimanna et al., 2011) serves as a source of new cells. Inflammatory cells also likely play a role in exacerbating pancreatic damage, as recent studies have shown a substantial role for stromal cells in contributing to damage (Guerra et al., 2011). We thus sought to determine whether ER stress-induced loss of a large portion of the exocrine compartment could represent a clinically relevant system for studying pancreatic regeneration.

Our studies have shown that acinar cell regeneration following Cre-mediated *Xbp1* ablation and subsequent loss of acinar cells is accompanied by cell cycle reentry and proliferation of both the acinar and centroacinar compartments. This proliferation results in a substantial recovery of the acinar lineage from a minority of acinar cells that failed to delete both Xbp1 alleles. Importantly, this system leads to large-scale acinar destruction accompanied by a mixed inflammatory response that is reminiscent of human patient samples. We thus believe that this model represents a preferred alternative to standard damage systems, combining the inflammatory environment seen in weaker, chemically-induced models with the intrinsic, massive acinar cell loss observed in transgenic models that fail to generate inflammation. Further follow-up studies may also take advantage of the generous window of opportunity for studying regenerative signaling events, as the prolonged recovery time (several weeks) is a distinct advantage over the rapid regeneration observed following chemical treatments. Indeed, the use of ER stress as a means of inducing extensive damage may more accuratly represent a chronic damage state than existing methods requiring frequent hourly treatments inducing supramaximal levels of aberrant zymogen secretion.

While both the demonstration of XBP1 as an element of acinar cell homeostasis and the establishment of a novel model of pancreatic damage and regeneration are important aspects of our work, we believe the most promising use of our data lies in the establishment of MIST1 as a new component of the unfolded protein response. This is because tumor cells often overcome regulatory mechanisms mediated by intrinsic stress pathways as a necessary component of tumor initiation and promotion (Li et al., 2011). Indeed, recent work has shown that restoration/induction of the UPR in cancer cells can restore the ability of certain chemotherapeutics to kill previously resistant cell types (Martins et al., 2011). Thus, increased knowledge regarding downstream targets of major UPR components may aid in the discovery of new compounds to facilitate current treatments for pancreatic and other secretory malignancies.

We have shown that *Mist1* expression is correlated both *in vivo* and *in vitro* with ER stress, indicating a physiological response suggesting a role in the UPR. We furthermore demonstrated that this activation was directly due to *Xbp1* expression, and XBP1 was capable of binding to elements of the *Mist1* promoter in order to activate transcription.

Finally, we revealed that a number of putative MIST1 gene targets, determined via bioinformatic analysis of genome-wide expression data, are expressed in a pattern suggesting a correlation with MIST1 protein, indicating that these targets may be the means by which MIST1 exerts an influence on the unfolded protein response. These data may allow the targeting of specific MIST1 effectors, or MIST1 itself, as a means of compromising normal UPR function in transformed cells. This, in turn, could provide an approach to switching cellular ER stress responses from the adaptive to the apoptotic phases of the UPR. Such a treatment could be combined with other cytotoxic and chemotherapeutic treatment options in order to provide an extra “push” to cells that may be responsive to standard drug and radiation therapy, but only submaximally initiating damage/apoptotic cascades.

In summary, our work has generated a more complete understanding of how the UPR, and specifically XBP1, play a role in maintaining and sustaining the homeostatic balance in highly secretory pancreatic acinar cells. We show that XBP1 is an indispensable part of the mammalian UPR in cells with high demand for secreted products, and that the ER stress imparted by loss of *Xbp1* can be used as a means to study pancreatic disease *in vivo*. We furthermore show that XBP1 may exert influence on cell processes both within and outside the canonical UPR via its direct interaction with MIST1. We believe that exploring the molecular events mediated by the XBP1/MIST1 interaction should be an important goal of future work focused on understanding and manipulating exocrine cell fate in pancreatic disease.

LIST OF REFERENCES

Acosta-Alvear, D., Zhou, Y., Blais, A., Tsikitis, M., Lents, N.H., Arias, C., Lennon, C.J., Kluger, Y., and Dynlacht, B.D. (2007). XBP1 controls diverse cell type- and condition-specific transcriptional regulatory networks. Molecular Cell *27*, 53–66.

Adler, G., Hupp, T., and Kern, H.F. (1979). Course and spontaneous regression of acute pancreatitis in the rat. Virchows Archiv. A, Pathological Anatomy and Histology *382*, 31–47.

Alahari, S., Mehmood, R., Johnson, C.L., and Pin, C.L. (2011). The absence of MIST1 leads to increased ethanol sensitivity and decreased activity of the unfolded protein response in mouse pancreatic acinar cells. PloS One *6*, e28863.

Alberts, B., Johnson, A., Lewis, J., Raff, M., Roberts, K., and Walter, P. (2007). Molecular Biology of the Cell (New York: Garland Science).

Bachem, M.G., Schneider, E., Groß, H., Weidenbach, H., Schmid, R.M., Menke, A., Siech, M., Beger, H., Grünert, A., and Adler, G. (1998). Identification, culture, and characterization of pancreatic stellate cells in rats and humans. Gastroenterology *115*, 421–432.

Baeyens, L., Bonné, S., Bos, T., Rooman, I., Peleman, C., Lahoutte, T., German, M., Heimberg, H., and Bouwens, L. (2009). Notch signaling as gatekeeper of rat acinar-to-beta-cell conversion in vitro. Gastroenterology *136*, 1750–60.e13.

Banin, S. (1998). Enhanced Phosphorylation of p53 by ATM in Response to DNA Damage. Science *281*, 1674–1677.

Bommiasamy, H., Back, S.H., Fagone, P., Lee, K., Meshinchi, S., Vink, E., Sriburi, R., Frank, M., Jackowski, S., Kaufman, R.J., et al. (2009). ATF6alpha induces XBP1-independent expansion of the endoplasmic reticulum. Journal of Cell Science *122*, 1626–1636.

Brembeck, F.H., Schreiber, F.S., Deramaudt, T.B., Craig, L., Rhoades, B., Swain, G., Grippo, P., Stoffers, D.A., Silberg, D.G., and Rustgi, A.K. (2003). The mutant K-ras oncogene causes pancreatic periductal lymphocytic infiltration and gastric mucous neck cell hyperplasia in transgenic mice. Cancer Res *63*, 2005–2009.

Brune, K., Abe, T., Canto, M., O'Malley, L., Klein, A.P., Maitra, A., Volkan Adsay, N., Fishman, E.K., Cameron, J.L., Yeo, C.J., et al. (2006). Multifocal neoplastic precursor lesions associated with lobular atrophy of the pancreas in patients having a strong family history of pancreatic cancer. The American Journal of Surgical Pathology *30*, 1067–1076.

Burgess, T.L., and Kelly, R.B. (1987). Constitutive and regulated secretion of proteins. Annual Review of Cell Biology *3*, 243–293.

Capoccia, B.J., Lennerz, J.K.M., Bredemeyer, A.J., Klco, J.M., Frater, J.L., and Mills, J.C. (2011). Transcription factor MIST1 in terminal differentiation of mouse and human plasma cells. Physiological Genomics *43*, 174–186.

Carrière, C., Young, A.L., Gunn, J.R., Longnecker, D.S., and Korc, M. (2009). Acute pancreatitis markedly accelerates pancreatic cancer progression in mice expressing oncogenic Kras. Biochemical and Biophysical Research Communications *382*, 561–565.

Case, R.M. (1978). Synthesis, intracellular transport and discharge of exportable proteins in the pancreatic acinar cell and other cells. Biological Reviews of the Cambridge Philosophical Society *53*, 211–354.

Casola, S. (2010). Mouse models for miRNA expression: the ROSA26 locus. Methods in Molecular Biology (Clifton, N.J.) *667*, 145–163.

Chakrabarti, A., Chen, A.W., and Varner, J.D. (2011). A review of the mammalian unfolded protein response. Biotechnology and Bioengineering *108*, 2777–2793.

Chappell, W.H., Steelman, L.S., Long, J.M., Kempf, R.C., Abrams, S.L., Franklin, R.A., Bäsecke, J., Stivala, F., Donia, M., Fagone, P., et al. (2011). Ras/Raf/MEK/ERK and PI3K/PTEN/Akt/mTOR inhibitors: rationale and importance to inhibiting these pathways in human health. Oncotarget *2*, 135–164.

Clauss, I.M., Gravallese, E.M., Darling, J.M., Shapiro, F., Glimcher, M.J., and Glimcher, L.H. (1993). In situ hybridization studies suggest a role for the basic region-leucine zipper protein hXBP-1 in exocrine gland and skeletal development during mouse embryogenesis. Developmental Dynamics : an Official Publication of the American Association of Anatomists *197*, 146–156.

Collins, M.A., Bednar, F., Zhang, Y., Brisset, J.-C., Galbán, S., Galbán, C.J., Rakshit, S., Flannagan, K.S., Adsay, N.V., and Pasca di Magliano, M. (2012). Oncogenic Kras is required for both the initiation and maintenance of pancreatic cancer in mice. The Journal of Clinical Investigation *122*, 639–653.

Cooper, G. (2000). The Golgi Apparatus. In The Cell: A Molecular Approach. 2nd Edition, (Sinauer Associates),.

Cox, A.D., and Der, C.J. (2003). The dark side of Ras: regulation of apoptosis. Oncogene *22*, 8999–9006.

Cox, J.S., and Walter, P. (1996). A novel mechanism for regulating activity of a transcription factor that controls the unfolded protein response. Cell *87*, 391–404.

Criscimanna, A., Speicher, J.A., Houshmand, G., Shiota, C., Prasadan, K., Ji, B., Logsdon, C.D., Gittes, G.K., and Esni, F. (2011). Duct Cells Contribute to Regeneration of Endocrine and Acinar Cells Following Pancreatic Damage in Adult Mice. Gastroenterology.

Cyr, D.M., and Hebert, D.N. (2009). Protein quality control-linking the unfolded protein response to disease. Conference on “From Unfolded Proteins in the Endoplasmic Reticulum to Disease”. EMBO Rep *10*, 1206–1210.

Daneshmand, S., Quek, M.L., Lin, E., Lee, C., Cote, R.J., Hawes, D., Cai, J., Groshen, S., Lieskovsky, G., Skinner, D.G., et al. (2007). Glucose-regulated protein GRP78 is up-regulated in prostate cancer and correlates with recurrence and survival. Human Pathology *38*, 1547–1552.

Dawra, R., Sharif, R., Phillips, P., Dudeja, V., Dhaulakhandi, D., and Saluja, A.K. (2007). Development of a new mouse model of acute pancreatitis induced by administration of L-arginine. American Journal of Physiology. Gastrointestinal and Liver Physiology *292*, G1009–18.

Deitcher, D. (2002). Exocytosis, endocytosis, and development. Seminars in Cell & Developmental Biology *13*, 71–76.

Detlefsen, S., Sipos, B., Feyerabend, B., and Klöppel, G. (2005). Pancreatic fibrosis associated with age and ductal papillary hyperplasia. Virchows Archiv : an International Journal of Pathology *447*, 800–805.

DeToma, A.S., Salamekh, S., Ramamoorthy, A., and Lim, M.H. (2012). Misfolded proteins in Alzheimer’s disease and type II diabetes. Chemical Society Reviews *41*, 608–621.

DiRenzo, D.M. (2012). Identifying Mist1 Regulated Genes In Pancreatic Acinar Cell Homeostasis and Carcinogenesis. Thesis Document.

Direnzo, D., Hess, D.A., Damsz, B., Hallett, J.E., Marshall, B., Goswami, C., Liu, Y., Deering, T., Macdonald, R.J., and Konieczny, S.F. (2012). Induced Mist1 Expression Promotes Remodeling of Mouse Pancreatic Acinar Cells. Gastroenterology *143*, 469–480.

Doherty, G.J., and McMahon, H.T. (2009). Mechanisms of endocytosis. Annual Review of Biochemistry *78*, 857–902.

Dufour, M.C., and Adamson, M.D. (2003). The epidemiology of alcohol-induced pancreatitis. Pancreas *27*, 286–290.

Edlund, H. (2002). Pancreatic organogenesis--developmental mechanisms and implications for therapy. Nat Rev Genet *3*, 524–532.

Elayat, A.A., El-Naggar, M.M., and Tahir, M. (1995). An immunocytochemical and morphometric study of the rat pancreatic islets. Journal of Anatomy *186 (Pt 3*, 629–637.

Elsasser, S., and Finley, D. (2005). Delivery of ubiquitinated substrates to protein-unfolding machines. Nature Cell Biology *7*, 742–749.

Farrow, B., and Evers, B.M. (2002). Inflammation and the development of pancreatic cancer. Surgical Oncology *10*, 153–169.

Federovitch, C.M., Ron, D., and Hampton, R.Y. (2005). The dynamic ER: experimental approaches and current questions. Current Opinion in Cell Biology *17*, 409–414.

Feil, R., Wagner, J., Metzger, D., and Chambon, P. (1997). Regulation of Cre recombinase activity by mutated estrogen receptor ligand-binding domains. Biochem Biophys Res Commun *237*, 752–757.

Fendrich, V., Esni, F., Garay, M. V, Feldmann, G., Habbe, N., Jensen, J.N., Dor, Y., Stoffers, D., Jensen, J., Leach, S.D., et al. (2008). Hedgehog signaling is required for effective regeneration of exocrine pancreas. Gastroenterology *135*, 621–631.

Flaherty, D.P., Golden, J.E., Liu, C., Hedrick, M., Gosalia, P., Li, Y., Milewski, M., Sugarman, E., Suyama, E., Nguyen, K., et al. (2010). Selective small molecule activator of the apoptotic arm of the UPR. In Probe Reports from the NIH Molecular Libraries,.

Friedrich, G., and Soriano, P. (1991). Promoter traps in embryonic stem cells: a genetic screen to identify and mutate developmental genes in mice. Genes & Development *5*, 1513–1523.

Fukuda, M. (2008). Regulation of secretory vesicle traffic by Rab small GTPases. Cellular and Molecular Life Sciences : CMLS *65*, 2801–2813.

Gao, F., Liu, Q.-C., Zhang, S., Zhuang, Z.-H., Lin, C.-Z., and Lin, X.-H. (2012). PRSS1 intron mutations in patients with pancreatic cancer and chronic pancreatitis. Molecular Medicine Reports *5*, 449–451.

Garber, K. (2010). Stromal depletion goes on trial in pancreatic cancer. Journal of the National Cancer Institute *102*, 448–450.

Garside, V.C., Kowalik, A.S., Johnson, C.L., DiRenzo, D., Konieczny, S.F., and Pin, C.L. (2010). MIST1 regulates the pancreatic acinar cell expression of Atp2c2, the gene encoding secretory pathway calcium ATPase 2. Experimental Cell Research *316*, 2859–2870.

Glickman, J.N., and Kornfeld, S. (1993). Mannose 6-phosphate-independent targeting of lysosomal enzymes in I-cell disease B lymphoblasts. The Journal of Cell Biology *123*, 99–108.

Grampp, G.E., Sambanis, A., and Stephanopoulos, G.N. (1992). Use of regulated secretion in protein production from animal cells: an overview. Advances in Biochemical Engineering/biotechnology *46*, 35–62.

Guerra, C., Mijimolle, N., Dhawahir, A., Dubus, P., Barradas, M., Serrano, M., Campuzano, V., and Barbacid, M. (2003). Tumor induction by an endogenous K-ras oncogene is highly dependent on cellular context. Cancer Cell *4*, 111–120.

Guerra, C., Schuhmacher, A.J., Canamero, M., Grippo, P.J., Verdaguer, L., Perez-Gallego, L., Dubus, P., Sandgren, E.P., and Barbacid, M. (2007). Chronic pancreatitis is essential for induction of pancreatic ductal adenocarcinoma by K-Ras oncogenes in adult mice. Cancer Cell *11*, 291–302.

Guerra, C., Collado, M., Navas, C., Schuhmacher, A.J., Hernández-Porras, I., Cañamero, M., Rodriguez-Justo, M., Serrano, M., and Barbacid, M. (2011). Pancreatitis-induced inflammation contributes to pancreatic cancer by inhibiting oncogene-induced senescence. Cancer Cell *19*, 728–739.

Guo, F., Lin, E.A., Liu, P., Lin, J., and Liu, C. (2010). XBP1U inhibits the XBP1S-mediated upregulation of the iNOS gene expression in mammalian ER stress response. Cellular Signalling *22*, 1818–1828.

Haas, I.G. (1994). BiP (GRP78), an essential hsp70 resident protein in the endoplasmic reticulum. Experientia *50*, 1012–1020.

Habbe, N., Shi, G., Meguid, R.A., Fendrich, V., Esni, F., Chen, H., Feldmann, G., Stoffers, D.A., Konieczny, S.F., Leach, S.D., et al. (2008). Spontaneous induction of murine pancreatic intraepithelial neoplasia (mPanIN) by acinar cell targeting of oncogenic Kras in adult mice. Proc Natl Acad Sci U S A *105*, 18913–18918.

Harding, H.P., Novoa, I., Zhang, Y., Zeng, H., Wek, R., Schapira, M., and Ron, D. (2000). Regulated translation initiation controls stress-induced gene expression in mammalian cells. Molecular Cell *6*, 1099–1108.

Heinemeyer, W., Kleinschmidt, J.A., Saidowsky, J., Escher, C., and Wolf, D.H. (1991). Proteinase yscE, the yeast proteasome/multicatalytic-multifunctional proteinase: mutants unravel its function in stress induced proteolysis and uncover its necessity for cell survival. The EMBO Journal *10*, 555–562.

Hernández-Muñoz, I., Skoudy, A., Real, F.X., and Navarro, P. (2008). Pancreatic ductal adenocarcinoma: cellular origin, signaling pathways and stroma contribution. Pancreatology : Official Journal of the International Association of Pancreatology (IAP) ... [et Al.] *8*, 462–469.

Hess, D.A., Humphrey, S.E., Ishibashi, J., Damsz, B., Lee, A.H., Glimcher, L.H., and Konieczny, S.F. (2011). Extensive Pancreas Regeneration Following Acinar-Specific Disruption of Xbp1 in Mice. Gastroenterology *141*, 1466–1476.

Hetz, C., Lee, A.-H., Gonzalez-Romero, D., Thielen, P., Castilla, J., Soto, C., and Glimcher, L.H. (2008). Unfolded protein response transcription factor XBP-1 does not influence prion replication or pathogenesis. Proceedings of the National Academy of Sciences of the United States of America *105*, 757–762.

Hidalgo, M. (2010). Pancreatic Cancer. New England Journal of Medicine *362*, 1605–1617.

Hingorani, S.R., and Tuveson, D.A. (2003). Ras redux: rethinking how and where Ras acts. Curr Opin Genet Dev *13*, 6–13.

Ho, C.-K., Kleeff, J., Friess, H., and Büchler, M.W. (2005). Complications of pancreatic surgery. HPB : the Official Journal of the International Hepato Pancreato Biliary Association *7*, 99–108.

Hogan, B.L. (1996). Bone morphogenetic proteins: multifunctional regulators of vertebrate development. Genes & Development *10*, 1580–1594.

Homann, O.R., and Johnson, A.D. (2010). MochiView: versatile software for genome browsing and DNA motif analysis. BMC Biology *8*, 49.

Houbracken, I., De Waele, E., Lardon, J., Ling, Z., Heimberg, H., Rooman, I., and Bouwens, L. (2011). Lineage tracing evidence for transdifferentiation of acinar to duct cells and plasticity of human pancreas. Gastroenterology *141*, 731–41, 741.e1–4.

Hruban, R.H., Adsay, N. V, Albores-Saavedra, J., Anver, M.R., Biankin, A. V, Boivin, G.P., Furth, E.E., Furukawa, T., Klein, A., Klimstra, D.S., et al. (2006). Pathology of genetically engineered mouse models of pancreatic exocrine cancer: consensus report and recommendations. Cancer Res *66*, 95–106.

Hruban, R.H., Maitra, A., and Goggins, M. (2008). Update on pancreatic intraepithelial neoplasia. Int J Clin Exp Pathol *1*, 306–316.

Hsu, S.-C., TerBush, D., Abraham, M., and Guo, W. (2004). The exocyst complex in polarized exocytosis. International Review of Cytology *233*, 243–265.

Huang, H., Daniluk, J., Liu, Y., Chu, J., Li, Z., Ji, B., and Logsdon, C.D. (2013). Oncogenic K-Ras requires activation for enhanced activity. Oncogene 1–4.

Huh, W.J., Esen, E., Geahlen, J.H., Bredemeyer, A.J., Lee, A.H., Shi, G., Konieczny, S.F., Glimcher, L.H., and Mills, J.C. (2010). XBP1 controls maturation of gastric zymogenic cells by induction of MIST1 and expansion of the rough endoplasmic reticulum. Gastroenterology.

Hwang, R.F., Moore, T., Arumugam, T., Ramachandran, V., Amos, K.D., Rivera, A., Ji, B., Evans, D.B., and Logsdon, C.D. (2008). Cancer-associated stromal fibroblasts promote pancreatic tumor progression. Cancer Research *68*, 918–926.

Iida, K., Li, Y., McGrath, B.C., Frank, A., and Cavener, D.R. (2007). PERK eIF2 alpha kinase is required to regulate the viability of the exocrine pancreas in mice. BMC Cell Biol *8*, 38.

Itoh, H., Komatsuda, A., Ohtani, H., Wakui, H., Imai, H., Sawada, K.-I., Otaka, M., Ogura, M., Suzuki, A., and Hamada, F. (2002). Mammalian HSP60 is quickly sorted into the mitochondria under conditions of dehydration. European Journal of Biochemistry / FEBS *269*, 5931–5938.

Iwawaki, T., Akai, R., Kohno, K., and Miura, M. (2004). A transgenic mouse model for monitoring endoplasmic reticulum stress. Nat Med *10*, 98–102.

Jackson, E.L., Willis, N., Mercer, K., Bronson, R.T., Crowley, D., Montoya, R., Jacks, T., and Tuveson, D.A. (2001). Analysis of lung tumor initiation and progression using conditional expression of oncogenic K-ras. Genes & Development *15*, 3243–3248.

Jaffray, C., Mendez, C., Denham, W., Carter, G., and Norman, J. (2000). Specific pancreatic enzymes activate macrophages to produce tumor necrosis factor-alpha: role of nuclear factor kappa B and inhibitory kappa B proteins. Journal of Gastrointestinal Surgery : Official Journal of the Society for Surgery of the Alimentary Tract *4*, 370–7; discussion 377–8.

Jensen, J.N., Cameron, E., Garay, M. V, Starkey, T.W., Gianani, R., and Jensen, J. (2005). Recapitulation of elements of embryonic development in adult mouse pancreatic regeneration. Gastroenterology *128*, 728–741.

Jha, R.K., Ma, Q., Sha, H., and Palikhe, M. (2009). Acute pancreatitis: a literature review. Medical Science Monitor : International Medical Journal of Experimental and Clinical Research *15*, RA147–56.

Ji, B., Bi, Y., Simeone, D., Mortensen, R.M., and Logsdon, C.D. (2002). Human pancreatic acinar cells do not respond to cholecystokinin. Pharmacology & Toxicology *91*, 327–332.

Ji, B., Tsou, L., Wang, H., Gaiser, S., Chang, D.Z., Daniluk, J., Bi, Y., Grote, T., Longnecker, D.S., and Logsdon, C.D. (2009). Ras activity levels control the development of pancreatic diseases. Gastroenterology *137*, 1072–82, 1082 e1–6.

Jia, D., Sun, Y., and Konieczny, S.F. (2008). Mist1 regulates pancreatic acinar cell proliferation through p21 CIP1/WAF1. Gastroenterology *135*, 1687–1697.

Jungermann, J., Lerch, M.M., Weidenbach, H., Lutz, M.P., Krüger, B., and Adler, G. (1995). Disassembly of rat pancreatic acinar cell cytoskeleton during supramaximal secretagogue stimulation. The American Journal of Physiology *268*, G328–38.

Kaufman, R.J. (2002). Orchestrating the unfolded protein response in health and disease. The Journal of Clinical Investigation *110*, 1389–1398.

Kelly, R.B. (1985). Pathways of protein secretion in eukaryotes. Science (New York, N.Y.) *230*, 25–32.

Khare, V., and Eckert, K.A. (2002). The proofreading 3'-->5' exonuclease activity of DNA polymerases: a kinetic barrier to translesion DNA synthesis. Mutation Research *510*, 45–54.

Kim, H. (2008). Cerulein pancreatitis: oxidative stress, inflammation, and apoptosis. Gut and Liver *2*, 74–80.

Kim, I., and Rao, H. (2010). Degradation of Misfolded Secretory and Membrane Proteins and Associated Diseases. eLS.

Kimmig, P., Diaz, M., Zheng, J., Williams, C.C., Lang, A., Aragón, T., Li, H., and Walter, P. (2012). The unfolded protein response in fission yeast modulates stability of select mRNAs to maintain protein homeostasis. eLife *1*, e00048.

Klöppel, G., and Maillet, B. (1993). Pathology of acute and chronic pancreatitis. Pancreas *8*, 659–670.

Klöppel, G., Detlefsen, S., and Feyerabend, B. (2004). Fibrosis of the pancreas: the initial tissue damage and the resulting pattern. Virchows Archiv : an International Journal of Pathology *445*, 1–8.

Koong, A.C., Chauhan, V., and Romero-Ramirez, L. (2006). Targeting XBP-1 as a novel anti-cancer strategy. Cancer Biology & Therapy *5*, 756–759.

Kopp, J.L., Von Figura, G., Mayes, E., Liu, F.-F., Dubois, C.L., Morris, J.P., Pan, F.C., Akiyama, H., Wright, C.V.E., Jensen, K., et al. (2012). Identification of Sox9-dependent acinar-to-ductal reprogramming as the principal mechanism for initiation of pancreatic ductal adenocarcinoma. Cancer Cell *22*, 737–750.

Kowalik, A.S., Johnson, C.L., Chadi, S.A., Weston, J.Y., Fazio, E.N., and Pin, C.L. (2007). Mice lacking the transcription factor Mist1 exhibit an altered stress response and increased sensitivity to caerulein-induced pancreatitis. American Journal of Physiology. Gastrointestinal and Liver Physiology *292*, G1123–32.

Kubisch, C.H., Sans, M.D., Arumugam, T., Ernst, S.A., Williams, J.A., and Logsdon, C.D. (2006). Early activation of endoplasmic reticulum stress is associated with arginine-induced acute pancreatitis. American Journal of Physiology. Gastrointestinal and Liver Physiology *291*, G238–45.

De La O, J., Emerson, L.L., Goodman, J.L., Froebe, S.C., Illum, B.E., Curtis, A.B., and Murtaugh, L.C. (2008). Notch and Kras reprogram pancreatic acinar cells to ductal intraepithelial neoplasia. Proc Natl Acad Sci U S A *105*, 18907–18912.

Lee, A.H., Iwakoshi, N.N., and Glimcher, L.H. (2003). XBP-1 regulates a subset of endoplasmic reticulum resident chaperone genes in the unfolded protein response. Molecular and Cellular Biology *23*, 7448–7459.

Lee, A.H., Chu, G.C., Iwakoshi, N.N., and Glimcher, L.H. (2005). XBP-1 is required for biogenesis of cellular secretory machinery of exocrine glands. EMBO J *24*, 4368–4380.

Lee, E., Nichols, P., Spicer, D., Groshen, S., Yu, M.C., and Lee, A.S. (2006). GRP78 as a novel predictor of responsiveness to chemotherapy in breast cancer. Cancer Research *66*, 7849–7853.

Lee, K., Tirasophon, W., Shen, X., Michalak, M., Prywes, R., Okada, T., Yoshida, H., Mori, K., and Kaufman, R.J. (2002). IRE1-mediated unconventional mRNA splicing and S2P-mediated ATF6 cleavage merge to regulate XBP1 in signaling the unfolded protein response. Genes & Development *16*, 452–466.

Lee, S., Hur, E., Ryoo, I., Jung, K.-A., Kwak, J., and Kwak, M.-K. (2012). Involvement of the Nrf2-proteasome pathway in the endoplasmic reticulum stress response in pancreatic β-cells. Toxicology and Applied Pharmacology *264*, 431–438.

Lerch, M.M., and Adler, G. (1994). Experimental animal models of acute pancreatitis. International Journal of Pancreatology : Official Journal of the International Association of Pancreatology *15*, 159–170.

Li, X., Zhang, K., and Li, Z. (2011). Unfolded protein response in cancer: the physician's perspective. Journal of Hematology & Oncology *4*, 8.

Lombardi, B., Estes, L.W., and Longnecker, D.S. (1975). Acute hemorrhagic pancreatitis (massive necrosis) with fat necrosis induced in mice by DL-ethionine fed with a choline-deficient diet. The American Journal of Pathology *79*, 465–480.

Lu, X., Xu, T., Qian, J., Wen, X., and Wu, D. (2002). Detecting K-ras and p53 gene mutation from stool and pancreatic juice for diagnosis of early pancreatic cancer. Chinese Medical Journal *115*, 1632–1636.

Lugea, A., Nan, L., French, S.W., Bezerra, J.A., Gukovskaya, A.S., and Pandol, S.J. (2006). Pancreas recovery following cerulein-induced pancreatitis is impaired in plasminogen-deficient mice. Gastroenterology *131*, 885–899.

Lugea, A., Tischler, D., Nguyen, J., Gong, J., Gukovsky, I., French, S.W., Gorelick, F.S., and Pandol, S.J. (2011). Adaptive unfolded protein response attenuates alcohol-induced pancreatic damage. Gastroenterology *140*, 987–997.

Ma, Y., and Hendershot, L.M. (2004). The role of the unfolded protein response in tumour development: friend or foe? Nature Reviews. Cancer *4*, 966–977.

Mains, R.E., Cullen, E.I., May, V., and Eipper, B.A. (1987). The role of secretory granules in peptide biosynthesis. Annals of the New York Academy of Sciences *493*, 278–291.

Maitra, A., and Hruban, R.H. (2008). Pancreatic cancer. Annu Rev Pathol *3*, 157–188.

Marchand, A., Tomkiewicz, C., Magne, L., Barouki, R., and Garlatti, M. (2006). Endoplasmic reticulum stress induction of insulin-like growth factor-binding protein-1 involves ATF4. The Journal of Biological Chemistry *281*, 19124–19133.

Martins, I., Kepp, O., Schlemmer, F., Adjemian, S., Tailler, M., Shen, S., Michaud, M., Menger, L., Gdoura, A., Tajeddine, N., et al. (2011). Restoration of the immunogenicity of cisplatin-induced cancer cell death by endoplasmic reticulum stress. Oncogene *30*, 1147–1158.

Mayer, M.P., and Bukau, B. (2005). Hsp70 chaperones: cellular functions and molecular mechanism. Cellular and Molecular Life Sciences : CMLS *62*, 670–684.

Mayer, M., Kies, U., Kammermeier, R., and Buchner, J. (2000). BiP and PDI cooperate in the oxidative folding of antibodies in vitro. The Journal of Biological Chemistry *275*, 29421–29425.

Mayerle, J., Sendler, M., and Lerch, M.M. (2013). Secretagogue (Caerulein) induced pancreatitis in rodents. The Pancreapedia: Exocrine Pancreas Knowledge Base.

McClellan, A.J., Tam, S., Kaganovich, D., and Frydman, J. (2005). Protein quality control: chaperones culling corrupt conformations. Nature Cell Biology *7*, 736–741.

McCormick, F. (1993). Signal transduction. How receptors turn Ras on. Nature *363*, 15–16.

McNaught, K.S., Olanow, C.W., Halliwell, B., Isacson, O., and Jenner, P. (2001). Failure of the ubiquitin-proteasome system in Parkinson's disease. Nature Reviews. Neuroscience *2*, 589–594.

Means, A.L., Meszoely, I.M., Suzuki, K., Miyamoto, Y., Rustgi, A.K., Coffey Jr., R.J., Wright, C. V, Stoffers, D.A., and Leach, S.D. (2005). Pancreatic epithelial plasticity mediated by acinar cell transdifferentiation and generation of nestin-positive intermediates. Development *132*, 3767–3776.

Meda, P. (1996). Gap junction involvement in secretion: the pancreas experience. Clinical and Experimental Pharmacology & Physiology *23*, 1053–1057.

Mellman, I. (1996). Endocytosis and molecular sorting. Annual Review of Cell and Developmental Biology *12*, 575–625.

Mellman, I., and Nelson, W.J. (2008). Coordinated protein sorting, targeting and distribution in polarized cells. Nature Reviews. Molecular Cell Biology *9*, 833–845.

Mills, J.C., and Taghert, P.H. (2012). Scaling factors: transcription factors regulating subcellular domains. BioEssays : News and Reviews in Molecular, Cellular and Developmental Biology *34*, 10–16.

Mimura, N., Fulciniti, M., Gorgun, G., Tai, Y., Cirstea, D., Santo, L., Fabre, C., Minami, J., Ohguchi, H., Kiziltepe, T., et al. (2012). Blockade of XBP1 splicing by inhibition of IRE1 α is a promising therapeutic option in multiple myeloma. Blood *119*, 5772–5781.

Minami, K., Okuno, M., Miyawaki, K., Okumachi, A., Ishizaki, K., Oyama, K., Kawaguchi, M., Ishizuka, N., Iwanaga, T., and Seino, S. (2005). Lineage tracing and characterization of insulin-secreting cells generated from adult pancreatic acinar cells. Proceedings of the National Academy of Sciences of the United States of America *102*, 15116–15121.

Mitchell, K.J., Pinson, K.I., Kelly, O.G., Brennan, J., Zupicich, J., Scherz, P., Leighton, P.A., Goodrich, L. V, Lu, X., Avery, B.J., et al. (2001). Functional analysis of secreted and transmembrane proteins critical to mouse development. Nature Genetics *28*, 241–249.

Mori, K. (2009). Signalling pathways in the unfolded protein response: development from yeast to mammals. Journal of Biochemistry *146*, 743–750.

Nawrocki, S.T., Carew, J.S., Dunner Jr., K., Boise, L.H., Chiao, P.J., Huang, P., Abbruzzese, J.L., and McConkey, D.J. (2005a). Bortezomib inhibits PKR-like endoplasmic reticulum (ER) kinase and induces apoptosis via ER stress in human pancreatic cancer cells. Cancer Res *65*, 11510–11519.

Nawrocki, S.T., Carew, J.S., Pino, M.S., Highshaw, R.A., Dunner Jr., K., Huang, P., Abbruzzese, J.L., and McConkey, D.J. (2005b). Bortezomib sensitizes pancreatic cancer cells to endoplasmic reticulum stress-mediated apoptosis. Cancer Res *65*, 11658–11666.

Neubauer, K., Knittel, T., Armbrust, T., and Ramadori, G. (1995). Accumulation and cellular localization of fibrinogen/fibrin during short-term and long-term rat liver injury. Gastroenterology *108*, 1124–1135.

Niederau, C., Ferrell, L.D., and Grendell, J.H. (1985). Caerulein-induced acute necrotizing pancreatitis in mice: protective effects of proglumide, benzotript, and secretin. Gastroenterology *88*, 1192–1204.

Oates, P.S., and Morgan, R.G. (1982). Pancreatic growth and cell turnover in the rat fed raw soya flour. The American Journal of Pathology *108*, 217–224.

Ohta, T., and Fukuda, M. (2004). Ubiquitin and breast cancer. Oncogene *23*, 2079–2088.

Okada, T., Yoshida, H., Akazawa, R., Negishi, M., and Mori, K. (2002). Distinct roles of activating transcription factor 6 (ATF6) and double-stranded RNA-activated protein kinase-like endoplasmic reticulum kinase (PERK) in transcription during the mammalian unfolded protein response. The Biochemical Journal *366*, 585–594.

Okamoto, H. (1999). The Reg gene family and Reg proteins: with special attention to the regeneration of pancreatic beta-cells. Journal of Hepato-biliary-pancreatic Surgery *6*, 254–262.

Olivier, M., Hollstein, M., and Hainaut, P. (2010). TP53 mutations in human cancers: origins, consequences, and clinical use. Cold Spring Harbor Perspectives in Biology *2*, a001008.

Omary, M.B., Lugea, A., Lowe, A.W., and Pandol, S.J. (2007). The pancreatic stellate cell: a star on the rise in pancreatic diseases. The Journal of Clinical Investigation *117*, 50–59.

Oslowski, C.M., and Urano, F. (2010). The binary switch between life and death of endoplasmic reticulum-stressed beta cells. Current Opinion in Endocrinology, Diabetes, and Obesity *17*, 107–112.

Oslowski, C.M., and Urano, F. (2011). Measuring ER stress and the unfolded protein response using mammalian tissue culture system. Methods in Enzymology *490*, 71–92.

Pandol, S., Edderkaoui, M., Gukovsky, I., Lugea, A., and Gukovskaya, A. (2009). Desmoplasia of pancreatic ductal adenocarcinoma. Clinical Gastroenterology and Hepatology : the Official Clinical Practice Journal of the American Gastroenterological Association *7*, S44–7.

Pandol, S.J., Gorelick, F.S., Gerloff, A., and Lugea, A. (2010). Alcohol abuse, endoplasmic reticulum stress and pancreatitis. Digestive Diseases (Basel, Switzerland) *28*, 776–782.

Parsons, B.L., and Meng, F. (2009). K-RAS mutation in the screening, prognosis and treatment of cancer. Biomarkers in Medicine *3*, 757–769.

Perez-Mancera, P.A., and Tuveson, D.A. (2006). Physiological analysis of oncogenic K-ras. Methods Enzymol *407*, 676–690.

Pin, C.L., Bonvissuto, A.C., and Konieczny, S.F. (2000). Mist1 expression is a common link among serous exocrine cells exhibiting regulated exocytosis. Anat Rec *259*, 157–167.

Pin, C.L., Rukstalis, J.M., Johnson, C., and Konieczny, S.F. (2001). The bHLH transcription factor Mist1 is required to maintain exocrine pancreas cell organization and acinar cell identity. J Cell Biol *155*, 519–530.

Pines, J., and Lindon, C. (2005). Proteolysis: anytime, any place, anywhere? Nature Cell Biology *7*, 731–735.

Reddy, R.K., Mao, C., Baumeister, P., Austin, R.C., Kaufman, R.J., and Lee, A.S. (2003). Endoplasmic reticulum chaperone protein GRP78 protects cells from apoptosis induced by topoisomerase inhibitors: role of ATP binding site in suppression of caspase-7 activation. The Journal of Biological Chemistry *278*, 20915–20924.

Reimold, A.M., Etkin, A., Clauss, I., Perkins, A., Friend, D.S., Zhang, J., Horton, H.F., Scott, A., Orkin, S.H., Byrne, M.C., et al. (2000). An essential role in liver development for transcription factor XBP-1. Genes Dev *14*, 152–157.

Reimold, A.M., Iwakoshi, N.N., Manis, J., Vallabhajosyula, P., Szomolanyi-Tsuda, E., Gravallese, E.M., Friend, D., Grusby, M.J., Alt, F., and Glimcher, L.H. (2001). Plasma cell differentiation requires the transcription factor XBP-1. Nature *412*, 300–307.

Richter, K., Haslbeck, M., and Buchner, J. (2010). The heat shock response: life on the verge of death. Molecular Cell *40*, 253–266.

Ron, D., and Walter, P. (2007). Signal integration in the endoplasmic reticulum unfolded protein response. Nat Rev Mol Cell Biol *8*, 519–529.

Rooman, I., and Real, F.X. (2011). Pancreatic ductal adenocarcinoma and acinar cells: a matter of differentiation and development? Gut.

Rovira, M., Scott, S.G., Liss, A.S., Jensen, J., Thayer, S.P., and Leach, S.D. (2010). Isolation and characterization of centroacinar/terminal ductal progenitor cells in adult mouse pancreas. Proc Natl Acad Sci U S A *107*, 75–80.

Rukstalis, J.M., Kowalik, A., Zhu, L., Lidington, D., Pin, C.L., and Konieczny, S.F. (2003). Exocrine specific expression of Connexin32 is dependent on the basic helix-loop-helix transcription factor Mist1. J Cell Sci *116*, 3315–3325.

Samali, A., Fitzgerald, U., Deegan, S., and Gupta, S. (2010). Methods for monitoring endoplasmic reticulum stress and the unfolded protein response. International Journal of Cell Biology *2010*, 830307.

Schmid, R.M. (2002). Acinar-to-ductal metaplasia in pancreatic cancer. J. Clin. Invest. *109*, 2.

Shaffer, A.L., Shapiro-Shelef, M., Iwakoshi, N.N., Lee, A.-H., Qian, S.-B., Zhao, H., Yu, X., Yang, L., Tan, B.K., Rosenwald, A., et al. (2004). XBP1, downstream of Blimp-1, expands the secretory apparatus and other organelles, and increases protein synthesis in plasma cell differentiation. Immunity *21*, 81–93.

Shi, C., Hong, S.M., Lim, P., Kamiyama, H., Khan, M., Anders, R.A., Goggins, M., Hruban, R.H., and Eshleman, J.R. (2009a). KRAS2 mutations in human pancreatic acinar-ductal metaplastic lesions are limited to those with PanIN: implications for the human pancreatic cancer cell of origin. Mol Cancer Res *7*, 230–236.

Shi, G., Zhu, L., Sun, Y., Bettencourt, R., Damsz, B., Hruban, R.H., and Konieczny, S.F. (2009b). Loss of the Acinar-Restricted Transcription Factor Mist1 Accelerates Kras-Induced Pancreatic Intraepithelial Neoplasia. Gastroenterology.

Shi, G., Direnzo, D., Qu, C., Barney, D., Miley, D., and Konieczny, S.F. (2012). Maintenance of acinar cell organization is critical to preventing Kras-induced acinar-ductal metaplasia. Oncogene.

Siegel, R., Naishadham, D., and Jemal, A. (2013). Cancer statistics, 2013. CA: a Cancer Journal for Clinicians *63*, 11–30.

Slack, J.M. (1995). Developmental biology of the pancreas. Development *121*, 1569–1580.

So, J.-S., Hur, K.Y., Tarrio, M., Ruda, V., Frank-Kamenetsky, M., Fitzgerald, K., Koteliansky, V., Lichtman, A.H., Iwawaki, T., Glimcher, L.H., et al. (2012). Silencing of lipid metabolism genes through IRE1α-mediated mRNA decay lowers plasma lipids in mice. Cell Metabolism *16*, 487–499.

Soriano, P. (1999). Generalized lacZ expression with the ROSA26 Cre reporter strain. Nat Genet *21*, 70–71.

Spaargaren, M., Bischoff, J.R., and McCormick, F. (1995). Signal transduction by Ras-like GTPases: a potential target for anticancer drugs. Gene Expression *4*, 345–356.

Spiotto, M.T., Banh, A., Papandreou, I., Cao, H., Galvez, M.G., Gurtner, G.C., Denko, N.C., Le, Q.T., and Koong, A.C. (2010). Imaging the unfolded protein response in primary tumors reveals microenvironments with metabolic variations that predict tumor growth. Cancer Research *70*, 78–88.

Sriburi, R., Jackowski, S., Mori, K., and Brewer, J.W. (2004). XBP1: a link between the unfolded protein response, lipid biosynthesis, and biogenesis of the endoplasmic reticulum. The Journal of Cell Biology *167*, 35–41.

Sriburi, R., Bommiasamy, H., Buldak, G.L., Robbins, G.R., Frank, M., Jackowski, S., and Brewer, J.W. (2007). Coordinate regulation of phospholipid biosynthesis and secretory pathway gene expression in XBP-1(S)-induced endoplasmic reticulum biogenesis. The Journal of Biological Chemistry *282*, 7024–7034.

Stetler-Stevenson, W.G. (1996). Dynamics of matrix turnover during pathologic remodeling of the extracellular matrix. The American Journal of Pathology *148*, 1345–1350.

Strobel, O., Dor, Y., Alsina, J., Stirman, A., Lauwers, G., Trainor, A., Castillo, C.F., Warshaw, A.L., and Thayer, S.P. (2007). In vivo lineage tracing defines the role of acinar-to-ductal transdifferentiation in inflammatory ductal metaplasia. Gastroenterology *133*, 1999–2009.

Su, K.H., Cuthbertson, C., and Christophi, C. (2006). Review of experimental animal models of acute pancreatitis. HPB : the Official Journal of the International Hepato Pancreato Biliary Association *8*, 264–286.

Su, R., Li, Z., Li, H., Song, H., Bao, C., Wei, J., and Cheng, L. (2010). Grp78 promotes the invasion of hepatocellular carcinoma. BMC Cancer *10*, 20.

Suh, D.H., Kim, M.-K., Kim, H.S., Chung, H.H., and Song, Y.S. (2012). Unfolded protein response to autophagy as a promising druggable target for anticancer therapy. Annals of the New York Academy of Sciences *1271*, 20–32.

Szegezdi, E., Logue, S.E., Gorman, A.M., and Samali, A. (2006). Mediators of endoplasmic reticulum stress-induced apoptosis. EMBO Reports *7*, 880–885.

Takayanagi, S., Fukuda, R., Takeuchi, Y., Tsukada, S., and Yoshida, K. (2013). Gene regulatory network of unfolded protein response genes in endoplasmic reticulum stress. Cell Stress & Chaperones *18*, 11–23.

Tanaka, T., Tsujimura, T., Takeda, K., Sugihara, A., Maekawa, A., Terada, N., Yoshida, N., and Akira, S. (1998). Targeted disruption of ATF4 discloses its essential role in the formation of eye lens fibres. Genes to Cells : Devoted to Molecular & Cellular Mechanisms *3*, 801–810.

Thiele, C., Gerdes, H.H., and Huttner, W.B. (1997). Protein secretion: puzzling receptors. Current Biology : CB *7*, R496–500.

Todd, D.J., Lee, A.-H., and Glimcher, L.H. (2008). The endoplasmic reticulum stress response in immunity and autoimmunity. Nature Reviews. Immunology *8*, 663–674.

Todd, D.J., McHeyzer-Williams, L.J., Kowal, C., Lee, A.-H., Volpe, B.T., Diamond, B., McHeyzer-Williams, M.G., and Glimcher, L.H. (2009). XBP1 governs late events in plasma cell differentiation and is not required for antigen-specific memory B cell development. The Journal of Experimental Medicine *206*, 2151–2159.

Tran, T., Jia, D., Sun, Y., and Konieczny, S.F. (2007). The bHLH domain of Mistl is sufficient to activate gene transcription. Gene Expression *13*, 241–253.

Tsang, K.Y., Chan, D., Bateman, J.F., and Cheah, K.S.E. (2010). In vivo cellular adaptation to ER stress: survival strategies with double-edged consequences. Journal of Cell Science *123*, 2145–2154.

Tuveson, D.A., Zhu, L., Gopinathan, A., Willis, N.A., Kachatrian, L., Grochow, R., Pin, C.L., Mitin, N.Y., Taparowsky, E.J., Gimotty, P.A., et al. (2006). Mist1-KrasG12D knock-in mice develop mixed differentiation metastatic exocrine pancreatic carcinoma and hepatocellular carcinoma. Cancer Res *66*, 242–247.

Urano, F., Wang, X., Bertolotti, A., Zhang, Y., Chung, P., Harding, H.P., and Ron, D. (2000). Coupling of stress in the ER to activation of JNK protein kinases by transmembrane protein kinase IRE1. Science (New York, N.Y.) *287*, 664–666.

Vitale, A., and Denecke, J. (1999). The endoplasmic reticulum-gateway of the secretory pathway. The Plant Cell *11*, 615–628.

Wacker, I., Kaether, C., Krömer, A., Migala, A., Almers, W., and Gerdes, H.H. (1997). Microtubule-dependent transport of secretory vesicles visualized in real time with a GFP-tagged secretory protein. Journal of Cell Science *110 (Pt 1*, 1453–1463.

Walter, P., and Ron, D. (2011). The unfolded protein response: from stress pathway to homeostatic regulation. Science (New York, N.Y.) *334*, 1081–1086.

Wang, G., Yang, Z.-Q., and Zhang, K. (2010). Endoplasmic reticulum stress response in cancer: molecular mechanism and therapeutic potential. American Journal of Translational Research *2*, 65–74.

Wang, R.N., Klöppel, G., and Bouwens, L. (1995). Duct- to islet-cell differentiation and islet growth in the pancreas of duct-ligated adult rats. Diabetologia *38*, 1405–1411.

Watanabe, S., Abe, K., Anbo, Y., and Katoh, H. (1995). Changes in the mouse exocrine pancreas after pancreatic duct ligation: a qualitative and quantitative histological study. Archives of Histology and Cytology *58*, 365–374.

Whitcomb, D.C. (2004). Inflammation and Cancer V. Chronic pancreatitis and pancreatic cancer. Am J Physiol Gastrointest Liver Physiol *287*, G315–9.

Wiest, D.L., Burkhardt, J.K., Hester, S., Hortsch, M., Meyer, D.I., and Argon, Y. (1990). Membrane biogenesis during B cell differentiation: most endoplasmic reticulum proteins are expressed coordinately. The Journal of Cell Biology *110*, 1501–1511.

Williams, J.A. (2010). Regulation of acinar cell function in the pancreas. Current Opinion in Gastroenterology *26*, 478–483.

Wu, J., Rutkowski, D.T., Dubois, M., Swathirajan, J., Saunders, T., Wang, J., Song, B., Yau, G.D.-Y., and Kaufman, R.J. (2007). ATF6alpha optimizes long-term endoplasmic reticulum function to protect cells from chronic stress. Developmental Cell *13*, 351–364.

Yamamoto, K., Yoshida, H., Kokame, K., Kaufman, R.J., and Mori, K. (2004). Differential contributions of ATF6 and XBP1 to the activation of endoplasmic reticulum stress-responsive cis-acting elements ERSE, UPRE and ERSE-II. Journal of Biochemistry *136*, 343–350.

Yamamoto, K., Sato, T., Matsui, T., Sato, M., Okada, T., Yoshida, H., Harada, A., and Mori, K. (2007). Transcriptional induction of mammalian ER quality control proteins is mediated by single or combined action of ATF6alpha and XBP1. Developmental Cell *13*, 365–376.

Yan, L., McFaul, C., Howes, N., Leslie, J., Lancaster, G., Wong, T., Threadgold, J., Evans, J., Gilmore, I., Smart, H., et al. (2005). Molecular analysis to detect pancreatic ductal adenocarcinoma in high-risk groups. Gastroenterology *128*, 2124–2130.

Yoshida, H., Oku, M., Suzuki, M., and Mori, K. (2006). pXBP1(U) encoded in XBP1 pre-mRNA negatively regulates unfolded protein response activator pXBP1(S) in mammalian ER stress response. The Journal of Cell Biology *172*, 565–575.

Zhang, P., McGrath, B., Li, S., Frank, A., Zambito, F., Reinert, J., Gannon, M., Ma, K., McNaughton, K., and Cavener, D.R. (2002). The PERK eukaryotic initiation factor 2 alpha kinase is required for the development of the skeletal system, postnatal growth, and the function and viability of the pancreas. Molecular and Cellular Biology *22*, 3864–3874.

Zhao, Y., Li, X., Cai, M.-Y., Ma, K., Yang, J., Zhou, J., Fu, W., Wei, F.-Z., Wang, L., Xie, D., et al. (2013). XBP-1u suppresses autophagy by promoting the degradation of FoxO1 in cancer cells. Cell Research.

Zhu, L., Tran, T., Rukstalis, J.M., Sun, P., Damsz, B., and Konieczny, S.F. (2004). Inhibition of Mist1 homodimer formation induces pancreatic acinar-to-ductal metaplasia. Mol Cell Biol *24*, 2673–2681.

Zhu, L., Shi, G., Schmidt, C.M., Hruban, R.H., and Konieczny, S.F. (2007). Acinar cells contribute to the molecular heterogeneity of pancreatic intraepithelial neoplasia. Am J Pathol *171*, 263–273.

APPENDICES

Appendix A: ChIP Enrichment Scores and E-box Analysis for all MIST1 Candidate Effectors

Identification		*ChIP-Seq*			
Gene abbr.	**Name**	**Enrichment**		**E-boxes**	
		Locations	**Fold**	**GC**	**TA**
Alg12	asparagine-linked glycosylation 12	Promoter	2.3	1	0
Alg2	asparagine-linked glycosylation 2	Promoter	3.0	2	2
Amfr	Autocrine motility factor receptor	Intron 4	7.0	1	1
Arcn1	archain 1	Intron 1	5.0	0	1
Arfgap3	ADP-ribosylation factor GTPase activating protein 3	In 1, Ex 2	5.8, 3.8	1, 2	0
Atf4	Activating transcription factor 4	Upstream	3.0	2	0
Atf6	Activating transcription factor 6	Intron 1	5.0	0	2
Atp2a2	ATPase, Ca++ transporting, cardiac muscle, slow twitch 2	Intron 1	8.0	1	0
Atxn3	Ataxin 3	Upstream (-900)	2.0	1	1
Bet1	blocked early in transport 1	Promoter	2.8	1	0
Cct7	Chaperonin containing Tcp1, subunit 7 (eta)	Promoter	9.0	1	0
Cebpb	CCAAT/enhancer binding protein (C/EBP), beta	Exon 1	3.7	2	0
Copz1	coatomer protein complex, subunit zeta 1	Intron 1	23.0	0	1
Creb3l3	CAMP responsive element binding protein 3-like 3	Intron 3	4.0	1	0
Creb3l1	cAMP responsive element binding protein 3-like 1	Promoter	10.0	2	0
Derl1	Der1-like domain family, member 1	Promoter	2.0	1	0
Dnajb11	DnaJ (Hsp40) homolog, subfamily B, member 9	Exon 1/TSS	4.0	1	0
Dnajb9	DnaJ (Hsp40) homolog, subfamily B, member 11	-2.5K	3.0	0	1
Dnajc1	DnaJ (Hsp40) homolog, subfamily C, member 1	Prom, In 1	7.8, 8.0	0, 2	1, 0
Dnajc10	DnaJ (Hsp40) homolog, subfamily C, member 10	Promoter (2), In 1	15.0	2, 0, 0	0, 0, 2

Dnajc3	DnaJ (Hsp40) homolog, subfamily C, member 3	Intron 1	3.5	0	2
Dnajc4	DnaJ (Hsp40) homolog, subfamily C, member 4	Exon 1	2.7	1	0
Edem1	ER degradation enhancer, mannosidase alpha-like 1	Intron 1 (2)	17, 4.5	0, 1	1, 1
Edem3	ER degradation enhancer, mannosidase alpha-like 3	Prom, In 1	7, 4.5	1, 1	0, 1
Eif2a	eukaryotic translation initiation factor 2A	Intron 1	3.5	0	0
Eif2ak3	Eukaryotic translation initiation factor 2 alpha kinase 3	Intron 2	2.7	0	0
Ern1	Endoplasmic reticulum (ER) to nucleus signalling 1	Intron 1 (2)	5.7, 21	1, 1	0
Ero1L	ERO1-like (S. cerevisiae)	Promoter, In 1, In 2	6, 6, 10	0,0,1	1,0,0
Ero1Lb	ERO1-like beta (S. cerevisiae)	Promoter	NO CTRL	0	0
Erp44	Endoplasmic reticulum protein 44	Intron 1	2.5	0	2
Fbxo6	F-box protein 6	Intron 1	8.0	0	0
Fkbp10	FK506 binding protein 10	Upstream -1K	2.1	1	0
Fkbp11	FK506 binding protein 11	Exon 1/TSS	2.4	1	0
Fkbp14	FK506 binding protein 14	Promoter	7.0	2	0
Gcc1	golgi coiled coil 1	Promoter	7.0	0	1
Golga3	golgi autoantigen, golgin subfamily a, 3	Intron 1	6.0	1	0
Golga4	golgi autoantigen, golgin subfamily a, 4	Intron 1	4.0	1	0
Golgb1	golgi autoantigen, golgin subfamily b, macrogolgin 1	Upstream -4K	9.0	1	0
Golph3	golgi phosphoprotein 3	Intron 2	10.0	0	2
Gopc	golgi associated PDZ and coiled-coil motif containing	Intron 1	7.0	0	1
Gorasp2	golgi reassembly stacking protein 2	Promoter	3.0	2	2
H13	histocompatibility 13	Intron 1	2.3	4	0
H47	Histocompatibility 47	Ex 1, In 2	2, 10	2, 1	0, 0
Herpud1	Homocysteine-inducible, endoplasmic reticulum stress-inducible, ubiquitin-like domain member 1	Intron 1	2.3	0	0
Hmox1	heme oxygenase (decycling) 1	Exon 1/TSS	3.3	2	1
Hsp90b1	heat shock protein 90 alpha (cytosolic), class B member 1	Intron 4	4.0	1	0
Hspa13	Heat shock protein 2	Upstream -1k	8.0	1	1
Hspa2	heat shock protein 70 family, member 13	Promoter	4.0	0	0
Hsph1	Heat shock 105kDa/110kDa protein 1	Intron 1	5.0	2	0
Htra2	HtrA serine peptidase 2	Intron 2	2.1	4	0

Htra4	HtrA serine peptidase 4	Intron 8	2.7	0	0
Hyou1	hypoxia up-regulated 1	Exon 1/Intron 1	7.0	1	0
Kdelr2	KDEL (Lys-Asp-Glu-Leu) endoplasmic reticulum protein retention receptor 2	Upstream -2K	23.0	1	0
Lman1	lectin, mannose-binding, 1	Exon 1	9.0	0	0
Manf	Mesencephalic astrocyte-derived neurotrophic factor	Exon 1	3.7	1	1
Mapk10	Mitogen-activated protein kinase 10	Intron 1	10.0	0	0
Mapk9	Mitogen-activated protein kinase 9	Intron 1	10.0	2	0
Mbtps1	Membrane-bound transcription factor peptidase, site 1	Exon 1/TSS	11.0	1	0
Mbtps2	Membrane-bound transcription factor peptidase, site 2	Upstream (-3K)	6.0	1	0
Mcfd2	multiple coagulation factor deficiency 2	Intron 1	4.0	0	1
Mgat2	mannoside acetylglucosaminyltransferase 2	Promoter	5.5	0	0
Mogs	mannosyl-oligosaccharide glucosidase	Exon 4	10.0	1	0
Nploc4	Nuclear protein localization 4 homolog (S. cerevisiae)	Intron 1	12.5	0	1
Nucb1	Nucleobindin 1	Intron 1	4.7	1	0
Ormdl3	ORM1-like 3 (S. cerevisiae)	Upstream (-3K), Ex 1	10, 5	1, 1	0
Os9	Amplified in osteosarcoma	Prom, In 3	10, 4	1, 0	0, 2
PDI/Pdia3	Protein disulfide isomerase associated 3	Promoter	14.0	2	0
Pdia4	protein disulfide isomerase associated 4	Ex 1, In 1 X 2	13, 4, 8	1, 0, 1	0, 1, 0
Pfdn2	Prefoldin 2	Exon 1/TSS	3.0	0	0
Pfdn5	Prefoldin 5	Intron 2	3.0	0	0
Piga	phosphatidylinositol glycan anchor biosynthesis, class A	Intron 4	8.0	1	0
Ppib	peptidylprolyl isomerase B	Intron 1	3.5	2	0
Ppp1r15b	Protein phosphatase 1, regulatory (inhibitor) subunit 15b	Intron 1	7.7	2	0
Rab33b	RAB33B, member of RAS oncogene family	Exon 1/TSS	2.3	1	0
Rnf139	Ring finger protein 139	Ex 1, In 1	5, 3.7	0, 1	0, 0
Rnf5	Ring finger protein 5	Intron 1	2.5	0	1
Rpn1	Ribophorin I	Intron 1 (2)	3, 3	1, 0	0, 0
Rrbp1	ribosome binding protein 1	Intron 1	7.0	1	0
Sdf2l1	stromal cell-derived factor 2-like 1	Exon 1/TSS, In 1	7, 7	1, 1	0, 0
Sec11a	SEC11 homolog A (S. cerevisiae)	Upstream -1K	5.0	1	0
Sec11c	SEC11 homolog C (S. cerevisiae)	Intron 1	4.5	1	1

Sec31a	Sec31 homolog A (S. cerevisiae)	Intron 1	4.0	0	0
Sec61a1	Sec61 alpha 1 subunit (S. cerevisiae)	Intron 1	3.0	0	0
Sec61b	Sec61 beta subunit	Intron 2	3.8	2	1
Sec61g	SEC61, gamma subunit	-1K, In 1	6, 4	1, 0	0, 0
Sec62	SEC62 homolog (S. cerevisiae)	Intron 1	3.0	1	0
Sec63	SEC63-like (S. cerevisiae)	Intron 1 (2)	5, 4.3	1, 2	1, 0
Sel1l	Sel-1 suppressor of lin-12-like (C. elegans)	Upstream (-1.5K), In 1	8, 5.5	0, 1	0, 0
Selm	selenoprotein M	Exon 1/TSS	3.0	0	0
Serp1	signal peptidase complex subunit 3 homolog (S. cerevisiae)	Intron 2	2.7	1	0
Sil1	Endoplasmic reticulum chaperone SIL1 homolog (S. cerevisiae)	Intron 1	12.0	1	1
Spcs2	signal peptidase complex subunit 2 homolog (S. cerevisiae)	Intron 1	6.0	1	0
Spcs3	signal recognition particle 68	-1K, In 1, In 2	9, 12, 16	1, 0, 2	0, 1, 1
Srebf1	Sterol regulatory element binding transcription factor 1	Intron 1	3.5	0	0
Srebf2	Sterol regulatory element binding factor 2	Upstream (-3K)	10.0	1	0
Srp19	signal recognition particle 19	Intron 2	3.7	1	0
Srp54a	signal recognition particle 54A	Exon 1/TSS	11.0	1	0
srp68	signal recognition particle receptor	Intron 1	6.0	2	1
Srpr	signal sequence receptor, gamma	Intron 1	4.8	1	0
Srprb	signal recognition particle receptor, B subunit	Intron 1	7.0	0	0
Ssr1	signal sequence receptor, alpha	Promoter		1	0
Ssr3	translocating chain-associating membrane protein 1	Intron 1	3.5	0	2
Stx18	syntaxin 18	Intron 1 X 3	6, 2.3, 4.8	1, 2, 1	0, 0, 0
Surf4	surfeit gene 4	Exon 1/TSS	3.7	1	0
Syvn1	Synovial apoptosis inhibitor 1, synoviolin	Upstream (-3K)	8.0	0	1
Tor1a	Torsin family 1, member A (torsin A)				
Tram1	Stress-associated endoplasmic reticulum protein 1	Intron 1 X 4	4.3, 2.5, 2.8, 4.3	2, 1, 0, 0	0, 0, 1, 1
Txndc11	thioredoxin domain containing 11	Intron 1 (2)	4, 5	0, 0	0, 0
Txndc5	thioredoxin domain containing 5	Intron 1		1	0
Ube2g2	Ubiquitin-conjugating enzyme E2G 2	Intron 1	2.7	0	0
Ubxn4	UBX domain protein 4	Exon 1	2.0	0	0
Uggt1	UDP-glucose glycoprotein glucosyltransferase 1	Exon 1/TSS, In 1	2, 2.3	1, 0	0, 0
Uso1	USO1 vesicle docking factor	Intron 1	3.7	2	0
Usp14	Ubiquitin specific peptidase 14	Promoter	3.0	1	0

Vamp2	vesicle-associated membrane protein 2	Upstream (-1K), In 1	2.5, 5.0	4, 0	0, 0
Vamp4	vesicle-associated membrane protein 4	Promoter	6.0	0	0
Vamp7	vesicle-associated membrane protein 7	NO DATA			
Vcp	Valosin containing protein	Promoter, In 1, In 2	5, 2.8, 4.7	1, 1, 1	0, 1, 0
Xbp1	X-box binding protein 1	Promoter	3.5	1	0
Yipf5	Yip1 domain family, member 5	Exon 1/TSS	6.0	0	0

Appendix B: MIST1 Candidate Effectors With No ChIP Enrichment

Identification		*ChIP-Seq*			
Gene abbr.	Name	Enrichment		E-boxes	
		Locations	Fold	GC	TA
Atf5	Activating transcription factor 5	N/A	N/A	N/A	N/A
Atf6b	Activating transcription factor 6 beta	N/A	N/A	N/A	N/A
Bax	Bcl2-associated X protein	N/A	N/A	N/A	N/A
Bet1l	blocked early in transport 1-like	N/A	N/A	N/A	N/A
Bfar	bifunctional apoptosis regulator	N/A	N/A	N/A	N/A
Blzf1	basic leucine zipper nuclear factor 1	N/A	N/A	N/A	N/A
Calr	Calreticulin	N/A	N/A	N/A	N/A
Canx	Calnexin	N/A	N/A	N/A	N/A
Cct4	Chaperonin containing Tcp1, subunit 4 (delta)	N/A	N/A	N/A	N/A
CHOP/Ddit3	component of oligomeric golgi complex 3	N/A	N/A	N/A	N/A
Cog3	component of oligomeric golgi complex 6	N/A	N/A	N/A	N/A
Cog6	coatomer protein complex, subunit beta 1	N/A	N/A	N/A	N/A
Copb1	coatomer protein complex, subunit beta 2 (beta prime)	N/A	N/A	N/A	N/A
Copb2	coatomer protein complex, subunit epsilon	N/A	N/A	N/A	N/A
Cope	coatomer protein complex, subunit gamma 1	N/A	N/A	N/A	N/A
Copg	CAMP responsive element binding protein 3	N/A	N/A	N/A	N/A
Creb3	DNA-damage inducible transcript 3	N/A	N/A	N/A	N/A
Dad1	defender against cell death 1	N/A	N/A	N/A	N/A
Ddost	dolichyl-di-phosphooligosaccharide-protein glycotransferase	N/A	N/A	N/A	N/A
Derl2	Der1-like domain family, member 2	N/A	N/A	N/A	N/A
Dnajb2	DnaJ (Hsp40) homolog, subfamily B, member 2	N/A	N/A	N/A	N/A

Dolpp1	dolichyl pyrophosphate phosphatase 1	N/A	N/A	N/A	N/A
Ern2	Endoplasmic reticulum (ER) to nucleus signalling 2	N/A	N/A	N/A	N/A
Erp29	endoplasmic reticulum protein 29	N/A	N/A	N/A	N/A
Fkbp1b	FK506 binding protein 1b	N/A	N/A	N/A	N/A
Fkbp2	FK506 binding protein 2	N/A	N/A	N/A	N/A
Fkbp7	FK506 binding protein 7	N/A	N/A	N/A	N/A
Ganab	Alpha glucosidase 2 alpha neutral subunit	N/A	N/A	N/A	N/A
Ganc	Glucosidase, alpha; neutral C	N/A	N/A	N/A	N/A
Ggcx	gamma-glutamyl carboxylase	N/A	N/A	N/A	N/A
Golph3l	golgi phosphoprotein 3-like	N/A	N/A	N/A	N/A
Gosr2	golgi SNAP receptor complex member 2	N/A	N/A	N/A	N/A
Hspa1L	Heat shock protein 1-like	N/A	N/A	N/A	N/A
Hspa4	Heat shock protein 4	N/A	N/A	N/A	N/A
Hspa4L	Heat shock protein 4 like	N/A	N/A	N/A	N/A
Hspa5	Heat shock protein 5	N/A	N/A	N/A	N/A
Hspb9	Heat shock protein, alpha-crystallin-related, B9	N/A	N/A	N/A	N/A
Insig1	Insulin induced gene 1	N/A	N/A	N/A	N/A
Insig2	Insulin induced gene 2	N/A	N/A	N/A	N/A
Kdelr3	KDEL (Lys-Asp-Glu-Leu) endoplasmic reticulum protein retention receptor 3	N/A	N/A	N/A	N/A
Lepre1	leprecan 1	N/A	N/A	N/A	N/A
Lman2	lectin, mannose-binding 2	N/A	N/A	N/A	N/A
Mapk8	Mitogen-activated protein kinase 8	N/A	N/A	N/A	N/A
Pdia6	protein disulfide isomerase associated 6	N/A	N/A	N/A	N/A
Ppia	Peptidylprolyl isomerase A	N/A	N/A	N/A	N/A
Prkcsh	Protein kinase C substrate 80K-H	N/A	N/A	N/A	N/A
Rab3a	RAB3A, member RAS oncogene family	N/A	N/A	N/A	N/A
Rabac1	Rab acceptor 1 (prenylated)	N/A	N/A	N/A	N/A
Rcn3	reticulocalbin 3, EF-hand calcium binding domain	N/A	N/A	N/A	N/A
Rpn2	ribophorin II	N/A	N/A	N/A	N/A
Scap	SREBF chaperone	N/A	N/A	N/A	N/A
Sec22b	SEC22 vesicle trafficking protein homolog B (S. cerevisiae)	N/A	N/A	N/A	N/A
Sec23a	SEC23A (S. cerevisiae)	N/A	N/A	N/A	N/A

Sec23b	SEC23B (S. cerevisiae)	N/A	N/A	N/A	N/A
Sec24d	Sec24 related gene family, member D	N/A	N/A	N/A	N/A
Srp9	signal recognition particle 9	N/A	N/A	N/A	N/A
Ssr2	signal sequence receptor, beta	N/A	N/A	N/A	N/A
Ssr4	signal sequence receptor, delta	N/A	N/A	N/A	N/A
Stx5a	syntaxin 5A	N/A	N/A	N/A	N/A
Tcp1	T-complex protein 1	N/A	N/A	N/A	N/A
Ube2j2	Ubiquitin-conjugating enzyme E2, J2 homolog (yeast)	N/A	N/A	N/A	N/A
Ufd1l	Ubiquitin fusion degradation 1 like	N/A	N/A	N/A	N/A
Uggt2	UDP-glucose glycoprotein glucosyltransferase 2	N/A	N/A	N/A	N/A
Wfs1	Wolfram syndrome 1 homolog	N/A	N/A	N/A	N/A
Yif1a	Yip1 interacting factor homolog A (S. cerevisiae)	N/A	N/A	N/A	N/A

Appendix C: Relative Fold Change in *MIST1^{WT}*, *MIST1^{KO}*, and *MIST1^{KO};LSL-MIST1^{MYC}* for MIST1 Candidate Effectors With ChIP Enrichment and Significant Expression Differences in *MIST1^{WT}* vs. *MIST1^{KO}*

Identification		Array Data				
Gene abbr.	Name	Expression fold change			P-value (WT vs. KO)	Rescue
		WT	KO	Rescue		
Alg12	asparagine-linked glycosylation 12	1	1.20	1.01	0.0260	Full
Arcn1	archain 1	1	-1.21	-1.16	0.0400	Partial
Arfgap3	ADP-ribosylation factor GTPase activating protein 3	1	-2.23	-1.35	0.0001	Partial
Atp2a2	ATPase, Ca++ transporting, cardiac muscle, slow twitch 2	1	-1.34	-1.04	0.0460	Full
Copz1	coatomer protein complex, subunit zeta 1	1	-3.19	-1.07	0.0000	Full
Creb3l1	cAMP responsive element binding protein 3-like 1	1	1.32	1.11	0.0070	Partial
Dnajb11	DnaJ (Hsp40) homolog, subfamily B, member 9	1	1.26	1.22	0.0560	None
Dnajb9	DnaJ (Hsp40) homolog, subfamily B, member 11	1	1.19	1.14	0.0880	None
Dnajc1	DnaJ (Hsp40) homolog, subfamily C, member 1	1	-1.82	-1.12	0.0001	Partial
Dnajc3	DnaJ (Hsp40) homolog, subfamily C, member 3	1	-1.216	1.077	0.0370	Partial
Dnajc4	DnaJ (Hsp40) homolog, subfamily C, member 4	1	1.334	1.05	0.0005	Partial
Edem3	ER degradation enhancer, mannosidase alpha-like 3	1	-1.75	-1.11	0.0003	Partial
Eif2a	eukaryotic translation initiation factor 2A	1	-1.16	-1.2	0.0670	None
Ero1Lb	ERO1-like beta (S. cerevisiae)	1	-1.27	-1.33	0.0130	None
Erp44	Endoplasmic reticulum protein 44	1	-1.24	-1.18	0.0040	None
Fbxo6	F-box protein 6	1	-1.22	1.07	0.0600	Partial
H13	histocompatibility 13	1	-1.28	1.01	0.0490	Full
H47	Histocompatibility 47	1	-1.16	-1.11	0.0880	Partial
Htra2	HtrA serine peptidase 2	1	-2.78	-1.48	0.0000	Partial
Mapk9	Mitogen-activated protein kinase 9	1	-1.24	1.01	0.0197	Full

Mcfd2	multiple coagulation factor deficiency 2	1	-1.20	-1.04	0.0650	Full
Mogs	mannosyl-oligosaccharide glucosidase	1	-1.56	-1.20	0.0056	Partial
Os9	Amplified in osteosarcoma	1	-1.77	-1.24	0.0001	Partial
PDI/Pdia3	Protein disulfide isomerase associated 3	1	1.24	1.2	0.0890	None
Pdia4	protein disulfide isomerase associated 4	1	1.40	1.36	0.0630	None
Pfdn2	Prefoldin 2	1	1.17	1.08	0.0320	Partial
Pfdn5	Prefoldin 5	1	1.17	1	0.0010	Full
Piga	phosphatidylinositol glycan anchor biosynthesis, class A	1	2.56	1.34	0.0003	Partial
Ppib	peptidylprolyl isomerase B	1	1.13	1.04	0.0061	Full
Ppp1r15b	Protein phosphatase 1, regulatory (inhibitor) subunit 15b	1	-1.22	1	0.0530	Full
Rnf139	Ring finger protein 139	1	-1.264	-1.11	0.0410	Partial
Rrbp1	ribosome binding protein 1	1	1.21	1.18	0.0040	None
Sec11a	SEC11 homolog A (S. cerevisiae)	1	1.21	1.08	0.0240	Partial
Sec11c	SEC11 homolog C (S. cerevisiae)	1	-2.62	-1.74	0.0000	Partial
Sec31a	Sec31 homolog A (S. cerevisiae)	1	-1.20	-1.05	0.0630	Partial
Sec61b	Sec61 beta subunit	1	-1.33	-1.16	0.0148	Partial
Sec61g	SEC61, gamma subunit	1	1.18	1.12	0.0990	Partial
Sec62	SEC62 homolog (S. cerevisiae)	1	1.15	1.16	0.0560	None
Selm	selenoprotein M	1	-1.17	-1.20	0.0810	None
Serp1	signal peptidase complex subunit 3 homolog (S. cerevisiae)	1	-1.567	-1.19	0.0001	Partial
Spcs2	signal peptidase complex subunit 2 homolog (S. cerevisiae)	1	-1.16	-1.03	0.0450	None
Spcs3	signal recognition particle 68	1	-1.61	-1.29	0.0004	Partial
srp68	signal recognition particle receptor	1	-1.45	-1.13	0.0019	Partial
Srpr	signal sequence receptor, gamma	1	-1.35	-1.14	0.0010	Partial
Ssr3	translocating chain-associating membrane protein 1	1	-1.16	-1.04	0.0305	Full
Stx18	syntaxin 18	1	-1.19	-1.10	0.0630	Partial
Surf4	surfeit gene 4	1	1.20	-1.02	0.0730	Full
Syvn1	Synovial apoptosis inhibitor 1, synoviolin	1	-1.386	-1.17	0.0850	Partial

Tram1	Stress-associated endoplasmic reticulum protein 1	1	-1.80	-1.19	0.0000	Partial
Ube2g2	Ubiquitin-conjugating enzyme E2G 2	1	-1.2	-1.02	0.0750	Full
Ubxn4	UBX domain protein 4	1	-1.301	-1.032	0.0450	Full
Uso1	USO1 vesicle docking factor	1	-1.18	-1.11	0.0710	Partial
Xbp1	X-box binding protein 1	1	1.16	1.21	0.0640	None
Yipf5	Yip1 domain family, member 5	1	-1.27	-1.27	0.0606	None

Appendix D: Relative Fold Change In *MIST1^{WT}, MIST1^{KO}, and MIST1^{KO};LSL-MIST1^{MYC}* For MIST1 Candidate Effectors With ChIP Enrichment But no Significant Expression Changes Between *MIST1^{WT}* vs. *MIST1^{KO}*

Identification		Array Data			
Gene abbr.	Name	Expression fold change			P-value (WT vs. KO)
		WT	KO	Rescue	
Alg2	asparagine-linked glycosylation 2	1	-1.22	-1.09	>0.1
Amfr	Autocrine motility factor receptor	1	1.1	-1.07	>0.1
Atf4	Activating transcription factor 4	1	-1.12	-1.23	>0.1
Atf6	Activating transcription factor 6	1	-1.01	1.08	>0.1
Atxn3	Ataxin 3	1	1.12	-1.09	>0.1
Bet1	blocked early in transport 1	1	1.04	-1.09	>0.1
Cct7	Chaperonin containing Tcp1, subunit 7 (eta)	1	-1.05	0.93	>0.1
Cebpb	CCAAT/enhancer binding protein (C/EBP), beta	1	1.06	-1.1	>0.1
Creb3l3	CAMP responsive element binding protein 3-like 3	1	-1.02	1.02	>0.1
Derl1	Der1-like domain family, member 1	1	1.09	-1.09	>0.1
Dnajc10	DnaJ (Hsp40) homolog, subfamily C, member 10	1	1.11	-1.67	>0.1
Edem1	ER degradation enhancer, mannosidase alpha-like 1	1	-1.12	-1.05	>0.1
Eif2ak3	Eukaryotic translation initiation factor 2 alpha kinase 3	1	1.05	-1.11	>0.1
Ern1	Endoplasmic reticulum (ER) to nucleus signalling 1	1	-1.02	1.05	>0.1
Ero1L	ERO1-like (S. cerevisiae)	1	-1.14	1.21	>0.1
Fkbp10	FK506 binding protein 10	1	1.24	1.19	>0.1
Fkbp11	FK506 binding protein 11	1	1.05	-1.07	>0.1
Fkbp14	FK506 binding protein 14	1	1.08	1.26	>0.1
Gcc1	golgi coiled coil 1	1	-1.14	-1.16	>0.1
Golga3	golgi autoantigen, golgin subfamily a, 3	1	1.14	-1.03	>0.1
Golga4	golgi autoantigen, golgin subfamily a, 4	1	-1.16	1.01	>0.1

Golgb1	golgi autoantigen, golgin subfamily b, macrogolgin 1	1	1.19	1.14	>0.1
Golph3	golgi phosphoprotein 3	1	-1.13	-1.02	>0.1
Gopc	golgi associated PDZ and coiled-coil motif containing	1	1.16	-1.13	>0.1
Gorasp2	golgi reassembly stacking protein 2	1	1.05	-1.13	>0.1
Herpud1	Homocysteine-inducible, endoplasmic reticulum stress-inducible, ubiquitin-like domain member 1	1	1.08	-1.15	>0.1
Hmox1	heme oxygenase (decycling) 1	1	1.15	1.09	>0.1
Hsp90b1	heat shock protein 90 alpha (cytosolic), class B member 1	1	1.16	1.23	>0.1
Hspa13	Heat shock protein 2	1	-1.20	-1.39	.0.1
Hspa2	heat shock protein 70 family, member 13	1	-1.02	-1.04	>0.1
Hsph1	Heat shock 105kDa/110kDa protein 1	1	-1.03	1.003	>0.1
Htra4	HtrA serine peptidase 4	1	-1.04	1.14	>0.1
Hyou1	hypoxia up-regulated 1	1	1.16	1.12	>0.1
Kdelr2	KDEL (Lys-Asp-Glu-Leu) endoplasmic reticulum protein retention receptor 2	NO DATA			
Lman1	lectin, mannose-binding, 1	1	-1.20	1.00	>0.1
Manf	Mesencephalic astrocyte-derived neurotrophic factor	1	1.07	-1.02	>0.1
Mapk10	Mitogen-activated protein kinase 10	1	1.05	1.33	>0.1
Mbtps1	Membrane-bound transcription factor peptidase, site 1	1	1.09	1.13	>0.1
Mbtps2	Membrane-bound transcription factor peptidase, site 2	1	1	1.03	>0.1
Mgat2	mannoside acetylglucosaminyltransferase 2	1	1.06	-1.33	>0.1
Nploc4	Nuclear protein localization 4 homolog (S. cerevisiae)	1	-1.11	-1.03	>0.1
Nucb1	Nucleobindin 1	1	1.075	-1.07	>0.1
Ormdl3	ORM1-like 3 (S. cerevisiae)	1	1.04	1.17	>0.1
Rab33b	RAB33B, member of RAS oncogene family	1	1.13	-1.04	>0.1
Rnf5	Ring finger protein 5	1	-1.11	-1.24	>0.1
Rpn1	Ribophorin I	1	1.08	1.115	>0.1
Sdf2l1	stromal cell-derived factor 2-like 1	1	1.01	-1.02	>0.1

Sec61a1	Sec61 alpha 1 subunit (S. cerevisiae)	1	-1.07	1.07	>0.1
Sec63	SEC63-like (S. cerevisiae)	1	-1.12	1.06	>0.1
Sel1l	Sel-1 suppressor of lin-12-like (C. elegans)	1	-1.12	-1.13	>0.1
Sil1	Endoplasmic reticulum chaperone SIL1 homolog (S. cerevisiae)	1	1.12	1.13	>0.1
Srebf1	Sterol regulatory element binding transcription factor 1	1	-1.2	1.08	>0.1
Srebf2	Sterol regulatory element binding factor 2	1	1	1.14	>0.1
Srp19	signal recognition particle 19	1	1.00	-1.23	>0.1
Srp54a	signal recognition particle 54A	NO DATA			
Srprb	signal recognition particle receptor, B subunit	1	-1.25	-1.12	>0.1
Ssr1	signal sequence receptor, alpha	1	1.01	1.01	>0.1
Tor1a	Torsin family 1, member A (torsin A)	1	1.12	1.07	>0.1
Txndc11	thioredoxin domain containing 11	1	-1.03	-1.34	>0.1
Txndc5	thioredoxin domain containing 5	1	1.15	1.14	>0.1
Uggt1	UDP-glucose glycoprotein glucosyltransferase 1	1	-1.01	1.13	>0.1
Usp14	Ubiquitin specific peptidase 14	1	1.16	1.03	>0.1
Vamp2	vesicle-associated membrane protein 2	1	-1.02	-1.01	>0.1
Vamp4	vesicle-associated membrane protein 4	1	-1.07	-1.03	>0.1
Vamp7	vesicle-associated membrane protein 7	1	1.01	-1.35	>0.1
Vcp	Valosin containing protein	1	1.08	-1.04	>0.1

VITA

David A. Hess was born on August 7th, 1982 in Doylestown, PA to Herbert and Lolita Hess. David graduated from Central Bucks East High School in June 2000 and attended the Pennsylvania State University in State College, PA. He completed his Bachelor of Science degree in Biology in May 2004. He then spent two years teaching Life Sciences and World Geography in Atlanta, GA as part of the Teach for America program, followed by one year spent as a laboratory technician at Procter and Gamble in Hunt Valley, MD. David began his graduate studies in August 2007 in the Department of Biological Sciences at Purdue University, joining the lab of Dr. Stephen Konieczny in the spring of 2008. He initially investigated the effects of high-level RAS expression on pancreatic development before refocusing on the transcription factors XBP1 and MIST1 and their role in maintaining acinar cell homeostasis via the unfolded protein response. David published a number of peer-reviewed articles and earned fellowships and awards from the Purdue Center for Cancer Research and the American Pancreatic Association. Upon completion of his Ph D., David will pursue post-doctoral training in order to gain more expertise and broaden his skill set in preparation for conducting independent research as a primary investigator.

PUBLICATIONS

Hess, D. A., Humphrey, S. E., Ishibashi, J., Damsz, B., Lee, A. H., Glimcher, L. H., & Konieczny, S. F. (2011). Extensive Pancreas Regeneration Following Acinar-Specific Disruption of Xbp1 in Mice. Gastroenterology, 141(4), 1466–1476. doi:10.1053/j.gastro.2011.06.045

Direnzo, D., Hess, D. A., Damsz, B., Hallett, J. E., Marshall, B., Goswami, C., Liu, Y., et al. (2012). Induced Mist1 Expression Promotes Remodeling of Mouse Pancreatic Acinar Cells. Gastroenterology, 143(2), 469–480. doi:10.1053/j.gastro.2012.04.011